Mechanism of the Hsp90 Chaperone Cycle: Investigation of Divalent Ion Binding and Conformational Change

Dipali Patel

A thesis submitted for the degree of

Doctor of Philosophy

September 2011

Institute of Structural and Molecular Biology

University College London

Declaration

The work presented in this thesis was undertaken at University College London. With the exception of the NMR spectra recorded at 700 MHz by Dr Eleanor Williams (UCL), I, Dipali Patel confirm that the work presented in this thesis is my own. Where information has been derived from other sources, I confirm that this has been indicated in the thesis.

Abstract

Hsp90 chaperones a large number of client proteins that perform diverse functions including roles in signal transduction and cell cycle regulation. Since a subset of these clients are proto-oncogenes, Hsp90 has emerged as a target for anti-cancer therapeutics. The chaperone function of Hsp90 involves an ATP-dependent cycle of conformational changes: recently, X-ray crystallography and fluorescence resonance energy transfer (FRET) have provided evidence that these changes occur primarily within the N-terminal and middle domains of the protein which are thought to form a closed conformation following ATP binding that facilitates ATP hydrolysis.

The research described herein is broadly divided into two sections. Initially we investigate the thermodynamics of nucleotide binding to the isolated N-terminal domain of Hsp90 (N-Hsp90) and the role of the divalent Mg^{2+} ion in this interaction. This provides a rationale for how the binding of two structurally similar nucleotides, AMP-PNP (Adenosine 5′-(β,γ-imido)triphosphate tetralithium salt hydrate); an ATP analogue) and ADP that differ in structure by a single phosphate group, produce significantly different thermodynamic signatures. Isothermal titration calorimetry was used to characterize the thermodynamic profiles of nucleotide binding to N-Hsp90 and various mutants of N-Hsp90. The effect of incorporation of another divalent ion when compared to the native Mg^{2+} ion in the binding of the AMP-PNP ligand has a significant effect on the thermodynamic properties of complex formation. By substituting different cations in the solvent we were able to establish the potential importance of the hydration properties of the metal ion in the associated observed heat capacities and resulting conformational changes of the domain.

Secondly, we investigated the conformational changes associated with the turnover of ATP by the full length Hsp90 protein. It is well know that the conformational changes that take place post ATP binding and hydrolysis are responsible for the activation of Hsp90 and its role in the chaperoning of the large plethora of clientele that it has been associated with. Investigating the nature of the conformational changes associated with the full length Hsp90 during its ATP cycle using double electron-electron resonance (DEER) spectroscopy revealed previously unknown dynamics of the chaperone even in the absence of AMP-PNP. Furthermore, this method also revealed additional rearrangements whereby all three domains of Hsp90 undergo opening and closing in the absence and presence of the nucleotide. Furthermore, the crystal structure of the full length Hsp90 in complex with AMP-PNP and the co-chaperone Sba1/p23 revealed a conformation where the M domains of the dimer are shown to be in close association to one another; our data suggests that this state is only achieved upon the binding of the co-chaperone Sba1/p23, and not as a result of AMP-PNP binding as has previously been suggested. The findings from the DEER data provide a potential mechanism in which Sba1/p23 ‘halts’ the ATP cycle of Hsp90 in an ATP ‘active’ state, thereby enabling Sba1/p23 to recruit and process its client proteins. The additional conformational rearrangements observed in our study could be viewed as potential targets for the development of innovative therapeutics against this highly diverse molecular chaperone.

Acknowledgements

As a wise man once said:

"Everyday I remind myself that my inner and outer life are based on the labours of other men, living and dead, and that I must exert myself in order to give in the same measure as I have received and am still receiving" - Albert Einstein

We cannot begin to comprehend the amount of unconditional love and support we receive from the people who are responsible for our very existence, of how they dedicate their existence in order to better ours. I for one know, with no regret, that no amount of goodness in my life will come even significantly close to the devotion that I have and continue to receive from my parents. And for this reason, I dedicate this thesis to my mother as she always has been the driving force in my life. She taught me the most important value, and that is to never seek success out of greed or betrayal, as that success would be short-lived, if you need to fall a few times and hurt yourself to achieve success then this way is more rewarding. A mere thank you is not enough, your beautiful pure soul is what has made me into who I am today, and your soul continues to live in my heart, I love you.

This thesis reflects the unconditional support of my two supervisors, Professor John Ladbury, whom without I would never have been given the opportunity to undertake a PhD, and whose persistence and guidance made me always want to excel further, in fact he is the reason for why I am, I hope, a better scientist, thank you. And to Dr. Chris Kay for his infinite support and guidance. His teaching and encouragement, not only in my research, but in showing me to believe in myself is invaluable to me, he is the reason for why I am, I hope, a more confident scientist, thank you.

In the laboratory I have had the honour of working with many great scientists, each whom I have learned from. I would like to thank Dr. Roger George, Dr. Zamal Ahmed, Dr. Eleanor Williams, Dr. Sunita Sardiwal, Dr. Asvi Francois, Dr. Tsai Meng-Lin, Dr. Chi-Chuan Lin, Dr. Paul Leonard, Dr. Ragini Ghosh, Dr. Tjelvar Olssen, Dr. Annika Schuller,

Dr. Claire Stevens, Dr. Katharina Pirker, Dr. Lisa Cabrita, Dr. Chris Waudby, Kin Suen, David Fallaize, Helene Launay, Vishal Sanchania, Marc Warner, Micha Kunze and every one in the 6th floor lab who have encouraged me over the last four years. Thank you to Rumeza Hanif, Qing Cai, Batoul Farran, and Marta Wojnowska as without our never-ending justified 'breaks' I would most definitely have ended up quitting and working in Sainsbury's..

Thank you to my family and friends for their support and enthusiasm, and for helping me to always see the brighter side, even when this seemed impossible. In particular, to my sister Nishita Patel, your vision of me as your role model is my inspiration to never let you down, and to always be the version of me I see through your eyes. I would like to especially thank Kacper Rogala, without whom I would not have gotten through the last few months of my PhD, his strange taste in music and weird humour somehow brought me solace. Finally, one person has supported me not only during four of the toughest years for me as of yet, but ever since I can remember, and there are no words to show the appreciation I feel for never letting me give up and in pushing me to always be the best I can be, even when I didn't believe I could. Your value is eternal to me, thank you.

Dipali Patel

September 2011

Contents page

List of Figures

List of Tables

List of Abbreviations

ACES	-	N-(2-acetaamino)-2-aminoethanesulfonic acid
ADP	-	Adenosine diphosphate
AEBSF	-	4-(2-Aminoethyl)benzenesulfonylfluoride hydrochloride
AMP-PNP	-	Adenosine 5′-(β,γ-imido) triphosphate tetralithium salt hydrate
ATP	-	Adenosine triphosphate
Ca^{2+}	-	Divalent calcium ion
CD	-	Circular dichroism or C-domain
DEER	-	Double electron electron resonance
E.Coli	-	*Escherichia coli*
E64	-	L-transepoxysuccinyl-leucylamino-[4-guanidino] butane
EDTA	-	Ethylene-diamine-tetraacetic acid
EM	-	Electron microscopy
EPR	-	Electron paramagnetic resonance
FRET	-	Fluorescence resonance energy transfer
GHKL	-	Gyrase, histidine kinase, mutL
G153A	-	N-terminal domain mutant of Hsp90. Residue Gly153 mutated to Ala
G154A	-	N-terminal domain mutant of Hsp90. Residue Gly154 mutated to Ala
GR	-	Glucocorticoid receptor
HEPES	-	4-(2-hydroxyethyl)-1-piperazineethanesulfonic acid
Hsp90	-	Heat shock protein 90
$Hsp90^{[MTSSL]}$	-	Heat shock protein 90 spin labelled
HSQC	-	Heteronuclear single quantum coherence
IPTG	-	Isopropyl-β-D-thiogalactopyranoside
ITC	-	Isothermal titration calorimetry
kDa	-	Kilodaltons
LB	-	Luria bertani
MD	-	Middle domain
Mg^{2+}	-	Divalent magnesium ion
Mn^{2+}	-	Divalent manganese ion

MTSSL	-	Methanethiosulfonate spin label
N	-	Stoichiometry
ND	-	N domain
Ni-NTA	-	Nickel-charged nitriloacetic acid
NMR	-	Nuclear magnetic resonance
N-Hsp90	-	N-terminal domain of Hsp90
NTS	-	N-terminal strand
PAGE	-	Polyacrylamide gel electrophoresis
PDB	-	Protein data bank
ppm	-	parts per million
PR	-	Progesterone receptor
SDS-PAGE	-	Sodium dodecyl sulphate-polyacrylamide gel electrophoresis
T101I	-	N-terminal domain mutant of Hsp90. Residue Thr101 mutated to Ile
T221	-	N-terminal domain mutant of Hsp90. Residue Thr22 mutated to Ile
TNF	-	Tumour necrosis factor
TPR	-	Tetratricopeptide repeat
Tris	-	Tris(hydroxymethyl)aminomethane
UV	-	Ultra violet
WT	-	Wild type
ΔC_p	-	Change in heat capacity
ΔG	-	Change in Gibbs free energy
ΔH	-	Change in enthalpy
ΔS	-	Change in entropy

Chapter 1
Introduction

Heat shock proteins (Hsps) represent one of the major sets of regulatory proteins within the cell, and pose as a crucial element for cellular survival. Despite a large body of research on Hsps there is a significant gap in our knowledge on their mechanism of action.

The large family of Hsps share a high degree of homology with one other, with the yeast homologue from *Saccharomyces cerevisiae*, known as Hsp82, sharing up to a 70% similarity with the human homologue. Picard *et al.*[1] demonstrated that human Hsp90 is able to successfully restore yeast viability when the wild type gene for *S.Cerevisiae* is knocked out, and therefore yeast Hsp90 provides an excellent representative for human Hsp90. This thesis adopts the yeast Hsp of 90kDa (Hsp90) to study the thermodynamic effects of nucleotide binding resulting from the conformational changes within the ATP-binding domain, and to study the conformational changes throughout the full length Hsp90 during its ATP cycle.

1.1 The Hsp90 chaperone

The 90 kDa family of heat shock proteins are ubiquitous molecular chaperones representing approximately 1% of total cellular protein in eukaryotes. However during cellular stress, this level rises further. Hsp90 provides one of the major defence systems with respect to heat shock in eukaryotes and is responsible for vital functions within the cell, some of which include cell-cycle regulation, signal transduction and hormone responsiveness.

Different heat shock proteins are responsible for different stages of cellular function; the members of the 70 and 60 kDa heat shock proteins, Hsp70 and GroEL respectively, are required for the early stages of protein folding, whereas Hsp90 appears to be associated with the later stages of protein folding of a large range of 'client' proteins[2]. The clients of Hsp90 include a number of kinases and transcription factors, such as steroid hormone

receptors and proto-oncogenes, and these clients require a specific set of co-chaperones in order to be regulated. It has been found that the co-chaperones of Hsp90 determine its client specificity[3]. The role of these chaperone/co-chaperone complexes in the processing of these client proteins is not well understood, although these complexes have been implicated in inducing conformational changes within the client or allowing post-translational modifications such as phosphorylation or dephosphorylation, i.e. the phosphorylation of Ser13 by Caesin kinase II (CK2) within the co-chaperone Cdc37 has been shown to be essential for the formation of productive Hsp90-Cdc37-client kinase complexes[4].

Hsp90 can be divided into three discrete folded domains. The first is the N-terminal domain (also referred to as N-Hsp90 in this thesis); N-Hsp90 is composed of approximately 216 amino acids with a molecular weight of approximately 24 kDa. This domain is mainly involved in ATP binding and bears two functional regions, that is the N-terminal strand (also referred to as NTS in this thesis) and the ATP lid. The middle domain (also referred to as MD in this thesis) is composed of approximately 287 amino acids (from residues 273-560) with a molecular weight of approximately 33 kDa; this domain has also been shown to be involved directly in the ATP interaction. And finally, the C-terminal domain (also referred to as CD in this thesis), which consists of approximately 148 amino acids (from residues 561-709) and bears a molecular weight of approximately 16 kDa. This domain contains a conserved region involved in the binding of TPR (tetratricopeptide repeat)-containing co-chaperones and client proteins. All domains of Hsp90 have been shown to be involved in interactions with various co-chaperones and client proteins.

The extensive roles exhibited by the Hsp90 molecular chaperone are entirely dependent on its ability to bind and hydrolyse ATP, which occurs within N-Hsp90. However although ATP binding and hydrolysis is concentrated to N-Hsp90, the conformational changes resulting from this association have been observed throughout all domains of the chaperone[5-8], details of which will be discussed later. Hsp90 C-terminal domains are responsible for the constitutive dimerisation of the protein as well as being involved in the association of Hsp90 with various co-chaperone-client proteins that are thought to recognise a conserved MEEDV region within this domain[9,10].

The network of conformational changes occurring after ATP binding and hydrolysis are

responsible for co-chaperone association and successful processing of clients handled by the Hsp90 chaperone. Numerous groups have reported various intermediate conformations that Hsp90 adopts during its ATP cycle[11-13] together with a large number of solved structures of the isolated domains[7,8,14 15] and full-length Hsp90[16-18] bound with various ligands and/or co-chaperone-client complexes. However although these studies have provided us with key information on the various conformations of Hsp90, they correspond to 'snapshots' of the chaperone at various intermediates during its ATP cycle and are associated with limitations of the technique employed such as the static nature of crystallography and cryo-electron microscopy. Therefore in order to understand the extensive dynamic nature of the Hsp90 molecular chaperone, techniques such as isothermal titration calorimetry (ITC)[7,19-21], nuclear magnetic resonance spectroscopy (NMR)[3,5,8,15,22,23], fluorescence studies[6,11,12,24], and mutational analysis[7,9,13,25,26] have all been adopted to probe the diversity of conformational changes within the protein.

A large number of studies investigating the structure and function of Hsp90 have limited themselves to the isolated N-terminal domain of the protein primarily due to the fact that this domain alone encompasses the binding site for ATP. Furthermore, N-Hsp90 has a molecular weight of approximately 24 kDa and therefore is suitable for investigation by techniques that are subject to molecular weight limitations, e.g. NMR spectroscopy. In addition, N-Hsp90 cannot dimerize in the absence of the other domains thus making it tractable to investigate as a monomer. The complexity of associated conformational changes within the chaperone are evident from the studies carried out to date and in order to understand the dynamic nature of Hsp90 and therefore how it processes the various clientele, it is crucial to resolve the intricate details of the Hsp90 machinery.

1.2 Protein clientele of Hsp90

As mentioned earlier, Hsp90 plays a key role in the activity of 'client' proteins that are involved in a large number of regulatory cellular processes. In addition to the requirement of Hsp90 to bind and hydrolyse ATP, the regulation of these client proteins requires Hsp90 to associate with a plethora of co-chaperones. For example the co-chaperone Cdc37 (or the mammalian homologue p50) is required for the activation of specific protein kinase clients of Hsp90 via serine phosphorylation within the Cdc37

molecule[4,27]. Contrary to this, not all clients of Hsp90 require regulation via Cdc37 phosphorylation, and so there continues to be extensive efforts into studying the modes of action adopted by Hsp90-co-chaperone complexes in order to elucidate how the diverse client proteins of Hsp90 are processed and regulated.

The clients of Hsp90 can be divided into three distinct groups. The largest group of clientele are the protein kinases such as PKB/Akt, LKB1, Raf-1, ErbB2, Bcr-Abl, Src-family kinases, and cyclin-dependent kinases[28]. The second group encompasses the transcription factors including nuclear steroid receptors such as glucocorticoid receptors (GR), progesterone receptors (PR) and, estrogen receptors. The third group is that of structurally unrelated proteins. The website 'HSP90 Interactors' provides regular updates of the continually expanding list of the Hsp90 clientele; http://www.picard.ch/downloads/Hsp90interactors.pdf

The diverse clients of Hsp90 have very little in common in terms of their nature of association with the chaperone complexes; for example, the tyrosine kinase receptor $pp60^{v\text{-}Src}$ requires brief association with Hsp90 immediately after it is synthesized, whereas the GR is associated with Hsp90 for a longer period allowing it to remain in an activated state[25]. The multitude of oncogenic protein kinases processed via Hsp90 has engendered Hsp90 as a target for cancer therapeutics[29], as inhibition of Hsp90 would lead to degradation of proteins involved in cancer pathways, or ultimately cell death via apoptosis[30].

1.3 The structural features of Hsp90

The full-length Hsp90 protein exists as a constitutive homodimer with a molecular weight of approximately 166 kDa. Three functional domains constitute this homodimer as mentioned earlier; N-Hsp90, the MD, and the CD. Each of these domains has been found to exhibit distinct roles in the functioning of the Hsp90 chaperone system and interestingly these roles are coupled during the conformational cycle of the protein. A series of conformational changes beginning within N-Hsp90 upon ATP binding take place, the effects of which have been observed throughout all domains of Hsp90. Further rearrangements have also been demonstrated within all domains of Hsp90 upon co-

chaperone association, changes which are independent of the primary binding site of the co-chaperone involved. Ali *et al*.[16] published the first crystal structure of the full-length yeast Hsp90 protein and this structure was in good agreement with the individually determined structures of the various isolated domains of Hsp90.

1.3.1 N Domain

The crystal structure of the N-terminal domain of yeast Hsp90 was found to run from residue 1 to residue 216[7]. In the same year that the yeast N-terminal Hsp90 structure was determined, the human N-terminal Hsp90 structure was also solved[31]; these two studies further confirmed the high degree of similarity between yeast and human Hsp90. Figure 1.1 shows the yeast and human N-Hsp90 structures illustrating the high homology in their tertiary structures. Both structures show an eight-stranded β-sheet, which forms the base of the ligand binding pocket and α-helices flanking either side of this pocket.

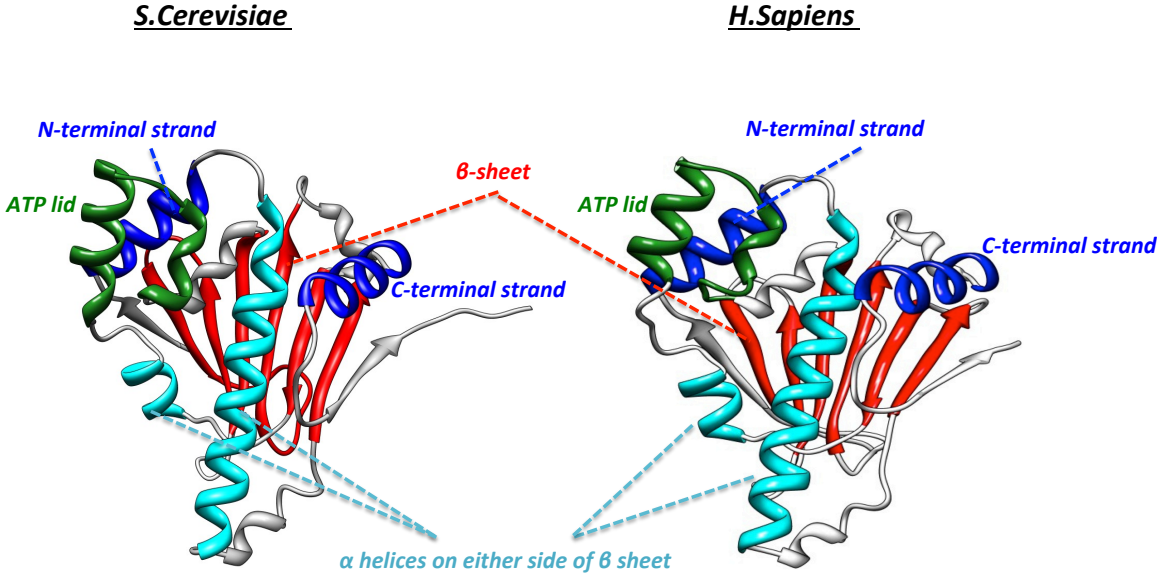

Figure 1.1 Ribbon representations of the *Saccharomyces cerevisiae* (PDB 1AMW; refer to Appendix 1) and *Homo sapiens* (PDB 1YES) N-Hsp90 structure, highlighting the important structural features shared by both species.

Stebbins *et al*.[31] first identified this β-sheet binding pocket to be involved with the antitumor agent geldanamycin (GA), and from this study it was speculated that the binding pocket could also accommodate the client proteins of Hsp90 , concluding that GA served as

an competitive inhibitor of N-Hsp90 client proteins.

The N-terminal region of DNA gyrase, which is an ATP-binding domain from the family of type II topoisomerases , was found to share a similar topology to N-Hsp90[32], and after multiple sequence alignment of the region which comprises the ATP binding properties of DNA gyrase, it was found that this region is also conserved in other Hsp90 sequences[33]. In light of these studies, Prodromou *et al.*[7] solved the complex of yeast N-Hsp90 in association with both ADP (adenosine 5′-diphosphate) and ATP at a resolution of 2.5 and 2.0 Å respectively, which confirmed Hsp90 as an ATP-binding protein. Furthermore, they found that ATP and ADP bind N-Hsp90 in a 1:1 stoichiometry, with binding affinities of approximately 132 μM and 29 μM respectively, and in contrast to the nature of the GA interaction with human N-Hsp90 proposed by Stebbins *et al.*[31], Prodromou *et al*. found that rather GA acts as a mimetic of ADP/ATP binding to yeast N-Hsp90. The bound nucleotide was found to make several contacts with the protein, most of which are solvent-mediated. A Mg^{2+} ion was unambiguously identified in the binding pocket due to an octahedral coordination between a solvent water molecule interacting with the oxygens of the α and β phosphates, the side chain amide oxygen of Asn37, and three other solvent water molecules, and although the Mg^{2+} ion was not visible in the solved crystal structures, calorimetric studies found that N-Hsp90 bears no nucleotide-binding abilities in the absence of Mg^{2+}[7].

1.3.2 The NTS and the ATP lid

In a structural comparison of the N-terminal fragment of the *E.coli* DNA gyrase B-ATP complex and the *S.Cerevisiae* N-Hsp90-nucleotide complex, a high degree of variation was found in one particular region of the above structures, comprising residues 95-119 and 94-124 respectively. It was found that this helical segment was highly disordered in the DNA gyrase B structures appearing to fold over the nucleotide-binding site and making contacts with the adenine base and phosphates of the ATP molecule[34]. The structural analysis of the same region in N-Hsp90 showed this segment to be packed against residues 10-27[7], a region defined as the N-terminal strand (or NTS) in both structures, an observation also demonstrated for the human N-Hsp90 structure[31]. Figure 1.1 presents the position of these regions for both human and yeast N-Hsp90 structures. Based

on the apparent dynamics of the segment closing over the ATP binding pocket (in the case of DNA gyrase B), it was given the name of the ATP lid.

In DNA gyrase B, the NTS appears to be involved in a dimerisation interaction with a second DNA gyrase B molecule, whereas in N-Hsp90, this strand forms the amino-terminal end of the β-sheet structure. The crystal structure of the yeast N-Hsp90/nucleotide complex shows the ATP lid to be stabilised in the 'open' conformation, as would be expected from the strong hydrophobic contacts seen between the ATP lid residues and the NTS residues, portraying the distinct difference in the behaviour of this lid in comparison to DNA gyrase B. Nevertheless, there are a large number of similarities in structural details of the contacts made between both N-Hsp90 and DNA gyrase B with ATP, further illustrating the structural conservation between type II topoisomerases and Hsp90s[33], and as a result of these similarities Hsp90 was soon included in a family of proteins called Gyrase, Hsp90, Histidine Kinase, MutL (GHKL).

Through mutational studies Prodromou *et al*.[13] demonstrated the existence of a similar mechanism in Hsp90 to that seen in DNA gyrase B in terms of ATP lid closure resulting in dimer formation, further illustrating the similarities in ATP binding to DNA gyrase B. However the exact role of this lid closure in potential client protein binding or merely enhancing the stability of the dimerised N domain state remained unclear. The first crystal structure of full-length yeast Hsp90 in complex with an ATP analogue, AMP-PNP, was solved[16] providing evidence for the necessary closure of the ATP lid, as was demonstrated via an A107N mutation that forced the lid closed promoting dimerisation of the N domains of the Hsp90 dimer. Furthermore, a strand-swap event of the NTS with the same region within the partner protomer of the Hsp90 dimer was also evident in this structure. Figure 1.2 illustrates the two conformational changes upon AMP-PNP binding. Ali *et al*.[16] demonstrated that the closure of the ATP lid exposes a hydrophobic surface which leads to N domain association upon burial of the same region within the partner N domain[13], and this was demonstrated by a mutation (A107N) which stabilised the lid in a closed conformation thereby promoting N domain dimerisation. Furthermore, the structure provided evidence of nucleotide-induced conformational changes affecting other domains of Hsp90 connected to the ATP lid region[5], which could be essential to successful ATP hydrolysis, demonstrating the extent of flexibility of the Hsp90 chaperone.

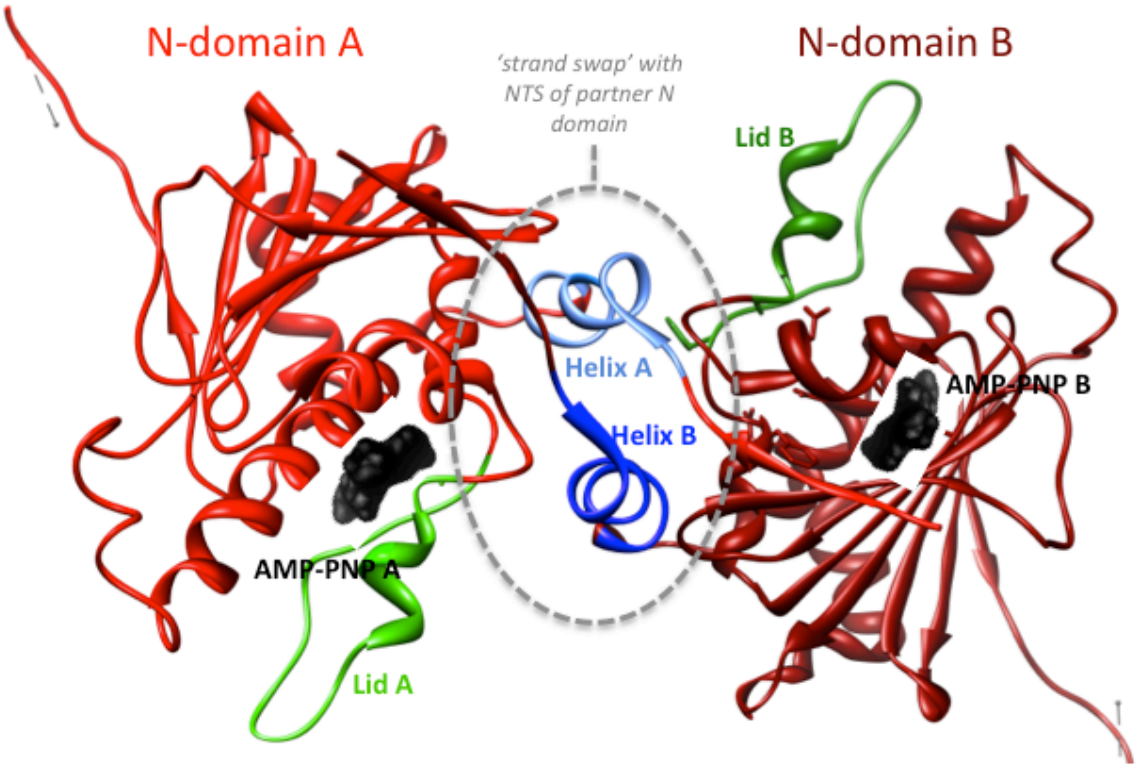

Figure 1.2 Ribbon representation of the N-terminal domains of full-length Hsp90 (PDB 2CG9[16]; refer to Appendix 1), highlighting AMP-PNP (black), the ATP lid (green) in the closed form, NTS formed by helix A and B (blue) showing a 'strand swap' with partner N domains, and the ATP lid closed over the bound AMP-PNP. N domain B uses same colour scheme as N domain A but in a darker shade.

1.3.3 Nucleotide-N-Hsp90 contacts

The bound nucleotide makes a large number of contacts with N-Hsp90, most of which are solvent-mediated. The first crystal structure[7] of the isolated N-Hsp90 in complex with both ADP and ATP showed the N6 of the adenine moiety and the O2 of the ribose sugar each making a direct hydrogen bond between Asp79 and Asn92 of N-Hsp90, with all other possible hydrogen-bonding contacts mediated indirectly to the protein via water molecules. The adenine base makes further contacts with the protein by hydrogen bonds through water molecules to Leu34, Asp79, Thr171, and Gly83. The N3 of the adenine, the O2 of the ribose, and the N7 of the adenine moiety interact with a water molecule bound to Asn92 and Asn37 respectively. A van der Waals contact between a hydrophobic region of the adenine to the side chain of Met84 also exists.

In terms of the phosphodiester of the nucleotide, the α phosphate hydrogen bonds to Asn37 and Phe124, the β phosphate hydrogen bonds via the putative Mg^{2+} ion to Lys98 together with several solvent water molecules in the binding pocket, whereby one of these solvent molecules may interact with the oxygens of the α and β phosphates, Asn37, and three other water molecules in an octahedral coordination potentially identified as a Mg^{2+} ion. It has been demonstrated calorimetrically that N-Hsp90 bears no nucleotide-binding capability in the absence of Mg^{2+}, and crystals of N-Hsp90 grown in the presence of the divalent ion failed to show bound ions eliminating the possibility of the protein having an inherent ion-binding site, and as a result suggested that N-Hsp90 binds a nucleotide-ion complex[7].

The isolated N-Hsp90 crystal structure in complex with the adenine-containing nucleotides failed to show interactions mediated vi the terminal γ phosphate, but a clear interaction between this phosphate and an Arg380 residue within the M domain of Hsp90 was later observed in the crystal structure of the full-length Hsp90 in complex with AMP-PNP and the co-chaperone Sba1/p23[16]. Further contacts between the γ phosphate with Gln119, Gly121, Val122, and Gly123 via hydrogen bonds were also visible, together with slight differences in interactions between the β phosphate and the protein in comparison to the isolated N-Hsp90-nucleotide complex.

1.3.4 Hsp90 inhibitors

Understanding the detail of Hsp90 inhibitor interactions is important since it can provide insight into the key recognition features of the ATP binding site. Hsp90 research to date has so far demonstrated the existence of two naturally occurring inhibitors, whereby inhibition refers to diminishing the ability of Hsp90 to bind and therefore hydrolyse ATP. The first such inhibitor, geldanamycin (GA) and analogues thereof (17-AAG and 17-DMAG), which was found as a naturally occurring ansamycin antitumor antibiotic, was initially found to bind in the deep pocket (mentioned above) of human N-Hsp90, where it was presumed to mimic the interaction of a client substrate to Hsp90.

Radicicol is another antitumor antibiotic, which was shown to be involved in the accelerated turnover and degradation of the kinase Raf-1 in a similar fashion to the

ansamycin inhibitor GA. It was only later that both GA and radicicol were found to be involved in the inhibition of the folding and activation of target proteins by the Hsp90 chaperone through diminishing the ability of Hsp90 to bind and hydrolyse ATP. Roe *et al*.[21] demonstrated the ability of radicicol to potently inhibit the specific ATPase activity of Hsp90 and reported the crystal structure of the complex of yeast N-Hsp90 to radicicol.

The crystal structure of GA bound to yeast N-Hsp90 shares a high homology with that of the human N-Hsp90[7,31]. Both GA and radicicol are orientated in the binding pocket in different conformations as illustrated in Figure 1.3; GA binds with its macrocyclic ansamycin ring containing the conjugated bonds system directed toward the bottom of the binding pocket and the benzoquinone ring toward the top of the pocket, whereby the GA structure is folded over so that the two ends of the GA molecule are approximately parallel. Radicicol on the other hand binds to N-Hsp90 in a manner where its aromatic ring is directed toward the bottom of the binding pocket and the macrocycle containing the conjugated bond system is orientated toward the top of the pocket forming a folded conformation that is perpendicular rather than parallel, like the GA structure [21].

Although both GA and radicicol differ in their chemical structures (shown in Figure 1.4), the similarity in which they bind to N-Hsp90, both in the folded conformation shown in Figure 1.3 and in terms of the contacts made between the protein and ligand, surprisingly resembled that of the ADP-bound N-Hsp90 complex[7]. ADP binds to N-Hsp90 in an orientation which enables the ribose and α phosphate to come into close contact with the adenine moiety, also resembling an apparent folded conformation like that of GA and radicicol. Upon investigation of the binding site contacts of the three ligands stated above, one specific interaction appears to be a shared feature: a direct hydrogen bond via the N6 of the adenine to the carboxyl group of Asp79, a residue which also makes an indirect hydrogen bond via a tightly bound water molecule to the N1 of the adenine, rendering the Asp79 residue critical for complex formation. Interestingly, the position of the bound water molecule changes by less than 0.5 Å between the three ligand-bound complexes[21]. Figure 1.3 demonstrates the high degree of similarity in the interactions of GA and radicicol with N-Hsp90.

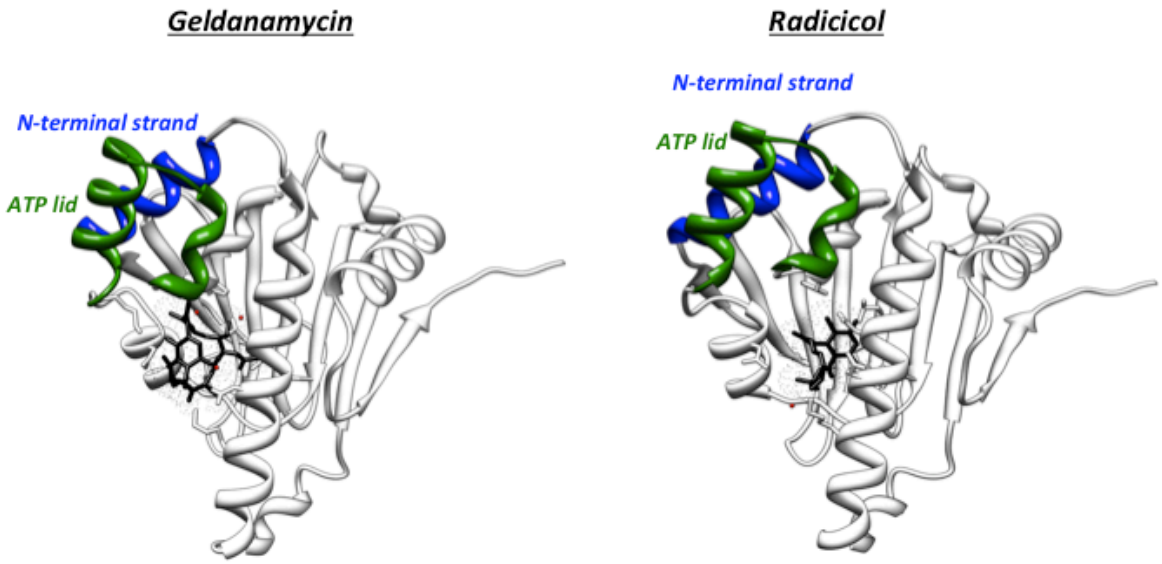

Figure 1.3 Structure of the N-terminal domains of Hsp90 in complex with geldanamycin (PDB 1A4H; refer to Appendix 1) and radicicol (PDB 1BGQ; refer to Appendix 1)

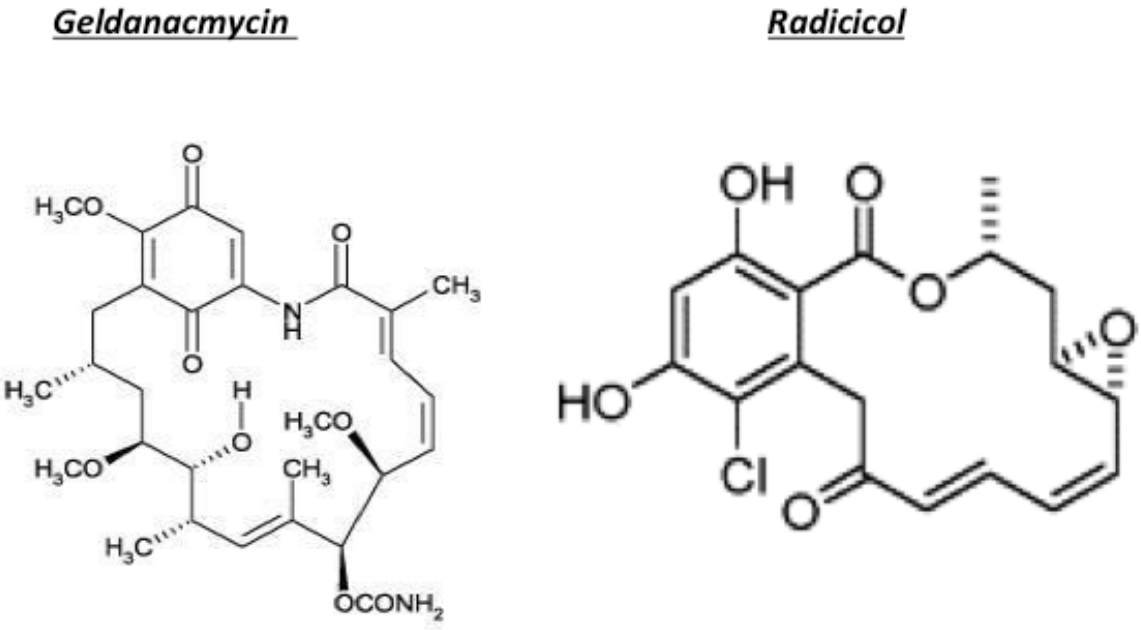

Figure 1.4 Chemical structures of geldanamycin and radicicol

A study carried out Dehner *et al.*[23] using NMR spectroscopy revealed a large number of chemical shifts within N-Hps90 complexes of the ADP, AMP-PNP, GA, and radicicol bound conformations. They used the ligand free or 'apo' N-Hsp90 backbone resonance

assignment[35] to determine the regions that undergo the greater number of chemical shift changes as a means of establishing possible residues involved directly in complexation formation. Three distinct regions revealed major chemical shift changes in the N-Hsp90-AMP-PNP complex; these include the ATP lid region (residues 90-120), which represented the most significant change upon nucleotide association, the NTS (residues 10-22), and the back of the ligand binding pocket (residues 150-210).

ADP association shows a similar profile to the AMP-PNP data, however particular residues around the ATP lid and NTS region differ in their chemical shift pattern from the AMP-PNP spectra. Radicicol and GA show rather different NMR profiles to both ADP and AMP-PNP in that the overall binding pocket is less affected with radicicol binding, particularly the ATP lid and NTS. Moreover, only a certain region of the β sheet structure that makes the back of the binding pocket is affected by radicicol binding. GA on the other hand showed the most significant chemical shift changes upon complex formation with N-Hsp90 in comparison to the ADP, AMP-PNP, and radicicol spectra. The ATP lid and NTS are largely affected by GA association, where shift patterns for Ile82 and Asn92 could not be followed, a situation not observed with nucleotide association. Like radicicol association, the back of the binding pocket encompassing the β sheet structure is affected in a similar manner with GA.

In comparison to the binding affinity of N-Hsp90 to ADP, which was calorimetrically determined to be approximately 29 μM[7] in a 1:1 stoichiometry, Roe *et al*.[21] established the binding affinities of GA and radicicol to be approximately 0.7 μM and 2.7 nM respectively, also in a 1:1 fashion. The binding affinities established in this study demonstrate the potency of the GA and radicicol inhibitors in diminishing the ATP binding capability of Hsp90.

1.3.5 Thermodynamics of nucleotide and ligand binding

Although the available structural information for nucleotide and ligand binding to Hsp90 provides valuable insight into the local and global changes taking place within Hsp90, a deeper understanding is required in order to extract the finer details of these interactions allowing us to establish how binding to the same site on Hsp90 reveals distinctly dramatic changes.

Determining the thermodynamics of an interaction could potentially lead to details on the nature of the interaction and hence one can extract structural information from the relationship between the thermodynamic parameters obtained from such an investigation, such as enthalpy (ΔH), entropy (ΔS), and free energy changes (ΔG).

Roe *et al*.[21] first determined the thermodynamic profiles of GA and radicicol binding, where they demonstrated that both inhibitors exert different modes of binding as is also evident through the differences in the regions of N-Hsp90 affected by both molecules. Both bind with favourable enthalpies where GA shows a slightly more favourable enthalpy (of -44.9 kJ mol^{-1}) than radicicol (of -22.8 kJ mol^{-1}). In contrast however, radicicol binds with a significantly large favourable entropy (of +87.5 kJ mol^{-1}) where as GA binds with an entropic penalty (of-33.9 kJ mol^{-1}). Based on the information provided by this study, a favourable entropy would suggest that radicicol is able to displace much of the solvent molecules at the binding interface between protein and ligand without direct replacement of these molecules with functional groups. GA however, displaces the solvent molecules by substitution with functional groups. The large discrepancy in the entropic cost of each interaction and the similar enthalpic contributions could explain the difference in potency of GA and radicicol interactions, in that the strong affinity of radicicol to Hsp90 could derive from entropy-related effects.

A study by Nilapwar.[19] later determined the thermodynamics of the interaction of N-Hsp90 with ADP and AMP-PNP together with that for GA and its analogues 17-AAG and 17-DMAG. The relative binding affinities of all interactions were also determined. AMP-PNP bound to N-Hsp90 with a K_d of approximately 130 μM and ADP bound with an approximate 5-fold stronger affinity of 22 μM; GA was found to bind to N-Hsp90 with an affinity of approximately 1 μM. The nucleotide interactions of this study illustrated that both AMP-PNP and ADP interactions are enthalpically driven, where ADP shows a more favourable change in observed enthalpy (of -75.2 kJ mol^{-1}, and AMP-PNP of -35.9 kJ mol^{-1}, at 15°C) and AMP-PNP shows a more entropically favourable profile (of -13.1 kJ mol^{-1}, ADP of -47.9 kJ mol^{-1}, at 15°C). In this instance, it is also evident that both nucleotides have different modes of binding, but the larger entropic penalty of the ADP interaction cannot explain the stronger affinity exhibited by this molecule in the same way as the radicicol or GA interaction. GA and its analogues also bound to N-Hsp90 in an

enthalpically-driven mechanism and in this instance, these compounds showed a more favourable change in entropy in comparison to the nucleotide compounds, a feature that explains the approximate 20-40 fold stronger affinity of these inhibitors compared to both ADP and AMP-PNP.

The change in heat capacity (ΔC_p) of a system can provide further information on the nature of protein-ligand or protein-protein interactions. This function is a result of changes in enthalpy with temperature[36]. Changes in this thermodynamic parameter can reflect widespread changes derived from local events as a result of bond alterations, release or sequestering of solvent molecules at the binding interface, burial of surface area upon complex formation, conformational changes within protein structure, and additional smaller effects[19]. Interestingly, both AMP-PNP and ADP showed completely opposite changes in observed heat capacities further confirming their rather distinct modes of binding to N-Hsp90. ADP heat capacity changes were in agreement with a situation which results in burial of surface area upon complex formation. AMP-PNP however, showed an anomalous positive change in observed heat capacity. Nilapwar *et al*.[19] by a method of elimination, came to the conclusion that the positive heat capacity exhibited by the AMP-PNP interaction could be partially attributed to the closure of the ATP-lid, which results in the exposure of an hydrophobic patch to the bulk solvent. However, although the ATP lid region has been shown to move upon ATP association in various nucleotide and ligand bound states, it is still not clearly understood to what extent this lid moves in the ATP-bound Hsp90 complex since there is no available structure so far illustrating the effect of the lid on ATP binding alone. Therefore in order to gain a clearer understanding of the source of this anomalous positive heat capacity, other possible contributing factors must be considered.

1.3.6 The M Domain

The crystal structure of the Hsp90 middle domain (M domain or MD) was solved by x-ray crystallography by Meyer *et al*.[5]. The crystal structure of the 33 kDa middle domain, which runs from residues 273-560 was obtained with a with a resolution of 2.5 Å. This domain has considerable similarity in architecture with other members of the GHKL family members, i.e. DNA gyrase B and MutL. Figure 1.4 shows the structure of the M domain,

which can be divided into three regions. The first region encompasses an α-β-α sandwich, which is composed of a three-turn α helix and random loops, a five strand β-sheet, and a six-turn α helix. This region then leads to a small segment formed by three short α helices, and this is followed by another segment of an α-β-α sandwich. The crystallographic data for the structure beyond residue 525 showed disorder and therefore could not be incorporated into the final published structure. The region between residues 378-384 also showed some degree of disorder. Interestingly, this is the region in which a catalytic residue (Arg380) lies, which has been speculated to interact with the γ-phosphate of the bound ATP within the N domain of Hsp90[7,13,37].

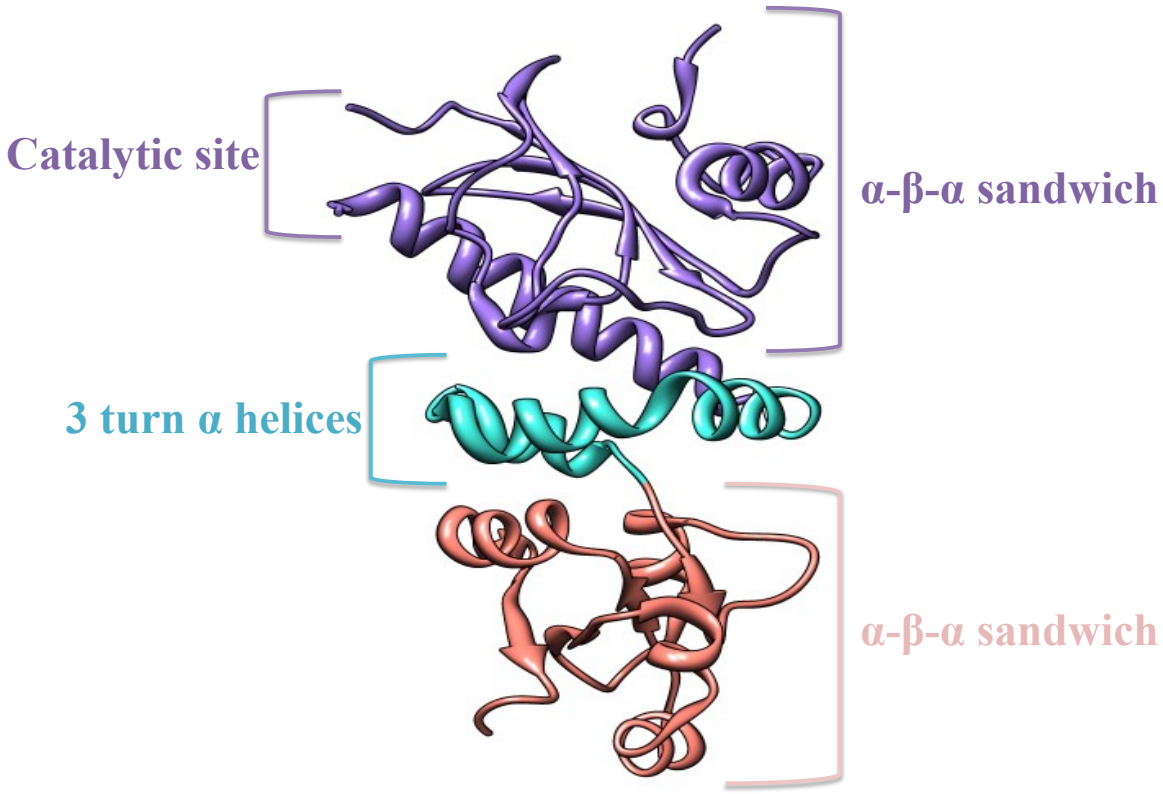

Figure 1.5 Ribbon representation of the M domain of yeast Hsp90 (PDB 1HK7[5]; refer to Appendix 1), highlighting residues 273-409 (purple), 411-443 (cyan), 444-525 (pink), and the region in which the catalytic Arg380 residue sits.

MutL and DNA gyrase B have also been shown to contain a similar fold of their M domains to the structure of the yeast Hsp90 M domain shown above. However the structures of MutL and DNA gyrase B differ in the polypeptide connecting strands which are short irregular segments in Hsp90 but structured helices in the other protein structures.

Furthermore is the structure beyond the three-turn α helix, which in the structure of DNA gyrase B continues to a seven-turn α helix. This helix is also present in Hsp90 forming the first helix of the second α-β-α sandwich, although it is much shorter by comparison.

Unlike DNA gyrase B and MutL whose N and M domains are connected with a continuing secondary structure, Hsp90 N and M domains are connected by a long unstructured charged linker composed of approximately 50 residues, and was found to be vital for Hsp90 function *in vivo*[38] and *in vitro*[39] demonstrating importance in the overall flexibility of the protein during its conformational cycle. Although the crystal structure of full length yeast Hsp90 has been solved in complex with AMP-PNP and the co-chaperone p23[16], the protein construct used to obtain the crystals was one in which the charged linker region had to be shortened to 8 residues with a sequence of LQHMASBD. Therefore although a minimal charged linker was found necessary to maintain yeast viability *in vivo*, the ultimate function of this charged linker region remains elusive[38]. A study by Hainzl *et al.*[39] found that this charged linker region is crucial for the regulation of Hsp90 function in the processing of client proteins by co-chaperones by enabling flexibility of Hsp90 during its conformational cycle. Furthermore, it was found that full deletion of this charged linker region retains a folded structure of the chaperone and function in terms of ATP binding and hydrolysis, however the rate of ATP hydrolysis is reduced.

Structural alignments of the M domains of DNA gyrase B and MutL structures with the crystallized yeast M domain revealed a corresponding catalytic loop found within the first α-β-α sandwich known to 'sense' the presence of the γ phosphate of the bound ATP molecule in the case of DNA gyrase B and MutL[5]. For the Hsp90 M domain, this catalytic loop corresponds to residues 375-388, and mutational studies found the critical requirement of Arg380 and Gln384 in both maintaining cell viability and ATPase function of Hsp90 indicating direct involvement in the catalysis of ATP hydrolysis. The involvement of the Arg380 residue was later revealed in the full-length crystal structure of yeast Hsp90 in complex with AMP-PNP and p23, where the side chain was shown to point directly into the ATP binding pocket[16]. Further mutational studies involving a hydrophobic patch adjacent to this catalytic loop, which centres around Phe349 and Val348, revealed its involvement in inter-domain contact of N and M domains proving it to be essential for efficient ATPase activity. The catalytic loop containing residues 375-388 was also found to include a binding

site for the co-chaperone Aha1; mutation of the Glu381 residue proved to almost completely abolish stimulation of Hsp90 by Aha1 but still maintained Hsp90 ATPase activity, whereas the Phe349 mutations showed hyperresponsiveness of Aha1 to Hsp90[5].

The M domain of Hsp90 contains further interesting features including a hydrophobic patch situated in the inner segments of the M domain in context of the Hsp90 dimer; this patch forms part of an amphipathic loop that is made up of a hydrophobic side and a positively charged side. Mutations to this hydrophobic patch were studied in order to establish the potential role of this feature in client protein association by Hsp90, and it was found that the mutation of Trp300 leads to severe retardation of v-Src activation by Hps90, without affecting ATPase activity[5]. Further studies revealed the importance of this hydrophobic patch in Hsp90-mediated activation of other clients, such as PKB/Akt and glucocorticoid receptors[25,40].

1.3.7 C Domain

The carboxyl-terminal domain (C domain or CD) of Hps90 serves the main function of constitutive dimerisation, and therefore provides the amino-terminal domains with the correct geometry in order for them to form transient dimers upon ATP binding. As mentioned earlier, deletion of the C domain of Hsp90 leads to diminished ATP hydrolysis and impairs yeast viability[9,13,38]. Furthermore, a conserved region within the C domain has been implicated in interactions with co-chaperones and clients of Hsp90. The first structural representation of the Hsp90 C domain was provided by Harris *et al*.[22] who obtain a crystal of the C domain of the *E.coli* Hsp90 homologue HtpG with a resolution of 2.6 Å (Figure 1.6a).

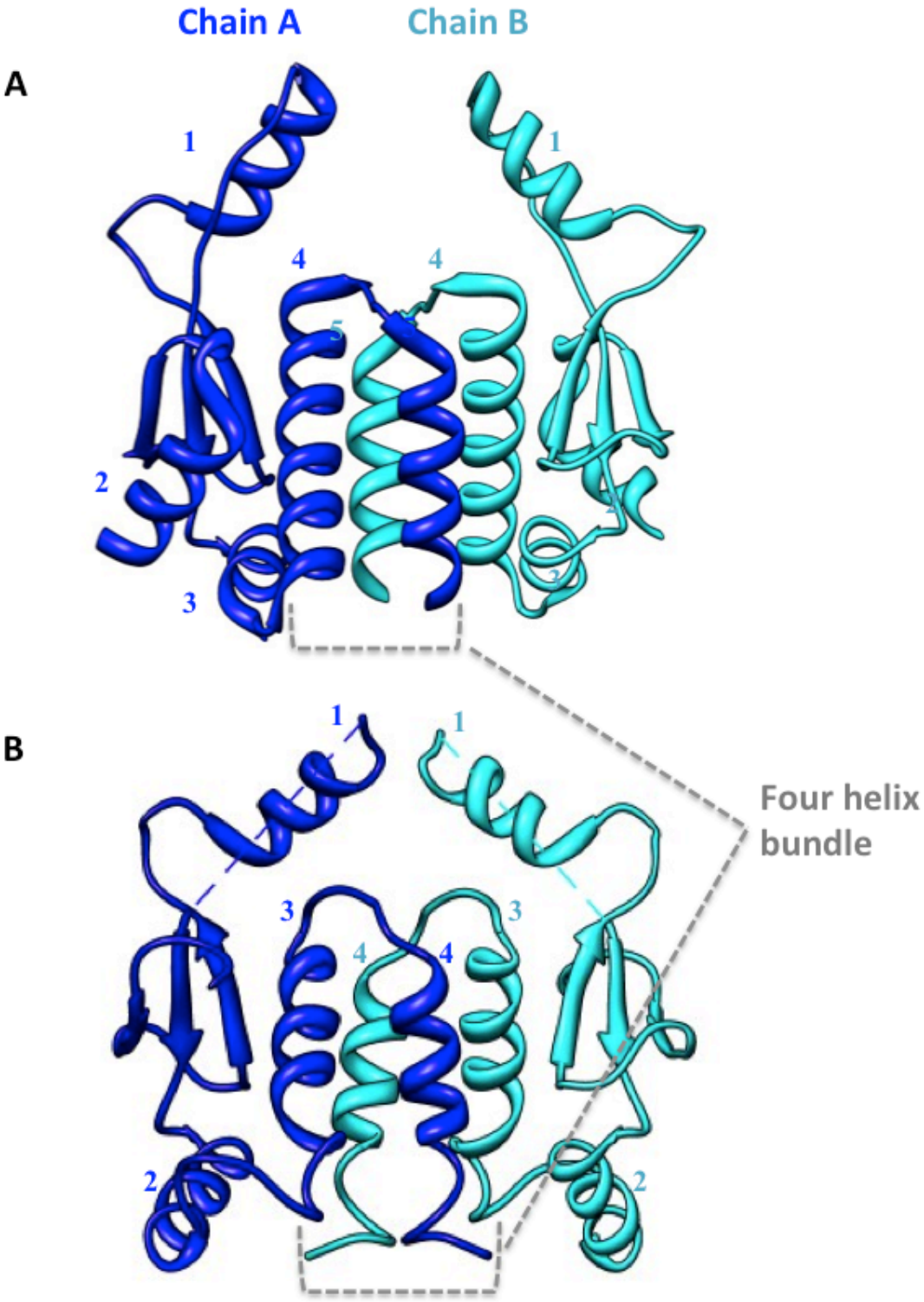

Figure 1.6 Ribbon representation of the dimeric Hsp90 C domain with chain A (blue) and chain B (cyan) of **A,** *E.Coli* HtpG (PDB 1SF8[22]; refer to Appendix 1) and **B,** *S.Cerevisiae* Hsp90 (2CG9[16]; refer to Appendix 1) highlighting the four helix bundle that incorporates the dimerisation interface.

Shortly after the determination of the structure of HtpG, the crystal structure of the full length yeast Hsp90 was solved[16] which was in good agreement with the structure of HtpG (Figure 1.5b). The C domain, which runs from residues 561-709, begins with a short α helix (α1 in both HtpG and Hsp90). This helix projects toward the N terminal end of the structure and is involved in a dimeric interaction with the partner protomer in yeast Hsp90, in contrast, this projecting helix is in a significantly different orientation in the HtpG structure. Helix 1 is followed by a small 3-stranded antiparallel β sheet. Within this β sheet is another short helix (only present in HtpG numbered α2). The β sheet segment is then followed by three (for HtpG; α3-α5) or two (for Hsp90; α3-α4) α helices, where the last two helices form the bulk of the dimerisation interface with the equivalent helices in the partner protomer as part of a four helix bundle. The dimerisation interface between the partner C domains buries a large surface area and exhibits a binding affinity of 24 nM for HtpG and 60 nM for yeast Hsp90[15]. Mass spectrometry H/D exchange studies revealed significant changes in the C domains upon radicicol binding to N-Hsp90. A single highly exposed amide in the ligand free HtpG protein became highly inaccessible to solvent upon inhibitor binding. Furthermore, the central strand of this β sheet and the flanking loop regions that form part of the interface with the M domain in HtpG showed significant changes upon radicicol binding, which suggested a tightening of the interaction between the two domains[41]. The bacterial Hsp90 naturally lacks the conserved MEEVD motif within the C domain, which for yeast Hsp90 has been implicated in the binding of co-chaperones, and this region in the yeast homologue is disordered, therefore it is still somewhat ambiguous how the C domain of Hsp90 is involved in the co-chaperone regulation of Hsp90 function.

The regulation of Hsp90 function by post-translational modifications such as phosphorylation, acetylation, and S-nitrosylation has long been studied, and revealed interesting features of the Hsp90 chaperone in client protein activation. S-nitrosylation, which is the modification of a cysteine residue by nitric oxide (NO), was found to affect ATPase activity of human Hsp90[42]. The cysteine residue involved is highly conserved in most eukaryotic Hsp90 and in some bacterial isoforms, however in the yeast Hsp90, this cysteine residue is replaced (Ala577 in yeast Hsp90). In yeast Hsp90, residue 577 is located on the 3-stranded β sheet within the M domain (mentioned earlier) and has been involved in the conformational changes associated with ligand binding to N-Hsp90. Mutational studies

of Ala577 revealed some variants resulting in enhanced ATPase activity and some resulting in a reduced ATPase activity of the Hsp90 dimer. Furthermore, the S-nitrosylation of the Ala577Cys mutant significantly reduced the ATPase activity by approximately 50%. The stimulation of Aha1 by Hsp90 was also investigated with the S-nitrosylated Ala577Cys mutant, which appeared to be significantly impaired, and this effect was specific to Aha1 since other co-chaperones tested such as Crp6, p23/Sba1, and Hop/Sti1 exhibited no difference in the regulation of Hsp90 ATPase activity. This study clearly demonstrated the regulatory importance of the Ala577 residue, however circular dichroism (CD) and NMR spectroscopy showed no evidence for possible structural changes induced by the modification of the Ala577 residue. FRET analysis revealed that mutations of the Ala577 residue affected dimer formation in an ATP-affinity dependent manner, and mutations which led to stronger N domain dimer formation (A577I) led to stronger client protein activation by Hsp90.

A study by Ratzke *et al*.[24] using single-molecule FRET (sm-FRET) later revealed that the assumed homodimeric nature of the Hsp90 via the C domain is indeed not true. The study demonstrated the fast opening and closing of the previously found high affinity dimerised C domain, in a way that is independent of N terminal domain dimerisation, such that the C domains are 'open' when the N domains are 'closed' and vice versa. The distance between the two C domains of the Hsp90 dimer in the open and closed C domain states were shown to be 6.4 nm and 4.3 nm respectively, the latter distance of which is in good agreement with the crystal structure of the full-length yeast Hsp90[16]. The demonstration of C domain dynamics proposes a new picture of Hsp90 dynamics as opposed to the previously assumed structure of a C domain dimerised Hsp90, and proposes a new view of Hsp90-regulated client activation, a feature which might be exploited for the development of novel therapeutics.

1.4 The ATP cycle of Hsp90

Extensive investigations have been directed at the various conformations of the Hsp90 molecular chaperone during its ATPase cycle, and whilst the solved crystal structures of the various isoforms of both the isolated domains of Hsp90 and the full-length yeast Hsp90 provide valuable insight into certain states of the ligand-free and ligand bound

Hsp90 molecule, these structures demonstrate 'static' pictures of the Hsp90 chaperone in one of its many conformational states. In order to understand the various states of this molecular machine, it is crucial to determine as many of the conformational states that Hsp90 adopts upon ATP binding and hydrolysis. Only then can we gain a clearer view of how this protein aids in the regulation of its clientele. A number of methods have been utilised to visualise the Hsp90 ATP cycle, these include cryo-electron microscopy and FRET studies.

1.4.1 Structural detail of ATP cycle determined by cryo-EM

Shaiu *et al*.[43] demonstrated a chaperone cycle for Hsp90 based on the structural depiction of the nucleotide-free, AMP-PNP, and ADP bound states of the full-length *E.Coli* HtpG molecule. In the nucleotide-free conformation, HtpG adopts an 'open' conformation whereby all three domains of each protomer present hydrophobic elements to the large central cleft formed by the dimer. This structure showed various angles in the electron micrographs suggesting that this conformation is rather flexible and probably poses the state that is most likely to interact with client proteins due to the exposure of a large hydrophobic area; this is especially plausible for the *E.Coli* HtpG molecule, which has been shown to lack co-chaperone association. The extent to which the nucleotide-free HtpG opens is largely owed to the rigidity of the M-C domain contacts. AMP-PNP binding leads to a conformation of HtpG that is in good agreement with the structure of the full-length yeast Hsp90 in complex with AMP-PNP and p23. ADP binding (Figure 1.7) induced a novel compact globular conformation, with a narrowing of the central cleft bringing together the hydrophobic segments exposed in the 'open' conformation and thereby promoting the release of bound clients. The cryo-EM structures displayed two regions that exhibited significant differences to previously demonstrated structures. One is the region occupying the helices corresponding to the NTS and ATP lid of the N domain of Hsp90, whereby the ATP lid is either shown to be ordered or disordered in the open and closed states respectively. The second region is α2 (Figure 1.5a) in the C domain. This helix is in an exposed amphipathic loop that is shown to be ordered in the isolated C domain structure[22], but is disordered in the full length structure obtained by Shaiu *et al*.[43].

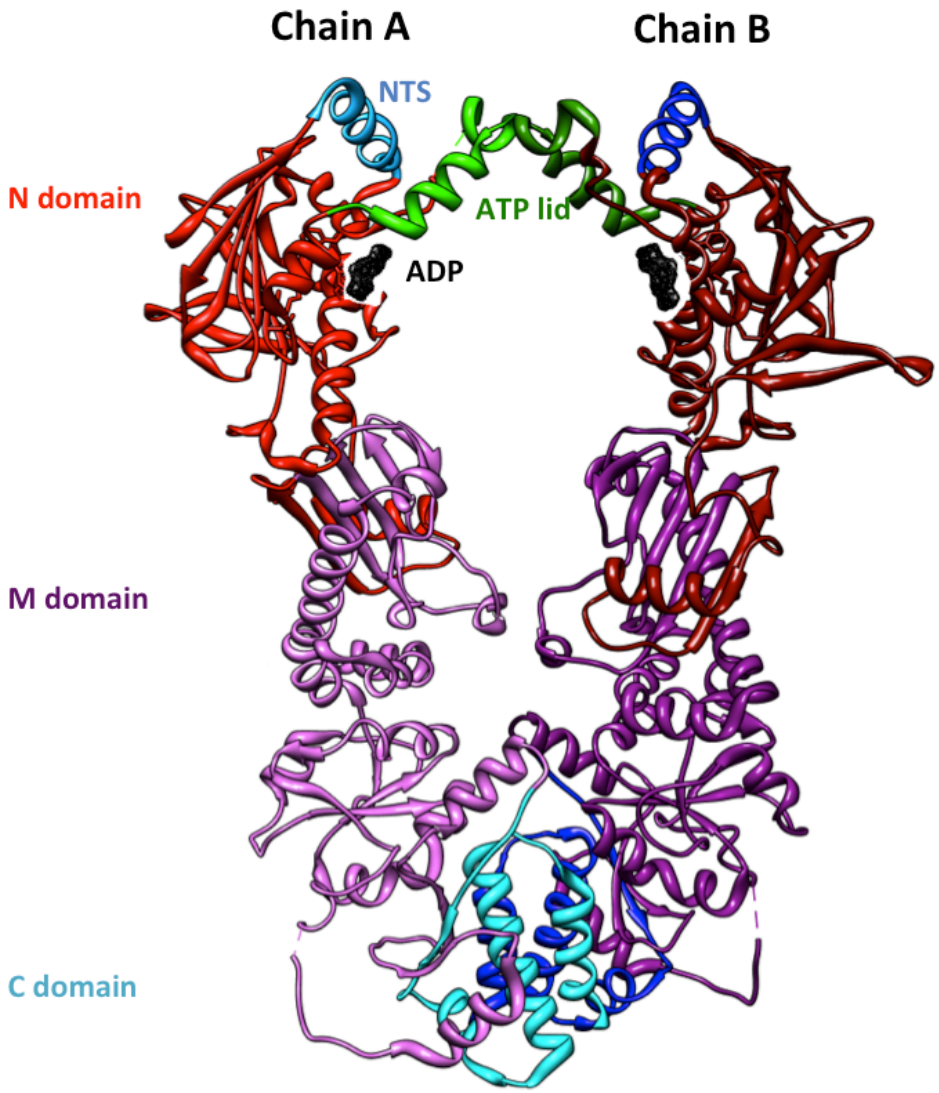

Figure 1.7 Structure of HtpG in the ADP-bound conformation (PDB 2IOP; refer to Appendix 1) conformations.

The model for the *E.Coli* Hsp90 chaperone cycle by cryo-EM (as illustrated in Figure 1.8) begins with the nucleotide-free conformation that presents a structure in which the Hsp90 dimer is in the 'open' state resulting in exposure of a large hydrophobic surface from each protomer of the dimer directed towards the central cleft; this conformation provides the most probable conformation for promoting client protein association due to its hydrophobic characteristic. The structure of the 'open' conformation show that the nucleotide binding pocket is occupied by parts of residues Phe123 and Gln122 and probably drive lid rearrangement to the more polar conformation observed for the isolated N domain, which demonstrates a 'lid open' Hsp90. This 'lid open' conformation would not fit the current

model of the N and M domain contacts, which involves the interaction of a closed lid with a catalytic residue within the M domain. And thus ATP binding induces either a disordering of the lid or a reorientation of the N and M domains. Alternatively, client protein binding could disrupt the interactions observed in the 'open' dimer leading to an N-M domain conformation that favours nucleotide binding. Lid rearrangement would decrease the overall surface hydrophobicity, but client protein association could potentially continue as a result of the continued exposure of the lid and the amphipathic helix of the C domain (mentioned earlier). As discussed above, it was found that a catalytic arginine residue (Arg336 in HtpG and Arg380 in yeast Hsp90) interacts with the bound nucleotide via the closure of the ATP lid over the nucleotide-binding pocket, promoting ATP hydrolysis. The closure of the ATP lid exposes another hydrophobic surface at the back of the lid, which is now involved in the interaction with the partner N domain resulting in N domain dimerisation. Shaiu *et al*.[43] suggested that N domain dimerisation could potentially remodel bound clients and therefore reduce the affinity of the Hsp90-client interaction. As eukaryotic Hsp90 interacts with co-chaperones, this reduced intrinsic affinity of the client protein interaction caused by N domain dimerisation could be increased by the association of co-chaperones with Hsp90.

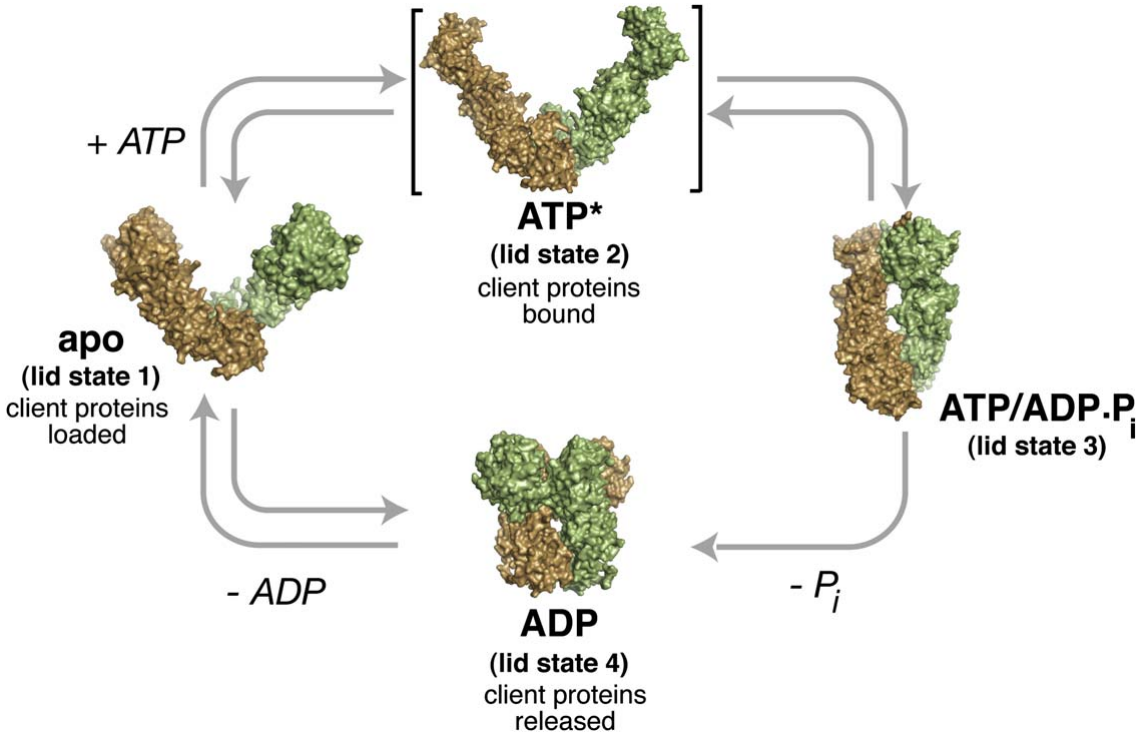

Figure 1.8 ATP cycle of HtpG by cryo-EM

Once hydrolysis of the ATP takes place, this would result in the reversal of the interaction between the bound nucleotide and the catalytic arginine residue leading to the compact ADP-bound conformation of the Hsp90 dimer. Cryo-EM studies found that the lid in this conformation induces a very compact conformation facilitating the complete release of client proteins. Ultimately, nucleotide release would revert the Hsp90 dimer back to the 'open' conformation exhibiting the large hydrophobic central cleft, allowing for another chaperone cycle to take place.

1.4.2 Structural detail of ATP cycle determined by FRET

A study by Hessling *et al.*[11] used FRET to determine the yeast Hsp90 chaperone cycle by attaching donor and acceptor fluorophores to engineered cysteine residues at positions Asp61 (N domain) and Gln385 (M domain). These sites were chosen due to their surface-exposed nature and the low probability of these sites affecting Hsp90 function. A double mutant at positions Asp61 and Gln333 was also created to complement the single mutant data, which was also able to exhibit the functionality of yeast Hsp90 reconstituted into a knockout strain. The successful observation of differentially labelled heterodimers was

determined by changes in the FRET efficiencies of the donor and acceptor signals. The addition of ATPγS (adenosine 5'-O-(3-thio)triphosphate; a slow-hydrolysed ATP analogue) led to the observation of a k_{cat} value that was in good agreement with the known value for Hsp90 ATPase activity, suggesting that these changes represent the rate-limiting step of the Hsp90 ATP cycle. The time-dependent FRET efficiencies observed with ATPγS yielded complex reaction kinetics, which could not be fit to a single-step reaction, and due to this it was suggested that nucleotide binding to Hsp90 induced intermediate conformations that became dominant in the minute time scale following ATPγS addition; the data fit a 5-state reaction cycle. The doubly-labelled mutant revealed the necessity of inter-N domain dimerisation in order for rearrangements between intra N and M domains to occur. Furthermore, in the absence of nucleotide or in the presence of ATP, the FRET complex was shown to dissociate within 120s, whereas with ATPγS this time was 50 times longer, indicating a fast hydrolysis reaction for ATP. Anaytical ultracentrifugation further confirmed the dissociation of the Hsp90 dimer in the absence of nucleotide, but the dissociation of the dimer was also demonstrated with the ADP-bound complex, a result which is in disagreement with a compact dimer seen with cryo-EM structure of HtpG[43]. The use of the non-hydroylsable ATP analogue, AMP-PNP, revealed no dimer dissociation thus confirming this nucleotide leads to a stable N-terminally dimerised Hps90 molecule. The results of this FRET study revealed yet another representation of the Hsp90 chaperone cycle depicted in Figure 1. In this model the 'open' Hsp90 dimer binds ATP in a fast reaction, followed by the slow formation of a complex in which N domains are still in the 'open' state (I_1); this step could represent the stage in which the ATP lid closes over the nucleotide binding pocket and also the release of the NTS. The rearrangements within the N domain then leads to the formation of the N terminal dimerised Hsp90 (I_2) resulting in the rearrangements of the N and M domains induced by the interaction between the catalytically active arginine residue, forming the 'closed' state that represents the ATP 'active' state. As a result of ATP hydrolysis and ADP + pi release from the binding pocket, the Hsp90 dimer reverts back to the 'open' state. Conformational changes as a result of ADP-induced affects (as described by Shaiu *et al*.[43] for HtpG) would not be seen by FRET as they do not contribute to the rate-limiting step of the hydrolysis reaction.

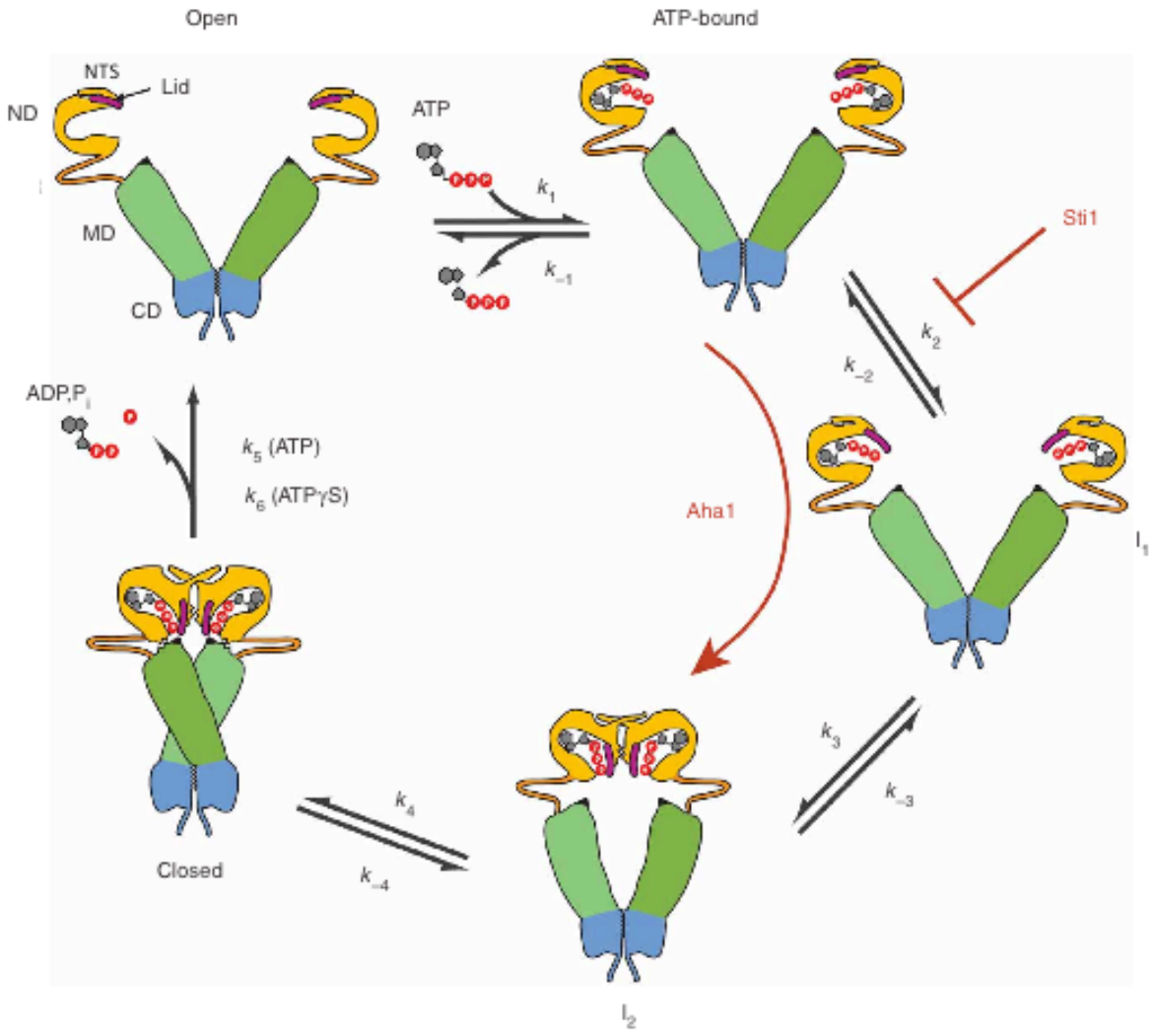

Figure 1.9 The proposed ATP cycle of the Hsp90 chaperone using FRET[11]

A single-molecule FRET (sm-FRET) study[6] using the same sites as above (Asp61 and Gln385) provided another representation of the Hsp90 ATP cycle, which allowed for the determination of rate constants without any of the assumptions associated with techniques such as FRET alone due to intrinsic averaging of such experiments. In a system such as Hsp90, where the conformational states seem largely abundant, it is important to understand all dynamics of the system in order to gain a full picture of the regulatory roles such a system poses. In this study, like the bulk FRET study described above, the mutants were labelled with donor and acceptor fluorophores and conformational changes of the differentially labelled heterodimers were observed upon ligand binding as a result of changes in the FRET signal. Dimer dissociation was prevented by the addition of a coiled coil motif at the C terminus and the mutants were immobilised onto a surface. The results

from this study showed opening and closing of the Hsp90 dimer on a timescale that was much faster than a single ATP hydrolysis cycle (100s for the construct used). Both nucleotide-free and ADP-bound states revealed the same FRET efficiencies. AMP-PNP however, resulted in a long N-terminal closed state with no conformational fluctuations on a second timescale, suggesting that Hsp90 is stabilised to this closed conformation for many minutes. These results are in good agreement with the observations made with the bulk FRET study described above. The data revealed four clear states of Hps90 during its ATP cycle, using the existing crystal structures to illustrate the four steps. Two states represent the N-terminal 'open' dimer and two states represent the N-terminal 'closed' dimer. Although the FRET efficiencies show no significant difference between the two open states and the two closed states, the differences in the dwell-times between each sub-state illustrate differential rate constants of each state proposed.

Both FRET and sm-FRET studies revealed no observable conformation changes upon ADP binding as previously suggested by cryo-EM studies with the *E.coli* HtpG homologue[43], indicating that if an ADP-bound conformation exists in yeast Hsp90 then it must be short-lived and minimally populated during the ATP cycle. Furthermore, these studies revealed an open N domain dimer distance of approximately 8.3 nm and a closed N domain dimer distance of approximately 5.2 nm, which are in good agreement with the predictions of the distance between the mutated residues used in these studies from the published crystal structure[16]. Furthermore, a more recent sm-FRET study[24] also revealed the opening and closing of the C domains of the Hsp90, an observation which has never been addressed in previous studies of a similar nature. The functional significance of this opening and closing is currently unclear, however it is evident that the large number of conformational changes associated with Hsp90 during its ATP cycle must accrue to its role in the regulation of co-chaperone associated client processing.

1.5 Co-chaperone regulation of Hsp90 function

Research has found that Hsp90 displays a high degree of specificity for particular target proteins, for example, playing crucial roles in the processing of the steroid receptor superfamily (i.e. glucocorticoid/progesterone receptors) and some kinases (i.e. the tumour necrosis factor (TNF) receptor, p60). The way in which these target proteins is regulated

are via a network of Hsp90-co-chaperone complexes. The association of the various co-chaperones of Hsp90 has been found to take place via each of the domains of the Hsp90 dimer, and depending on the site of interaction, the co-chaperones exhibit a specific function[44].

The tetratricopeptide repeat (TPR) domain-containing co-chaperones bind to a conserved MEEDV motif located on the C terminal domain of Hsp90, although not all co-chaperones in this class bind to this region[44]. The co-chaperones that do bind to Hsp90 via their TPR domain at the C domain are usually involved in a larger multicomplex network. Another class of Hsp90 co-chaperones is characterised by the molecules that alter the ATPase activity of the protein. These co-chaperones are usually found to associate with the N and M domains of the Hps90 dimer and either increase or decrease ATPase activity. In addition to their ability to influence the ATP activity, a few of these co-chaperones have also been found to be involved in client recruitment to Hsp90.

The mechanism of these Hsp90-co-chaperone complexes coupled with ATP hydrolysis in inducing the regulation of the target proteins of Hsp90 is essential to understand the pathology of certain disease states associated with Hsp90, and will aid in the development of effective therapeutics against this molecular chaperone.

1.5.1 The role of Sba1/p23 in the chaperone-client cycle

The association of Sba1 (or mammalian homologue p23) with Hsp90 was identified when it was co-purified with Hsp90 from various tissue types, it was later found that the Hps90-Sba1 complex plays a role in the recruitment and processing of steroid receptors such as the progesterone receptor in an ATP-Mg^{2+}. The bound Sba1 dissociates post ATP hydrolysis[45,46]. Furthermore, the ATPase inhibitor geldanamycin was found to inhibit the association of Sba1 with Hsp90 in a similar way to the ADP-bound or nucleotide-free Hsp90, neither of which showed association with Sba1. In addition, mutations within the N domain that abolish ATP binding were also shown to prevent Sba1 association[47]. The results from this study indicate that Sba1 most probably binds to the N domain of Hsp90, although a later study found the association of Sba1 with both the N and M domains[48].

A study by Prodromou *et al*.[13] demonstrated that the isolated N domain although fully capable of binding ATP or AMP-PNP, is not sufficient for its interaction with Sba1. Furthermore, cross-linking and mutational studies demonstrated the association of Sba1 to a dimeric Hsp90 molecule, even in the absence of the C terminal dimerisation interface, indicating that Sba1 preferentially binds to the N domain-dimerised Hsp90 and slows down the ATPase cycle possibly by stabilizing the N domain dimerisation interface[49]. In contrast, Siligardi *et al*.[20] showed through ITC that when AMP-PNP was omitted, Sba1 bound to Hsp90 but with an approximate 70-fold weaker affinity compared to an AMP-PNP bound Hsp90. Furthermore, a mutant that displays a stronger N domain dimerised Hsp90 showed stronger binding of Sba1 than the nucleotide free protein, although again, this interaction was not as strong as the AMP-PNP bound Hsp90 mutant. These results are in good agreement with previous observations of Sba1 association not being directly ATP-dependent, but rather it is dependent on a stabilised N domain dimer, a conformation achieved upon ATP binding. The stoichiometry of the Sba1:Hsp90 complex remains ambiguous, with studies reporting a 1:1[20] or 2:1[50]. In contrast to the relatively weak affinity of the nucleotide-free yeast Hsp90 to bind Sba1, human Hsp90 was found to associate with Sba1 with an affinity that was 5 fold stronger. Furthermore dimeric human Hsp90 binds two Sba1 molecules simultaneously[51], a stoichiometry also seen with the yeast proteins[50]. Surprisingly McLaughlin *et al*.[51] found that the Sba1:Hsp90 interaction leads to the complete inhibition of the ATPase cycle of human Hsp90 by 'locking' the ATP-bound state of the chaperone, a state which has also been shown to have a high affinity for client proteins.

The crystal structure of the full-length yeast Hsp90 in complex with Sba1[16] provides the first structural view of the localization of the Sba1 protein on the Hsp90 dimer further conforming that Sba1 binds to the Hsp90 dimer in a 2:1 stoichiometry. The structure (Figure 1.10) shows Sba1 contacting both N and M domains, the latter of which was also seen in NMR chemical shift patterns[3]. It is clear from the structure why the absence of N domain dimerisation would lead to reduced Sba1 affinity, since one end of the Sba1 is shown to bind the N domain of one Hsp90 protomer and the other end binds to the N domain of the partner protomer (Figure 1.11). Thus the lack of N domain dimerisation would probably destabilise both N domain contacts with p23.

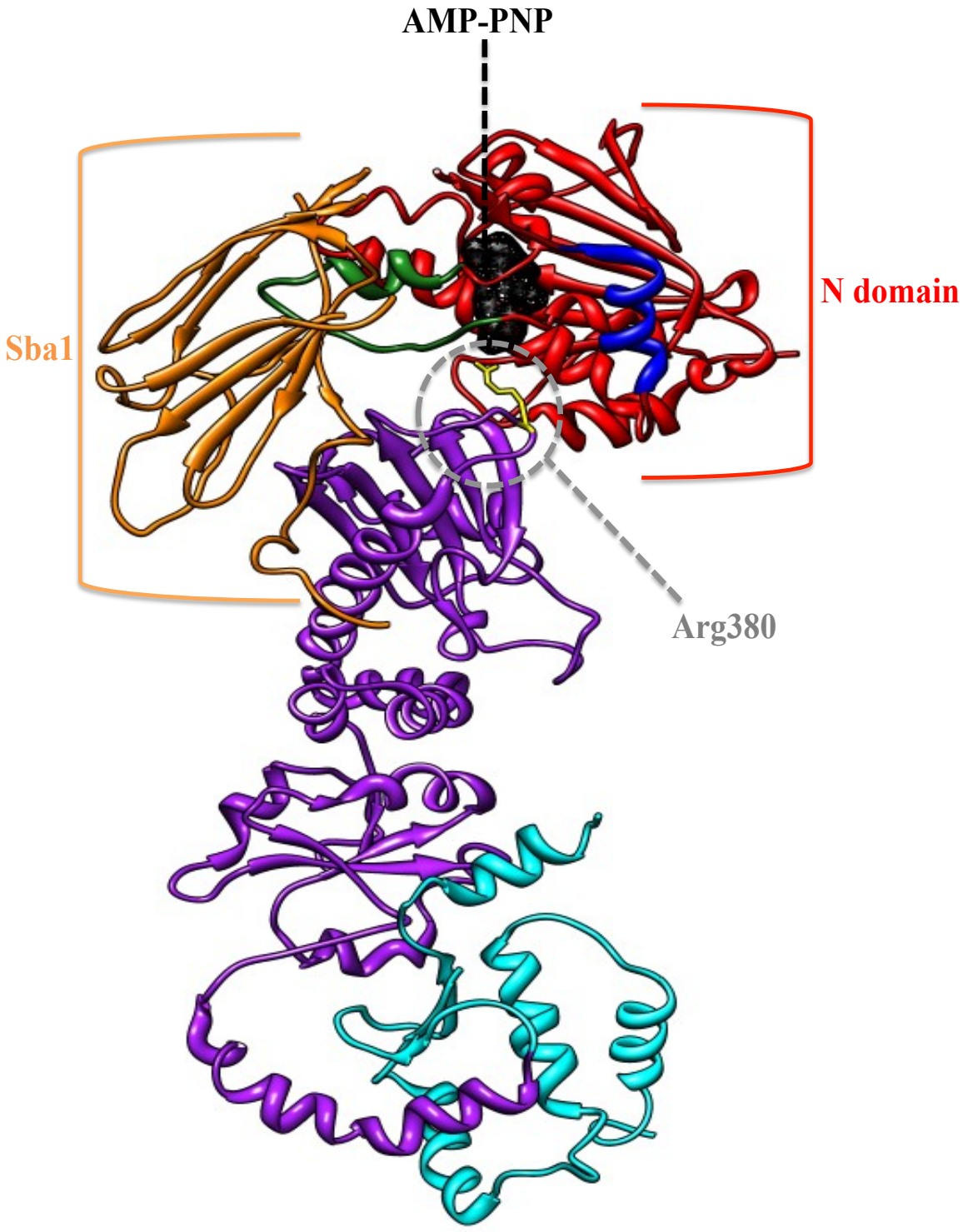

Figure 1.10 Ribbon representation of one (of two) protomers of the crystal structure of full-length yeast Hsp90 in complex with AMP-PNP (black) and Sba1[16] (orange), highlighting contacts of Sba1 with the N domain (red) and M domain (purple). Also highlighted is the NTS (blue) and ATP lid (green) region of the N domain, and the catalytic Arg380 residue (grey) of the M domain.

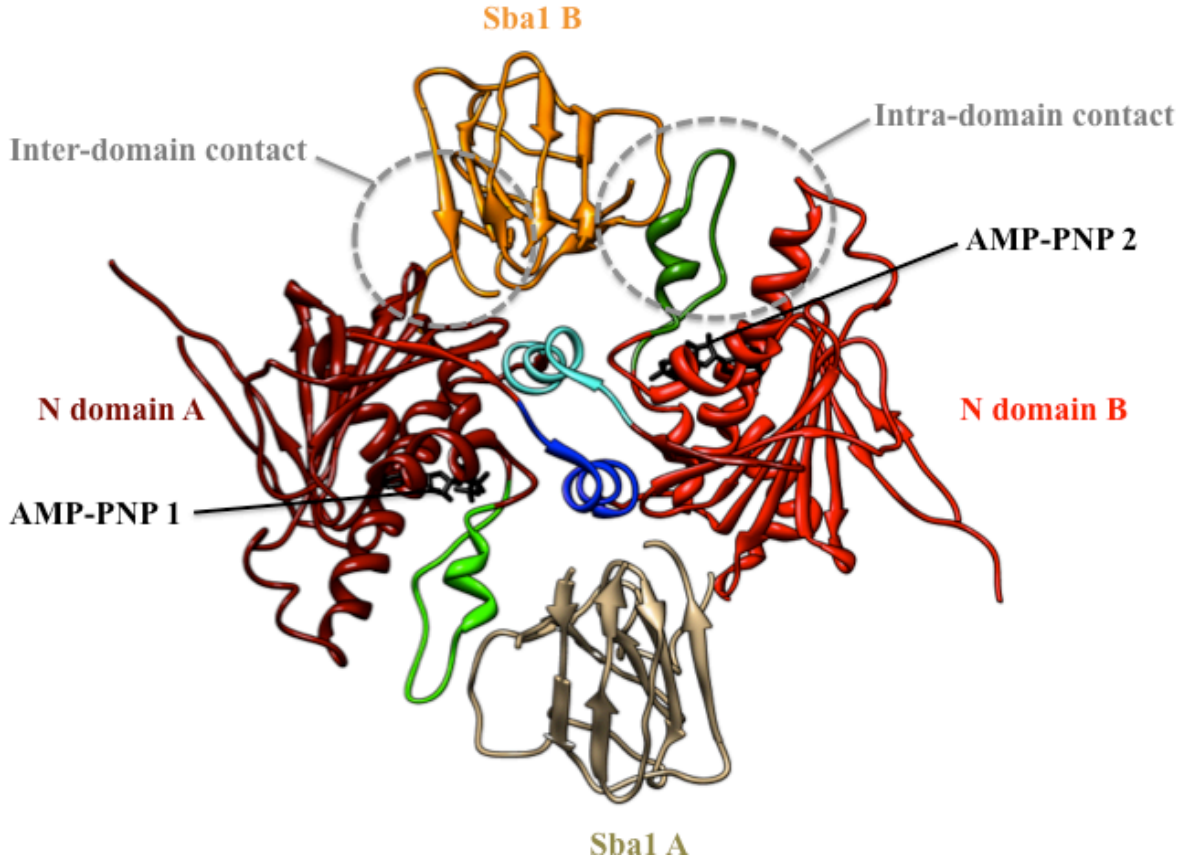

Figure 1.11 Ribbon representation of the top view of the Hsp90:Sba1 complex[16], highlighting both inter- (with the ATP lid of the N domain of one Hsp90 protomer) and intra-domain (with the surface of the N domain of the second Hsp90 protomer) contacts of the bound Sba1.

Furthermore, the association of p23 with the N and M domain of each Hsp90 protomer may prevent the complete docking of N and M domains by acting as a 'barrier'. The docking of the N and M domains of each Hsp90 protomer allows the interaction between the catalytic Arg380 residue (within the M domain) with the bound ATP. Thus p23 association may inhibit the hydrolysis of ATP, but stabilise the ATP-bound Hsp90 conformation, as a result this would 'halt' the ATP cycle and promote client association.

1.5.2 The role of Aha1 in the chaperone-client cycle

Aha1 (activator of Hsp90 ATPase) is another co-chaperone that binds directly to Hsp90 and has been demonstrated to be involved in the activation of client proteins *in vivo*,

such as the protein kinase v-Src[49]. Furthermore, it was demonstrated that Aha1 binds to the Hsp90 dimer in a 2:1 fashion and is able to coexist in complexes with the co-chaperones involved in the earlier stages of client folding (i.e. Hop/Sti1 and p50/Cdc37) and those involved in the later stages of client folding (i.e. Cyp40/Crp6 and p23/Sba1). Thus Aha1 possibly plays a role in the general up-regulation of Hsp90 function rather than being able to stabilise a particular conformation at a specific stage during the ATPase cycle. A homologue of Aha1, Hch1, was discovered to suppress a mutant allele of Hsp90 containing the residue Gly381[25]. Considering the location of this residue within the catalytic loop of the M domain next to the catalytic Arg380, it was suggested that Hch1 and/or Aha1 might bind directly to the M domain of Hsp90. This was later confirmed by ITC[52] experiments, which showed that although there is substantial binding between full-length Aha1 and Hsp90 (residues 273-560) with a K_d of approximately 3.8 μM, the affinity is significantly stronger for full-length Hsp90 (K_d = ~0.6 μM). The relative affinities of the two interactions suggests that although Aha1 is able to bind the isolated M domain of Hsp90, the stronger affinity of Aha1 for full length Hsp90 requires contributing interactions from the N and/or C domains of Hsp90 together with the M domain.

Since Hch1, which is shorter in length than Aha1, was able to significantly stimulate Hsp90 function, the corresponding residues within Aha1 (1-153; N-Aha1) were exploited for Hsp90 association; ITC revealed a K_d of approximately 1.75 μM, which is approximately 3-fold stronger than that obtained for full-length Aha1. These findings led to the successful crystallisation of the M domain of Hsp90 with the N domain of Aha1[52], a structure that showed a resolution of approximately 2.7Å. This structure provided a view of a parallel association between Hsp90 and Aha1 (Figure 1.12).

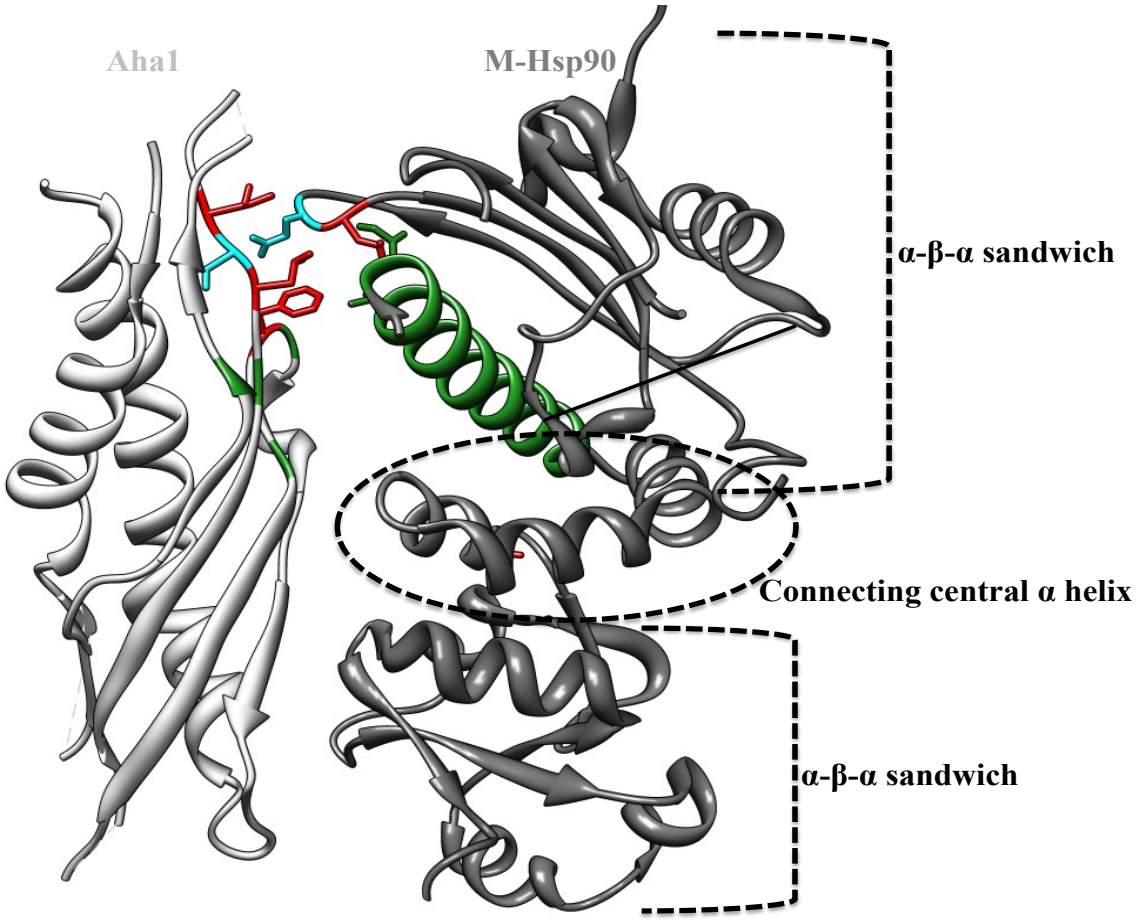

Figure 1.12 Ribbon representation of M-Hsp90 in complex with Aha1 (PDB 1USU[52]; refer to Appendix 1) highlighting the main interaction interface formed by hydrophobic (red) and two polar (cyan) interactions between the two proteins. Also highlighted is the hydrogen bonding and ion-pair interactions between the two interacting proteins (green).

Apart from the intimate hydrophobic interaction formed by the residues in the first α-β-α segment of the M domain of Hsp90 and the N terminal segment of the Aha1 protein (illustrated in Figure 1.8), the remaining interactions are relatively weak and polar, formed mainly by an extensive network of solvent-mediated interactions between the two proteins. As mentioned earlier, the catalytic Arg380 residue within the M domain of Hsp90 is thought to directly interact with the bound ATP molecule in the Hsp90 N domain. The loop bearing this residue (residues 370-390) shows considerable rearrangement in the Aha1-bound Hsp90 when compared to that in the Aha1-free M domain crystal structure[5] in that it re-orientates towards the N domain. Mutation of residues which alter the main interaction interface between Aha1 and the catalytic loop demonstrated an impairment in Aha1's ability to influence the ATP activity of Hsp90[52]. Furthermore, a study in which a mutant

designed to disrupt the interaction of the N and M domains of each Hsp90 protomer and thus prevent the interaction between the catalytic Arg380 residue and the bound ATP, ultimately inhibiting ATPase activity, demonstrated that Aha1 association to Hsp90 was able to reverse the effect of this mutation and restore ATPase activity. These data suggest Aha1 is responsible for the repositioning of the loop containing the catalytic Arg380 residue thereby activating the ATPase state of the Hsp90 chaperone[20].

1.5.3 The role of Cdc37/p50 in the chaperone-client cycle

The recruitment of many of Hsp90's protein kinase clients involves the association of the co-chaperone Cdc37 (or the mammalian homologue, p50), many of which directly bind Cdc37. Siligardi *et al.*[53] showed that Cdc37 binds to the Hsp90 as a homodimer (at its N domains) as a scaffold and acts to inhibit the ATPase function of Hsp90 and thus facilitate client loading. Furthermore, Cdc37 does not displace the Hsp90 inhibitor GA, but rather binds in conjunction with GA, suggesting that the N domain is not likely to provide the interface between Cdc37 and Hsp90. The observation of the simultaneous binding of two Cdc37 co-chaperones to Hsp90 provides the possibility of two different protein kinase clients being recruited to the co-chaperone:chaperone complex.

Roe *et al*.[28] later crystallised the core complex of p50 with yeast Hsp90 illustrating the interaction between co-chaperone and Hsp90 takes place in the N domain of Hsp90 in a 1:1 complex. As mentioned previously, the successful hydrolysis of ATP involves a large number of conformational changes within the Hsp90 N and M domains. The ability of Hsp90 to hydrolyse ATP must involve the formation of a stabilised N domain dimer, which predominantly involves the interaction of the hydrophobic surfaces formed by the closure of the so-called 'ATP lid' from both protomers. However the stable N domain dimer although crucial for ATP hydrolysis, does not lead to ATP hydrolysis. Additional contacts between N and M domains involving a catalytic loop within the M domain must take place for ATP hydrolysis to occur. The structure (Figure 1.13) clearly shows p50 interacting with the lid 'open' N domain of Hsp90, thus preventing the closure of the ATP lid over the nucleotide-binding pocket and ultimately inhibiting N and M domain contacts.

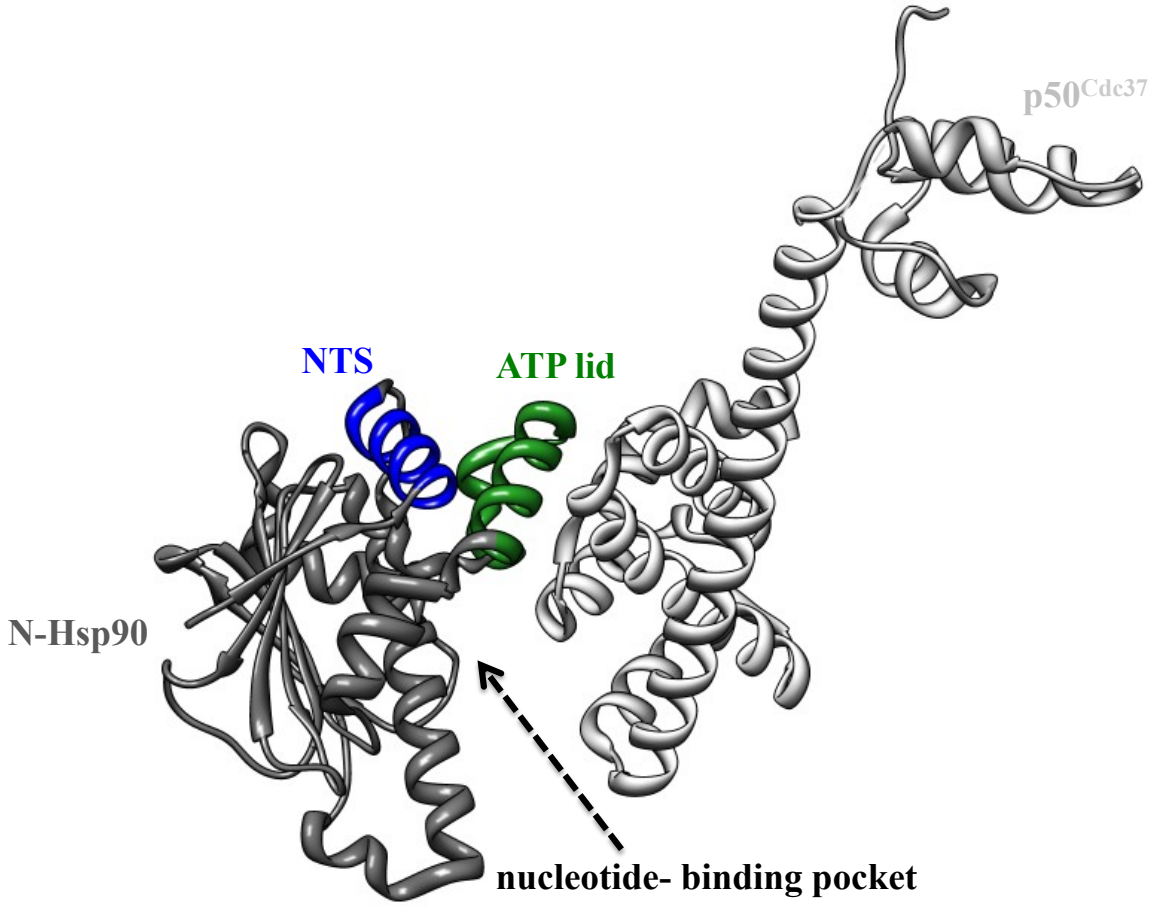

Figure 1.13 Ribbon representation of N-Hsp90 in complex with p50 (PDB 1US7[28]; refer to Appendix 1) highlighting the interface formed by the ATP lid region of the Hsp90 N domain with the N domain of the p50 molecule.

Furthermore, the structure indicates that p50 would sit in the junction between the two N domains of Hsp90 dimer, holding them in the 'open' conformation (approximately 40 Å apart) and therefore preventing their association, which would lead to the events that promote ATP hydrolysis.

1.5.4 The role of Sti1/Hop in the chaperone-client cycle

First described as a major component of the Hsp90 chaperone complex in yeast, the TPR-domain containing Sti1 co-chaperone (or the mammalian homologues, p60/Hop) was suggested to be an inhibitor of the ATPase activity of Hsp90, binding to Hsp90 in a 1:1 fashion[54]. Sti1 was later found to bind to the Hsp90 dimer as a dimer itself with a K_d of approximately 0.33 μM[55], simultaneously occupying both TPR-binding sites within the C

domains of the Hps90 dimer. Cpr6, also a TPR-binding co-chaperone does not affect the intrinsic ATPase activity of Hsp90, and was shown to be able to restore Hsp90 ATP function by displacing the bound Sti1. The similarities in affinities exhibited by Sti1 and Cpr6 (K_d = 0.2 μM) for Hsp90, and the fact that Cpr6 does not abolish ATPase activity, it was apparent the both co-chaperones bind to Hsp90 in a similar fashion. Furthermore it was shown that Sti1 is able to successfully displace the Hsp90 ATP inhibitor GA, interestingly suggesting a direct interaction between Sti1 and the N domain of Hsp90[55].

Pull down assays showed evidence that a number of other co-chaperones, including Hsp70, are present with Hsp90 and Sti1, but were not directly found associated with Sti1. Furthermore, Sti1 was not shown to bind with client proteins, suggesting that Sti1 is probably part of a larger complex of Hsp90:co-chaperones involved in the maturation and regulation of client proteins[56]. The recent cryo-EM structure of the human Hsp90:Hop complex[17] revealed that Hop does not simply mediate the Hsp70 co-chaperone in the Hsp90:co-chaperone complex. The binding of Hop to Hsp90 leads to two significantly large conformational changes (Figure 1.14); one is the rotation of the M and C domain junction that results in a substantially smaller 'open' angle. The second is the almost 90° rotation of the N domains of Hsp90 such that the interface between the N and M domains matches the ATP-bound Hsp90 state. Furthermore, this change results in the hydrophobic surface of the ATP lid coming into close proximity with the hydrophobic catalytic loop within the M domain that is known to bind the protein kinase client v-Src. The N domains are thus left in an orientation that would otherwise promote dimerisation and hence ATP hydrolysis, but instead are left in a hydrolysis-incompetent state. The conformational changes induced by Hop binding promote a state which is more efficient in binding client proteins, whereby the putative inter-dimer surfaces along the central cleft between both protomers of the Hsp90 dimer are left more accessible for client loading.

1.6 Summary

The considerable amount of flexibility the Hsp90 dimer evidentially plays a crucial role in the ability of Hsp90:co-chaperone complexes to recruit and process the varied clientele. This client loading function is narrowed down to two active components which serve as the 'signal' for Hsp90 to then carry out its regulatory functions; that is the

mechanism of ATP binding and hydrolysis and the local rearrangements within the N domain of Hsp90, and the conformational changes signalled throughout the entire length of the dimer as a result of this local binding event. It is therefore essential to de-convolute the intricate mechanism associated with the above two components of the Hsp90 conformational cycle before trying to understand the additional conformational affects of co-chaperone association, and ultimately client loading.

This thesis focuses on the local changes derived from nucleotide binding to the isolated ATP-binding N domain of Hsp90, particularly involving the contribution of the poorly studied but apparently indispensable Mg^{2+} ion in the nucleotide:protein complex using a combination of ITC, NMR spectroscopy and mutational studies. In addition, an investigation of the conformational changes affecting the other domains of the full-length Hsp90 dimer upon nucleotide and co-chaperone association are delineated using a type of EPR spectroscopy, named double electron electron resonance (DEER) spectroscopy. Together, the two studies contribute to a better understanding of the action of the Hsp90 molecular chaperone machinery and how it may regulates client proteins *in vivo*.

Chapter 2

Materials and methods

This chapter illustrates the methodology adopted in order to complete the various projects within this thesis. All reagents were purchased from Sigma-Aldrich, VWR or Melford unless otherwise stated, and were made using deionised water from an Elga Maxima Ultra-pure water purification system (of 10 mOhm purity) and sterilized by autoclaving at 123°C for 15 minutes.

As stated in Chapter 1, this thesis used the *S.Cerevisiae* Hsp90 for investigation of thermodynamics and conformational change upon nucleotide association; the isolated N terminal domain was used for the thermodynamic analysis of nucleotide binding, and the full length Hsp90 was used to study conformational change within all domains of the protein upon nucleotide association.

2.1 Protein constructs

Five protein constructs of the isolated N domain of Hps90 were used for thermodynamic analysis, all of which altered the proteins ability to bind its nucleotide ligands. The N terminal domain of Hsp90 used in this thesis runs from residues 4- 207 and has the following amino acid composition:

N terminal domain

ETFEFQAEITQLMSLIINTVYSNKEIFLRELISNASDALDKIRYKSLSDPKQLETEPDL
FIRITPKPEQKVLEIRDSGIGMTKAELINNLGTIAKSGTKAFMEALSAGADVSMIGQF
GVGFYSLFLVADRVQVISKSNDDEQYIWESNAGGSFTVTLDEVNERIGRGTILRLFL
KDDQLEYLEEKRIKEVIKRHSEFVAYPIQL

In addition to investigation of the wild-type N-Hsp90 domain, the above sequence was modified by a single amino acid residue (at any one time) in order to investigate the effects of various point mutations on the thermodynamics of ligand binding to N-Hsp90. The selected residues for mutational analysis were Thr22 and Thr101, both of which were

mutated to Ile22 and Ile101 respectively. Mutation of these residues stabilised the ATP lid in either an open or closed conformation, and were thus exploited for the thermodynamic effects upon nucleotide binding as a result of altering the ATP lid position. Gly153 and Gly154 were also selected for mutational analysis, and were mutated to Ala153 and Ala154 respectively. Mutation of these residues was as a result of the varied effect of these residues in the AMP-PNP bound N-Hsp90 NMR HSQC measurements in the presence of MgCl2 or CaCl2. The protocol for mutagenesis is described in section 2.5.

Nine protein constructs of the full-length Hsp90 were used for investigation of conformational change upon ligand binding using a type of electron paramagnetic resonance (EPR) spectroscopy, called double electron electron resonance (DEER) spectroscopy (Section 2.). In this instance, the wild-type protein could not be used due to the complete absence of cysteine residues in the protein sequence, so various positions were selected for single cysteine mutation. The full length Hsp90 protein sequence runs from residues 4-709. Residues 678-709 encode for the region in which TPR-binding clients or co-chaperones associate with Hsp90. However this region is not included in the protein construct utilised in this thesis. The full-length protein construct used in this thesis has the following amino acid composition:

Full length Hsp90

ETFEFQAEITQLMSLIINTVYSNKEIFLRELISNASDALDKIRYKSLSDPKQLETEPDL
FIRITPKPEQKVLEIRDSGIGMTKAELINNLGTIAKSGTKAFMEALSAGADVSMIGQF
GVGFYSLFLVADRVQVISKSNDDEQYIWESNAGGSFTVTLDEVNERIGRGTILRLFL
KDDQLEYLEEKRIKEVIKRHSEFVAYPIQLVVTKEVEKEVPIPEEEKKDEEKKDEEK
KDEDDKKPKLEEVDEEEEKKPKTKKVKEEVQQIEELNKTKPLWTRNPSDITQEEYN
AFYKSISNDWEDPLYVKHFSVEGQLEFRAILFIPKRAPFDLFESKKKKNNIKLYVRR
VFITDEAEDLIPEWLSFVKGVVDSEDLPLNLSREMLQQNKIMKVIRKNIVKKLIEAF
NEIAEDSEQFEKFYSAFSKNIKLGVHEDTQNRAALAKLLRYNSTKSVDELTSLTDY
VTRMPEHQKNIYYITGESLKAVEKSPFLDALKAKNFEVLFLTDPIDEYAFTQLKEFE
GKTLVDITKDFELEETDEEKAEREKEIKEYEPLTKALKEILGDQVEKVVVSYKLLD
APAAIRTGQFGWSANMERIMKAQALRDSSMSSYMSSKKTFEISPKSPIIKELKKRVD
EGGAQDKTVKDLTKLLYETALLTSGFSLDEPTSFASRINRLISLGLN

The residues selected for cysteine mutation are Ser17, Asp61, Ala103, Ser297, Ser363, Val391, His430, Thr511, and Met589.

The *S.Cerevisiae* construct of the co-chaperone p23, Sba1 was also used to study conformational changes during the Hsp90 chaperone cycle using DEER spectroscopy. The Sba1 protein sequence runs from residues 1-227 and has the following amino acid composition:

MASLEVLFQGPMSDKVINPQVAWAQRSSTTDPERNYVLITVSIADCDAPELTIKPSY
IELKAQSKPHVGDENVHHYQLHIDLYKEIIPEKTMHKVANGQHYFLKLYKKDLESE
YWPRLTKEKVKYPYIKTDFDKWVDEDEQDEVEAEGNDAAQGMDFSQMMGGAG
GAGGAGGMDFSQMMGGAGGAGSPDMAQLQQLLAQSGGNLDMGDFKENDEEDE
EEEIEPEVKA

All protein constructs included an N-terminal poly-histidine tag to allow for protein purification via Ni-NTA affinity chromatography (Section 2.9).

Wild-type Hsp90, T22I and T101I N-Hsp90 mutants, and Sba1 for the study on Hsp90 were obtained from Dr Chrisostomos Prodromou and Professor Laurence Pearl from the Institute of Cancer Research (ICR), London.

2.2 Competent cells

For the preparation of competent *Escherichia coli* (*E.Coli*) cells with a competency of 1 x10^7 colonies μg^{-1} plasmid DNA, the following regaents were prepared:

Transformation buffer I

30mM potassium acetate pH 5.8
100mM rubidium chloride (RbCl)
50mM manganese chloride ($MnCl_2$)
10mM calcium chloride ($CaCl_2$)
15% (w/v) glycerol

Slow addition of acetic acid was carried out to adjust pH.

Transformation buffer II

10mM Mops pH 6.8
10mM RbCl
75mM $CaCl_2$
15% (w/v) glycerol

The pH was adjusted with HCl or NaOH as required.

Final reagents were filter directly using a sterile 22µm filter.

Sterile LB media (using reagents stated in Section 2.3)

NZY+ broth (250ml in sterile distilled H_2O):
2.5 g of NZ amine (casein hydrolysate)
1.25 g of yeast extract
1.25 g of NaCl

The pH was adjusted to pH7.5 with NaOH and sterilised by autoclaving at 121°C.

Once the autoclaved broth cooled to room temperature, the following filter-sterilised supplements were added to the broth:
3.125 mL of 1 M $MgCl_2$
3.125 mL of 1 M $MgSO_4$
5 mL of 20% (w/v) glucose

2.2.1 Protocol for preparation of competent *E.coli* cells:

An *E.Coli* strain of BL21(DE3), DH5 or XL1 Blue was used to inoculate 5ml of sterile LB media and incubated overnight at 37°C in a shaking incubator at 200 rpm. 1ml of overnight culture was used to inoculate 50 mL of sterile LB media, which was grown at 37°C in a shaking incubator at 200 rpm until the cells reached an optical density (OD) of approximately 0.7 absorbance units at 600 nm.

The cells were then centrifuged at 4000 rpm for 10 minutes at 4°C in order to obtain the cell pellet. The supernatant was discarded using a sterile procedure before being disposed. The cell pellet was placed on ice for 15 minutes prior to being resuspended in 15 ml of transformation buffer I followed by incubation on ice for approximately 30 minutes (with gentle mixing).

The cell suspension was then centrifuged at 4000 rpm for 20 minutes at 4°C in order to collect the cell pellet. The supernatant was discarded using a sterile procedure before disposal. The cell pellet was then resuspended in 4 ml of transformation buffer II (on ice) and placed into 100 µl aliquots in sterile microcentrifuge and stored at -80°C until required.

2.3 Growth media

Luria-Bertani (LB) media:

For the culture of *E.Coli* strains, LB media was used. The composition of this media consisted of 10 g/l bacto-tryptone, or bacto-peptone, 5 g/l yeast extract, and 5 g/l NaCl. LB agar plates consisted of LB medium supplemented with 15 g/l agar poured evenly into Petri dishes. All media were made using deionised distilled H_2O (purity 10 mOhm; Elga) and sterilised by autoclaving at 123°C for 15 minutes prior to use.

Minimal media (M9)

The expression of isotopically enriched proteins for investigation by NMR spetroscopy was carried out using M9 media, consisting of 6 g/l Na_2HPO_4, 3 g/L KH_2PO_4 and 0.5 g/l NaCl. For the expression of [^{15}N]-labelled proteins, uniformly [^{15}N]-labelled $(NH_4)_2SO_4$ (Cambridge Isotope Laboratories) was used at 1 g/l; for [^{13}C]-labelled proteins,

uniformly labelled glucose (Cambridge Isotope Laboratories) was used at 2 g/l. This solution was pH adjusted to 7.4 and autoclaved. The following sterile filtered solutions were added per litre of media just before inoculation: 1 ml 1 M $MgCl_2$, 5 µl 1 M C aCl$_2$, 500 µl 0.01 M $FeSO_4$, 500 µl 1000X vitamins solution*, 500 µl 1000X micronutrient solution** and 500 µl 250 mg/ml carbenicillin .

Per Litre:

*1000X vitamins solution

0.4 g choline chloride
0.5 g Folic acid
0.5 g Pantothenic acid
0.5 g Nicotinamide
1.0 g Myo-inositol
0.5 g Pyridoxal HCl
0.5 g Thiamine HCl
0.05 g Riboflavin
1.0 g Biotin

**1000X micronutrient solution

3 µM ammonium molybdate
400 µM H_3BO_3
30 µM $CoCl_2$
10 µM $CuSO_4$
80 µM $MnCl_2$
10 µM $ZnSO_4$

2.4 Purification of plasmid DNA

Plasmid DNA was prepared from freshly transformed (section 2.6) *E. coli* XL1Blue cultures grown overnight in 5 ml LB media containing 250 µg/ml carbenecillin, and incubated at 37^{o}C with shaking at 200 rpm. The overnight culture was then pelleted by centrifugation at 4000 rpm for 15 minutes at 4^{o}C. The supernatant was discarded in a sterile manner, and the cell pellet was processed using a QIAprep Spin Miniprep kit (Qiagen) following the manufacture's protocol. The bacterial cells were lysed under alkaline conditions, and the lysate subsequently neutralised and adjusted to high-salt binding conditions. The spin columns contain a unique silica membrane that ensure only DNA is adsorbed, while RNA, cellular proteins and metabolites are not retained by the membrane but are found in the flow-through. Salts were removed by a wash step and the purified plasmid eluted from the QIAprep spin column using Elution Buffer (EB, Tris containing buffer, pH 7.0 – 8.5) or dH_2O.

2.5 Site-directed mutagenesis

Single amino acid mutants of the N-Hsp90 and full-length Hsp90 constructs were made using the Quikchange® Site-Directed Mutagenesis Kit (Stratagene). Mutagenesis of the full-length Hsp90 constructs would result in double cysteine labelled proteins due to the homodimeric nature of the full-length Hsp90 protein, and therefore can be studied using DEER spectroscopy. The basic procedure of the kit uses a supercoiled double-stranded DNA vector (dsDNA) harbouring the fragment of interest; so in this case it would be the insert corresponding to N-Hsp90 or full-length Hsp90. Two synthetic oligonucleotide primers containing the desired mutation, complementary to opposite strands of the vector, are both extended during the temperature cycling by the DNA polymerase, *PfuTurbo*. The extension of the oligonucleotide primers generates a mutated plasmid containing staggered nicks. After the completion of the temperature cycling, the mutated plasmid is treated with the endonuclease enzyme *Dpn1*, which is able to distinguish between methylated (the case for most *E.coli* strains) and hemimethylated DNA, and therefore the parental DNA template is digested resulting in a vector containing the newly synthesis nicked DNA including the desired mutation.

The Quikchange® Site-Directed Mutagenesis Kit comes with the following ingredients for the mutagenesis reaction:
PfuTurbo DNA polymerase (2.5 U/µl)
10x reaction buffer
dNTP mix
Dpn 1 restriction enzyme (10 U/µl)
E.coli Xl1-Blue supercompetent cells

The sythesised oligonucleotide primer sequences used for all mutagenesis reactions are listed in Table 2.1, and the parameters for the thermal cycling during the mutagenesis reactions are shown in Table 2.2.
The following considerations were made when designing the desired oligonucleotide primers:

- Both oligonucleotide primers must contain the desired mutation and anneal to the complementary sequences on opposite strands of the plasmid DNA.

- Oligonucleotide primers must be approximately 25-45 base pairs (bp) in length, generating a melting temperature (Tm) of ≥ 78°C. (Oligonucleotides longer than 45 bp may result in the formation of secondary structure potentially reducing mutagenesis efficiency).
- The desired mutation should be in the middle of the oligonucleotide primer sequence with approximately 10-15 bases either side of the mutation.
- The oligonucleotide primer sequences should have a minimum GC content of approximately 40%, and should terminate in one or more G/C bases.

Hsp90 mutant	PCR Primers (5' to 3')
N-Hsp90	
G153A	F:CTGGGAATCCAACGCT**GCT**GGTTCTTTCACTGTTA R: TAACAGTGAAAGAACCAGCAGCGTTGGATTCCCAG
G154A	F: CTGGGAATCCAACGCTGGT**GCT**TCTTTCACTGTTA R: TAACAGTGAAAGAAGCACCAGCGTTGGATTCCCAG
Full-length Hsp90	
S17C	F:CTGAAATTACTCAGTTGA**TGT**GTTTGATCATCAACACCGT R:GGTGTTGATGATCAAACACATCAACTGAGTAATTTCAGC
A61C	F:CAATTGGAAACAGAACCA**TGT**CTCTTTATTAGAATCACTCCA R:TGGAGTGATTCTAATAAAGAGACATGGTTCTGTTTCCAATTG
A103C	F:GCCAAGTCTGGTACCAAA**TGT**TTCATGGAAGCTCTATCTGCT R:AGCAGATAGAGCTTCCATGAAACATTTGGTACCAGACTTGGC
S297C	F:AATGCTTTCTATAAGTCTATT**TGT**AACGACTGGGAAGACCCATTGT R:ACAATGGGTCTTCCCAGTCGTTACAAATAGACTTATAGAAAGCATT
S363C	F: GACTTGATTCCAGAGTGGTTA**TGT**TTCGTCAAGGGTGTTGTTGAC R: GTCAACAACACCCTTGACGAAACATAACCACTCTGGAATCAAGTC
V391C	F: CAAAATAAGATCATGAAG**TGT**ATTAGAAAGAACATTGTCAAAAAG R: CTTTTTGACAATGTTCTTTCTAATACACTTCATGATCTTATTTTG
H430C	F: AAAAATATCAAGTTGGG**TGT**ATGTGAAGATACCCAAAACAGGGCT R: AGCCCTGTTTTGGGTATCTTCACATACACCCAACTTGATATTTTT
T511C	F:CCCAATTGATGAATACGCCTTC**TGT**CAATTGAAGGAATTCGAAGGTA R:TACCTTCGAATTCCTTCAATTGACAGAAGGCGTATTCATCAATTGGG
M589C	F:ATTTGGTTGGTCTGCTAAC**TGT**GAAAGAATCATGAAGGCTCAAGCCTT R:AAGGCTTGAGCCTTCATGATTCTTTCACAGTTAGCAGACCAACCAAAT

Table 2.1 Oligonucleotides used in the thermodynamic and structural analysis of Hsp90. Forward primer (F), reverse complement primer (R). Point of mutation (red).

Each mutagenesis reaction was composed of the following components:

5 µl 10x 10x reaction buffer

1 µl dsDNA template (concentration of 5-50 ng; either N-Hsp90/full-length Hsp90)

1.5 µl oligonucleotide primer 1 (125 ng)

1.5 µl oligonucleotide primer 2 (125 ng)

1 µl dNTP mix

The final reaction was made up to a final volume of 50 µl with ddH_2O and mixed gently

Immediately before starting the thermal cycling step, 1 µl of *PfuTurbo* DNA polymerase was added to the reaction mixture and mixed gently.

Cycle(s)	Temperature	Time
1	95°C	30 seconds
16-18	95°C	30 seconds
	55°C	1 minute
	68°C	1 minute/kb of plasmid

Table 2.2 Parameters used for thermal cycling of a single amino acid change mutagenesis reaction

2.6 Transformation into the BL21 (DE3) *E.Coli* protein expression strain

The appropriate volume (between 1-2 µl) of freshly prepared plasmid DNA (at 4°C) was incubated on ice with 50µl of thawed (on ice) BL21 (DE3) competent cells for 30 minutes. The cells were then given a 45 s heat-shock by placing the sample in a water bath at 42^{o}C. Following this, the cells were placed on ice for 10 s to recover from the heat-shock.

500 µl sterile LB media or NZY + broth (Section 2.2) was added to the cells and the solution was incubated at 37^{o}C for 1 hour with shaking at 200 rpm. The cells were then pelleted by centrifugation at 13500 rpm for 1 minute at room temperature, and the pellet was resuspended in 100 µl of sterile LB media. The 100 µl of cells were then spread, using a sterile streaking rod, onto an agar plate enriched with 250 µg/ml carbenecillin, and the plate was placed overnight in an incubator at 37^{o}C.

2.7 Preparation of glycerol stocks

A single colony selected from an agar plate was inoculated into 5 ml of sterile LB media containing 250 μg/ml carbenecillin. Cells were incubated overnight at 37^{o}C with shaking at 200 rpm. 500 μl of overnight culture was transferred into a cryogenic vial along with 500 μl of 70 % sterile glycerol and the vial was stored at -80^{o}C for long-term storage.

2.8 Protein expression

2.8.1 Small scale protein expression tests

Small-scale protein expression tests were typically performed in 100 ml sterile LB media. A single recombinant colony selected from a plate of freshly transformed *E. coli* BL21 (DE3) cells was used to inoculate 5 ml sterile LB media containing 250 μg/l carbenecillin. The cells were grown overnight at 37 ºC with shaking at 200 rpm. 1 ml of overnight culture was then used to inoculate 100 ml of sterile LB media fortified with 250 μg/l and subsequently incubated at 37 ºC with shaking at 200 rpm, until cells reached an OD_{600nm} = 0.6 - 0.8 absorbance units. The expression of protein was induced overnight with shaking at 200 rpm at a reduced temperature of 21 ºC with the addition of isopropyl-β-D-thiogalactopyranoside (IPTG) to a final concentration of 1 mM per Litre culture. The cells were then pelleted by centrifugation at 6000 rpm for 15 minutes, the supernatant was discarded in a sterile manner by autoclaving at 123 ºC for 15 minutes, and the cell pellet frozen at -20°C until required.

A sample of the pre- and post- induction cells were taken and analysed for protein expression using sodium dodecyl sulphate polyacrylamide gel electrophoresis (SDS-PAGE); Section 2.10; Figure 2.2-2.8).

2.8.2 Large scale protein expression of Hsp90 constructs

Protein expression was routinely performed in 2 l sterile LB media. A single colony of *E.Coli* BL21 (DE3) cells selected from a freshly transformed LB agar plate or 1

µl from a glycerol stock of the appropriate construct was used to inoculate 100 ml of sterile LB media supplemented with 250 µg/l carbenecillin and grown overnight at 37^{o}C with shaking at 200 rpm. 10 ml of the overnight culture was then sub cultured into 1 l of fresh sterile LB media supplemented with 250 µg/l carbenecillin and grown at 37^{o}C with shaking at 180 rpm until cells reached an OD_{600nm} of 0.6 - 0.8. Protein production was induced with 1 mM final concentration of IPTG and the temperature lowered to 21°C with cells growing overnight with shaking at 200 rpm. The cells were pelleted by centrifugation at 6000 rpm for 15 minutes at 4^{o}C. The supernantant was discarded in the same manner as stated in section 2.8.1 and the cell pellets were stored at -20^{o}C until required.

2.8.3 Large scale protein expression of isotopcally labelled N terminal Hsp90 constructs

A 4 l large-scale protein expression in LB media was transferred into 1 l of minimal media (M9 media). The same procedure as stated in section 2.8.2 was followed in order to obtain the cell pellet from the 4 l LB media. Subsequently, the pelleted cells were resuspended in 500 ml of minimal media fortified with 250 µg/l carbenecillin and incubated at 37^{o}C with shaking at 200 rpm for more than 1 hour to allow for sufficient ^{15}N labelling of the protein. Induction of protein expression was performed as in Section 2.8.2 and cell pellets stored at -20^{o}C until required.

2.9 Protein purification

All protein purification procedures were carried out with an AKTA purification system (Amersham) at 4 ^{o}C. The cells were defrosted on ice and resuspended in lysis buffer (Table 2.3). Protease inhibitors 4-(2-aminoethyl) benzenesulfonyl fluoride hydrochloride (AEBSF) 50mg/ml, benzamidine 50 mg/ml, and L-transepoxysuccinyl-leucylamido-[4-guanidino]butane (E-64) 20 mg/ml, were also added to the solution. Lysis of cells was carried out using a sonicator (15 x 10 s bursts with 50 s cooling intervals). The lysate containing the His-tagged Hsp90 construct was centrifuged at 18000 rpm for 45 minutes. A sample for SDS-PAGE analysis (Section 2.10; Figure 2.2-2.8) was taken from the pellet, and the pellet was discarded in a sterile manner using Virkon. The supernatant (cytoplasmic

fraction) was loaded onto a pre-equilibrated (NickelA; Table 2.3) 5 ml HisTrap NiNTA column (GE Healthcare, UK). A sample of the supernatant was also taken for SDS-PAGE analysis. Following complete loading of cell lysate onto the HisTrap NiNTA column at a flow rate of approximately 0.5-1 ml/min, a 4% wash (of NickelB; Table 2.3) of 5 column volumes (cv) was carried out to remove non-specifically bound proteins. The bound protein of interest was eluted using a gradient of 100% NickelB (Table 2.3).

For the full-length Hsp90 and Sba1 constructs, protein-containing fractions were purified further using a pre-equilibrated (QsephA; Table 2.3) anion-exchange Q-sepharose column (GE Healthcare). The fractions obtained after nickel affinity purification were concentrated to a maximum final volume of 5 ml using a 10 kDa cut off Vivaspin concentrator and diluted 10-fold with ddH_2O in order to lower the imidazole concentration of the sample to approximately 50 mM allowing for binding to the Q-sepharose column. After loading of the diluted protein sample at a flow rate of approximately 1 ml/min, the protein of interest was eluted off the column using a NaCl gradient from 0.2 – 2 M (QsephB; Table 2.3).

For all constructs, fractions containing the protein of interest were concentrated to a maximum volume of 5 ml using a 10 kDa cut off Vivaspin concentrator and loaded onto a pre-equilibrated (SEbuffer; Table 2.3) Superdex 200 gel filtration column for size-exclusion chromatography.

Buffer exchange

For DEER analysis, all full-length Hsp90 and Sba1 protein samples were transferred into the appropriate buffer during the size-exclusion chromatography step (DEERbuffer; Table 2.3), and concentrated to approximately 150 µM using a 10 kDa cut off Vivaspin concentrator, and transferred into 50 µl aliquots (+ 10% sterile glycerol) into cryogenic vials for long term storage at -80°C until required.

Protein samples for ITC/NMR analysis were loaded onto a pre-equilibrated (cation+buffer, cation+triplebuffer, or Ca^{2+}buffer) HiTrap desalting column and concentrated to the required concentration using a 10 kDa cut off Vivaspin concentrator. At each stage of the purification process, the column flow through was monitored by UV detection at 280 and 254 nm, and a 15 µl sample was removed for SDS-PAGE analysis (Section 2.10; Figure

2.2-2.8). Samples were stored at 4°C for short-term storage or -80°C (+ 10% sterile glycerol) for long-term storage until required.

Purification step	Buffer(s)	pH
Lysis	50 mM Tris base, 100 mM NaCl, 20 % (w/v) glycerol 1mM BME*	8.0
HisTrap NiNTA (Nickel)	NickelA: 50 mM Tris base, 100 mM NaCl 1mM BME*	8.0
	NickelB: 50 mM Tris base, 100 mM NaCl, 500 mM imidazole 1mM BME*	8.0
Anion exchange	QsephA: 50 mM Tris base, 50 mM NaCl, 5 mM EDTA 1mM BME*	8.0
	QsephB: 50 mM Tris base, 2 M NaCl, 5 mM EDTA 1mM BME*	8.0
Size exclusion	SEbuffer: 100 mM Tris base, 200 mM NaCl, 5mM EDTA	8.0
	DEERbuffer: 20mM Tris base, 5mM $MgCl_2$	8.0
Buffer exchange	Cation+buffer: 20 mM Tris base + 5 mM $MgCl_2$ or 2mM $CaCl_2$ or 1mM $MnCl_2$	8.0 5.0,6.0,7.0,8.0,9.0
	Cation+Triplebuffer: 100 mM ACES, 50 mM Tris base, 50 mM Ethanolamine + 5 mM $MgCl_2$ or 2mM $CaCl_2$ or 1mM $MnCl_2$	8.0
	Ca^{2+}buffer: 20mM Tris base, 2 mM $CaCl_2$	

Table 2.3 Composition of buffers used for the purification of N-Hsp90, full-length Hsp90, and Sba1.

**Note: 1mM BME (β-mercaptoethnol) was only added to the buffers used for the purification of full-length Hsp90 mutants in order to prevent the oxidation of the newly introduced cysteine residues.*

2.9.1 Labelling of full-length Hsp90 constructs for DEER spectroscopy analysis

For DEER spectroscopy, full-length Hsp90 cysteine mutants were labelled with the highly reactive nitroxide, methanethiosulfonate spin label (MTSSL), which conjugates thorough its C-terminal thioester to the sulfhydryl group of cysteine residues (Figure 2.1). Protein samples were then incubated with MTSSL (dissolved in 100% DMSO (dimethyl sulfoxide)) in a 1:20 ratio of protein:MTSSL, and incubated overnight at 4°C to allow for efficient labelling of cysteine mutants.

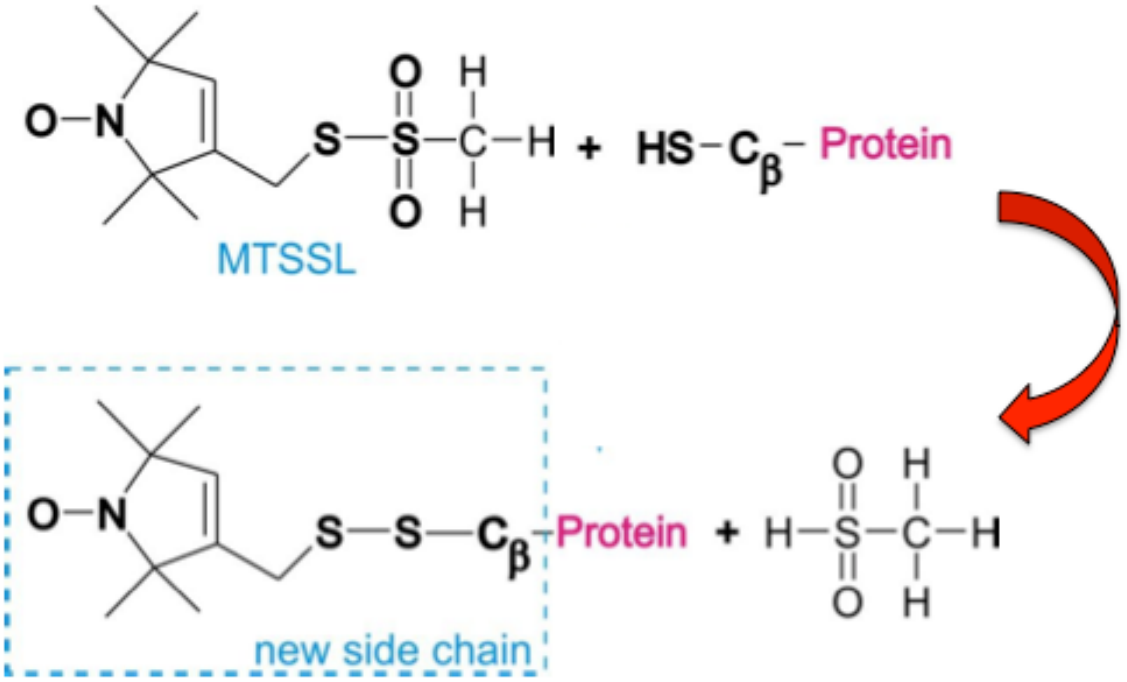

Figure 2.1 Schematic illustrating the MTSSL: Cysteine conjugation reaction.

Removal of excess spin label

Unbound spin label was removed by loading labelled protein samples onto a pre-equilibrated (DEERbuffer; Table 2.3) PD-10 desalting column, resulting in proteins that are larger than 5000 Da passing quickly through the column, and compounds smaller than 1000 Da such as MTSSL passing through the column more slowly.

The removal of excess MTSSL and the spin labelling efficiencies of the labelled protein samples were tested using cw-EPR (continuous wave) (Section 2.14), and the integrity of the Hsp90 dimer was tested by native PAGE analysis to confirm the presence of a dimeric Hsp90 species (Figure 2.7b).

2.10 PAGE analysis

2.10.1 SDS-PAGE

SDS-PAGE allows proteins to be separated according to size. Prior to loading protein samples onto a 10% SDS polyacrylamide gel (composition shown in Table 2.4), samples were denatured by negatively charged SDS in the loading buffer (2X SDS loading buffer: 62.5 mM Tris-HCl pH 6.8, 0.01 % bromophenol blue, 25 % SDS, and 25 % glycerol). A reducing agent such as BME (β-mercaptoethanol, also called 2-mercaptoethanol) or DTT was added to the sample to prevent disulphide formation. Complete denaturation of protein samples was achieved by following with heating at 95°C. Protein samples were centrifuged at 13500 rpm for 1 minute to pellet any aggregates that may have formed. The concentration of acrylamide determines the percentage of the composed gel, whereby a higher percentage gel creates a higher degree of resistance for the migrating proteins. A higher percentage gel allows for the resolution of small proteins and a lower percentage gel allows for the resolution of larger proteins. Samples were prepared in a 2:1 ratio of sample to 2X loading buffer.

Electrophoresis was carried out using MiniProtean II gel apparatus (Biorad) connected to a PowerPac 300 power supply (Biorad). Gel running buffer (14.4 g/l Glycine, 3.03 g/l Tris

base,1 g/l SDS) was used to fill both inner and outer chambers of the gel apparatus. Unstained Precision Plus protein standards (Biorad) were used as molecular weight markers unless otherwise stated. Polyacrylamide gels were electrophoresed at a constant voltage of 120 V for 75 minutes.

Reagents	Stacking gel (ml)	Resolving gel (ml)
30% acrylamide	0.5	1.7
H2O	2.0	2.55
3M Tris (pH 8.8)	1.0	0.625
10% SDS	0.040	0.050
10% ammonium persulphate	0.1	0.0375
Temed	0.005	0.010

Table 2.4 Composition of 10% SDS Polyacrylamide gel[57]

Following electrophoresis the gel was stained in a solution containing a Coomassie dye (40% methanol, 10% acetic acid, 50% dH_2O, 0.5 g/l coomassie brilliant blue), followed by heating for 30 seconds in a microwave, and left gently shaking for 15 minutes. Protein bands were visualized by washing the gel in a de-staining solution (40% methanol, 10% acetic acid, 50% dH_2O), followed by heating for 30 seconds in a microwave, and left gently shaking until protein bands were clearly visible with minimal background.

2.10.2 Native PAGE

Native-PAGE allows for the separation of proteins according to size in the native states. The setup of this type of PAGE is the same as for SDS-PAGE, however the loading buffer used to prepare samples differs in composition by a the lack of the SDS component. In addition, reducing agent was not added to the protein samples as Native-PAGE serves to observe the protein in its intact native set, allowing one to visualise the presence of potential higher order species.

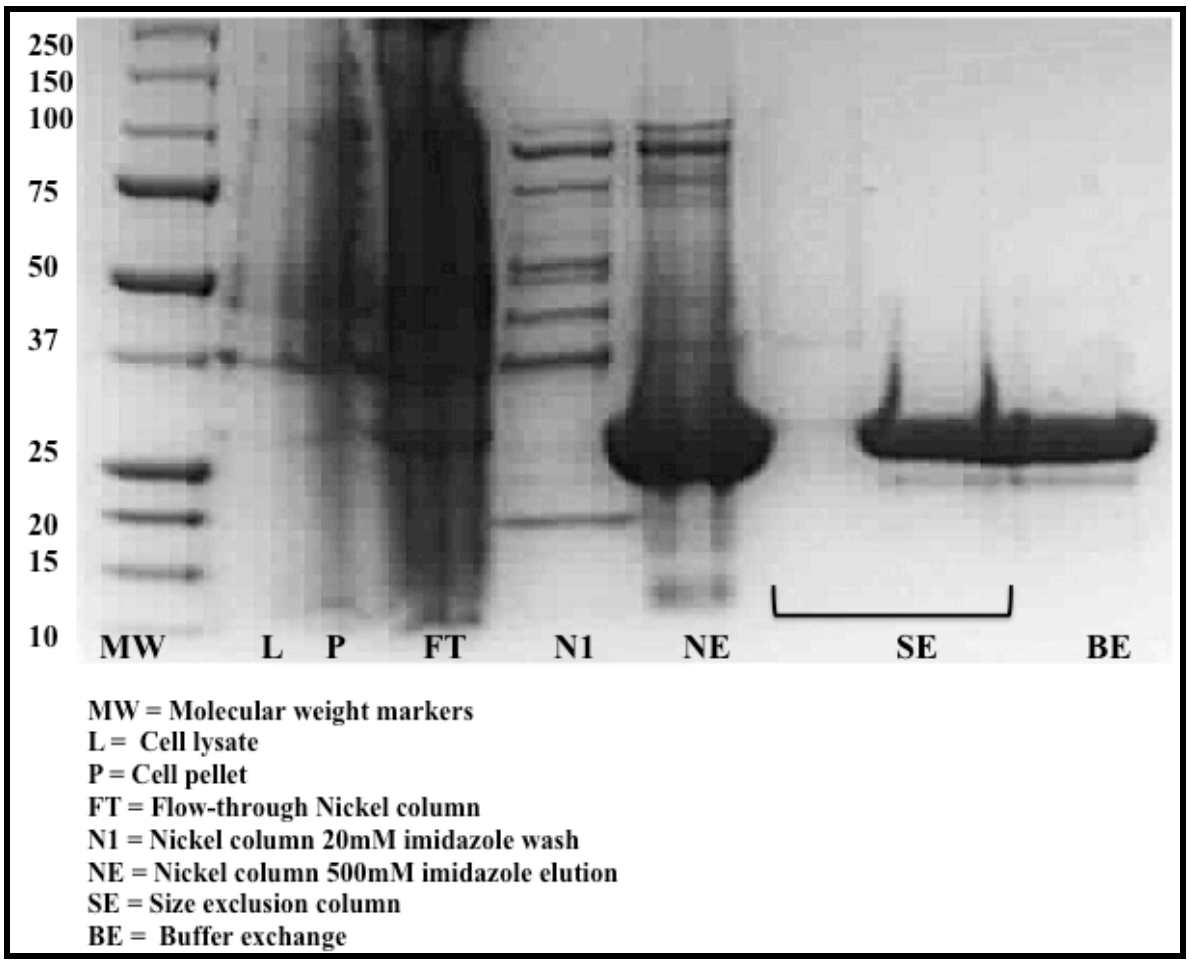

Figure 2.2 N-Hsp90 SDS-PAGE gel analysis of the purification of N-Hsp90.

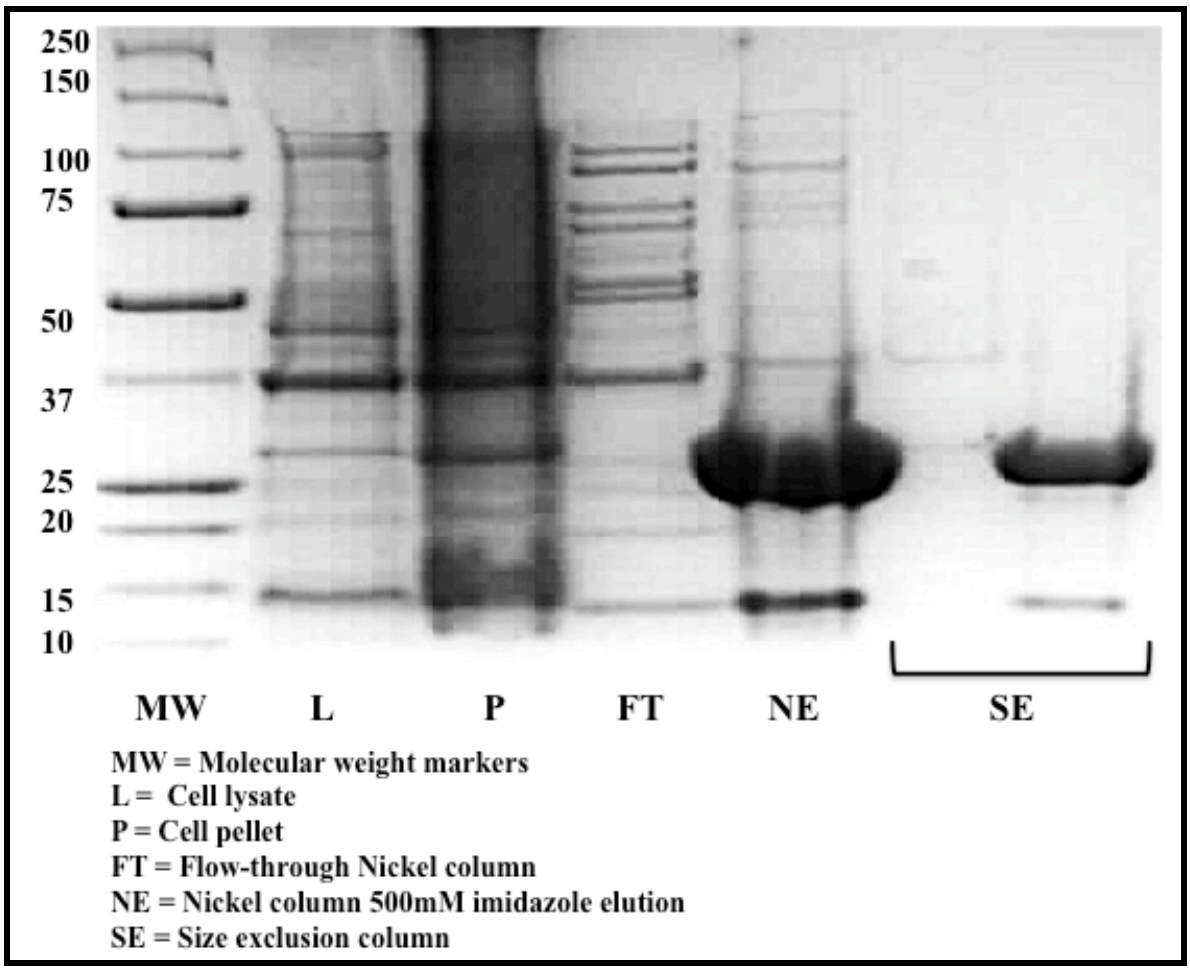

Figure 2.3 SDS-PAGE gel analysis of the purification of the N-Hsp90 mutant, T22I.

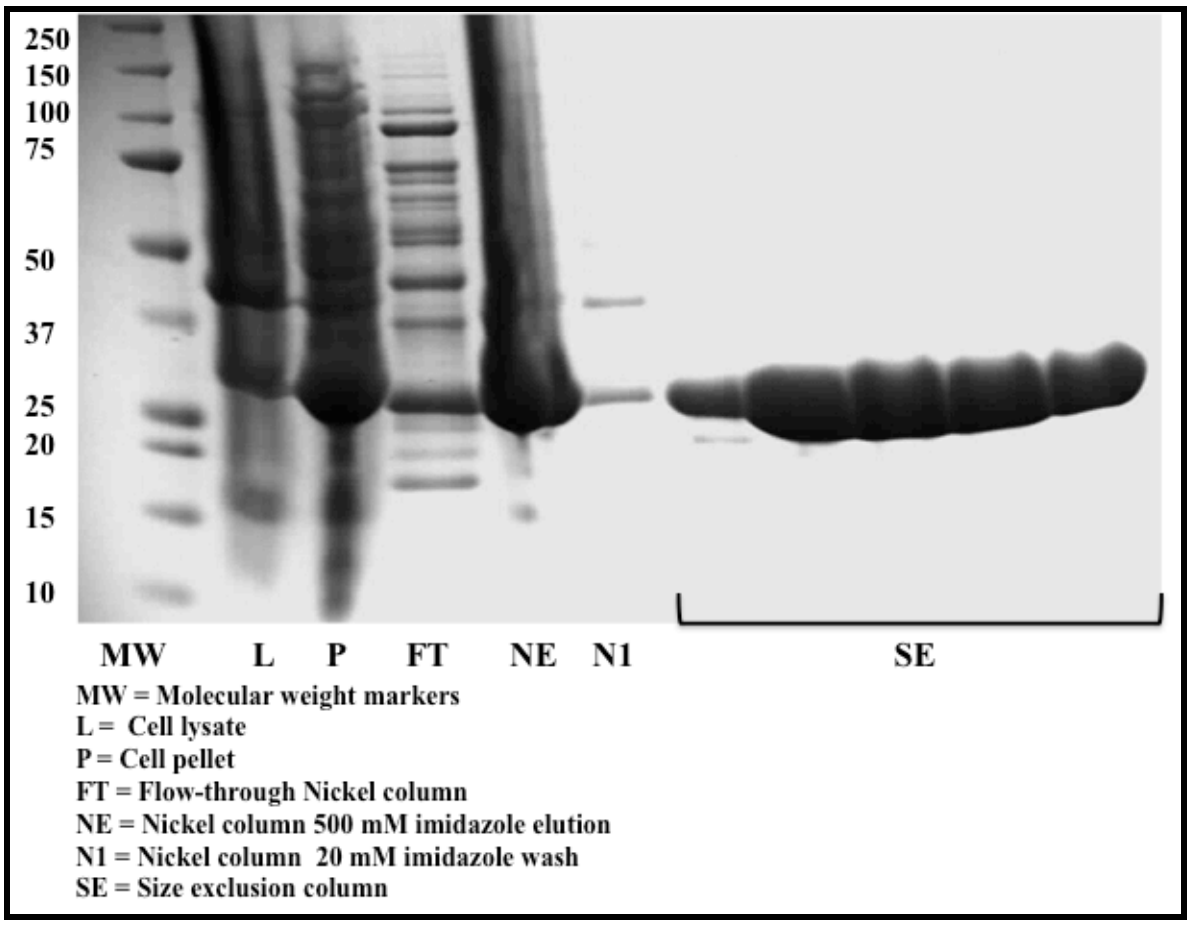

Figure 2.4 T101I SDS-PAGE gel analysis of the purification of the N-Hsp90 mutant, T101I.

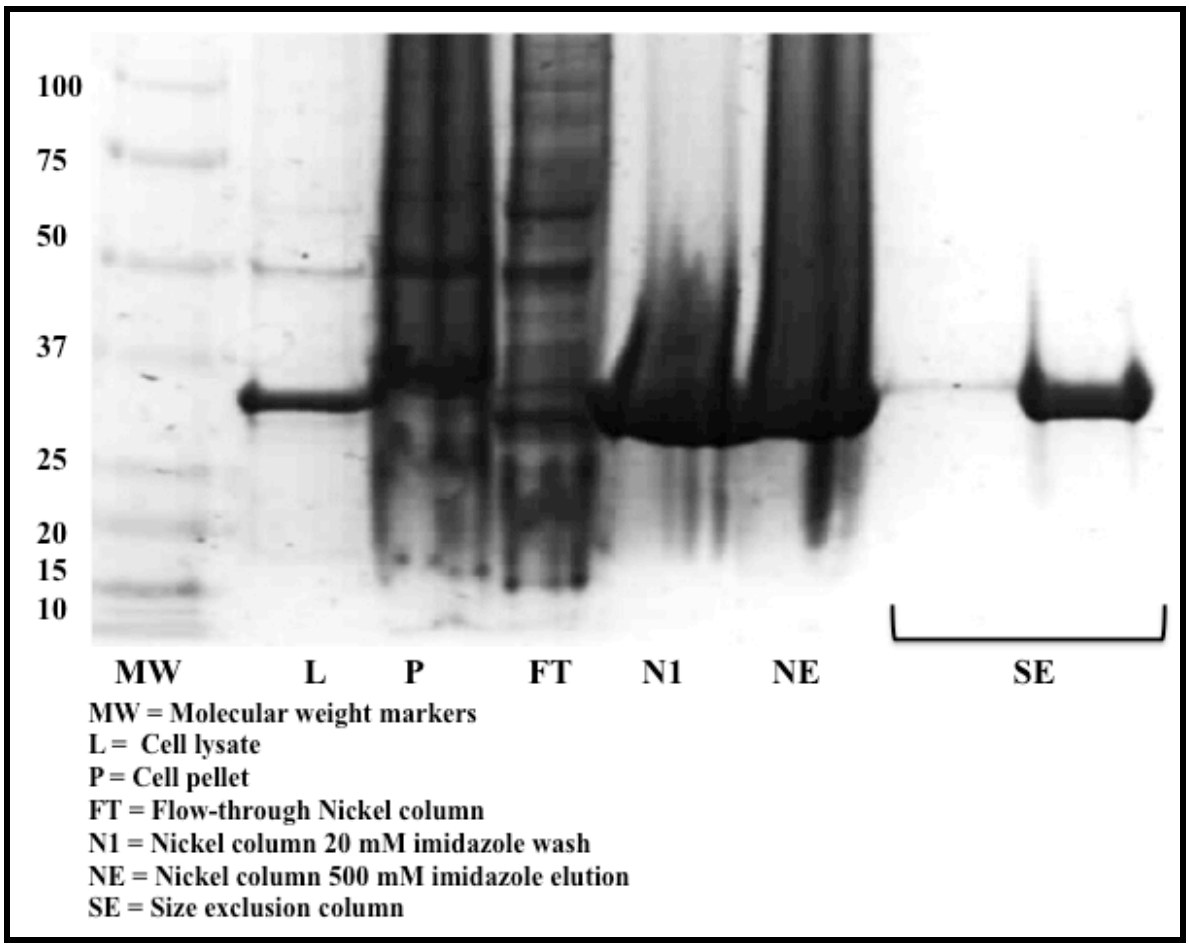

Figure 2.5 SDS-PAGE gel analysis of the purification of the N-Hsp90 mutant, G153A.

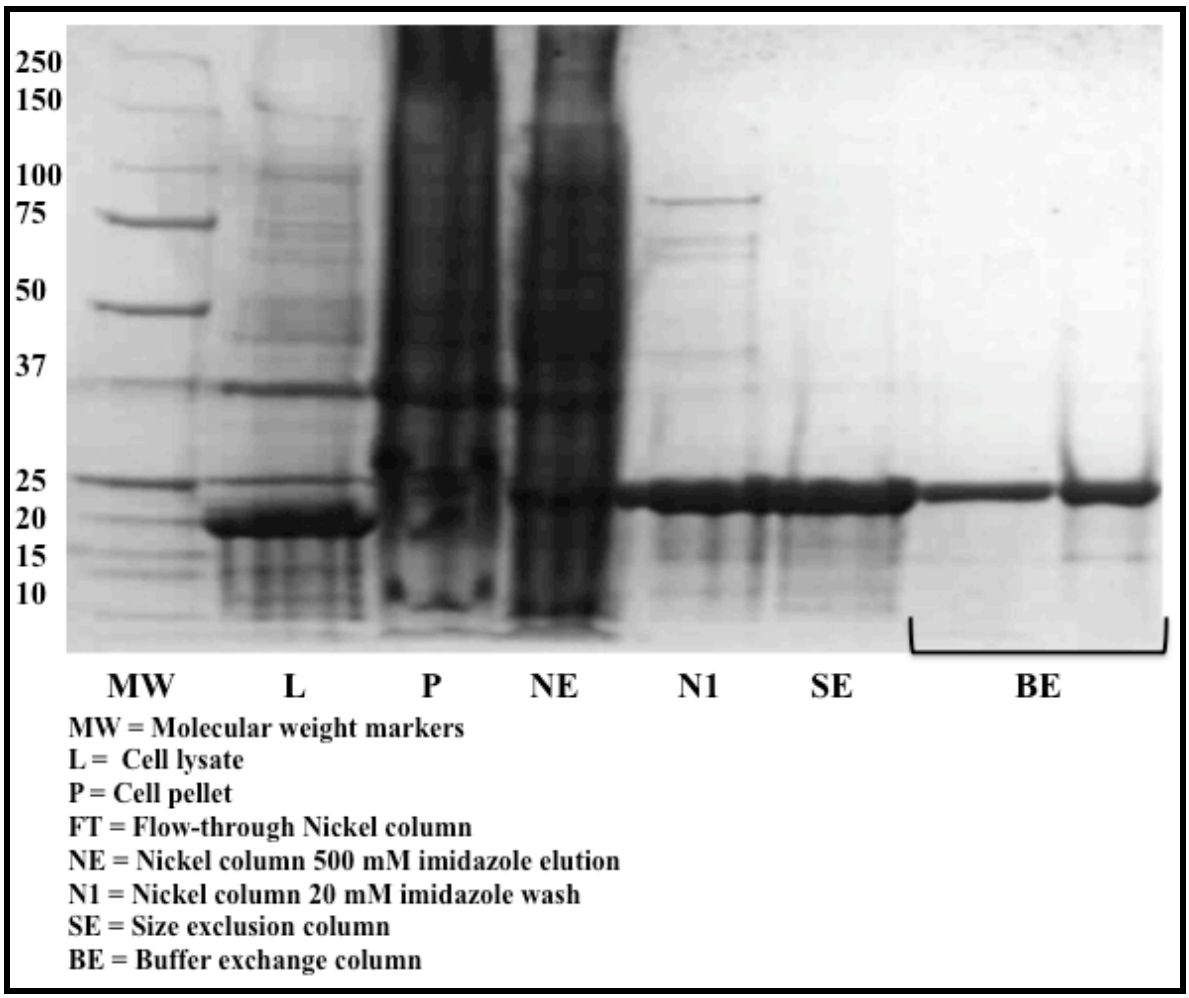

Figure 2.6 SDS-PAGE gel analysis of the purification of the N-Hsp90 mutant, G154A.

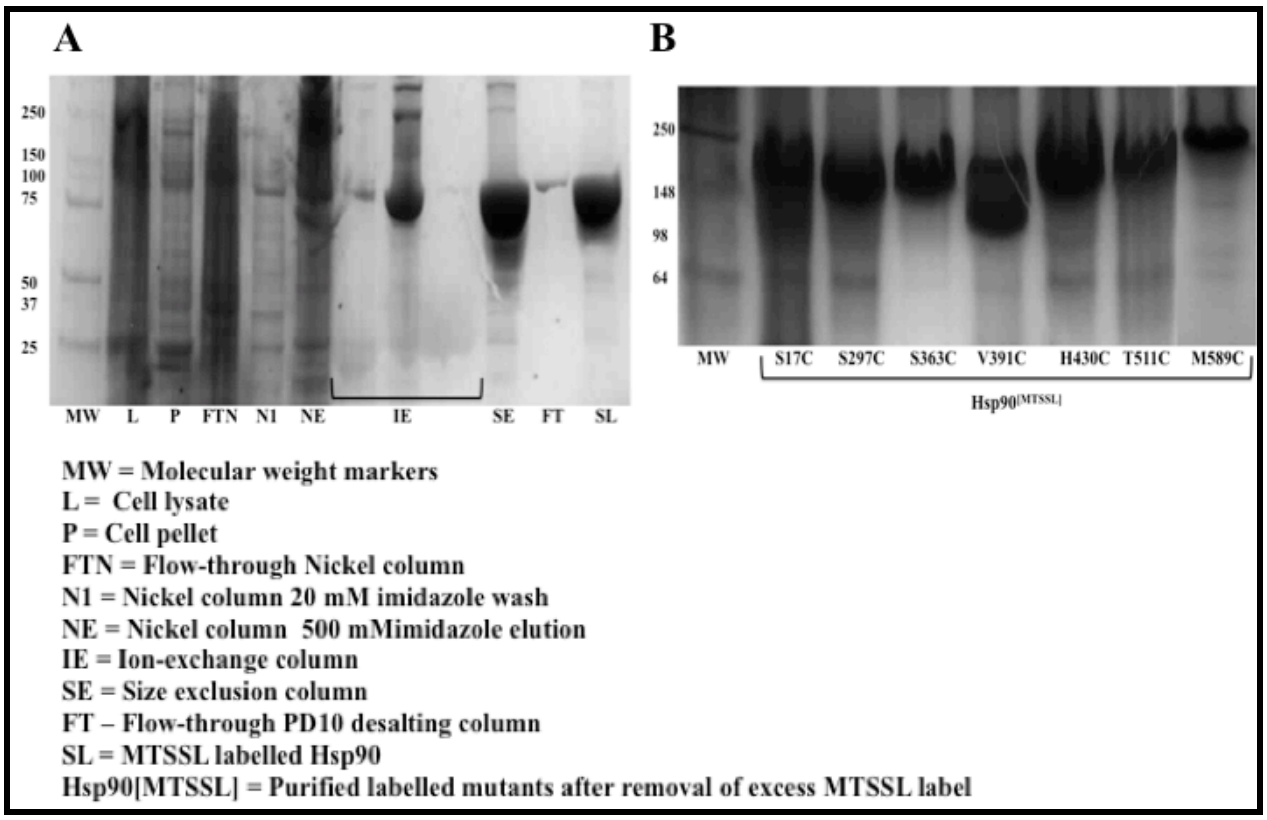

Figure 2.7 A, PAGE gel analysis of the purification of the Hsp90$^{[MTSSL]}$ mutants; one representative gel for all mutants as purification profiles were identical. **B*** ***(see below)*****,** Native PAGE gel analysis (under non-reducing conditions) of the final purified product for the Hsp90$^{[MTSSL]}$ mutants, showing the presence of a dominant dimeric Hsp90 with a small population of monomeric Hsp90.

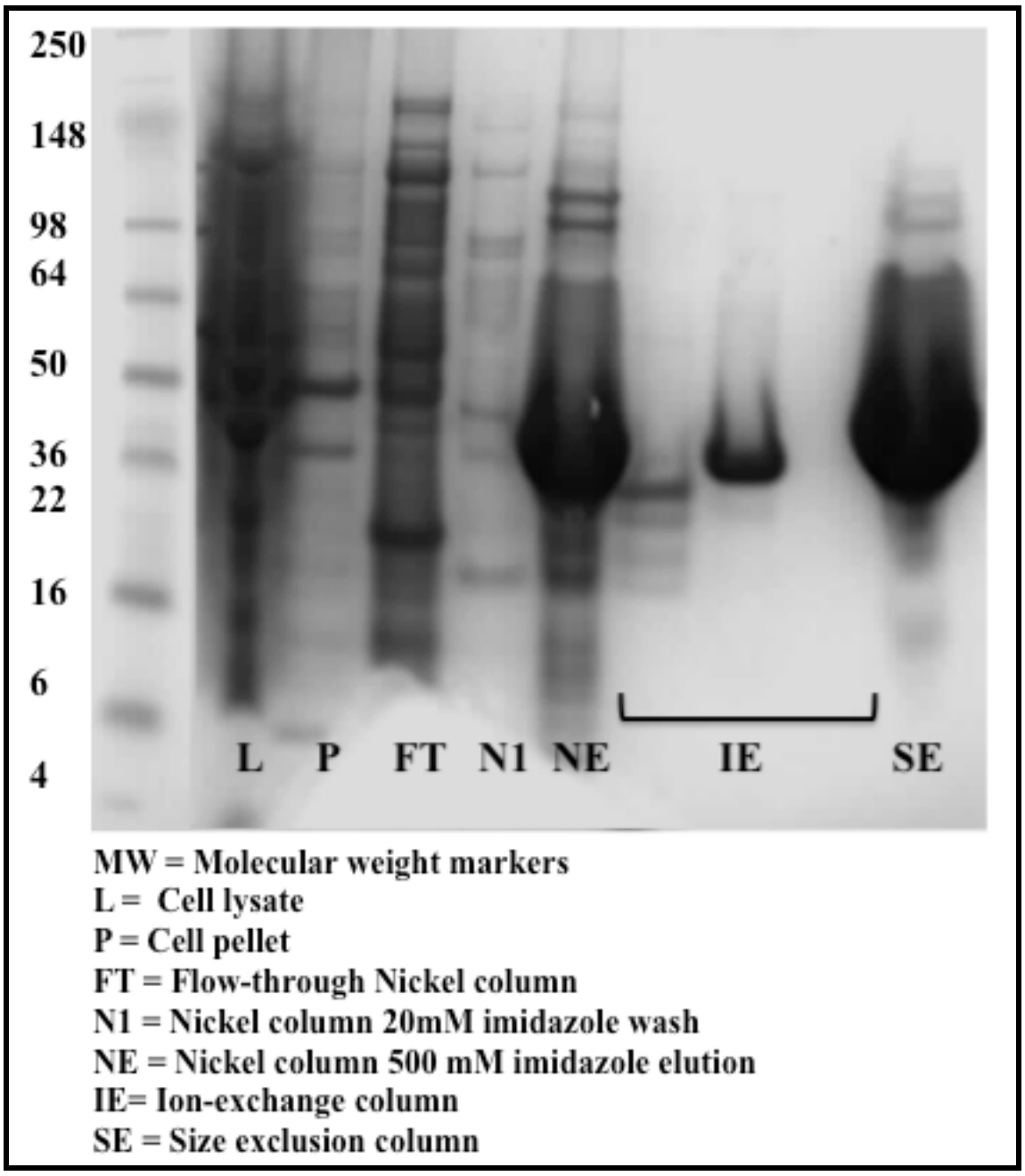

Figure 2.8*[(see below)] SDS-PAGE gel analysis of the purification of Sba1/p23.

**Note: the protein marker used in these instances was SeeBlue® Plus2 Pre-Stained Standard (Invitrogen).*

2.11 Determining protein concentration

Protein concentrations can be determined using the BioRad (BioRad) protein assay kit following the manufacture's protocol. This assay is derived from the Bradford method[58] and is based on the colour change of the Coomassie Brilliant Blue G-250 dye upon binding to the amino acid residues arginine, tryptophan, tyrosine, histidine, and phenylalanine. Free dye in solution has a absorption maxima at 470 and 650 nm, but when bound to protein has an absorption maximum at 595 nm. The colour change can therefore be quantified at 595 nm with a spectrophotometer and protein concentration determined by reference to a standard curve obtained with bovine serum albumin (BSA).

2.11.1 Absorbance spectra and measurement of protein concentration

UV-visible absorption spectra of the proteins were measured in a 1 ml quartz cuvette using a CARY100 Bio UV-Visible spectrophotometer. The molar extinction coefficient and molecular weight was calculated based on the amino acid sequence of the various protein constructs and are listed in Table 2.5. Protein concentrations were calculated using the Beer-Lambert law (Equation 2.1), which states that the absorbance at light at a specific wavelength (280 nm for proteins and 260 nm for nucleic acids) is directly proportional to the concentration of the protein/nucleic acid sample.

$$A_{280} = \varepsilon_{280}.C.l$$

A_{280}: the absorbance of the protein
ε_{280} : the molar extinction coefficient ($M^{-1}cm^{-1}$)
C : the protein concentration (M)
l : the path length (cm)

Equation 2.1

Protein construct	Molar extinction coefficient ($M^{-1}cm^{-1}$)	Molecular weight (k Da)
Wild-type N-Hsp90	14440	22.9
N-Hsp90 mutants: T22I,T101I,G153A,G154A	14440	23.0
Dimeric full-length Hsp90$^{[MTSSL]}$	114,600	155.4
Sba1	29910	26.5
AMP-PNP	14600	
ADP	14600	

Table 2.5 Predicted molar extinction coefficients and molecular weights of all protein samples and nucleotide ligands used in the thermodynamic and structural analysis of Hsp90.

2.12 Isothermal titration calorimetry (ITC)

Isothermal titration calorimetry (ITC), directly measures the heat or change in enthalpy (ΔH) evolved or absorbed as a result of the association between a 'ligand' and its 'macromolecule'. The syringe containing the ligand is titrated into the cell containing the macromolecule. The result of the additon of the two compoents within the syringe and cell results in heat either being evolved (exothermic) or absorbed (endothermic) within the sample cell. The release or absorption of heat is directly measured of the macromolecule on going from the free to the ligand bound state. When the macromolecule in the cell becomes fully saturated with ligand, the heat signal diminishes until only the background heat of dilution is observed. The heat of dilution is the heat that is released or absorbed as a result of the sample within the syringe being introduced into the buffer in which the macromolecule is contained within the cell.

A VP-ITC microcalorimeter (Microcal, Northampton, MA) was used to carry out all ITC experiments for this study, and Origin 7.0 (OriginLab, Nothampton, MA) was the software utilised to analyse the raw data. All experimental data obtained from the ITC titrations were fit using a non-linear least squares curve-fitting algorithm with three floating variables: stoichiometry, association constant ($K_a = 1/K_d$), and the change in enthalpy of the interaction.

The ITC experiment allows for the determination of the apparent equilibrium association constant (K_a; this term is equal to the inverse of the apparent equilibrium dissociation constant, i.e. $=1/K_d$) to be calculated. Based on the known concentration of the interactants the stoichiometry of the interaction (n)[59] can be calculated on fitting the binding isotherm to an appropriate model. The K_a obtained from an ITC experiment can then be used to calculate the change in entropy (ΔS) and the Gibbs free energy (ΔG). The relationship between ΔG and K_a is described by Equation 2.2, where *R* is the gas constant (8.134 J K^{-1} mol^{-1}) and *T* is the absolute temperature in degrees Kelvin. ΔG is also related to the ΔH and ΔS as shown in Equation 2.3.

$$\Delta G = -RT\ln K_a \qquad \textbf{Equation 2.2}$$

$$\Delta G = \Delta H - T\Delta S \qquad \textbf{Equation 2.3}$$

The ability of an ITC experiment to accurately obtain the binding constant is critically dependent upon the accurate determination of the concentrations of both the ligand and the macromolecule solutions. It is believed that the accuracy of thermodynamic information is largely dependent on the Wiseman (*c*) parameter, which is a unit-less parameter. The shape of an ITC binding isotherm changes according to the product of the association constant (K_a) and the (macromolecular) receptor concentration $[M]_t$ as shown in Equation 2.5, and they called this the *c* value, where *n* is the number of binding sites per receptor M[60].

$$C = K_a [M]n \qquad \textbf{Equation 2.5}$$

If the *c* value is less then ca.10, it is thought to lower the accuracy of the thermodynamic parameters obtained from an ITC experiment, and therefore the ITC experiment is limited for the use of high affinity systems. The accurate determination of the binding constant requires that the *c* value lies in the range 1-1000. Often, interactions with a strong affinity result in a sharp isotherm yielding a large *c* value, and one is unable to accurately determine K_a as the transition is too sharp and there are too few points to accurately fit the data. On the other hand, extremely weak interactions yield an isotherm that is close to linear whereby the heats od association are too small, and therefore the software again is unable to accurately fit the data[59].

All ITC binding studies with Hsp90 were carried out on the N terminal domain constructs detailed in Section 2.1 under a constant temperature and pressure in order to obtain the relevant thermodynamic parameters. Both protein sample and nucleotide ligand solutions were adjusted for any pH discrepancy and, in addition, both sample components were de-gassed prior to loading into the appropriate sample chamber according to the Microcal instructions. A purified protein sample of approximately 100 μM in an appropriate buffer (Table 2.3) was placed (using a 2 ml Hamilton syringe (Hamilton, Nevada)) into the sample cell, which has a cell volume of approximately 1.5 ml. The various nucleotide ligands were dissolved in the same buffer of the protein sample for a specific titration, and placed into the sample syringe, which has a volume of approximately 300 μl; the nucleotide ligands were used at a concentration that was 10-fold higher than of the protein sample to compensate for dilution during the course of the titration. Prior to the start of the titration, the sample cell containing the protein sample was allowed to equilibrate to the relevant temperature with the reference cell. The reference cell functions as a temperature reference, in that it is filled with water and serves to maintain a constant temperature with the sample cell containing the macromolecule. Each was carried out at a range of temperatures between 8 – 25 °C. N-Hsp90 wild-type and mutant constructs were tested with both ligands and all divalent metal ions. The ITC experimental parameters were set to 20 injections per titration with an initial injection of 2μL, followed by 19 injections of 15μL. The spacing interval parameter between each injection was set to 120 s for the first injection point followed by 19 injections at 240 s spacing intervals. All experiments were carried out at a constant pressure by using a closed ITC calorimeter. A reference power of 15 μcal/s, and a constant stirring speed of sample components of 300 rpm was used in all cases. Each titration was subsequently followed by a heat of dilution titration whereby the ligand was injected into the sample cell containing buffer alone (no protein). The data from this experiment was incorporated into the protein/ligand experimental data in order to yield the heat of the interaction itself.

2.12.1 Heat capacity

ITC experiments performed at different temperatures are together able to yield the change in the heat capacity (ΔC_p) of an interaction, which is defined by Equation 2.6 where *d* is the 'difference' in the associated parameter, and T is the absolute temperature.

$$\Delta C_p = d\Delta H/dT \qquad \textbf{Equation 2.6}$$

The change in constant pressure heat capacity is directly related to the change in enthalpy of a system with respect to temperature, therefore if ΔH is plotted against temperature for a number of titrations, the slope of the graph defines the ΔC_p[61]. Determining the change in heat capacity of a biomolecular system has the potential to provide a link to structural characteristics for the interaction due to the observed empirical correlation between ΔC_p and the buried surface area upon complex formation[62,63].

Changes in the heat capacity of a system can be the result of a number of contributing factors. The primary contribution is derived from the vibrational frequencies and internal rotations arising from variation in the degrees of freedom of each valence bond; therefore a change in the degrees of freedom of the interacting bonds will in turn affect the energy contribution required to raise the temperature of the system[62]. Gomez *et al.*[64] stated that the heat capacity of proteins is larger in solution than with that of the anhydrous protein or the unfolded protein, which indicates that the hydration of the protein molecule contributes positively to the heat capacity dependent upon the protein structure. Furthermore, this observation suggests that since the native hydrated protein exhibits a larger contribution to the heat capacity to that of the hydrated unfolded protein, the residues within the interior of the protein are those responsible for the discrepancy observed. The latter observation is related to the burial of the overall surface area of the protein chain that is the exposed and the solvent accessible polar and non-polar surface areas (SASA). Since the solvent exposed surface area of a native protein is generally composed of approximately 55% non-polar area, a positive contribution to the heat capacity of a system upon hydration is inevitable.

As mentioned above, the change in heat capacity is able to distinguish between hydrophobic and hydrophilic hydration, both of which result in a decrease in entropy due to

the release and/or displacement of water molecules at the protein-ligand interface, however result in completely opposite ΔC_p[65], whereby the hydration of non-polar surface is accompanied by a positive ΔC_p and hydration of polar surface is accompanied by a negative ΔC_p. The overall change in heat capacity can be the result of many contributing factors in a ligand binding reaction, however it is generally associated with gross changes of a system on going from the free state to the ligand bound state. Generally, upon complex formation, a negative change in heat capacity is observed as a result of the system moving to a state of greater order or favourable entropy[36,66]. However complex formation results in a wide array of 'side-effects', such as the release or sequestering of solvent molecules at the binding interface, changes in the protonation state of the protein or ligand, specific ion binding, and conformational change, all of which can have an affect on the observed ΔC_p[19].

2.13 Nuclear magnetic resonance spectroscopy

The nuclear magnetic resonance (NMR) spectra: [^{1}H,^{15}N] HSQC were acquired at a proton frequency of 700MHz on the Bruker Avance III spectrometer. All NMR experiments were set up with the help of Dr Eleanor Williams, using a 0.1 mM [^{1}H, ^{15}N]-labelled Hsp90 N terminal domain protein sample in the Cation+buffer containing $CaCl_2$ (Table 2.3). The sample contained 5% (v/v) D_2O to allow a frequency lock to adjust for drift in the magnetic field over the time course of the titration. All samples contained 0.02 % sodium 2,2-dimethyl-2-silane-pentane-5-sulphonate (DSS; w/v) to allow for chemical shift referencing recorded spectra to one another. The sample was placed in a standard 5 mm NMR tube (Wilmad Glass Co.Inc.). The bulk water signal was suppressed usin 'Watergate' or 'presaturation' methods. The protein sample was titrated with 50 µM increments of the nucleotide ligand AMP-PNP until a final nucleotide concentration of 1 mM was added to the protein sample.

NMR data was processed using NMRPipe spectral processing and analysis system[67] and viewed using NMRDraw. Processed data were converted to AZARA format and analysed using Collaborative Computing Project for NMR (CCPNMR) Analysis software v.2.1.3[68]. Chemical shifts were referenced to DSS. Peaks were picked either automatically using the CCPN software and subsequently edited by hand, or picked by hand entirely.

2.14 Electron paramagnetic resonance spectroscopy

A form of EPR spectroscopy, double electron electron resonance spectroscopy (DEER) was used to investigate the conformational transitions associated with nucleotide binding to full-length Hsp90, whereby various positions along the length of Hsp90 were labelled with the nitroxide spin label MTSSL (described in Section 2.9.1). DEER samples were used at a total volume of 50 µL at a concentration ratio of approximately 150:400 µM $Hsp90^{[MTSSL]}$ to ligand respectively. Samples were prepared by mixing $Hsp90^{[MTSSL]}$:ligand with 10% sterile glycerol and transferred into a quartz capillary of 2 mm inner diameter followed by freezing of the samples in liquid nitrogen immediately before placing into the sample resonator.

The spin labelling efficiency of each Hsp90 mutant was calculated by measuring the *cw*-EPR spectrum of the individual $Hsp90^{[MTSSL]}$ mutants and using the derived spectrum to calculate the second integral using the known protein concentration of each mutant as shown in Figure 2.9.

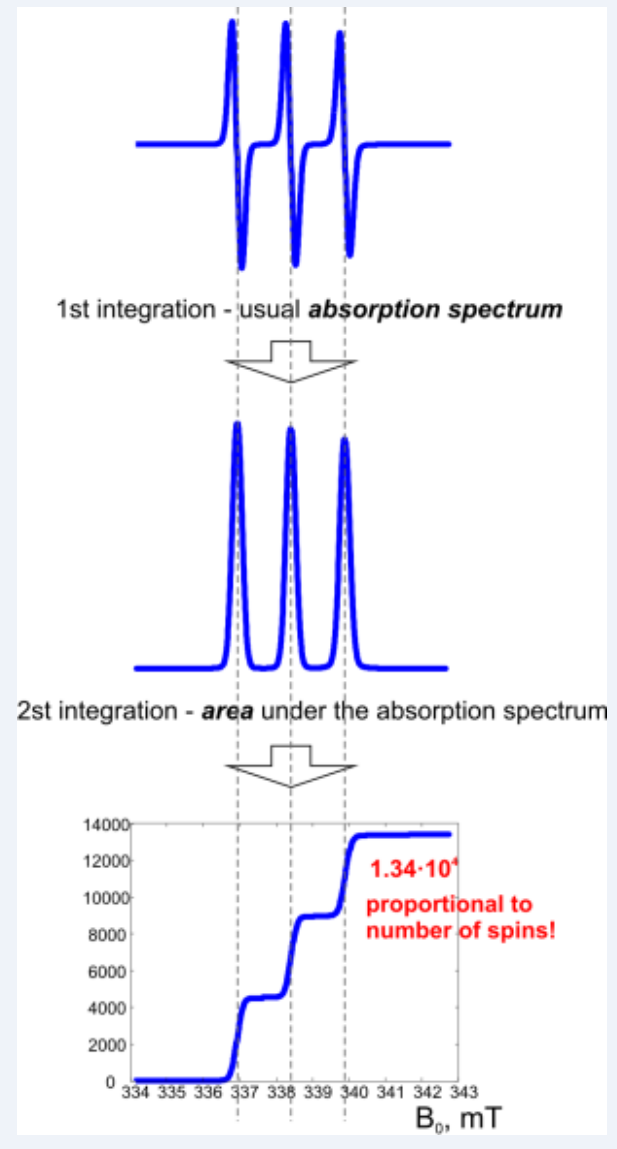

Figure 2.9 Double integral analysis of a nitroxide spectrum for the calculation of the spin labelling efficiency.

DEER measurements were performed at 50 K on a Bruker ELEXSYS E580 spectrometer operating at 9 GHz equipped with an ER-4118-X-MS-3W resonator. The four-pulse DEER sequence was chosen with $\pi/2(\nu_{obs})$-τ_1-$\pi(\nu_{obs})$-τ'- $\pi(\nu_{pump})$-$(\tau_1+\tau_2-t')$- $\pi(\nu_{obs})$-τ_2-*echo,* where the observe pulse length was 16 ns for π/2 and 32 ns for π pulses. The pump pulse length was 12 ns, the long interpulse delay was τ_2 = 3.2 µs. All other parameters were used according to Pannier *et al.*[69]. The DEER spectra were analysed using the program DeerAnalysis2011[70]. The background was corrected by a homology 3-dimensional fit.

Simulations were checked for stability according to the DEERAnalysis2011 manual. The technique of DEER spectroscopy is based on the dipolar interaction of two spin populations, when one spin population has been excited by a microwave pulse of different microwave frequency. The frequency *v* of the modulation amplitude of the spin population being excited is inversely proportional to the cube of the distance *r* between the two spin labels, as given in Equation 2.7.

$$\nu(r) = \frac{52.04 \text{ MHz nm}^{-3}}{r^3}$$

Equation 2.7

2.14.1 Rotamer Library Analysis (RLA)

In order to elucidate information on the possible relative orientations of the nitroxide spin labels and the distances between these possible orientations, a semi-dynamic structural model of the spin label can be used. In this model the dynamics of the spin label is represented by a discrete set of possible rotational isomers (rotamers). The program used in this work was kindly provided by Polyhach *et al.*[71]. Conformational structures of MTSSL were provided in a rotamer library, containing 98 MTSSL rotamer structures. The structures of the library had been generated by systemic variation of dihedral angles of MTSSL attached to a single cysteine residue. These determined structures of MTSSL can be attached to a specific position in a protein model, such as X-ray crystal structure obtained from the Protein Data Bank (PDB). The set of possible rotamers on the selected position is determined by calculating the probability of each particular rotamer of the library to occur in the protein structure. These probabilities are influenced by spatial restrictions of the MTSSL side chain due to its local environment defined by other protein atoms. Therefore, the free energy for each rotamer is computed considering the interaction between atoms of the label and atoms of the protein using a Lennard-Jones potential parameterised by an optimised potentials for liquid simulations (OPLS) force field. The Lennard-Jones potential takes the repulsion (clashes) and vanderWaals attraction of spin label and protein atoms into account.

The rotamer analysis was performed using the Hps90-AMP-PNP-p23 crystal structure (PDB: 2CG9) incorporating all residues that were present in the construct used in the

DEER studies (Section 2.1). The predicted distances based on the RLA analysis are discussed in detail in Chapter 5.

Chapter 3

Thermodynamic investigation of small ligand binding to N-Hsp90

3.1 Introduction

As discussed in Chapter 1, the binding of ATP to the Hsp90 dimer has been demonstrated to result in numerous conformational changes in order to form the fully bound ATP state of the chaperone, allowing ATP hydrolysis to then take place. As observed in previous studies, the binding of ATP not only induces conformational changes within the N-terminal domains of the Hsp90 dimer, but appears to be important in dictating conformational dynamics throughout the entire chaperone molecule. Therefore, investigating the binding of nucleotides to N-Hsp90 is crucial for providing an understanding of the biology and potentially informing the design of small molecules developed as therapeutics against this diverse chaperone.

Research on Hsp90 has so far yielded two crucial structures which would potentially represent the ATP bound N-terminally 'closed' Hsp90 complex[16], and the N-terminally 'open' ADP bound complex[7]. Other, more recent research, have focused on determining the ATP cycle of Hsp90 and its various conformational states using fluorescence resonance energy transfer (FRET)[11]. However, potential effects associated with the interaction of the Mg^{2+} ion in the ATP binding site has not been investigated in detail. This is surprising, as the absence of this ion results in no association of ATP to N-Hsp90. There are clear implications of the existence of conformational states which may not have been addressed in these studies due to factors such as limitations of the chosen experimental techniques. Therefore understanding the magnitude of motional changes this dynamic chaperone undergoes requires more information than of that provided by kinetic studies and static crystal structures.

This chapter describes the thermodynamic profiles involved in the interaction between N-Hsp90 and two adenine-containing nucleotides; the non hydrolysable

analogue of ATP, AMP-PNP (5′-(β,γ-imido) triphosphate) and ADP (adenosine 5′-diphosphate).

Isothermal titration calorimetry (ITC) was used to determine the thermodynamic parameters of these interactions. As discussed in Chapter 1, the transfer of heat either to or from the surroundings (exothermic or endothermic, respectively) between interacting molecules can be obtained via ITC. Such data can be used to quantify the change in enthalpy, $\Delta H°_{obs}$, the binding constant, K_a (=1/K_d), and the stoichiometry, *n*. The overall change in free energy, $\Delta G°_{obs}$, and entropy, $\Delta S°_{obs}$, can also be derived using the equation stated in Chapter 1. These parameters can all provide important information on the nature of the binding event and provide an insight to structural effects of binding by measuring the heat capacity change ($\Delta Cp°_{obs}$) associated with a given interaction. As discussed in Chapter 1, the removal of protein surface area from exposure to solvent upon ligand binding has been to shown to lead to negative $\Delta Cp°_{obs}$ values. The binding of AMP-PNP and ADP to N-Hsp90 leads to positive and negative $\Delta Cp°_{obs}$ (respectively)[19]. The observation of the binding of a small ligand to the same binding site resulting in completely opposite $\Delta Cp°_{obs}$ is unique. Furthermore, the positive $\Delta Cp°_{obs}$ observed upon AMP-PNP binding to N-Hsp90 is more pronounced when the native Mg^{2+} ion is substituted for another divalent ion.

This chapter focuses on the thermodynamic profiles of the nucleotide interactions with different divalent ions and the associated change in heat capacity effects. A detailed study focusing on the various effects which could give rise to a positive heat capacity change including the effect of opening and closing of the ‘ATP lid’ is investigated in order to determine the underlying cause of conformational changes.

3.2 Thermodynamic profiles of the interactions of N-Hsp90 with two adenine-containing nucleotides, AMP-PNP and ADP

ITC was used to measure the interactions of AMP-PNP and ADP with N-Hsp90 at different temperatures between 8–25 °C; the fitted isotherms for these interactions are shown in Figures 3.1 and 3.2.

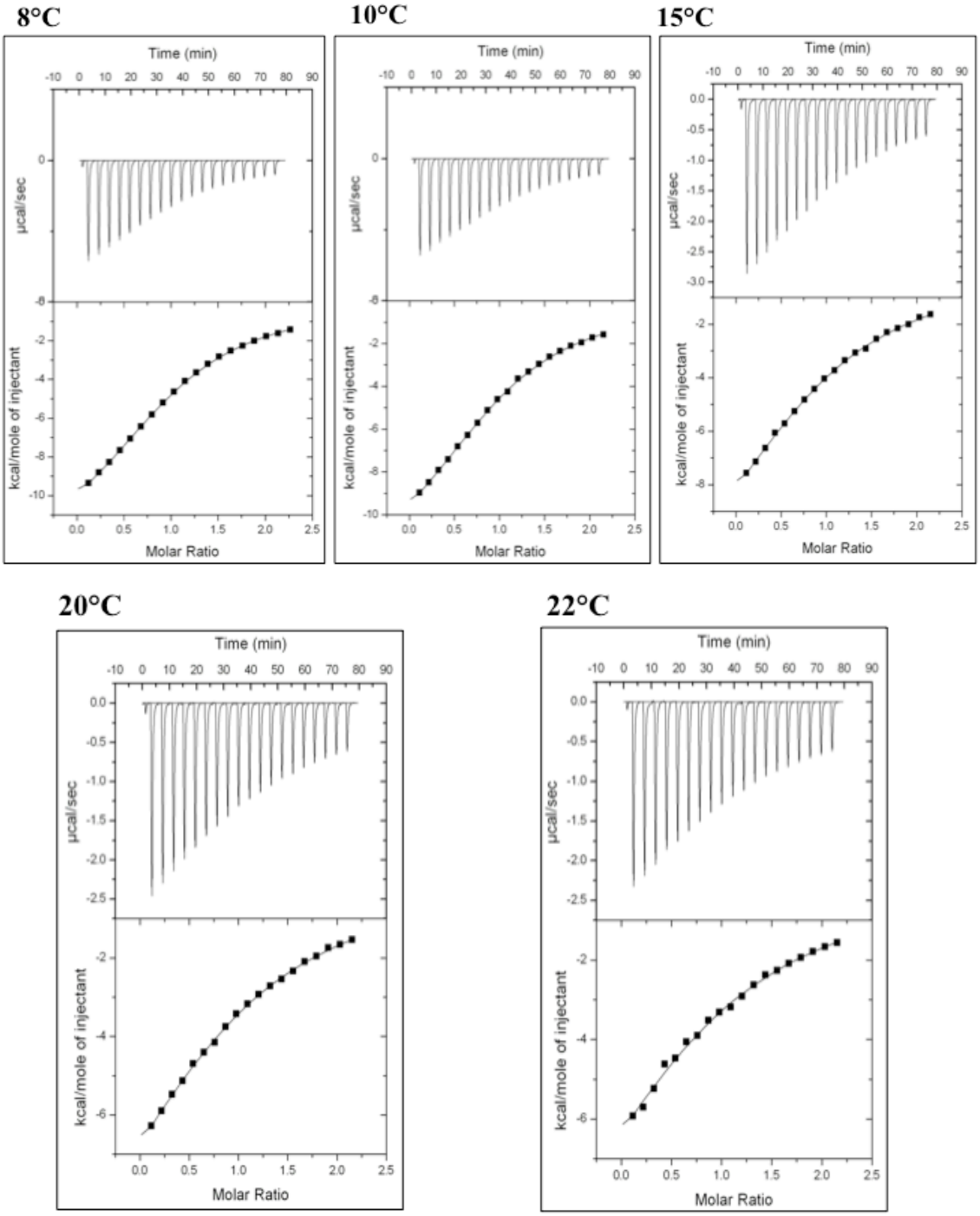

Figure 3.1 Raw and fitted data of the titration between N-Hsp90 and AMP-PNP in the presence of $MgCl_2$ at a range of temperatures between 8–22°C. The black line represents the least squares fit to a single-site binding model.

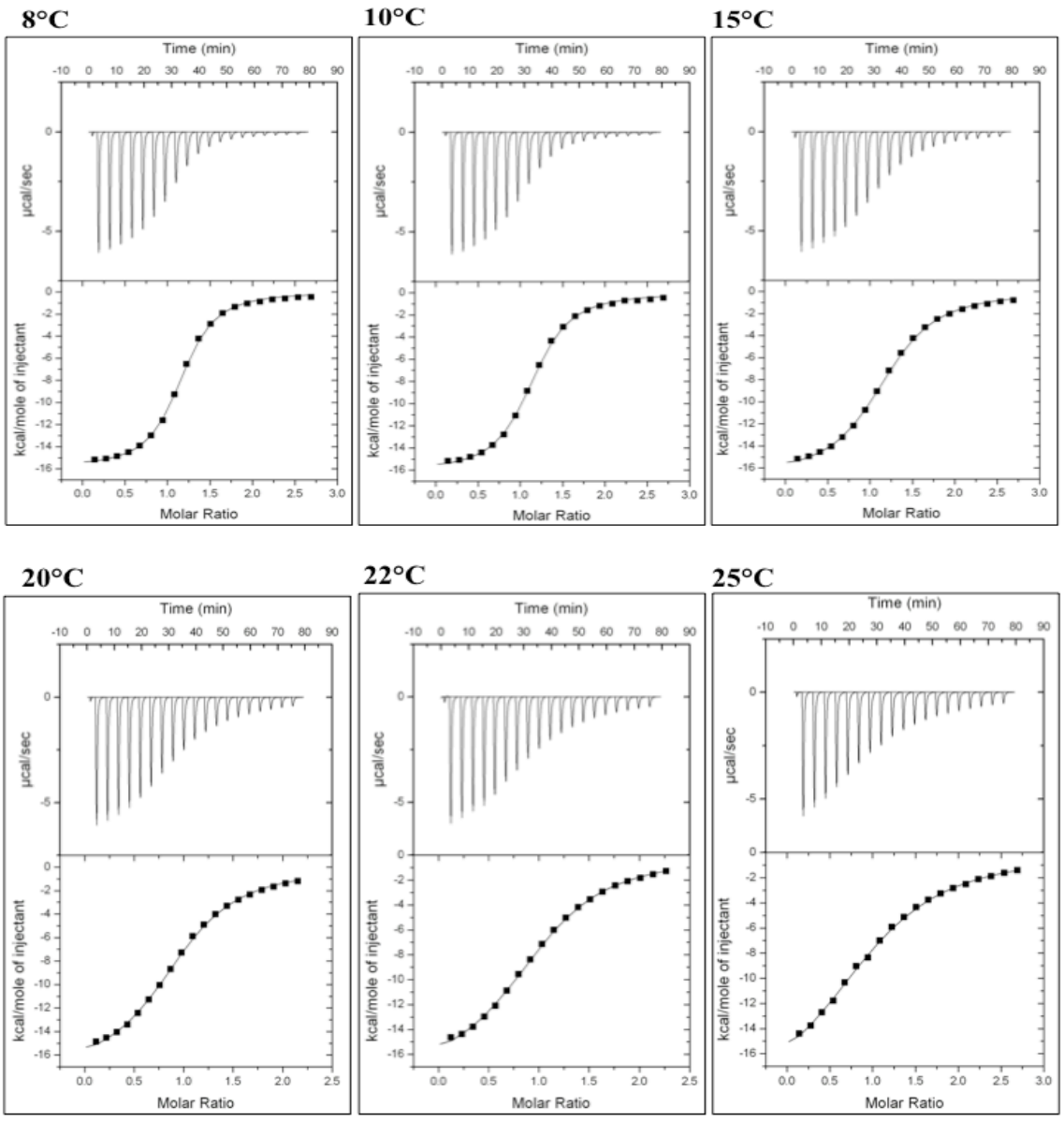

Figure 3.2 Raw and fitted data of the titration between N-Hsp90 and ADP in the presence of $MgCl_2$ at a range of temperatures between 8–25 °C. The black line represents the least squares fit to a single-site binding model.

The thermodynamic data obtained from the fitted isotherms is provided in Table 3.1. From the thermodynamic data derived from these interactions, it is clear all interactions are consistently exothermic and are enthalpically driven. ADP binding is generally of a stronger affinity (approximately 5 times that of AMP-PNP binding) and this interaction is associated with a more favourable change in observed enthalpy (ΔH°_{obs}) and a less favourable change in observed entropy ($T\Delta S^{\circ}_{obs}$). The less favourable entropy seen in the N-Hsp90:ADP interaction above may be a reflection of the large number of water molecules found present within the vacant binding site

becoming trapped upon binding of ADP, whereas the binding of AMP-PNP somehow leads to the trapping of less water, possibly the result of a different mode of binding than ADP. The additional phosphate group of the AMP-PNP (when compared to ADP) may play a role in forming additional contacts, mediated by the apparent closure of the ATP lid as previously reported. It has been demonstrated that the closure of the ATP lid results in the exposure of hydrophobic surface (back of the lid) to bulk solvent, an effect which is demonstrated by the general negative $T\Delta S°_{obs}$ seen with this interaction. The ATP cycle of Hsp90, as discussed in Chapter 1, involves the binding and hydrolysis of ATP resulting in the release of ADP and P_i. Interestingly, the results from the above titrations reveal that the binding of the product (ADP) may be of higher affinity than the substrate (AMP-PNP). This suggests that either the binding of AMP-PNP is not representative of the binding of the ATP substrate, or that binding of AMP-PNP to the isolated N-Hsp90 does not include the mechanism in which product is released and this could require contributions from the M and C domains.

	Temperature ° C	N	Error for N (+/-)	$\Delta H°_{obs}$ kJ mol^{-1}	Error for $\Delta H°_{obs}$ kJ mol^{-1} (+/-)	$T\Delta S°_{obs}$ kJ mol^{-1}	$\Delta G°_{obs}$ kJ mol^{-1}	K_d µM	Error for K_d µM (+/-)
AMP-PNP	8	1.0	0.01	-57.1	0.47	-33.3	-23.7	39.6	1.5
	10	1.0	0.01	-56.7	0.79	-33.2	-23.5	46.2	2.7
	15	0.9	0.04	-58.5	1.87	-35.6	-22.7	76.9	7.3
	20	1.0	0.05	-53.6	2.19	-31.1	-22.5	97.0	10.2
	22	1.0	0	-55.5	1.24	-33.2	-22.2	115.4	11.4
ADP	8	1.1	0.01	-66.3	0.37	-36.4	-29.8	2.8	0.6
	10	1.1	0.01	-67.3	0.40	-37.7	-29.5	3.6	0.4
	15	1.1	0.01	-69.7	0.44	-41.3	-28.4	7.0	0.5
	20	0.9	0.06	-72.8	0.66	-45.2	-27.4	12.8	0.9
	22	1.0	0.01	-74.0	0.68	-46.9	-27.1	15.8	1.1
	25	1.0	0.02	-83.8	1.5	-57.6	-26.1	27.1	3

Table 3.1 Thermodynamic parameters obtained from the interaction between N-Hsp90 with AMP-PNP and ADP in the presence of $MgCl_2$.

3.3 $\Delta Cp°_{obs}$ of the interaction between N-Hsp90 with AMP-PNP and ADP reveal opposite trends

As discussed in Chapter 1 the $\Delta Cp°_{obs}$ is, in many instances, associated with a system moving to a state of greater order, resulting in the usually observed negative $\Delta Cp°_{obs}$[19]. The $\Delta Cp°_{obs}$ of the interactions between N-Hsp90 and AMP-PNP and ADP was derived from the change in $\Delta H°_{obs}$ as a function of temperature as shown in Figure 3.3. The calculated values of $\Delta Cp°_{obs}$ show that AMP-PNP binding is associated with an anomalous positive heat capacity change of approximately +180 J mol^{-1}/°C, whilst ADP binding is associated with a negative heat capacity change of approximately -850 J mol^{-1}/°C.

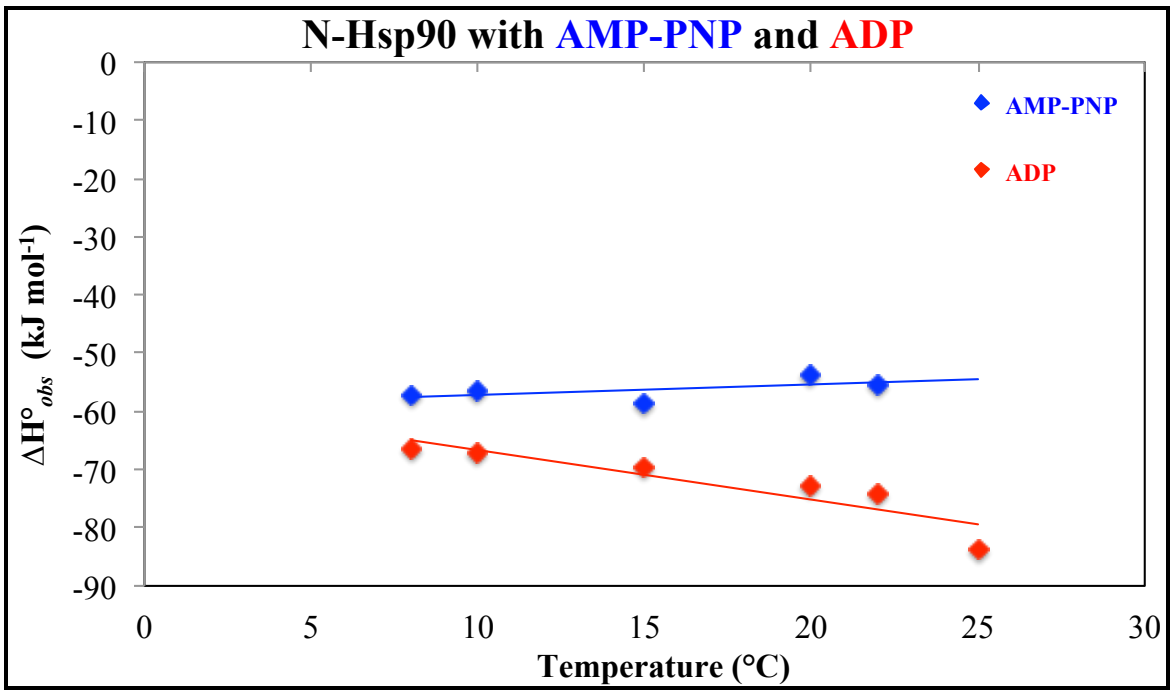

Figure 3.3 $\Delta H°_{obs}$ against temperature plots for nucleotide binding to N-Hsp90 in the presence of $MgCl_2$; the calculated $\Delta Cp°_{obs}$ are approximately +180 and -850 J mol^{-1}/°C for AMP-PNP and ADP respectively.

The contrasting heat capacities obtained for the two adenine-containing nucleotides to the same binding site in N-Hsp90 confirm the first observation of an interaction of different ligands to the same binding site resulting in both positive and negative $\Delta Cp°_{obs}$ as previously reported by Nilapwar *et al.*[19].

The structures of the adenine-containing nucleotides differ by a single phosphate group (Figure 3.4)

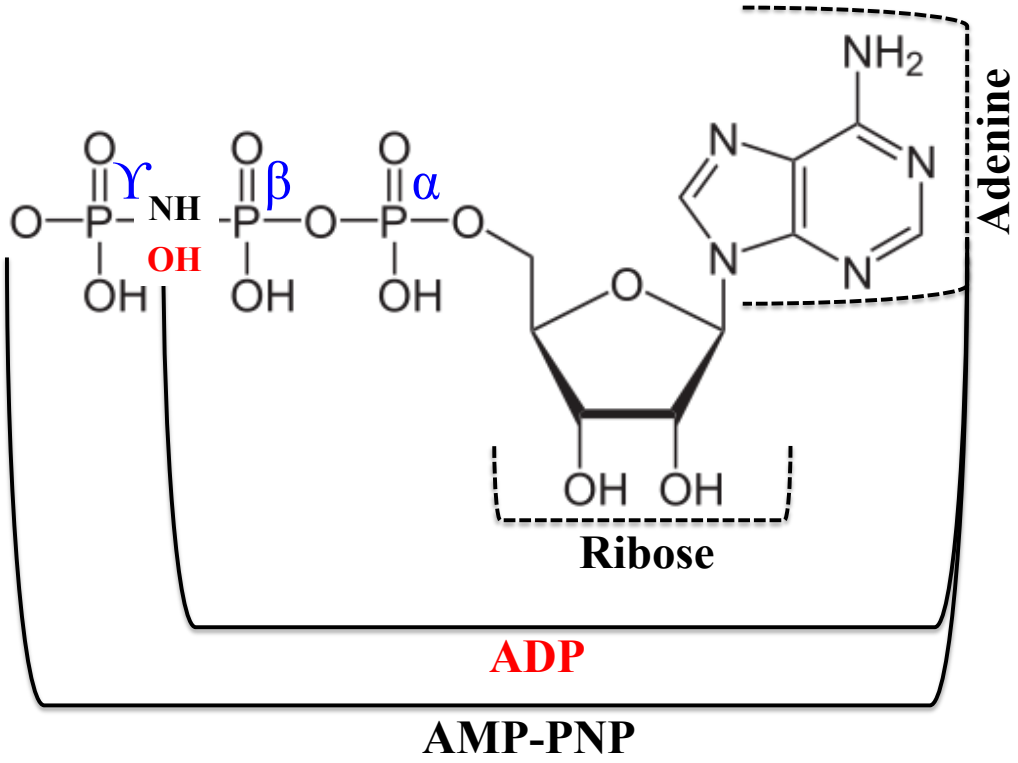

Figure 3.4 Structure of the two adenine containing nucleotides used in this study; for ADP, the –NH and terminal phosphate group of the AMP-PNP is replaced with an –OH group.

Previous structures of Hsp90 in complex with ATP/ADP[7,16,18,19] show that the majority of contacts made between the adenine ligands and the N-Hsp90 are mediated via water molecules that produce an extensive hydrogen bonding network. In comparison to the structures of the nucleotide–free N-Hsp90[37] and N-Hsp90:geldanamycin[31] complexes, the N-Hsp90:ADP complex[7] shows ten additional interfacial water molecules which are solvent exposed, three of which are shared with the nucleotide-free N-Hsp90 complex, and there are only two direct contacts between N-Hsp90 and ADP via the ribose and purine groups of the nucleotide. All other hydrogen bonding interactions between ADP and N-Hsp90 are mediated via water molecules.

The addition of the third phosphate group in AMP-PNP appears to have a destabilising effect upon the binding affinity, reducing it to a 5-fold lower value than that of ADP, shown in Table 3.1. Contrary to the binding of ADP, the AMP-PNP interaction is associated with a less favourable $\Delta H°_{obs}$ and more favourable $T\Delta S°_{obs}$.

3.4 Contributions to the anomalous positive change in heat capacity observed with AMP-PNP binding to N-Hsp90

The formation of a complex between two molecules is generally associated with a negative heat capacity change, and this is thought to be the result of the system moving to a state of greater order. This is usually derived from the phenomenon of the *hydrophobic effect*, i.e. the removal of non-polar surface area from water upon complex formation. On the contrary, the anomalous positive heat capacity associated with the binding of AMP-PNP to N-Hsp90 arises from the reduction of polar surface area[72,73], but can also be the result of a large number of other contributing factors. By considering these potential contributions individually, we can assess which of these factor(s) are the most likely cause of the positive $\Delta Cp°_{obs}$ seen in this study.

It was previously suggested that the potential cause of the positive change in heat capacity exhibited by the N-Hsp90:AMP-PNP interaction is the result of the closure of the 'ATP lid' upon AMP-PNP binding[19]. This view is further supported by the crystal structure of the Hsp90:AMP-PNP:Sba1/p23 complex[16], in which it was demonstrated that only a lid-closed Hsp90 leads to successful N-domain dimerisation. This conformational change exposes a hydrophobic surface to bulk solvent, formed by the back of the ATP lid. This exposure of hydrophobic surface could partially explain the observed thermodynamics, particularly in terms of the unfavourable $T\Delta S°_{obs}$ associated with the N-Hsp90:AMP-PNP interaction. Below are detailed experiments, which were designed to tease out the individual contributions of the metal ion, which is required for the successful interaction between N-Hsp90 and its nucleotide ligands. The results from these experiments will potentially enable us to enhance our understanding of the the interaction.

3.4.1. Magnesium ion binds to the adenine containing nucleotide with a negative $\Delta Cp°_{obs}$

The interaction between AMP-PNP and ADP to the N-Hsp90 is believed to involve the presence of a magnesium ion (Mg^{2+}), which in the AMP-PNP structure is shown to coordinate in an octahedral manner with the oxygens from the two phosphates (β and γ), Asn37, and three water molecules[19]. In the structural of N-Hsp90 bound to its nucleotide ligands, metal ions form an integral part of the complex. The possibility that the metal ion binds to the nucleotide prior to formation of the protein:nucleotide

complex leads to the importance of establishing the thermodynamic effect of the metal-nucleotide interaction.

The study by Nilapwar *et al.*[19] made mutations of the residues found to be involved in the water mediated-interactions between the nucleotide and N-Hsp90. It was found that one such mutation to Asn37, which is involved in a hydrogen bond between a water molecule coordinating the Mg^{2+}, resulted in the inability of AMP-PNP to bind N-Hsp90, illustrating that these water molecules were a crucial component of complex formation. To assess the importance of Mg^{2+} in the interaction between N-Hsp90 and AMP-PNP, titrations using ITC were carried out between AMP-PNP and ADP in the presence of 5mM $MgCl_2$ across a range of temperatures between 10–25 °C. The fitted isotherms for the interactions between AMP-PNP and $MgCl_2$ are shown in Figure 3.5.

Titrations were also carried out between ADP and $MgCl_2$ using the same conditions as with the AMP-PNP:$MgCl_2$ interaction, however the ADP saturated the magnesium within the first few (1-4) injections during the ITC experiment and so resulted in the shape of the isotherm being outside the limits of the *c* value for which a reliable fit can be obtained (refer to Chapter 2, page 82).

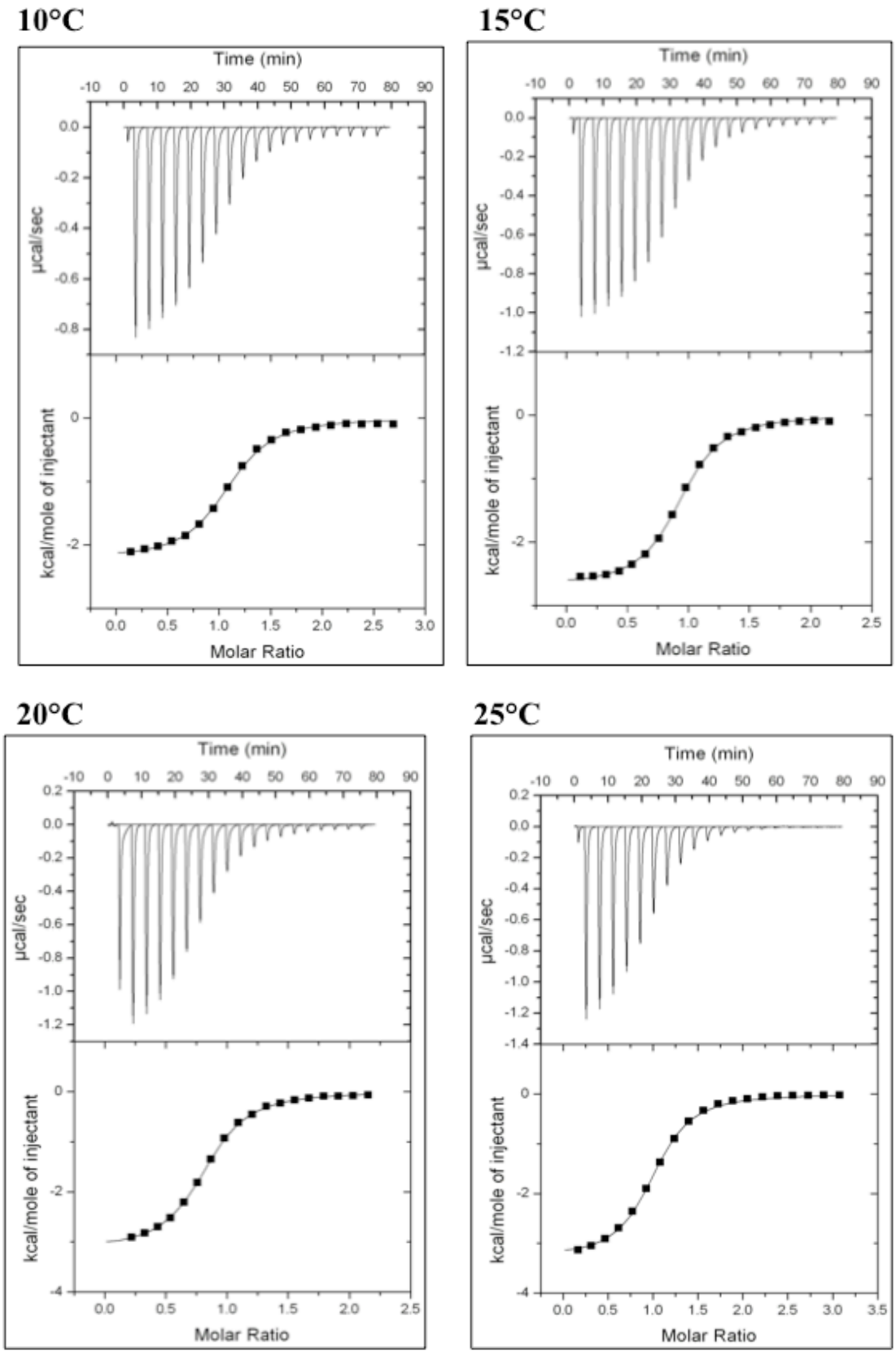

Figure 3.5 Raw and fitted data of the titration between AMP-PNP and $MgCl_2$ at a range of temperatures between 10–25 °C. The black line represents the least squares fit to a single site binding model.

The thermodynamic data obtained from the fitted isotherms shown above is provided in Table 3.2. From the thermodynamic data derived from these interactions, it is clear that the interaction between the nucleotide and the magnesium ion is consistently exothermic and is enthalpically driven. The binding between Mg^{2+} and AMP-PNP is of a higher affinity (approximately 5-fold larger than that between N-Hsp90:AMP-PNP), and in contrast to the N-Hsp90:AMP-PNP interaction, the AMP-PNP:Mg^{2+} interaction is associated with a less favourable $\Delta H°_{obs}$ and a more favourable $T\Delta S°_{obs}$. The favourable $T\Delta S°_{obs}$ seen with the AMP-PNP:Mg^{2+} interaction is reflective of the release of the interfacial water molecules present in the vacant ion-binding site into bulk solvent. As the nucleotide:ion complex binds to N-Hsp90, a less favourable $T\Delta S°_{obs}$ is observed and could be reflective of water at the nucleotide binding site becoming trapped. However this observation is more pronounced with the N-Hsp90:ADP interaction, which shows a much less favourable $T\Delta S°_{obs}$.

Temperature ° C	N	Error for N (+/-)	$\Delta H°_{obs}$ kJ mol^{-1}	Error for $\Delta H°_{obs}$ kJ mol^{-1} (+/-)	$T\Delta S°_{obs}$ kJ mol^{-1}	$\Delta G°_{obs}$ kJ mol^{-1}	Kd (µM)	Error for K_d µM (+/-)
10	1.0	0.01	-9.2	0.07	20.2	-29.5	3.5	0.5
15	0.9	0.01	-11.2	0.06	19.0	-30.3	3.1	0.3
20	0.9	0.01	-13.8	0.01	17.0	-30.8	3.2	0.3
25	0.8	0.01	-13.2	0.05	17.7	-30.8	3.9	0.2

Table 3.2 Thermodynamic parameters obtained from the interaction between AMP-PNP and $MgCl_2$.

Figure 3.6 illustrates that the $\Delta Cp°_{obs}$ for the binding of Mg^{2+} to AMP-PNP is negative (approximately -292 J mol^{-1}/°C) whereas AMP-PNP binding to N-Hsp90 in the presence of $MgCl_2$ was associated with the uncommon positive heat capacity of approximately +180 J mol^{-1}/°C.

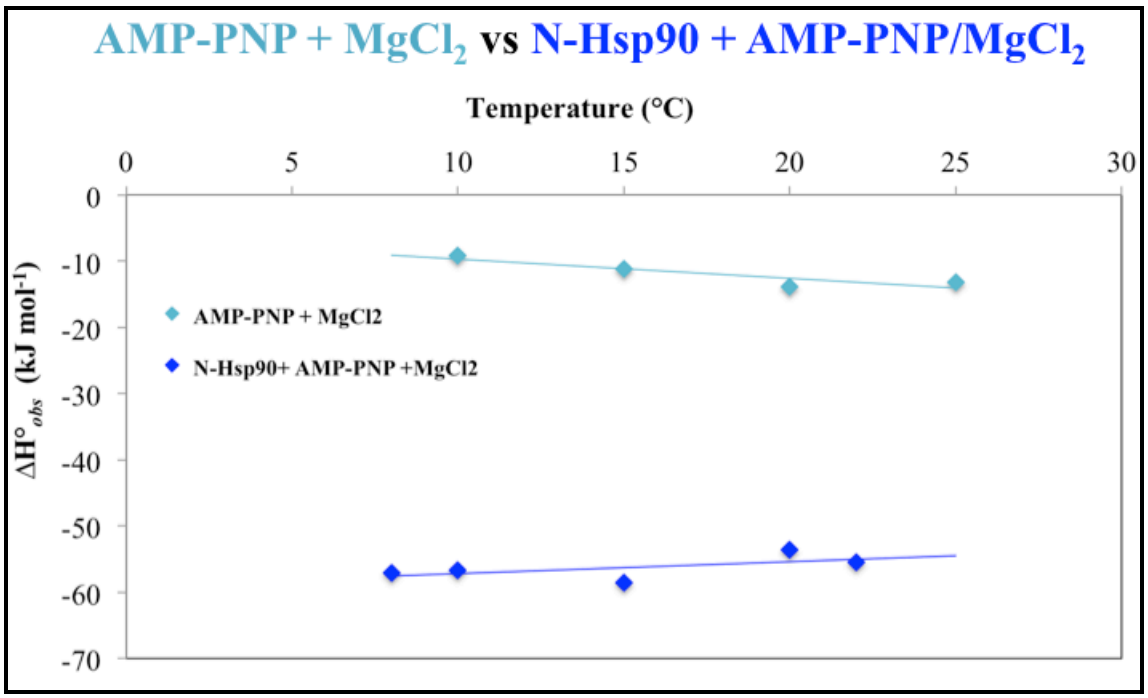

Figure 3.6 ΔH°_{obs} against temperature plots for $MgCl_2$ binding to AMP-PNP in comparison to the binding of N-Hsp90 with AMP-PNP in the presence of $MgCl_2$; the calculated ΔCp°_{obs} are approximately -292 and +180 J mol^{-1}/°C for AMP-PNP+$MgCl_2$ and N-Hsp90+AMP-PNP+$MgCl_2$ respectively.

From the above data, it is clear that Mg^{2+} is capable of binding to the nucleotide independent of its association with N-Hsp90. It is not clear however, whether the structure of the complex adopted by the metal-nucleotide interaction in isolation is the same as that seen in the N-Hsp90:nucleotide:ion interaction.

From the experiments involving AMP-PNP and ADP it appears that the terminal phosphate and the interactions mediated via this phosphate are strongly related to the positive heat capacity demonstrated in the interaction between N-Hsp90 and AMP-PNP. The magnesium ion is expected to reside in the junction between the β and γ phosphates of ATP and mutational studies showed that a residue (Asn37) involved in hydrogen bonding with a water molecule coordinating the magnesium ion is essential for complex formation[19]. Taking the experimental data and previous observations into consideration together with the observation that neither AMP-PNP nor ADP bind to N-Hsp90 in the absence of magnesium, the hypothesis that Mg^{2+} must play an important role in the contribution to the positive change in heat capacity observed in the interaction between N-Hsp90 and AMP-PNP was explored.

3.5. Assessing the importance of the magnesium ion by comparison with two other divalent metal ions; calcium (Ca^{2+}) and manganese (Mn^{2+})

Metal ions such as magnesium, are ubiquitous in nature and are well known for their crucial roles in many biochemical functions. One such function involves the role of these divalent ions in ATP hydrolysis[74]. In ATP hydrolysis reactions these divalent metal ions are located in close proximity to the phosphate chain. In *vitro* studies have shown that substitution of these ions for other divalent ions, e.g. Ca^{2+} or Mn^{2+} lead to significant changes in the cleavage efficiencies for the ATP phosphodiester[74]. Various studies have reported the use of the divalent ions Ca^{2+} and Mn^{2+} in substitution for Mg^{2+}, in experiments which are driven by ATP hydrolysis[74-79]. Whilst these studies reported successful ATP hydrolysis with the substituted divalent ions, they also reported significant discrepancies in the mode of binding of the substituted ions, particularly in relation to the hydration shells surrounding the metal ion.

3.5.1 Hydration properties of Mg^{2+}, Ca^{2+} and Mn^{2+} ions

Evidence has suggested that the hydration properties of metal ions are of crucial importance in their mechanisms in certain fundamental reactions, such as ATP hydrolysis[74]. Therefore, developing a clear understanding of their hydration characteristics and related dynamics is of importance for understanding a variety of biochemical functions.

In the Hsp90:ATP reaction, Mg^{2+} is the divalent metal ion found to be involved in the hydrolysis reaction, and in many instances, Mg^{2+} is generally found to possess an octahedral coordination geometry with some possible deviations in terms of its hydration shell. A study on the Hsp90 ATPase using molecular dynamics[74], showed that Mg^{2+} keeps an octahedral coordination by coordinating one oxygen atom of the ATP moiety and five water molecules. Any removal of water from the first solvation shell resulted in the recruitment of a new solvent molecule to the vacant site in a few picoseconds restoring the six- fold octahedral symmetry, indicating that its is the preferred configuration.

The divalent Ca^{2+} ion has also been shown to play a role in various ATPase reactions. However its coordination number has been found to vary between 6-8[80], suggesting that this particular divalent metal ion has a more flexible solvation shell in comparison to the stable Mg^{2+} ion. The microscopic details concerning the solvation shell of Ca^{2+} are still eluding an accurate experimental determination and its coordination number remains ambiguous. Computational simulations on Ca^{2+}[74] showed that the number of water molecules forming the first solvation shell seems to depend on the environment. When considering assessing the effects of the hydration properties of Mg^{2+} in the N-Hsp90:nucleotide interaction, the flexible hydration shell shown with Ca^{2+} would make it an ideal candidate as a substitute for the Mg^{2+}.

The paramagnetic metal ion Mn^{2+} has been demonstrated to be capable of replacing Mg^{2+} in many biochemical interactions, one of which includes ATP hydrolysis. Crystallographic studies[81] have shown divalent manganese having a preferred coordination number of six, similar to that of Mg^{2+}. As a result, Mn^{2+} has been commonly used as a mimetic of Mg^{2+} in many studies involving the ATP activity of various interactions. It is interesting to note that the atomic radius discrepancy between Mn^{2+} and Mg^{2+} is relatively large, with Mn^{2+} having an atomic radius of ~ 0.112 nm and Mg^{2+} having an atomic radius of ~ 0.160 nm. So potential thermodynamic effects that could result from this size discrepancy would have to be considered when making any conclusions in our experiments. Furthermore, the preference of Mn^{2+} for nitrogen and sulphur ligands could result in changes in the interaction between N-Hsp90 and nucleotide, thus affecting its direct comparison to Mg^{2+}.

3.6 Thermodynamics of N-Hsp90 binding to AMP-PNP and ADP in the presence of $CaCl_2$ and $MnCl_2$

Titrations were carried out using ITC and thermodynamic data was collected at a range of temperatures between 8–25 °C. The fitted isotherms of the titration between N-Hsp90 and AMP-PNP in the presence of 5mM $CaCl_2$ and $MnCl_2$ at a temperature of 15°C is shown in Figure 3.7. Figure 3.8 shows the fitted isotherms of the interaction between N-Hsp90 and ADP in the presence of these two divalent ions.

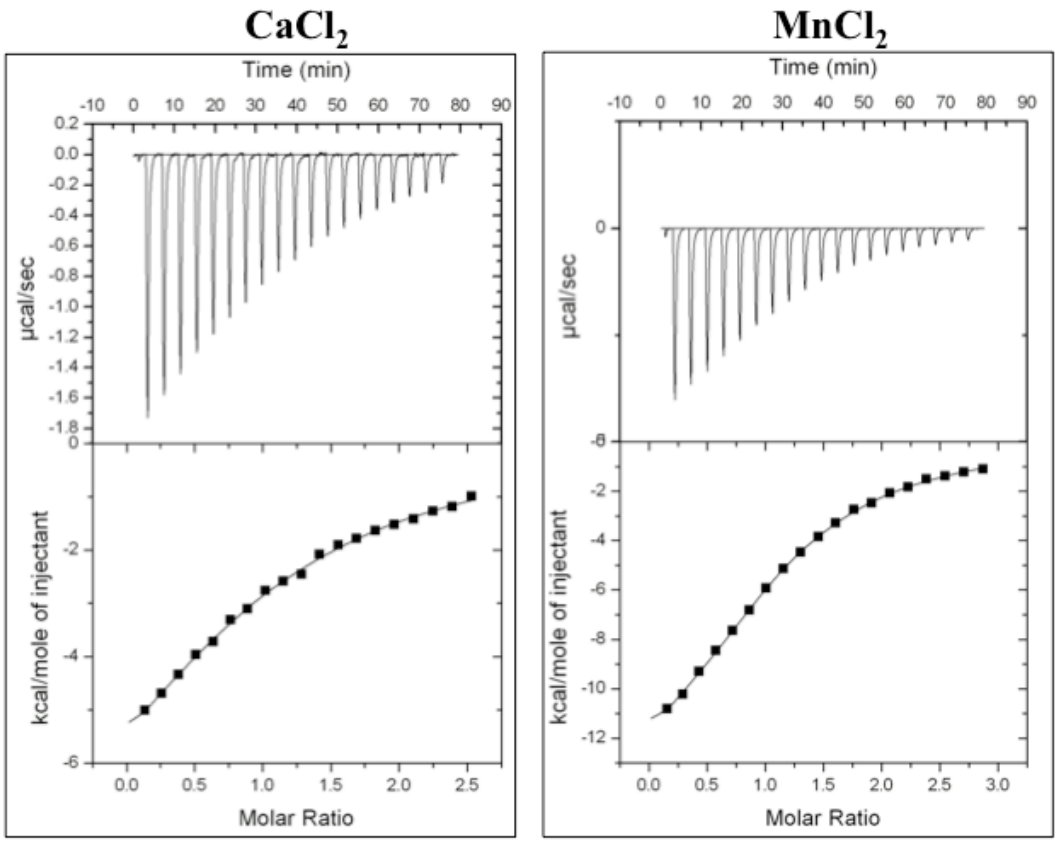

Figure 3.7 Raw and fitted data of the titration between N-Hsp90 and AMP-PNP in the presence of $CaCl_2$ and $MnCl_2$ at 15°C. The black line represents the least squares fit to a single site binding model.

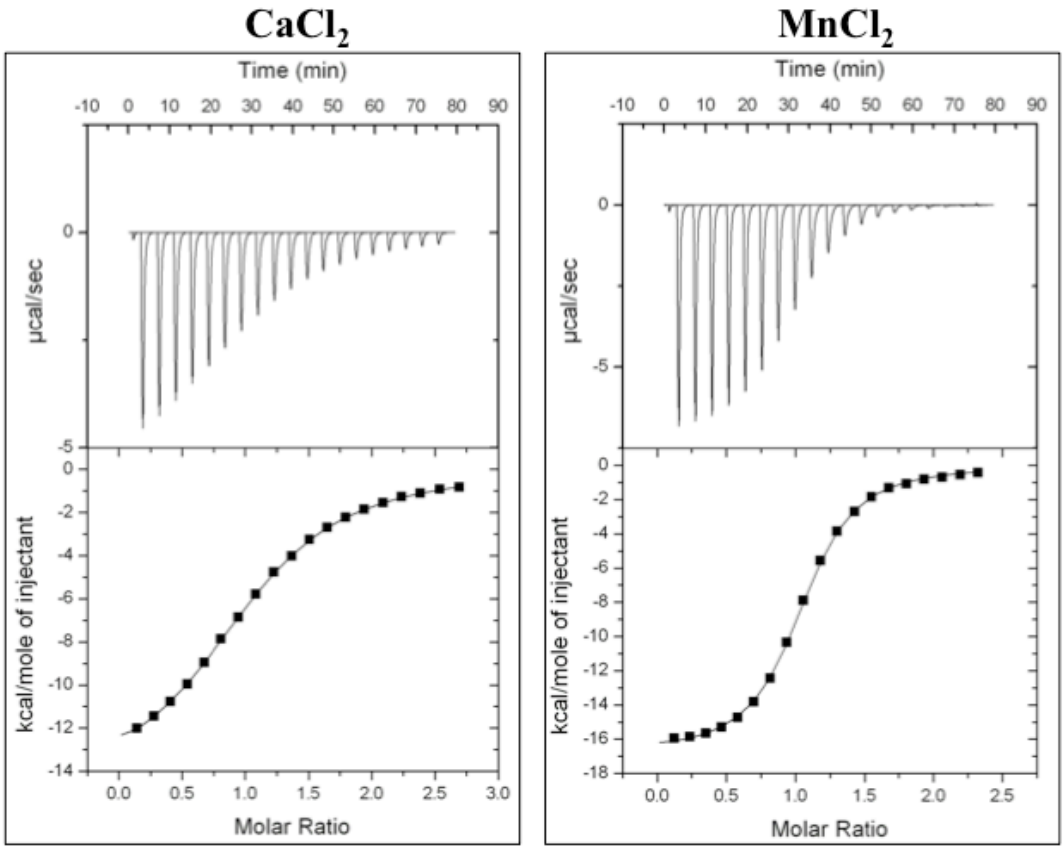

Figure 3.8 Raw and fitted data of the titration between N-Hsp90 and ADP in the presence of presence of $CaCl_2$ and $MnCl_2$ at 15°C. The black line represents the least squares fit to a single site binding model.

Tables 3.3 and 3.4 show the thermodynamic parameters of the interactions between N-Hsp90 and AMP-PNP and ADP in the presence of $Cacl_2$ and $MnCl_2$ respectively. The parameters presented demonstrate that the interactions between N-Hsp90 and AMP-PNP in the presence of both Ca^{2+} and Mn^{2+} is relatively weak when compared to that of the N-Hsp90:ADP interaction. This effect on affinity is also observed for the N-Hsp90:nucleotide interactions in the presence of $MgCl_2$ shown in Table 3.1.

	Temperature ° C	N	Error for N	$\Delta H°_{obs}$ kJ mol^{-1}	Error for $\Delta H°_{obs}$ kJ mol^{-1} (+/-)	$T\Delta S°_{obs}$ kJ mol^{-1}	$\Delta G°_{obs}$ kJ mol^{-1}	Kd µM	Error for K_d µM (+/-)
$CaCl_2$	8	1.0	0.03	-47.0	1.0	-24.2	-22.7	59.1	4.4
	10	1.0	0.04	-44.3	3.0	-21.5	-22.0	88.4	14.7
	15	1.0	0	-33.9	1.0	-11.1	-22.2	94.3	13.8
	22	1.0	0.3	-37.8	7.2	-14.0	-23.5	64.9	22.6
	25	1.0	0	-29.2	0.8	-6.6	-22.5	112.6	15.5
$MnCl_2$	8	1.1	0.01	-65.4	0.4	-39.8	-25.6	17.6	0.7
	10	1.1	0	-64.9	0.4	-39.4	-25.4	20.6	0.8
	15	1.0	0.01	-64.0	0.6	-38.9	-25.0	29.1	1.3
	20	1.0	0.01	-68.2	0.8	-44.0	-24.1	49.7	2.0
	22	1.1	0.03	-64.1	1.2	-39.8	-24.1	53.1	3.3
	25	1.0	0	-61.4	0.6	-37.2	-24.0	62.5	3.8

Table 3.3 Thermodynamic parameters obtained from the interaction between N-Hsp90 and AMP-PNP in the presence of $CaCl_2$ and $MnCl_2$.

	Temperature ° C	N	Error for N	ΔH°_{obs} kJ mol^{-1}	Error for ΔH°_{obs} kJ mol^{-1} (+/-)	$T\Delta S^{\circ}_{obs}$ kJ mol^{-1}	ΔG°_{obs} kJ mol^{-1}	Kd µM	Error for K_d µM (+/-)
$CaCl_2$	8	1.0	0.01	-60.3	0.1	-32.9	-27.3	8.4	0.2
	10	1.0	0.01	-60.3	0.1	-33.1	-27.2	9.6	0.3
	15	1.0	0.01	-61.8	0.2	-35.3	-26.4	16.4	0.3
	20	1.0	0.01	-62.3	0.7	-36.5	-25.7	25.9	1.7
	22	1.0	0.01	-64.1	0.6	-38.7	-25.3	33.3	1.4
	25	1.0	0.03	-65.7	1.2	-40.7	-24.9	43.6	3.1
$MnCl_2$	8	1.0	0.01	-64.6	0.9	-34.2	-30.4	2.2	0.5
	10	1.0	0.01	-66.7	0.1	-35.6	-31.0	1.9	0.1
	15	1.0	0.05	-70.3	0.2	-40.3	-29.9	3.7	0.2
	20	1.0	0.01	-72.2	0.2	-43.1	-29.0	6.7	0.3
	22	0.9	0.03	-104	2.7	-77.1	-27.2	15.1	3.0
	25	1.0	0.01	-80.1	0.5	-52.4	-27.5	15.0	0.8

Table 3.4 Thermodynamic parameters obtained from the interaction between N-Hsp90 and ADP in the presence of $CaCl_2$ and $MnCl_2$.

From the thermodynamic data derived, it is clear all interactions are consistently exothermic and are enthalpically driven as with the WT-N-Hsp90 interactions. The interactions in the presence of Ca^{2+} is of a weaker affinity, approximately 3-fold lower than that of both Mg^{2+} and Mn^{2+}, and this interaction is also associated with a less favourable ΔH°_{obs} more favourable $T\Delta S^{\circ}_{obs}$ than with Mg^{2+}/Mn^{2+}. Based on previous observations of the large number of interfacial water molecules present at the nucleotide binding site, the more favourable $T\Delta S^{\circ}_{obs}$ seen with the Ca^{2+} interactions could reflect its variable hydration shell in that it traps less of these interfacial water molecules than in the case of an ion that has a preferred stable hydration shell such as Mg^{2+}/Mn^{2+}. Thus, Ca^{2+} interaction results in the expulsion (rather than entrapment) of these interfacial water molecules into bulk solvent as reflected by the more favourable $T\Delta S^{\circ}_{obs}$.

The changes in heat capacity, ΔCp°_{obs} of the interaction between N-Hsp90 and AMP-

PNP in the presence of Ca^{2+} and Mn^{2+} also show the same anomalous positive $\Delta Cp°_{obs}$ as observed with the Mg^{2+} interaction. Data presented in Figure 3.9.

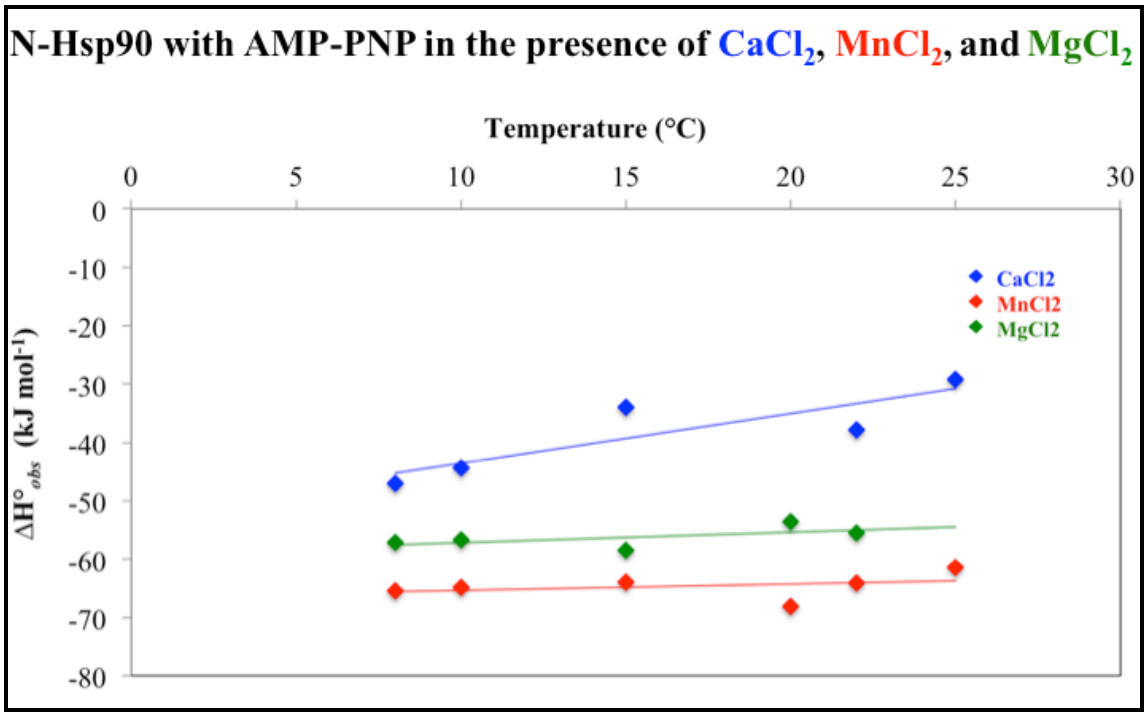

Figure 3.9 $\Delta H°_{obs}$ against temperature plots for AMP-PNP binding to N-Hsp90 in the presence of $CaCl_2$, $MnCl_2$, and $MgCl_2$; the calculated $\Delta Cp°_{obs}$ are approximately +853, +109 and +180 J mol^{-1}°/C respectively.

The data presented in Figure 3.9 show that in the Ca^{2+} interaction is associated with a much larger positive heat capacity of approximately +853 J mol^{-1}°/C than with the other ion interactions. Mn^{2+} binding is associated with a heat capacity change more comparable to that of Mg^{2+} (approximately +109 J mol^{-1}°/C and +180 J mol^{-1}°/C respectively).

Figure 3.10 shows the changes in heat capacity for the interaction between N-Hsp90 and ADP in the presence of Ca^{2+} and Mn^{2+}. The calculated $\Delta Cp°_{obs}$ values are negative for both metal ions as is also the trend seen with the Mg^{2+} interaction. As with the interaction between N-Hsp90 and AMP-PNP in the presence of Mg^{2+} and Mn^{2+}, the N-Hsp90:ADP interaction with these ions shows that manganese shares a $\Delta Cp°_{obs}$ similar to that of Mg^{2+} of -831 and -850 J mol^{-1}°/C respectively. The $\Delta Cp°_{obs}$ for the N-Hsp90:ADP interaction in the presence of Ca^{2+} is approximately -300 J mol^{-1}°/C, and is much less negative than for the other ion interaction with ADP.

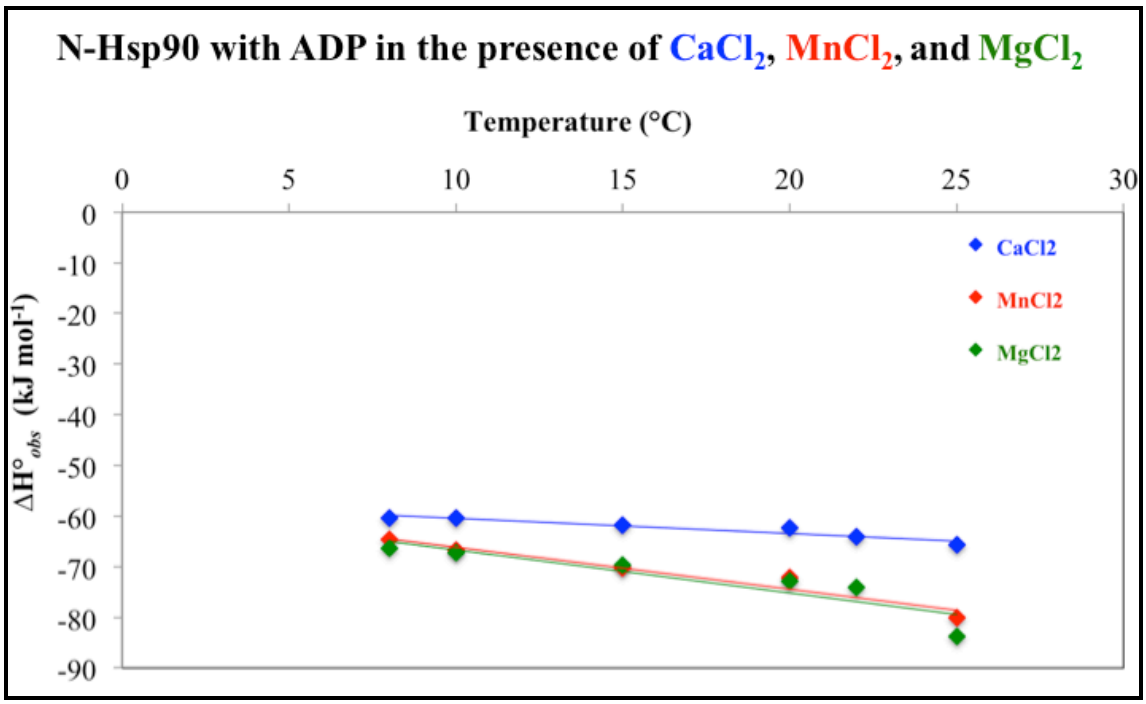

Figure 3.10 ΔH°_{obs} against temperature plots for ADP binding to N-Hsp90 in the presence of $CaCl_2$, $MnCl_2$, and $MgCl_2$; the calculated ΔCp°_{obs} are approximately -300, -831 and -850 J mol^{-1}°/C for the interactions with $CaCl_2$, $MnCl_2$, and $MgCl_2$ respectively.

The thermodynamic profiles for all interactions involving Mg^{2+} and Mn^{2+} share a large number of similarities, providing implications of their shared hydration shells in the observed thermodynamics. The trends in the changes in enthalpy, entropy, free energy, K_d, and ΔCp°_{obs} values for these interactions are extremely comparable as illustrated in Figure 3.11.

a

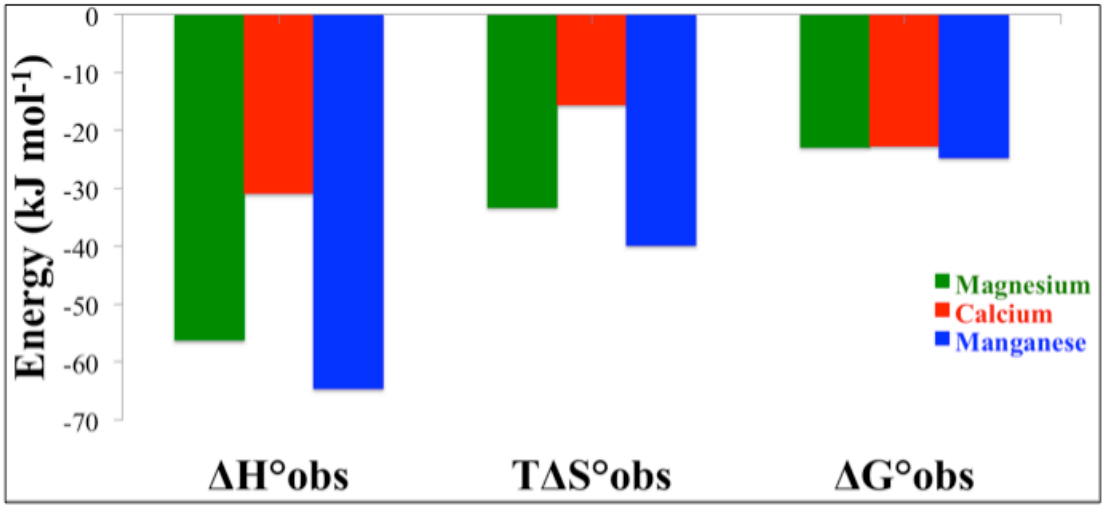

b

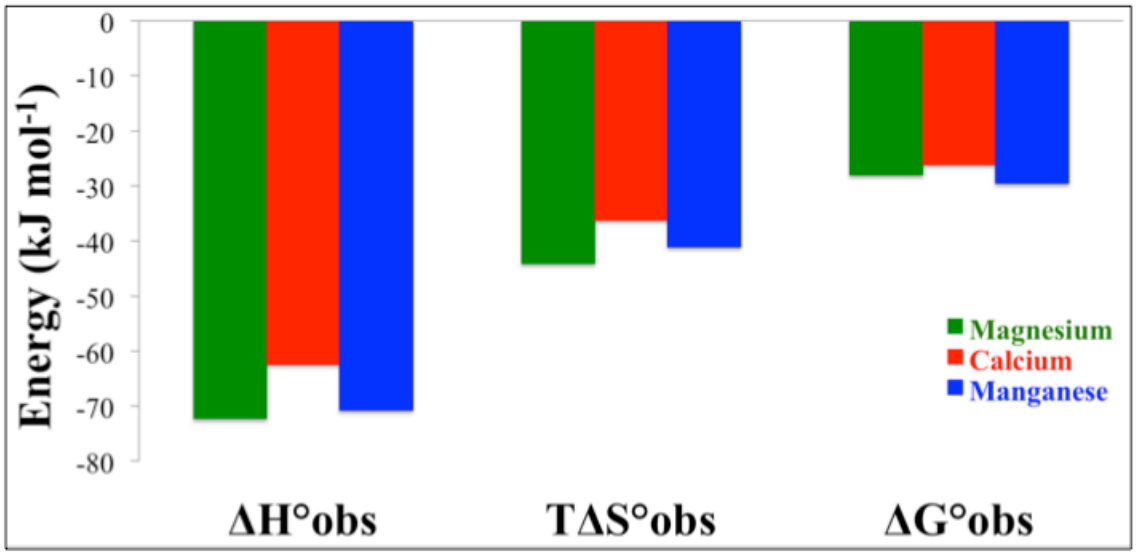

Figure 3.11 Comparison of the thermodynamic profiles of the interaction of N-Hsp90 with **a,** AMP-PNP and **b,** ADP in the presence of $MgCl_2$, $CaCl_2$, and $MnCl_2$.

All metal interactions are consistent in the observation of an anomalous positive heat capacity observed with AMP-PNP binding, which as mentioned earlier, is commonly associated with the burial of polar surface. However, the latter statement cannot be used to explain the large discrepancies in observed in the $\Delta Cp°_{obs}$ values for the Ca^{2+} ion

interactions when compared with that of Mg^{2+}/Mn^{2+}, therefore it is speculated that these discrepancies may accrue from the waters coordinating these metal ions.

3.7 Investigating the factors that can contribute to a positive heat capacity

Chapter 1 of this thesis highlights the possible factors which could contribute to a change in heat capacity such as, interfacial water molecules, effects of protonation, conformational changes in protein structure, changes in solvent-accessible surface area, and surface area changes derived from protein or ligand self-association. The following sections address each of these contributing factors by referring to experimental data and an extensive thermodynamic study carried out by Nilapwar *et al*.[19] on small ligand binding to N-Hsp90, including AMP-PNP and ADP.

3.7.1 Interfacial water molecules

A study by Nilapwar *et al*.[19] through mutational investigations found that the large number of water molecules involved in the interactions between N-Hsp90 with its nucleotide partners and inhibitor molecules are important for complex formation, since they showed a number of these water molecules being involved in indirect contacts with the protein and bound ligand. However, it was previously demonstrated that the incorporation of water molecules into a protein-ligand interface resulted in an increase in the negative change in heat capacity[82-84], rather than providing a positive change as seen with the N-Hsp90:ligand interaction. It has been reported that the effect on $\Delta Cp°_{obs}$ upon the burial of a single water molecule lies in the range -25 to -50 J mol^{-1} K^{-1}. Thus, the burial of the four commonly observed water molecules in the nucleotide-bound and inhibitor-bound complexes would amount to somewhere between -100 and -300 J mol^{-1} K^{-1} in terms of $\Delta Cp°_{obs}$. Thus sequestering of water molecules in the N-Hsp90:AMP-PNP binding site does not explain the positive $\Delta Cp°_{obs}$ observed in this interaction and therefore this observation must be the result of another cause.

The results of the above study provide further evidence for the potential importance of the hydration shells of the metal ion already demonstrated to a certain degree earlier in this chapter. If the burial of water molecules results in a negative $\Delta Cp°_{obs}$, as suggested by Nilapwar *et al*.[19], the substantially large positive heat capacity observed for the interaction between N-Hsp90 and AMP-PNP in the presence of Ca^{2+} when compared to that in the presence of Mg^{2+} could be a result of the lower number of water molecules

coordinating the Ca^{2+} ion, and burial of less water would result in a less negative and more positive $\Delta Cp°_{obs}$ as is observed.

3.7.2 Ligand self-association

Self-association or aggregation of either N-Hsp90 or the nucleotide would have a significant impact on the burial of surface area of the macromolecules involved in the interaction and also on the corresponding organisation of water molecules and dynamics of the protein. If the binding of the macromolecules was able to dissociate potential oligomers, a possible net increase in the exposed surface area could result, providing a positive $\Delta Cp°_{obs}$. Prodromou *et al.*[13] found no such evidence of self-association of the nucleotide-free N-Hsp90. Furthermore, Nilapwar *et al.*[19] ruled out potential dimerisation or aggregation events associated with N-Hsp90 using NMR spectroscopy. In addition, NMR spectroscopy of the nucleotide moiety and the adenine base itself revealed no evidence of base stacking of the nucleotide at concentrations used in this thesis. Furthermore, the ITC titrations carried out in this study showed no indication of aggregate formation under the particular solution conditions used, as would have been evident through irregular heats of dilutions

3.7.3 Protonation effects

Complex formation between a protein and a small molecule has the potential to change the local environment of labile protons within the protein and/or ligand. These changes could induce effects on the stability of the protonated state of either species leading to a labile group differing in its pK_a between the free and bound states. As a result, complex formation within a particular pH range could affect protonation events that could ultimately lead to changes in the thermodynamics of the interaction, including the $\Delta Cp°_{obs}$.

Nilapwar *et al.*[19] conducted an extensive study in which they used a triple buffer system to determine any potential protonation events that could be associated with complex formation between N-Hsp90 and AMP-PNP and ADP. They concluded that a single protonation event is apparent below pH 7.0, with $pK_{a\,(free)} = 5.7 \pm 0.2$ and $pK_{a\,(bound)} = 7.1 \pm 0.1$, as illustrated by a strong dependence on K_d and $\Delta H°_{obs}$ below pH 7.0. This protonation event was found to be associated with the AMP-PNP molecule. However, the experiments carried out in the above study and in this thesis were performed at pH

8.0, which is above the described pK_a values. Therefore it is unlikely that the unusual positive heat capacity observed in the interaction between N-Hsp90 and AMP-PNP in the presence of Mg^{2+} is derived from any protonation effects.

In view of the above findings, it was important to determine the effects of protonation that could potentially arise from the substitution of the native Mg^{2+} ion to Ca^{2+} or Mn^{2+}, since these ions could involve a different mechanism of complex formation in reference to hydrogen bonding or electrostatic interactions, which could lead to changes in protonation and therefore net changes in thermodynamics observed. Tables 3.5 and 3.6 illustrate the thermodynamic parameters observed from the interactions between N-Hsp90 and AMP-PNP in the presence of Ca^{2+} and Mn^{2+}, and also for the interaction between N-Hsp90 and ADP in the presence of Ca^{2+} at a pH range between 5.0-9.0. The results shown below are representative of the data observed at 15°C, however all titrations for each pH value were recorded at a temperature range between 10- 25°C.

	pH	N	Error for N (+/)	$\Delta H°_{obs}$ kJ mol^{-1}	Error for $\Delta H°_{obs}$ kJ mol^{-1} (+/-)	$T\Delta S°_{obs}$ kJ mol^{-1}	$\Delta G°_{obs}$ kJ mol^{-1}	Kd µM	Error for K_d µM (+/-)
AMP-PNP	5.5	0.9	0.52	-40.1	12.4	-19.0	-21.0	152.6	39.2
	6.0	0.9	0.41	-42.5	10.8	-20.7	-21.8	96.1	37.8
	7.0	1.1	0.53	-26.7	8.0	-5.3	-21.3	138.5	57.6
	8.0	1.1	0.66	-44.6	17.5	-24.7	-20.0	240.3	120.3
	9.0	0.9	0.44	-32.7	1.0	-9.2	-23.4	68.4	7.2
ADP	5.0	0.9	0.03	-169	41.4	-146.8	-22.1	78.7	11.2
	6.0	1.0	0.05	-38.3	1.3	-13.8	-24.4	37.1	4.1
	7.0	0.8	0.15	-79.5	8.6	-53.8	-25.6	22.9	4.8
	8.0	1.0	0.01	-65.6	0.4	-40.6	-24.9	29.9	1.0
	9.0	1.0	0.01	-65.6	0.5	-40.6	-24.9	31.0	1.7

Table 3.5 Thermodynamic parameters obtained from the interaction between N-Hsp90 with AMP-PNP and ADP in the presence of $CaCl_2$ at a pH range between 5.0–9.0. Data shown for 15°C.

pH	N	Error for N (+/-)	$\Delta H°_{obs}$ kJ mol^{-1}	Error for $\Delta H°_{obs}$ kJ mol^{-1} (+/-)	$T\Delta S°_{obs}$ kJ mol^{-1}	$\Delta G°_{obs}$ kJ mol^{-1}	Kd µM	Error for K_d µM (+/-)
5.0	1.0	0.05	-73.1	2.5	-47.4	-25.5	23.6	2.2
6.0	1.0	0.03	-46.5	0.9	-21.8	-24.7	33.5	2.3
7.0	1.0	0.11	-57.1	3.4	-33.4	-23.6	53.1	3.9
8.0	1.0	0.03	-52.2	1.4	-28.7	-23.3	58.8	5.4
9.0	1.1	0.06	-55.6	1.3	-32.6	-23.0	68.0	6.6

Table 3.6 Thermodynamic parameters obtained from the interaction between N-Hsp90 with AMP-PNP in the presence of $MnCl_2$ at a pH range between 5.0–9.0. Data shown for 15°C.

From Tables 3.5 and 3.6 it can be seen that there are small variations in the affinity of the interaction between N-Hsp90 with ADP in the presence of Ca^{2+} as with the data for the Mg^{2+} interaction demonstrated in the study by Nilapwar *et al.*[19]. However in comparison to the variation with the N-Hsp90:AMP-PNP interactions in the presence of Ca^{2+} and Mn^{2+}, these changes are negligible.

Although the errors in the calculated thermodynamic parameters are relatively large, particularly for the low pH titrations, these data follow the same trends as with the Mg^{2+} data reported by Nilapwar *et al.*[19].

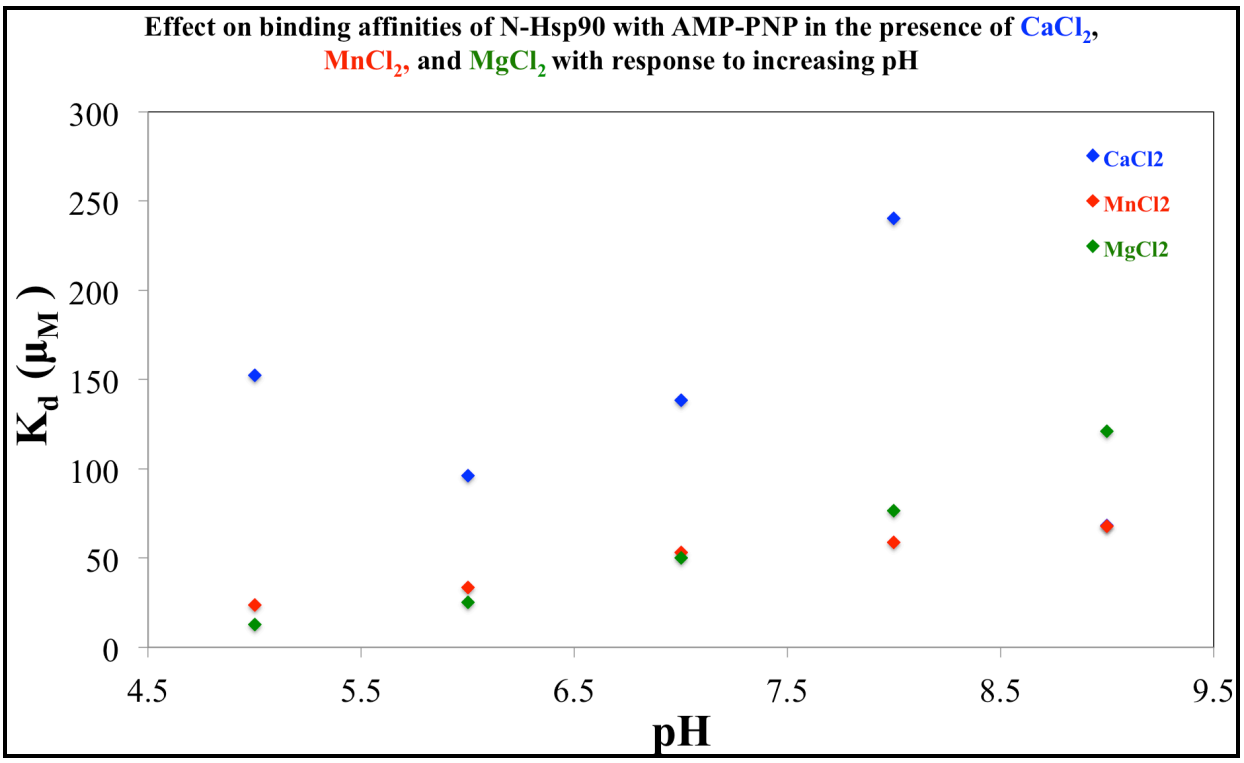

Figure 3.12 The pH dependence of the interaction between N-Hsp90 with AMP-PNP in the presence of $CaCl_2$, $MnCl_2$, and $MgCl_2$ recorded at 15°C. ($MgCl_2$ data was taken from Nilapwar *et al.*[19]).

Figure 3.12 illustrates the clear similarities between the binding affinities between the Mn^{2+} and Mg^{2+}interactions. The pH dependence of the interaction in the presence of Ca^{2+} is unreliable due to the constantly observed weak binding affinity shown in all conditions with this ion together with the increased errors associated with the measurement of the Kd and the stoichiometry, shown in Table 3.5. The *c* values of the fitted isotherms for the Ca^{2+} interactions were all below $c = 40$ (refer to Chapter 2, page 82), and therefore it was difficult to fit the raw data and hence derive accurate thermodynamic parameters.

In conclusion, it seems that the destabilisation in binding affinities in all metal ion interactions changes above pH 7.0 with AMP-PNP, but not with ADP. At low pH it seems that AMP-PNP binds with a similar K_d with all metal ion interactions, however the decrease in the strength of binding affinities above pH 7.0 is concomitant with the pH in which ATP changes its charged state from -3 to -4. And therefore if one assumes that the behaviour of ATP is similar to the behaviour of AMP-PNP, then this indicates a de-protonation event within the AMP-PNP moiety.

Bearing in mind that no such destabilisation of binding affinities is associated with ADP, this would lead us to the assumption that the γ phosphate is responsible for this protonation event. Furthermore, since the metal ion binding site is thought to reside in between the β and γ phosphates of the AMP-PNP, this could potentially explain the differences in the trends seen for all metal ions shown in Figure 3.12, in that each metal ion behaves differently in the N-Hsp90:AMP-PNP interaction.

The overall trend of a decrease in the strength of the K_d above pH 7.0 for all metal ion interactions is in agreement with the Mg^{2+} data reported by Nilapwar *et al.*[19], and therefore it can be assumed that the protonation event evident in the Ca^{2+} and Mn^{2+} interactions would also reflect that of a single protonation event with a $pK_{a\,(free)}$ and $pK_{a\,(bound)}$ similar to that of the Mg^{2+} interaction. Since the titrations carried out in this thesis were performed at pH 8.0, this is far above the pK_a values demonstrated above, and therefore the positive heat capacity observed in the N-Hsp90:AMP-PNP interaction must accrue from another source.

3.7.4 Conformational changes arising from the 'ATP lid'

Conformational changes associated with ligand binding can have a significant effect upon the heat capacity of a given system; these effects would generally arise from net changes in the degrees of freedom of atoms of the protein and/or ligand or from changes in solvation upon surface area burial[36,66,85]. Extensive research involving investigations into the consequences of binding of nucleotide and/or analogues thereof, including the N-Hsp90 inhibitors such as geldanamycin, have revealed significant changes in conformation of these ligands when compared to their respective apo structures[19]. However as demonstrated by Nilapwar *et al.*[19], most of the nucleotide-interactions are mediated by water molecules and are very much limited in terms of direct protein contacts.

NMR spectroscopic observations made by Nilapwar *et al.*[19], using the backbone assignment of N-Hsp90, revealed a significant number of chemical shift changes widely dispersed throughout this domain. However, the region which revealed the most variation was occupied by amino acid residues 81-123, a region occupied by the ATP lid (refer to Chapter 1, page 24). The binding of AMP-PNP affected most of the first helix of this lid region, a region found not affected by the binding of ADP, shown in

Figure 3.13. These chemical shift changes are also in good agreement with the crystal structure of the full length Hsp90-AMP-PNP-p23[16] complex, which shows a lid closed Hsp90, however it is important to note that the crystal structure harboured a mutation (A107N) which induced lid closure.

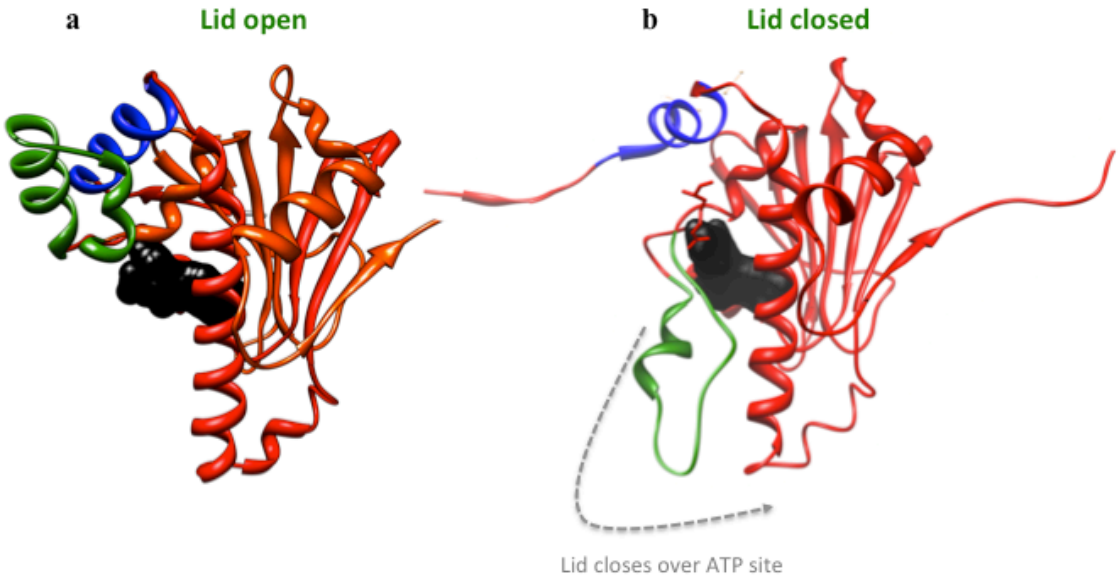

Figure 3.13, a, N-Hsp90 (red)-ADP (black) complex[7] highlighting the ATP lid (green) in the open conformation. **b,** N-Hsp90 (red)-AMP-PNP (black) complex[16] highlighting the lid in the closed conformation.

The demonstration of the different conformational changes induced by both ADP and AMP-PNP (which differ by a single phosphate), is surprising, as one would expect the structural change(s) upon ligand binding to a protein to commonly populate around local regions close to the ligand-binding site. The movement or closure of the ATP lid in the Hsp90 system has been proposed to reveal a hydrophobic surface derived from the back of the ATP lid, upon which a potential for a positive ΔCp°_{obs} could be discernable, by the exposure of this hydrophobic surface to the bulk solvent upon movement of this lid segment away from the main body of the protein and over the nucleotide binding site (illustrated in Figure 3.13b).

In order to assess the effects of potential ATP lid closure on the thermodynamics of the interaction between N-Hsp90 and AMP-PNP/ADP, individual mutants of N-Hsp90 in which the ATP lid was stabilised in either the open or closed conformation were used to carry out ITC analysis on.

T101 is buried in the lid open conformation as shown in Figure 3.14 and therefore would become exposed in the ATP bound N-Hsp90 as a result of lid closure (Figure 3.13b). Mutation to the more hydrophobic isoleucine stabilises the lid open conformation, hence should decrease ATP/AMP-PNP binding[16]. Since T101I stabilises the lid open conformation, this should resemble the ADP-bound N-Hsp90 complex, which shows an open lid[7]. Table 3.7 shows the thermodynamic parameters obtained from the interaction between N-Hsp90 and N-Hsp90-T101I with AMP-PNP and ADP in the presence of 5 mM $MgCl_2$.

	Temperature ° C	N	Error for N	$\Delta H°_{obs}$ kJ mol^{-1}	Error for $\Delta H°_{obs}$ kJ mol^{-1} (+/-)	$T\Delta S°_{obs}$ kJ mol^{-1}	$\Delta G°_{obs}$ kJ mol^{-1}	K_d µM	Error for K_d µM
AMP-PNP	8	1.0	0.03	-51.3	1.1	-26.1	-25.2	21.0	2.5
	10	0.9	0.03	-51.6	1.4	-26.2	-25.3	21.3	3.3
	15	1.0	0.03	-55.2	1.2	-30.3	-24.7	32.6	3.2
	20	1.0	0.05	-59.8	1.7	-35.5	-24.2	47.8	4.8
	22	0.9	0.52	-64.1	42.9	-40.2	-23.8	68.0	45.2
ADP	8	0.9	0.01	-68.2	0.4	-39.1	-29.0	4.0	0.4
	10	1.0	0.01	-65.2	0.4	-36.2	-28.8	4.7	0.4
	15	1.0	0.03	-78.6	1.5	-51.2	-27.3	11.3	1.7
	20	0.9	0.01	-69.4	0.6	-41.9	-27.3	13.4	0.9
	22	0.9	0.01	-77.2	0.7	-50.4	-26.7	18.5	1.1
	25	1.0	0.01	-76.0	0.3	-50.1	-25.9	29.2	0.8

Table 3.7 Thermodynamic parameters obtained from the interaction between N-Hsp90-T101I with AMP-PNP and ADP in the presence of $MgCl_2$ across a temperature range of 8-25 °C.

The involvement of T22 in the ATP-bound N-Hsp90 has been addressed in a study by Ali *et al.*[16], who illustrated the role of this residue in intermolecular and inter-domain rearrangements within the N and M domains of opposing protomers of the Hsp90 dimer. T22 resides on the main body of N-Hsp90 close to the top end of the ATP lid. Its mutation to the more hydrophobic isoleucine should reinforce its contact with the back

nucleotide-free N domain. However in the AMP-PNP-bound N domain, the catalytic loop has been shown to close over the nucleotide binding site[16], and as such T22 would come into contact with the catalytic loop of the partner N domain, thus reinforcing the dimerisation interface via lid closure in the context of the full-length dimeric Hsp90. Therefore the T22I mutation could stabilise either a lid-open or a lid-closed conformation. If the T22I mutation stabilises the lid-closed conformation, it should resemble the ATP-bound N-Hsp90 complex, which has been demonstrated to result in lid closure. And if the lid-open conformation is stabilised via the T22I mutation, then the thermodynamic effects of this mutant should resemble that of the T101I mutant, which stabilises a lid-open N domain. Table 3.8 shows the thermodynamic parameters obtained from the interaction between N-Hsp90-T22I with AMP-PNP and ADP in the presence of 5 mM $MgCl_2$

	Temperature ° C	N	Error for N	$\Delta H°_{obs}$ kJ mol^{-1}	Error for $\Delta H°_{obs}$ kJ mol^{-1} (+/-)	$T\Delta S°_{obs}$ kJ mol^{-1}	$\Delta G°_{obs}$ kJ mol^{-1}	K_d µM	Error for µM K_d
AMP-PNP	8	0.9	0.07	-29.6	13.1	-4.8	-24.7	25.7	3.9
	10	1.0	0.09	-32.9	1.7	-8.4	-24.4	30.9	5.7
	15	1.0	0.07	-28.5	1.1	-3.6	-24.9	30.5	4.7
	20	0.9	0.04	-34.6	0.9	-10.1	-24.5	43.1	3.2
	22	0.9	0.12	-35.9	2.7	-12.0	-23.8	60.2	10.1
	25	1.0	0.20	-40.2	5.6	-16.7	-23.6	74.0	17.2
ADP	8	0.9	0.01	-63.2	0.5	-34.9	-28.2	5.7	0.6
	10	0.9	0.01	-64.0	0.6	-36.2	-27.7	7.7	0.8
	15	1.0	0.01	-68.5	0.7	-41.6	-26.7	14.1	1.1
	20	1.0	0.01	-71.8	0.9	-45.8	-25.9	23.7	1.8
	22	1.1	0.01	-73.0	0.6	-47.2	-25.7	28.0	1.5
	25	1.1	0.01	-79.0	1.1	-53.9	-25.0	41.6	3.0

Table 3.8 Thermodynamic parameters obtained from the interaction between T22I with AMP-PNP and ADP in the presence of $MgCl_2$ across a temperature range of 8-25 °C.

3.7.4.1. Thermodynamics arising from lid closure in wild-type N-Hsp90 show similarities to a lid 'open' N-Hsp90

From the thermodynamic data given in Table 3.9, it is evident that when compared to the thermodynamics from WT-N-Hsp90 for both AMP-PNP and ADP interactions, the observed changes in enthalpy, entropy, free energy and K_d values are highly comparable with N-Hsp90-T101I and N-Hsp90-T22I in the ADP interaction.

Ligand	Construct	$\Delta H°_{obs}$ (kJ mol^{-1})	Error for $\Delta H°_{obs}$ (+/-)	$T\Delta S°_{obs}$ (kJ mol^{-1})	$\Delta G°_{obs}$ (kJ mol^{-1})	Kd (µM)	Error for K_d (+/-)
AMP-PNP	WT	-53.6	2.19	-31.1	-22.5	97.0	10.2
	T101I	-59.8	1.7	-35.5	-24.2	47.8	4.8
	T22I	-34.6	0.9	-10.1	-24.5	43.1	3.2
ADP	WT	-72.8	0.66	-45.2	-27.4	12.8	0.9
	T101I	-69.4	0.6	-41.9	-27.3	13.4	0.9
	T22I	-71.8	0.9	-45.8	-25.9	23.7	1.8

Table 3.9 Thermodynamic parameters obtained from the interaction between WT-N-Hsp90, N-Hsp90-TI01I, and N-Hsp90-T22I with AMP-PNP and ADP in the presence of $MgCl_2$. Data shown from ITC titrations at 20°C.

The thermodynamics presented, generally follow the same trend as that of WT N-Hsp90, in that all interactions are consistently exothermic and enthalpically driven. ADP binding shows a more favourable $\Delta H°_{obs}$ and a less favourable $T\Delta S°_{obs}$ than with AMP-PNP binding. As discussed earlier these observations are most likely due to the larger AMP-PNP moiety playing a role in trapping fewer water molecules at the binding interface and instead displacing these water molecules by the formation of new contacts between itself and N-Hsp90, possibly as a result of the movement of the ATP lid mediated via the γ-phosphate. With ADP, this ability to displace solvent molecules is likely to be impaired, as the closure of the ATP lid does not occur. Therefore the water molecules present in the binding site become trapped upon ADP binding, resulting in the entropic cost becoming less favourable.

As mentioned above, N-Hsp90-T101I stabilises the lid-open conformation, as with the WT N-Hsp90:ADP bound state. Therefore the comparable thermodynamics in this

instance would make sense for the data shown for the interaction between N-Hsp90-T101I with AMP-PNP and ADP, as does the negative $\Delta C_p°_{obs}$ shown in Figure 3.16. The K_d values for the WT-N-Hsp90:AMP-PNP interactions however, are not comparable to that for N-Hsp90-T101I with AMP-PNP. N-Hsp90-T101I is demonstrated to bind to AMP-PNP with a 2-fold stronger affinity compared with WT-N-Hsp90. The steric hindrance arising from potential ATP lid closure as a result of AMP-PNP binding to WT-N-Hsp90 could provide an understanding of the stronger binding affinity observed with N-Hsp90-T101I, which seems likely with an N-Hsp90 that has its ATP lid open, hence allowing the binding pocket to be more accessible.

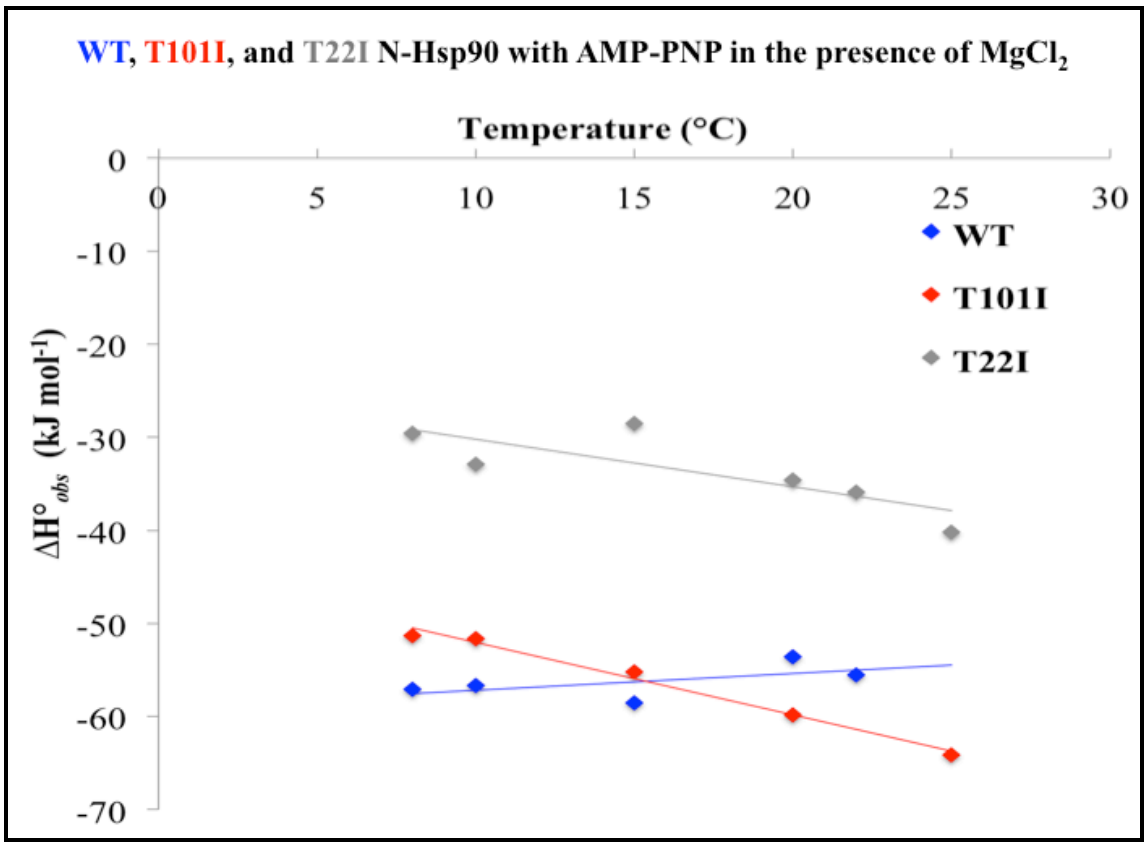

Figure 3.14 $\Delta H°_{obs}$ against temperature plots for AMP-PNP binding to WT N-Hsp90, N-Hsp90-T101I, and N-Hsp90-T22I in the presence of $MgCl_2$; the calculated $\Delta Cp°_{obs}$ are approximately +180, -779 and -512 J mol^{-1}/°C respectively.

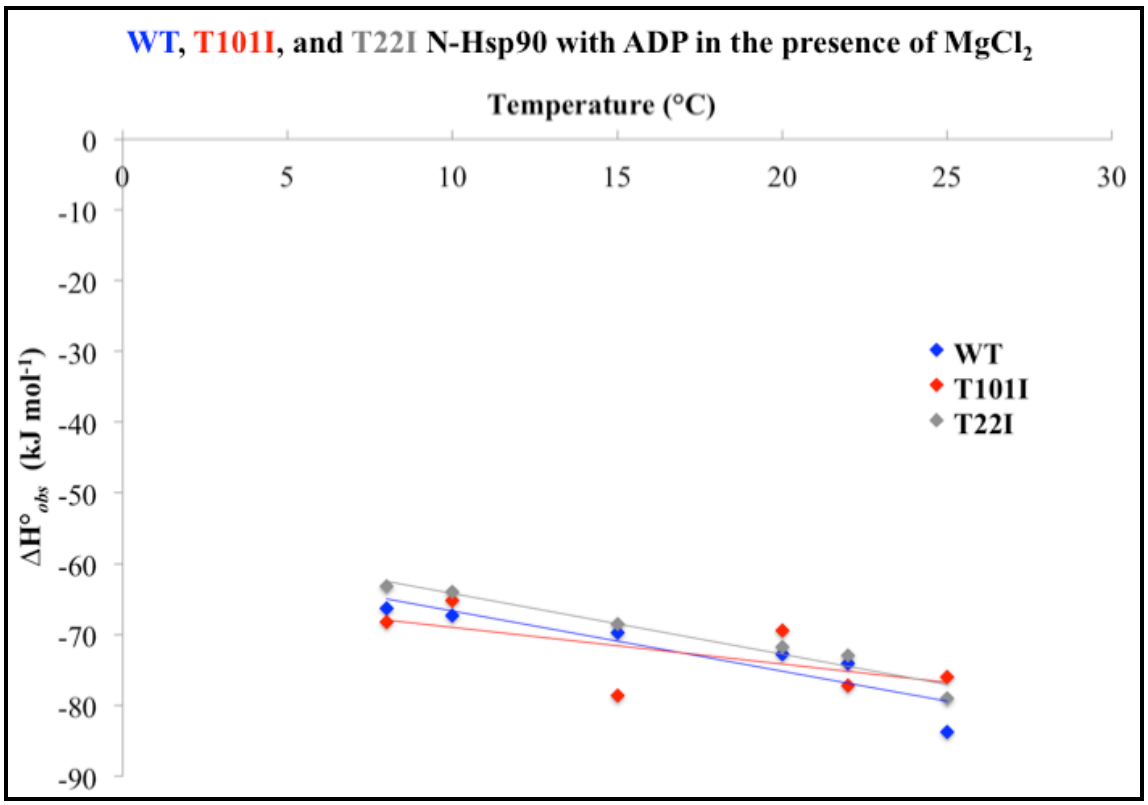

Figure 3.15 ΔH°_{obs} against temperature plots for ADP binding to WT N-Hsp90, N-Hsp90-T101I, and N-Hsp90-T22I in the presence of $MgCl_2$; the calculated ΔCp°_{obs} are approximately -850, -517 and -857 J mol^{-1}°/C respectively.

Figure 3.15 and 3.16 show the $\Delta C_p^{\circ}_{obs}$ for the interaction between WT-N-Hsp90, N-Hsp90-T101I and N-Hsp90-T22I with both nucleotides. The calculated $\Delta C_p^{\circ}_{obs}$ values for the interaction of AMP-PNP with WT-N-Hsp90, N-Hsp90-T101I and N-Hsp90-T22I are approximately +180 J mol^{-1}/°C, -779 J mol^{-1}°/C, and -512 J mol^{-1}°/C respectively. The negative value observed with the N-Hsp90-T101I:AMP-PNP interaction of approximately -779 J mol^{-1}/°C is in agreement with that of the WT-N-Hsp90:ADP interaction of approximately -850 J mol^{-1}/°C, which further validates that an open lid N-Hsp90 gives a negative change in heat capacity upon surface area burial through association with the nucleotide. This finding also holds true for ADP binding to N-Hsp90-T101I, which also shows a negative change in heat capacity with a value of approximately -517 J mol^{-1}/°C although to a lesser extent than with the WT-N-Hsp90:ADP interaction of approximately -850 J mol^{-1}/°C. The lower value for $\Delta C_p^{\circ}_{obs}$ seen with the N-Hsp90-T101I:ADP interaction compared with that of WT-N-Hsp90, can be due to the fact that the ATP lid in WT-N-Hsp90 is not in a 'fixed' position as

with N-Hsp90-T101I, and so more energy is probably required to control an ATP lid that is flexible in comparison to a lid that is 'fixed' to a specific conformation.

The negative value of $\Delta C_p°_{obs}$ (-779 J mol^{-1}/°C) seen with the N-Hsp90-T101I:AMP-PNP interaction in comparison to that of WT-N-Hsp90 (+180 J mol^{-1}/°C), provides evidence for the observation made by Nilapwar *et al*.[19] in that the positive heat capacity change observed with the WT-N-Hsp90:AMP-PNP interaction may be due to closure of the ATP lid, exposing a hydrophobic surface to the bulk solvent.

N-Hsp90-T22I, in which the ATP lid could be in either the open or closed conformation, also shows a 2-fold stronger binding affinity for AMP-PNP binding than with WT-N-Hsp90, demonstrating a lid that is more likely to be in the open conformation. These findings suggest that the ATP lid in WT-N-Hsp90 (which shows a weaker binding affinity with AMP-PNP compared with N-Hsp90-T22I) may be flexible, where it either switches between open and closed or is in a intermediate position between open/closed, causing destabilisation of the bound ATP, and full closure of the lid is possibly achieved once other conformational changes within the Hsp90 dimer take place, ultimately promoting ATP hydrolysis.

If we consider that the closure of the ATP lid is the sole reason for the observed positive heat capacity change seen with WT-N-Hsp90, then an N-Hsp90 in which the ATP lid is potentially stabilised to the closed conformation should also yield a positive heat capacity change regardless of which nucleotide it interacts with. Contrary to this hypothesis are the findings from the titrations between N-Hsp90-T22I and AMP-PNP and ADP. Figure 3.15 and 3.16 show that the binding of AMP-PNP and ADP to N-Hsp90-T22I results in a negative change in observed heat capacity. It is interesting to see that the $\Delta C_p°_{obs}$ value for ADP binding to a N-Hsp90-T22I is comparable to the WT-N-Hsp90:ADP interaction, as are the other thermodynamic parameters (Table 3.9), implying that supposed artificial lid closure does not affect the binding of ADP in terms of enthalpic and entropic costs. This validates an earlier observation of the possibility of the lid in N-Hsp90-T22I not being closed.

3.8 Dissecting the involvement of the divalent ion through effects on thermodynamics from the ATP lid

In order to scrutinize the thermodynamic effects of ATP lid closure in combination with metal ion hydration properties in reference to the observed positive heat capacity change of N-Hsp90 with AMP-PNP, the earlier approach of metal ion substitution would have to be utilised. If the apparent stable six coordinate divalent Mg^{2+} ion plays a crucial role in of the observed anomalous positive heat capacity, then the substitution of this ion would change the thermodynamics of the interaction between the ATP lid mutants N-Hsp90-T101I and N-Hsp90-T22I with AMP-PNP and ADP in a way that should be distinguishable.

The data so far suggest that AMP-PNP binds to WT-N-Hsp90 with a positive $\Delta C_p^\circ{}_{obs}$ in the presence of Mg^{2+}, Mn^{2+}, and Ca^{2+} with values of +180, +109, and +853 J mol^{-1}/°C respectively (Table 3.1 and 3.3). The thermodynamic effects of these interactions are enthalpically less favourable and entropically more favourable with Ca^{2+} than with Mg^{2+} and Mn^{2+}. This observation could potentially be related to the varied hydration shell of the Ca^{2+} ion in comparison to the more stable hydration shells of Mg^{2+} and Mn^{2+} ions.

It has been suggested that the closure of the ATP lid could be the reason for this observed positive heat capacity change with the AMP-PNP interaction. The demonstration of lid closure being the reason for the positive $\Delta C_p^\circ{}_{obs}$ is further validated by the negative $\Delta C_p^\circ{}_{obs}$ observed with the ADP interaction, which results in a lid-open N-Hsp90. Contrary to this are the thermodynamic effects of an N-Hsp90 mutant in which the ATP lid has potentially been stabilised to the closed conformation, which provides no evidence of a positive change in heat capacity, rather this mutant reflects a negative $\Delta C_p^\circ{}_{obs}$, similar that of the WT-N-Hsp90:ADP interaction. The results from N-Hsp90-T22I suggest that the mutation of Thr22 to Ile may not stabilise a lid-closed structure, which could then explain the similarities in thermodynamics with WT-N-Hsp90. An N-Hsp90 mutant in which the ATP lid is stabilised to the open conformation also results in a negative $\Delta C_p^\circ{}_{obs}$ as would be expected, since the interaction between WT-N-Hsp90 and ADP (forming a lid-open N-Hsp90) also results in a negative heat capacity change. And therefore, the inconclusive data so far suggest that the anomalous positive ΔC_p° seen with the WT-N-Hsp90:AMP-PNP interaction

although may seem to partially relate to the gross dynamics of the ATP lid, must also accrue from another source.

Figure 3.17 illustrates the comparison between the thermodynamic parameters obtained from the interaction between N-Hsp90-T101I and N-Hsp90-T22I with AMP-PNP in the presence of Mg^{2+}, Mn^{2+}, and Ca^{2+} with that of WT-N-Hsp90. As with WT-N-Hsp90, the interaction between N-Hsp90-T101I with AMP-PNP in the presence of Ca^{2+} is enthalpically less favourable and entropically more favourable than with Mg^{2+} and Mn^{2+}, further reflecting the ability of the varied hydration shell of the Ca^{2+} ion trapping less solvent molecules at the binding interface and rather expels these water molecules into bulk solvent. Surprisingly, the binding affinities (Figure 3.17c) for the interaction between N-Hsp90-T101I and N-Hsp90-T22I with AMP-PNP are extremely comparable in the presence of Mg^{2+}, further demonstrating a possible lid-open structure for N-Hsp90-T22I.

On the contrary, the interactions in the presence of Mn^{2+} and Ca^{2+} show weaker affinities for the N-Hsp90-T22I:AMP-PNP interaction. For the Ca^{2+} interaction, the weaker affinity could be due to a reduction in this ions ability to contribute to the hydrogen bonding network that is a prominent feature of the N-Hsp90-AMP-PNP interaction[19] as a result of its less hydrated solvation shell. For the Mn^{2+} interaction, a weaker affinity is surprising since the WT-N-Hsp90:AMP-PNP interaction in the presence of this ion results in an approximate 2-fold stronger affinity than with that of the Mg^{2+} interaction. These data suggest that there may be a variation in the hydration shell of Mn^{2+} in comparison to the six-coordinate Mg^{2+} ion (as previously mentioned), and this varied hydration shell can either impair (less water reduces hydrogen bonding capability) or hinder (entrapment of more water, reducing the degrees of freedom of water molecules at the protein/ligand interface) the interaction between N-Hsp90 and AMP-PNP. Considering the unfavourable $T\Delta S°_{obs}$ seen with the N-Hsp90-T22I:AMP-PNP interaction in the presence of Mn^{2+} when compared to that in the presence of Mg^{2+}/Ca^{2+}, a case of more water coordinating the Mn^{2+} ion seems likely.

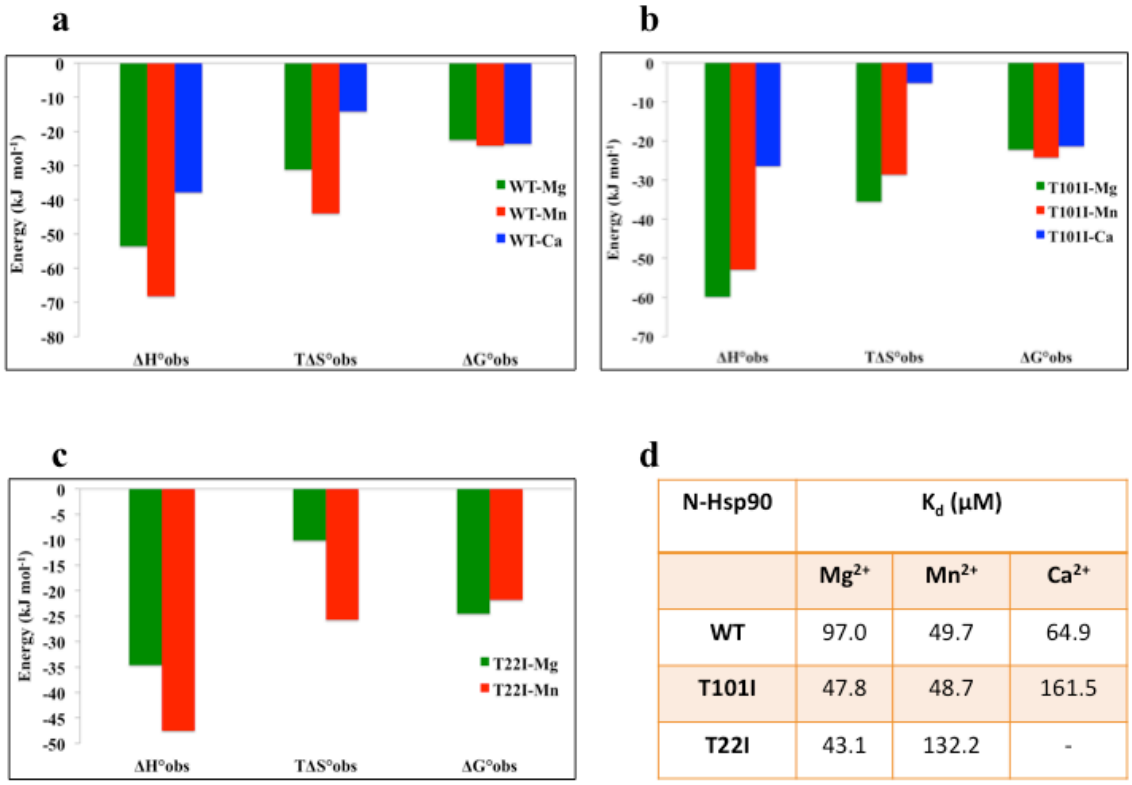

N-Hsp90	K_d (μM)		
	Mg^{2+}	Mn^{2+}	Ca^{2+}
WT	97.0	49.7	64.9
T101I	47.8	48.7	161.5
T22I	43.1	132.2	-

Figure 3.16 Comparison of the thermodynamic profiles of the interaction of AMP-PNP with **a,** WT-N-Hsp90, **b,** N-Hsp90-T101I, **c,** N-Hsp90-T22I in the presence of Mg^{2+}, Ca^{2+}, and Mn^{2+}. **d,** binding affinities of representative interactions. Data shown for titrations performed at 20°C.

Figure 3.18 shows the observed heat capacity changes for the interaction of AMP-PNP with WT-N-Hsp90, N-Hsp90-T101I, and N-Hsp90-T22I. A negative $\Delta C_p°_{obs}$ is observed for the interaction between AMP-PNP with both N-Hsp90-T101I and N-Hsp90-T22I in the presence of Mg^{2+} (approximately -779 and -512 J mol^{-1}/°C respectively). These values suggest that the closure of the ATP lid may not entirely be responsible for the observed positive heat capacity change seen with WT-N-Hsp90 (approximately +180 J mol^{-1}/°C). Interestingly, the interaction of AMP-PNP with N-Hsp90-T101I in the presence of Mn^{2+} and Ca^{2+} yields a positive $\Delta C_p°_{obs}$, with values of approximately +414 and +1262 J mol^{-1}/°C respectively. In contrast, N-Hsp90-T101I shows a value of approximately -779 J mol^{-1}/°C for the interaction with AMP-PNP in the presence of Mg^{2+}. These data strongly indicate the possibility of the contribution of the hydration shells of these ions giving rise to the variations in the changes in heat

capacity as N-Hsp90-T101I has its lid stabilised to the open conformation, and so its $\Delta C_p°_{obs}$ should reflect that of the WT-N-Hsp90:ADP interaction, which is negative.
The N-Hsp90-T101I interaction with AMP-PNP in the presence of Ca^{2+} results in a more favourable $T\Delta S°_{obs}$ than with that of the WT-N-Hsp90:AMP-PNP:Ca^{2+} interaction, further supporting the earlier hypothesis of an ATP lid that could be in an intermediate between open and closed, as an N-Hsp90 in which the lid is forced in the open conformation would trap less water than a lid that is 'flexible' as with WT-N-Hsp90.

The thermodynamic data for the interaction between N-Hsp90-T22I and AMP-PNP in the presence of Mg^{2+} again resulted in a negative observed heat capacity change with a $\Delta C_p°_{obs}$ value of approximately -512 J mol^{-1}/°C , although to a lesser extent than with N-Hsp90-T101I. This data strongly suggests that the lid in N-Hsp90-T22I could be open (as mentioned earlier), however the location of T22 behind the top of the catalytic loop in comparison to the location of T101 in close contact to the back bottom of the catalytic loop allows the catalytic loop in T22I to possibly destabilise slightly upon AMP-PNP binding, thus resulting in a less negative change in heat capacity in comparison to the T101I mutant. Contrary to this observation, is the observation of an almost linear change in observed heat capacity of approximately -7.0 J mol^{-1}/°C for the interaction between N-Hsp90-T22I with AMP-PNP in the presence of Mn^{2+}, and a heat capacity change that was undistinguishable with the Ca^{2+} interaction due to the extremely weak nature of the N-Hsp90-T22I:AMP-PNP interaction in the presence of this ion. These data suggest that for both Mn^{2+} and Ca^{2+} interactions, the effect of the T22I mutation has a significant effect on the gross thermodynamics of the system, unlike for the Mg^{2+} interaction, further supporting a view of the waters coordinating the metal ion to be of importance. For the Mg^{2+} interaction, the T22I mutation produces a more positive $\Delta C_p°_{obs}$ and a more favourable $T\Delta S°_{obs}$ when compared to that of WT-N-Hsp90, suggesting that the apparent closed lid traps less water, which is the opposite effect one would expect upon lid closure. These data therefore agree with the idea of the T22I mutation not actually producing a fully lid-closed N-Hsp90 post AMP-PNP binding as implied by a Thr:Ile mutation within this region. Furthermore, the less positive $\Delta C_p°_{obs}$ and less favourable $T\Delta S°_{obs}$ seen with the WT-N-Hsp90:AMP-PNP interaction in comparison to that of N-Hsp90-T22I, further supports the view of WT-N-Hsp90 adopting a lid conformation that could be in an intermediate between open and

closed, as partial lid closure would expose partial hydrophobic surface to bulk solvent as opposed to full lid closure.

On the contrary the interaction between N-Hsp90-T22I and AMP-PNP in the presence of Mn^{2+} produces a negative $\Delta C_p°_{obs}$ but a more favourable $T\Delta S°_{obs}$ in comparison to WT-N-Hsp90/Mn^{2+} (as with the same interaction in the presence of Mg^{2+}). These data again suggest that the apparent closed lid in the Mn^{2+} interaction probably traps less water than a lid that could be flexible.

a

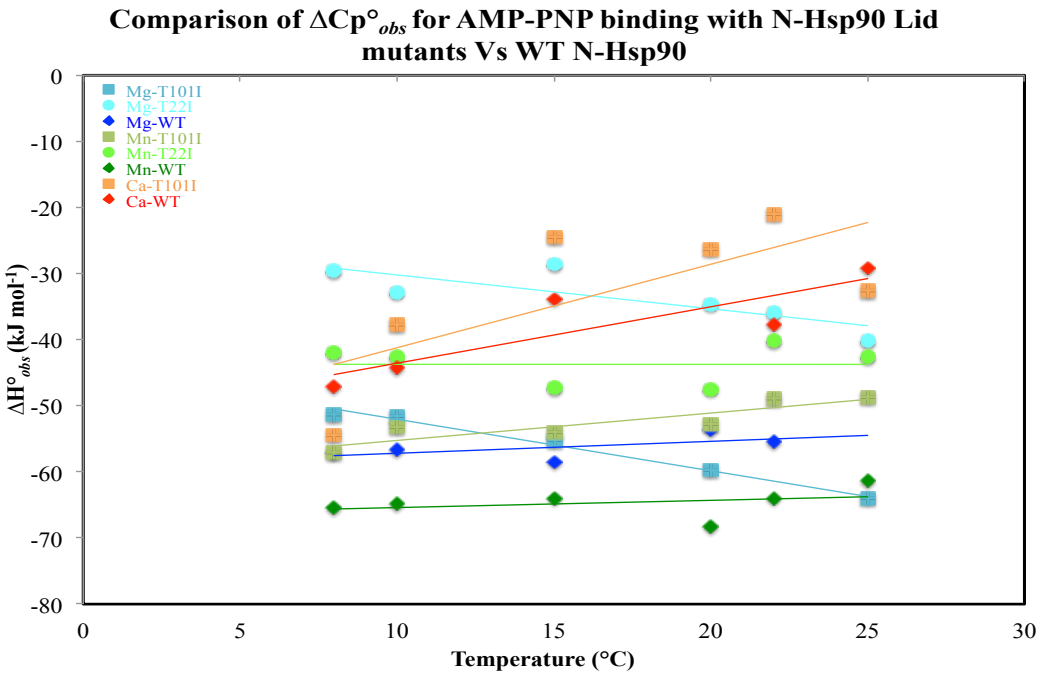

b

Construct	ΔCp°_{obs}
Mg-T101I	-779
Mg-T22I	-512
Mg-WT	+180
Mn-T101I	+414
Mn-T221I	-7.0
Mn-WT	+109
Ca-T101I	+1262
Ca-T22I	-
Ca-WT	+853

Figure 3.17 a, ΔH°_{obs} against temperature plots for AMP-PNP binding to N-Hsp90 lid mutants compared with WT-N-Hsp90 in the presence of $MgCl_2$, $MnCl_2$, and $CaCl_2$. **b,** Calculated values of $\Delta C_p^{\circ}{}_{obs}$ for N-Hsp90 lid mutants compared with WT-N-Hsp90 in the presence of $MgCl_2$, $MnCl_2$, and $CaCl_2$.

Figure 3.19 illustrates the comparison between the thermodynamic parameters obtained from the interaction between WT-N-Hsp90, N-Hsp90-T101I, and N-Hsp90-T22I with ADP in the presence of Mg^{2+}, Mn^{2+}, and Ca^{2+}.

The interaction of N-Hsp90-T101I and N-Hsp90-T22I with ADP in the presence all metal ions follows the same trend as with WT-N-Hsp90, in that all interactions are enthalpically more favourable and entropically less favourable.

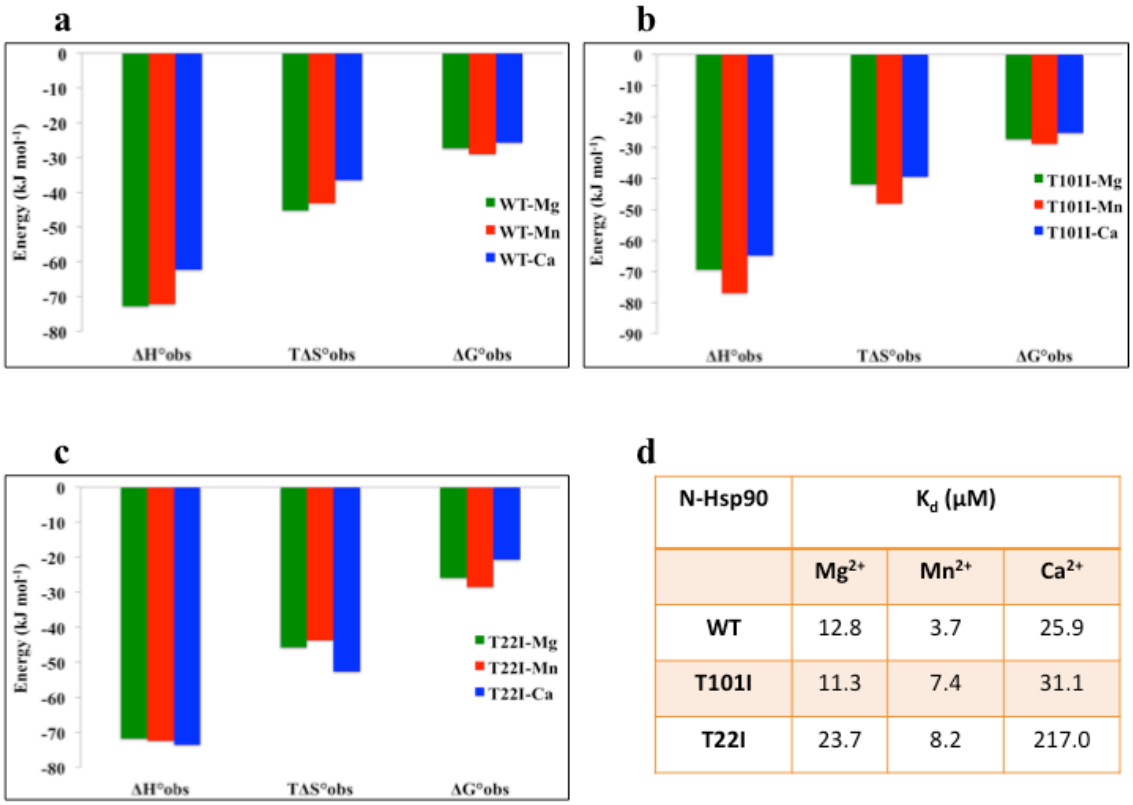

N-Hsp90	K_d (μM)		
	Mg^{2+}	Mn^{2+}	Ca^{2+}
WT	12.8	3.7	25.9
T101I	11.3	7.4	31.1
T22I	23.7	8.2	217.0

Figure 3.18 Comparison of the thermodynamic profiles of the interaction of ADP with **a,** WT-N-Hsp90, **b,** N-Hsp90-T101I, **c,** N-Hsp90-T22I in the presence of Mg^{2+}, Ca^{2+}, and Mn^{2+}. **d,** binding affinities of representative interactions. Data shown for titrations performed at 20°C.

Interestingly, the similarities observed between WT-N-Hsp90 and both lid mutants provides further evidence of the possibility of the lid in N-Hsp90-T22I not being fully closed. Furthermore, as with WT-N-Hsp90, a negative $\Delta C_p°_{obs}$ is derived upon ADP binding to both lid mutants in all ion-interactions as illustrated in Figure 3.20.

a

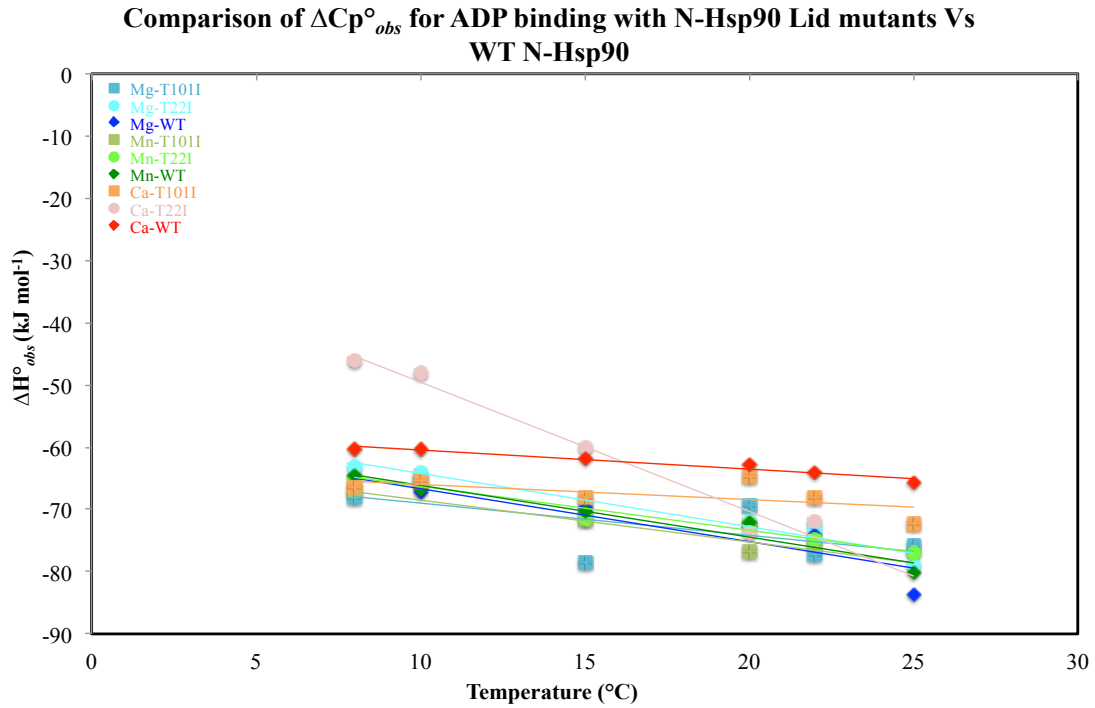

b

Construct	ΔCp°_{obs}
Mg-T101I	-517
Mg-T22I	-857
Mg-WT	-850
Mn-T101I	-671
Mn-T22I	-707
Mn-WT	-911
Ca-T101I	-242
Ca-T22I	-2077
Ca-WT	-307

Figure 3.19 ΔH°_{obs} against temperature plots for ADP binding to N-Hsp90 lid mutants compared with WT-N-Hsp90 in the presence of $MgCl_2$, $MnCl_2$, and $CaCl_2$. **b,** Calculated values of $\Delta C_p^{\circ}{}_{obs}$ for N-Hsp90 lid mutants compared with WT-N-Hsp90 in the presence of $MgCl_2$, $MnCl_2$, and $CaCl_2$.

WT-N-Hsp90 bares similarities to N-Hsp90-T22I in terms of the changes in heat capacity, further demonstrating a lid that is probably not in the fully closed conformation for N-Hsp90-T22I. N-Hsp90-T101I shows a less negative $\Delta C_p^{\circ}{}_{obs}$

possible flexibility of the ATP lid in WT-N-Hsp90. WT-N-Hsp90 is assumed to adopt an 'open' conformation upon binding of ADP and hence a negative $\Delta C_p°_{obs}$, a flexible ATP lid (as with WT-N-Hsp90) may induce further lid opening than a lid that is fixed to a specific open conformation (as with N-Hsp90-T101I).

The interaction between the lid mutants and ADP in the presence of Ca^{2+} revealed the most significant differences in $\Delta C_p°_{obs}$. N-Hsp90-T101I and WT-N-Hsp90 appear to have similar effects upon ADP binding, whereby WT-N-Hsp90 (like with the Mg^{2+} interaction) shows a slightly more negative $\Delta C_p°_{obs}$, again supporting the view of a flexible lid in WT N-Hsp90. The interaction between N-Hsp90-T22I and ADP in the presence of Ca^{2+} results in a much larger negative change in heat capacity of approximately -2077 $Jmol^{-1}/°C$ than with both N-Hsp90-T101I and WT-N-Hsp90 (of -242 and -307 $Jmol^{-1}/°C$ respectively). This data provides implications for the hydration shell of the Ca^{2+} ion playing a role in the derived $\Delta C_p°_{obs}$, as the other metal ion interactions of N-Hsp90-T22I appear to be comparable. Furthermore, the weak affinity of the interaction of N-Hsp90-T22I with ADP in the presence of Ca^{2+}, and an affinity that was unobtainable for the AMP-PNP interaction, also implicate the role of its hydration shell in the observed thermodynamics.

3.9 Summary

The data presented in this chapter strongly suggest that the positive heat capacity change observed in the interaction between N-Hsp90 and AMP-PNP does not arise solely due to conformational changes associated with the ATP lid and this was reflected in a derived negative $\Delta C_p°_{obs}$ for N-Hsp90 mutants in which the ATP lid was stabilised to both open and closed conformations. Furthermore, these data suggested that N-Hsp90-T22I, in which the lid could be stabilised to the open or closed conformation, binds with an affinity similar to that of N-Hsp90-T101I, in which the lid is stabilised to the open conformation. Both lid mutants show stronger binding affinities to that of WT-N-Hsp90. The stronger affinity observed for N-Hsp90-T101I is probably reflective of there being no structural hindrance (otherwise induced by lid movement) upon the binding of AMP-PNP. On the contrary, results from N-Hsp90-T22I demonstrate two potential observations; one is that the lid in this mutant is in the open conformation prior to AMP-PNP binding and this lid becomes partially destabilised upon AMP-PNP binding due to the location of the T22I mutation in comparison to the T101I mutation. And the second observation is that WT-N-Hsp90 could have an ATP lid that is in a

conformation between open and closed, and that partial closure of the ATP lid (or any conformational change of the lid) upon AMP-PNP binding leads to the weaker affinity observed with WT-N-Hsp90. In order to assess the true effects of ATP lid closure, a mutation close to the where the supposed closed ATP lid meets the main body of the N domain could be created, such as the A107N mutation used in the crystal structure of the full-length Hsp90 in complex with Sba1/p23[16].

Although a positive change in heat capacity is observed from the interaction between N-Hsp90 and AMP-PNP in the presence of Mg^{2+}, Mn^{2+}, and Ca^{2+}, the variations in $\Delta C_p°_{obs}$ observed with the different ions suggest alternative mechanisms of action. Furthermore, contrary to the negative heat capacity changes observed in the interaction of AMP-PNP with both N-Hsp90 lid mutants in the presence of Mg^{2+}, are the positive heat capacities observed with this interaction in the presence of Mn^{2+} and Ca^{2+}. Whereby the thermodynamic trends observed for Mn^{2+}, although enthalpically more favourable and entropically less favourable than with Mg^{2+}, are still comparable. The thermodynamics of all interactions in the presence of Ca^{2+} are consistently enthalpically less favourable and entropically more favourable then of that of the Mg^{2+} and Mn^{2+}interactions, demonstrating the possible role of the varied hydration shell of Ca^{2+}in the observed thermodynamics.

Chapter 4

Structural thermodynamic investigation of the Hsp90/ligand interaction through NMR

4.1 Introduction

As presented in Chapter 3, the binding of ATP (as mimicked by the non-hydrolysable analogue AMP-PNP) to the N-terminal domain of Hsp90 results in an anomalous positive $\Delta C_p°_{obs}$, which is not apparent in the interaction of this domain with ADP. The ADP interaction yields a negative $\Delta C_p°_{obs}$. Inhibitors of Hsp90, such as geldanamycin[19] also exhibit this negative $\Delta C_p°_{obs}$ on binding to N-Hsp90. The observation of opposite signs for $\Delta C_p°_{obs}$ for the binding of small molecules to the same binding site is unusual, particularly when one considers the fact that AMP-PNP and ADP differ in structure by a single phosphate. Factors which could give rise to a positive change in observed heat capacity have been evaluated in Chapter 3 through the use of ITC. The source of the positive $\Delta C_p°_{obs}$ is likely to be the result of a combination of more than one effect, these being a conformational change associated with the ATP lid upon AMP-PNP binding and the role of the hydration shell of the Mg^{2+} ion upon binding of AMP-PNP to N-Hsp90[11,16,19].

Previous studies have demonstrated that the divalent Mg^{2+} ion required for successful binding and hydrolysis of ATP in the Hsp90 system, sits in the junction between the two terminal phosphates of the ATP, and is involved in an extensive hydrogen bonding network between the protein and nucleotide[19]. The substitution of the native Mg^{2+} ion for Mn^{2+} in the AMP-PNP interaction with N-Hsp90 revealed comparable thermodynamic profiles, however, substituting the Mg^{2+} for Ca^{2+} revealed a $\Delta C_p°_{obs}$ which was approximately 7-fold more positive than for that of the Mg^{2+}interaction. Furthermore, metal ion substitution experiments with N-Hsp90 mutants where the ATP lid was stabilised to the open or closed conformation revealed completely opposite $\Delta Cp°_{obs}$ to the interactions of these mutants in the presence of Mg^{2+}. The data so far suggest that the variations observed in the $\Delta Cp°_{obs}$ values with the different metal ions must accrue from their individual hydration shell properties, since water has been shown to play a crucial role in the interaction between N-Hsp90 and its nucleotide

ligands. The hydration shells of the metal ions used in this study could explain the similarities observed in the thermodynamics between the N-Hsp90:nucleotide interactions in the presence of Mg^{2+} and Mn^{2+}, metal ions that have been shown to share common features in their hydrations shells[77,81,86]. Furthermore, the large discrepancies observed in the N-Hsp90:nucleotide interactions in the presence of Ca^{2+} could reflect its variable hydration shell[74].

In order to further address the possibility of the hydration properties of the metal ions playing a role in the $\Delta Cp°_{obs}$ for the N-Hsp90:AMP-PNP interaction, it is important to investigate if these divalent ions form different contacts between the protein and the nucleotide and whether they affect different amino acid residues, and if so, then how do they do this. This chapter uses nuclear magnetic resonance spectroscopy (NMR) in an attempt to extract potential variations in chemical shift changes for the interaction between N-Hsp90 with AMP-PNP in the presence of $MgCl_2$ and $CaCl_2$. ITC is used to investigate the thermodynamic effects of point mutations created to slightly alter the polarity of selected residues showing differences in the NMR titrations between the two metal ions in the N-Hsp90:AMP-PNP interaction. This chapter aims to reveal information on the structural basis of the anomalous $\Delta Cp°_{obs}$ seen with the N-Hsp90:AMP-PNP interaction in an attempt to provide insight into the nature of the interaction.

4.2 NMR reveals chemical shifts changes which are both common and unique in the interaction between N-Hsp90 with AMP-PNP in the presence of Mg^{2+} and Ca^{2+}

4.2.1 Sample preparation, data acquisition and processing

N-Hsp90 samples were prepared as described in Chapter 2 using ^{15}N-ammonium sulphate and ^{12}C-glucose, resulting in a singe isotopically labelled protein suitable for NMR spectroscopy. ^{15}N HSQC spectra were acquired using a spectrometer operating at 700 MHz using the experimental parameters described in Chapter 2. Data collection and processing was carried out by Dr Eleanor Williams (UCL) using CCPNmr software. Backbone resonances for N-Hsp90 were taken from published data from the group[19] and were used as a basis from which differences in chemical shifts were depicted in the interaction between N-Hsp90 with AMP-PNP in the presence of $CaCl_2$; this was

achieved by superimposing the apo and AMP-PNP bound spectra in the presence of $MgCl_2$ with the AMP-PNP bound spectra in the presence of $CaCl_2$.

4.2.2 Similarities in the interaction between AMP-PNP and N-Hsp90 in the presence of Ca^{2+} and Mg^{2+} observed using NMR spectroscopy

^{15}N HSQC spectra of N-Hsp90 were collected in the apo and AMP-PNP-bound states in the presence of $CaCl_2$; Figure 4.1 shows the spectral overlay between apo and AMP-PNP-bound N-Hsp90 in the presence of $CaCl_2$. These spectra were then compared to the ^{15}N HSQC spectra obtained from the interaction between N-Hsp90 and AMP-PNP in the presence of $MgCl_2$ from a previous study[19]; Figure 4.2 shows the spectral overlay between apo and AMP-PNP-bound N-Hsp90 in the presence of $MgCl_2$.

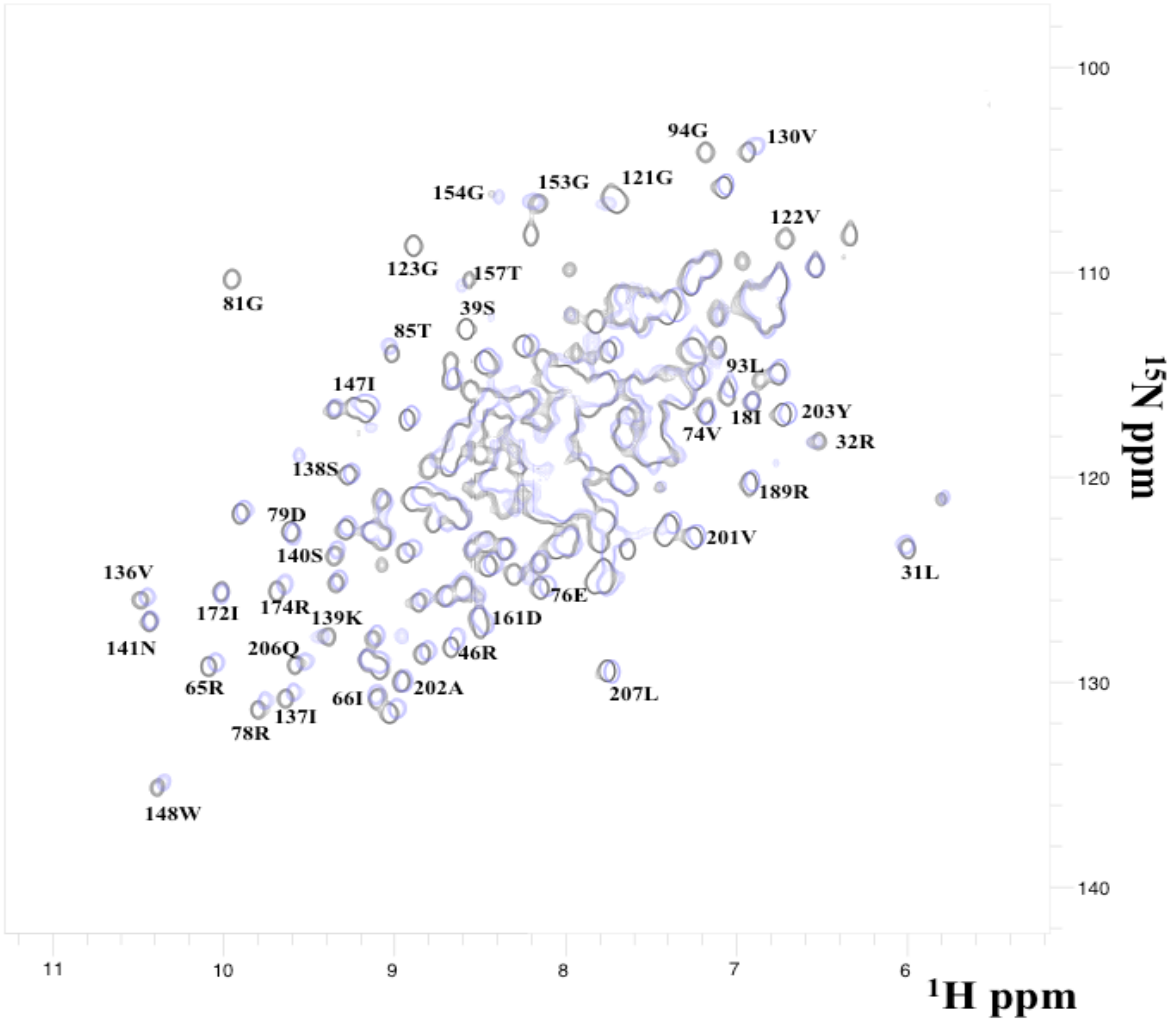

Figure 4.1 HSQC spectra of the apo and AMP-PNP-bound N-Hsp90. Overlay of the apo (black) and AMP-PNP bound N-Hsp90 representing the chemical shift changes in the presence of Ca^{2+} (blue).

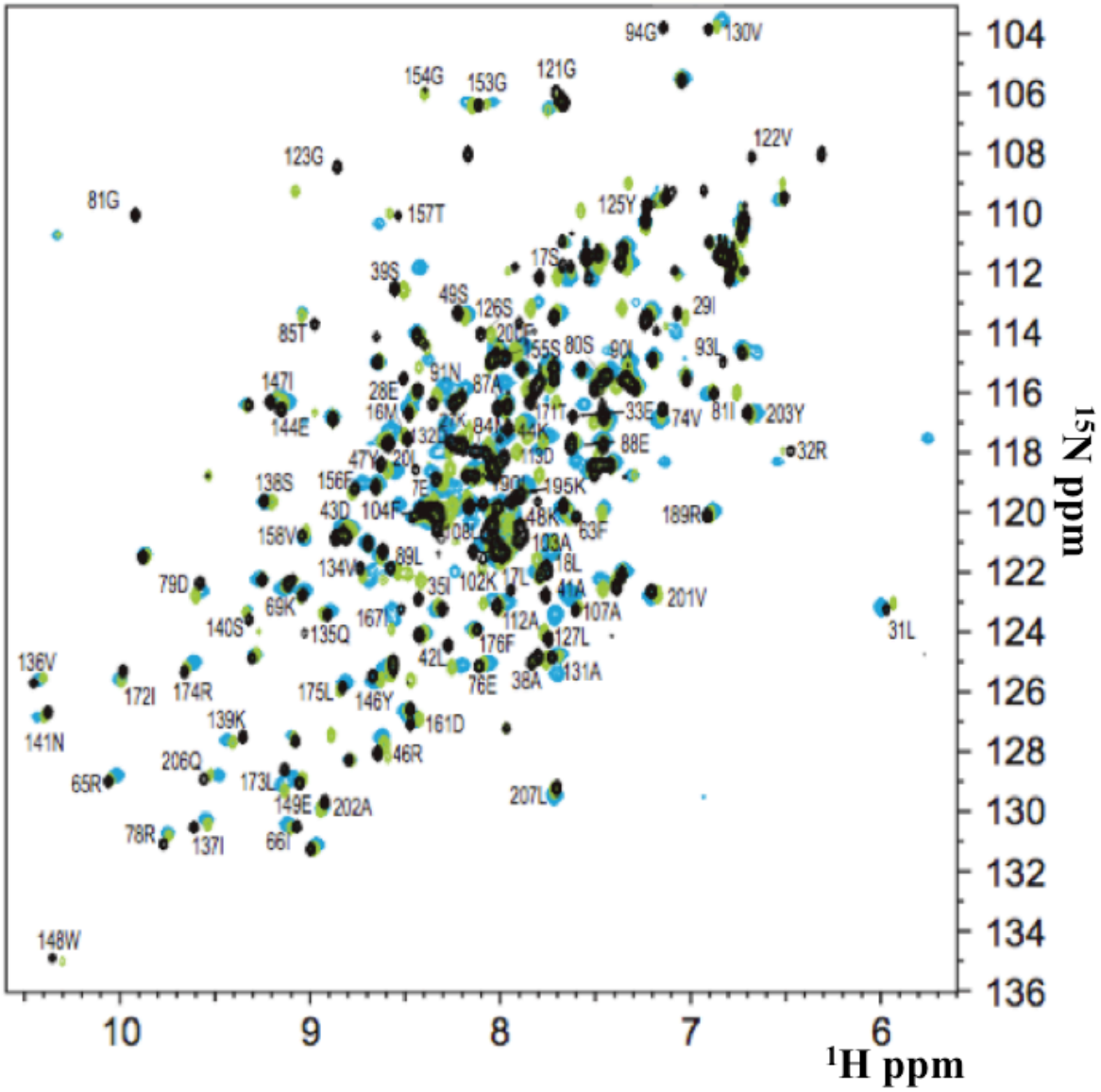

Figure 4.2 HSQC spectra of the apo and AMP-PNP bound N-Hsp90. Overlay of the apo (black) and AMP-PNP bound N-Hsp90 representing the chemical shift changes in the presence of Mg^{2+} (cyan). Data taken from Nilapwar *et al*.[19].

*The green data represents the spectrum of the interaction between N-Hsp90 and cAMP, which is not under investigation in this study.

The chemical shift changes that are shared between each interaction in the presence of the two metal ions are shown on the crystal structures of N-Hsp90 bound to ADP (a structure which represents the ligand-free/apo conformation) and AMP-PNP as illustrated in Figure 4.3.

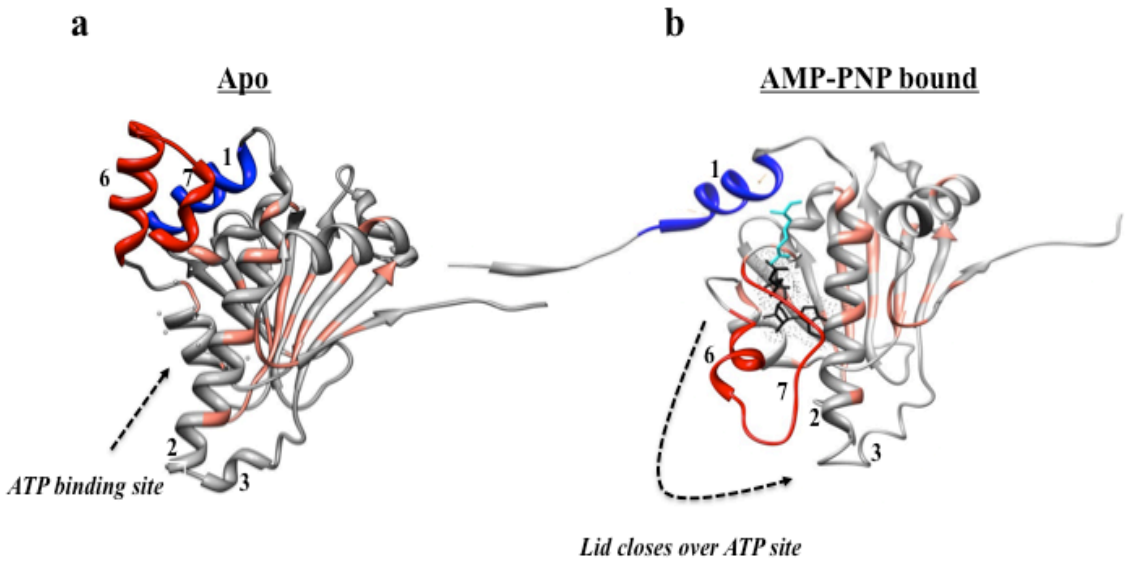

Figure 4.3 Chemical shift changes (pink) associated with N-Hsp90 in the ligand free and AMP-PNP-bound conformations that are shared between $CaCl_2$ and $MgCl_2$. **a,** N-Hsp90-ADP complex[7]. **b,** N-Hsp90-AMP-PNP complex highlighting the bound AMP-PNP (black)[16]. Both structures highlight the N-terminal strand (blue) and ATP lid (red). α-helices that are affected upon AMP-PNP association are numbered on each structure.

The figure shows numerous chemical shift changes that are common in the interaction between N-Hsp90 and AMP-PNP in the presence of both Ca^{2+} and Mg^{2+}. The number of common chemical shift changes in both metal ion interactions illustrate that the bulk of structural rearrangements occurring upon AMP-PNP binding are the result of local shifts around the nucleotide binding pocket and the rearrangement of the ATP lid as demonstrated in Chapter 3. The back of the nucleotide binding pocket is composed of a β-sheet structure and is largely affected upon AMP-PNP binding, whereby seven adjacent amino residues are affected in both metal interactions (Gln135, Val136, Ile137, Ser138, Lys139, and Ser140). These residues sit opposite the adenine moiety of the ATP molecule, suggesting that a disruption to these residues would result in a significant impact on the interaction between N-Hsp90 and AMP-PNP.

As has been previously demonstrated, ATP lid closure presents one of the major conformational changes upon ATP binding in N-Hsp90[8], and this can be seen from the extent in which the structures of α-helices 6 and 7 on Figure 43 are effected, whereby α-helix 7 completely unwinds on going from the nucleotide-free to the nucleotide-bound conformation. If lid closure indeed results upon ATP binding, this closed lid would

come into contact with the base of α-helix 2 (residues 27 – 51; Figure 4.3b), this is clearly evident by the chemical shift changes seen within this region. However, only two of the affected residues seem to show a close contact with the closed lid, Ser39 and Arg46. The chemical shift changes seen at the upper end of α-helix 2 (Ile29, Leu31, Arg32) could possibly be affected by the movement of the N-terminal strand (α-helix 1), a conformational rearrangement also observed upon ATP binding leading to the dimerisation of both N domains of the Hsp90 dimer.

Chapter 3 demonstrates how the ATP lid of N-Hsp90 could possibly be in an intermediate conformation between open/closed; the chemical shifts affecting the base of the α-helix 2 only show two residues being disrupted. When considering the effect of full lid closure, one would expect a larger disruption to the base of this α-helix as this helix is pushed into an almost upright position in the lid-closed conformation on going from lid-open to a lid-closed (Figure 4.2). The chemical shift changes observed in our NMR titrations of both metal ion interactions suggest that the repositioning of α-helix 2 upon AMP-PNP binding (as shown in the crystal structure) may actually be caused from a rearrangement of α-helix 1, rather than full lid closure as suggested[16]. If the latter speculation were true, this would fit well with observations made in Chapter 3 where it was suggested that the ATP lid in WT-N-Hsp90 could be in an intermediate between open/closed. Furthermore, the fully lid-closed Hsp90 structure demonstrated by Ali *et al.*[16] was induced via an A107N mutation (mentioned earlier) which forced the ATP lid in a closed conformation, allowing N domain dimerisation to take place. Furthermore, any additional conformational rearrangements associated with the ATP lid could result from co-chaperone association, an effect that would not be seen in our NMR titration on the isolated N-Hsp90 domain in the absence of both the A107N mutation and the co-chaperone Sba1/p23.

The disappearance of the cross peak for residues Leu93 and Gly94 (which form part of the ATP lid) for the interaction between N-Hsp90 and AMP-PNP in the presence of Ca^{2+} shown in as Figure 4.4 fits well with same interaction in the presence of Mg^{2+}, demonstrated by Nilapwar *et al*.[19] shown in Figure 4.5. The disappearance of the peaks for the above residues are a result of conformational exchange on the intermediate NMR timescale, where the change in frequency (or chemical shift change) is probably close to the frequency of the conformational change itself resulting in a disappearance of the

cross peaks for these residues. Nilapwar *et al.*[19] showed that the exchange of these two residues is as a result of ATP lid movement and indicative of N-Hsp90 being in the AMP-PNP –bound state. Therefore, the disappearance Gly94 in the Ca^{2+} interaction provided evidence for N-Hsp90 being in the AMP-PNP-bound conformation, at which point the titration of AMP-PNP into the sample containing N-Hsp90 and $CaCl_2$ was stopped.

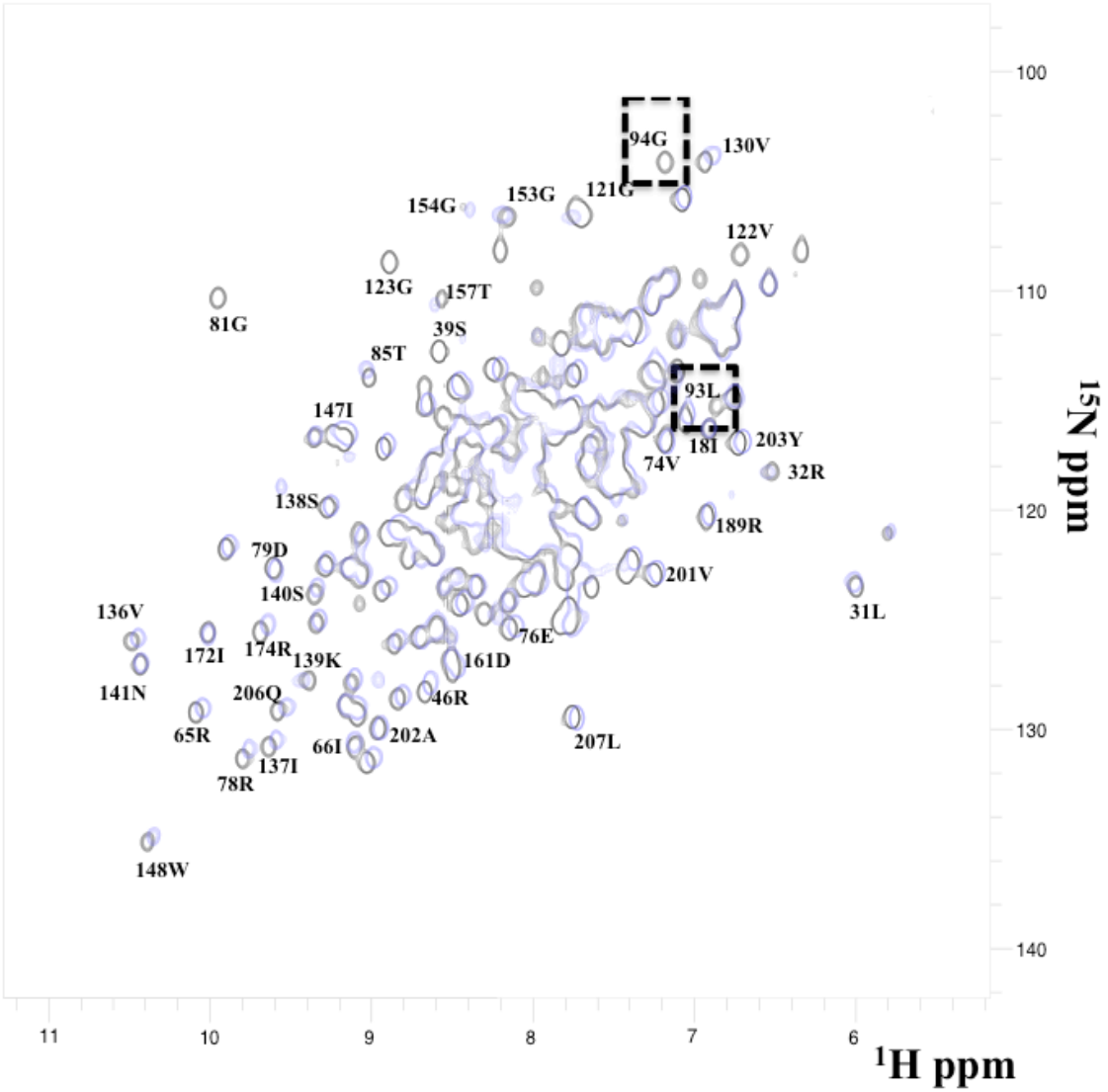

Figure 4.4 Overlay of the HSQC spectra of the apo and AMP-PNP bound N-Hsp90. Highlighting the disappearance of the cross peaks for residues Leu93 and Gly94 on going from the apo (black) to the AMP-PNP bound N-Hsp90 in the presence of Ca^{2+} (blue).

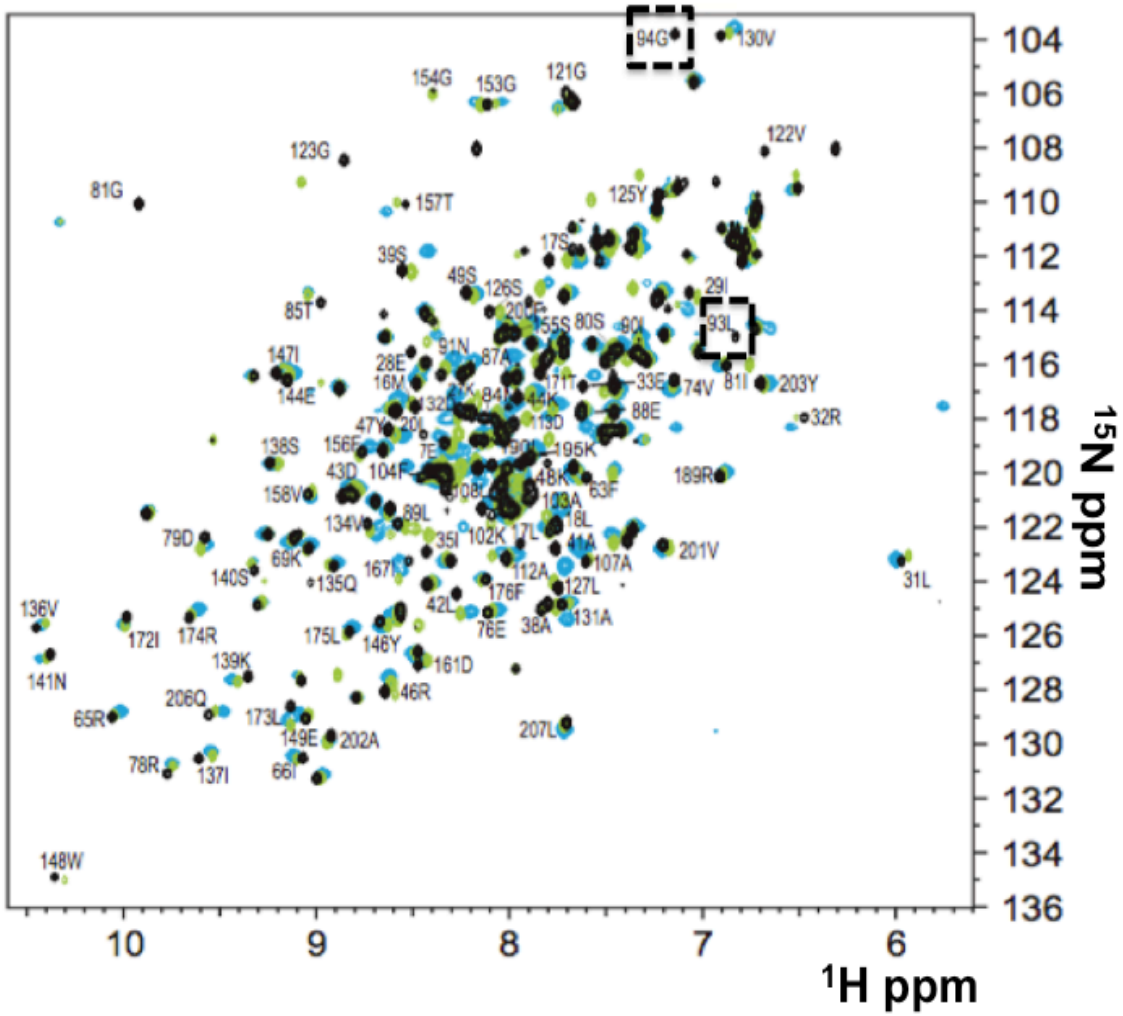

Figure 4.5 Overlay of the HSQC spectra of the apo and AMP-PNP bound N-Hsp90. Highlighting the disappearance of the cross peaks for residues Leu93 and Gly94 on going from the apo (black) to the AMP-PNP bound N-Hsp90 in the presence of Mg^{2+} (cyan).

Figure 4.6 illustrates where residues Leu93 and Gly94 reside in the AMP-PNP bound complex of the crystal structure of full-length Hsp90 in complex with AMP-PNP[16]. These residues lie at the base of the ATP lid, a region which is fully exposed in the ATP lid-open conformation, however upon apparent lid closure, this region encompassing the base of the lid appears to become buried, possibly reflected in the disappearance of the cross peaks corresponding to Leu 93 and Gly94.

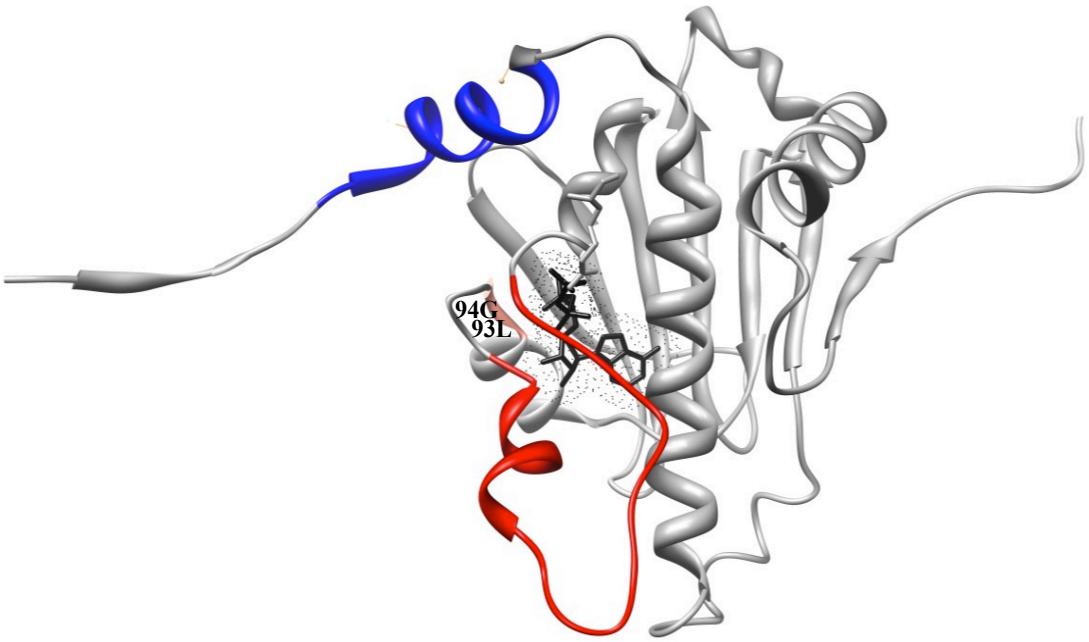

Figure 4.6 N-Hsp90-AMP-PNP complex[16] highlighting residues Leu93/Gly94 (pink), the ATP Lid (red), N-terminal strand (blue), and bound AMP-PNP (black).

4.2.3 Variations in the interaction between N-Hsp90 and AMP-PNP are observable in the presence of Ca^{2+} and Mg^{2+}

In addition to the chemical shift changes that are common between both ion interactions, there were also chemical shift changes that were unique to both ion interactions further implicating the effect of the divalent ion inducing conformational variations independent of that caused by the ATP molecule itself. Figure 4.7 highlights the regions of chemical shift changes that are unique in the interaction between N-Hsp90 with AMP-PNP in the presence of Ca^{2+}, and Figure 4.8 highlights the same residues for the Mg^{2+} interaction.

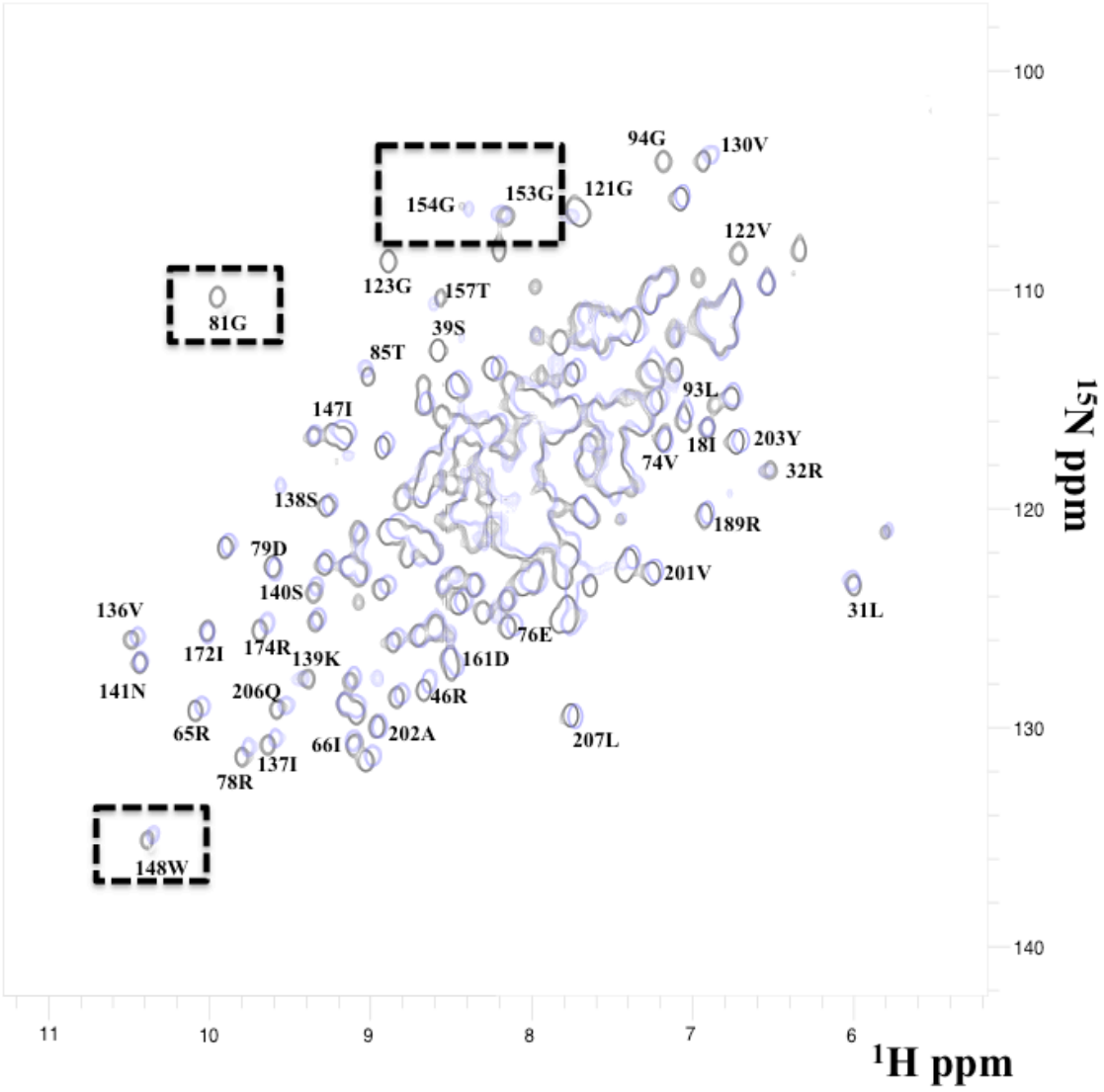

Figure 4.7 Overlay of the HSQC spectra of the apo and AMP-PNP bound N-Hsp90. Highlighting the unique chemical shifts in the interaction of N-Hsp90 on going from apo (black) with AMP-PNP in the presence of Ca^{2+} (blue).

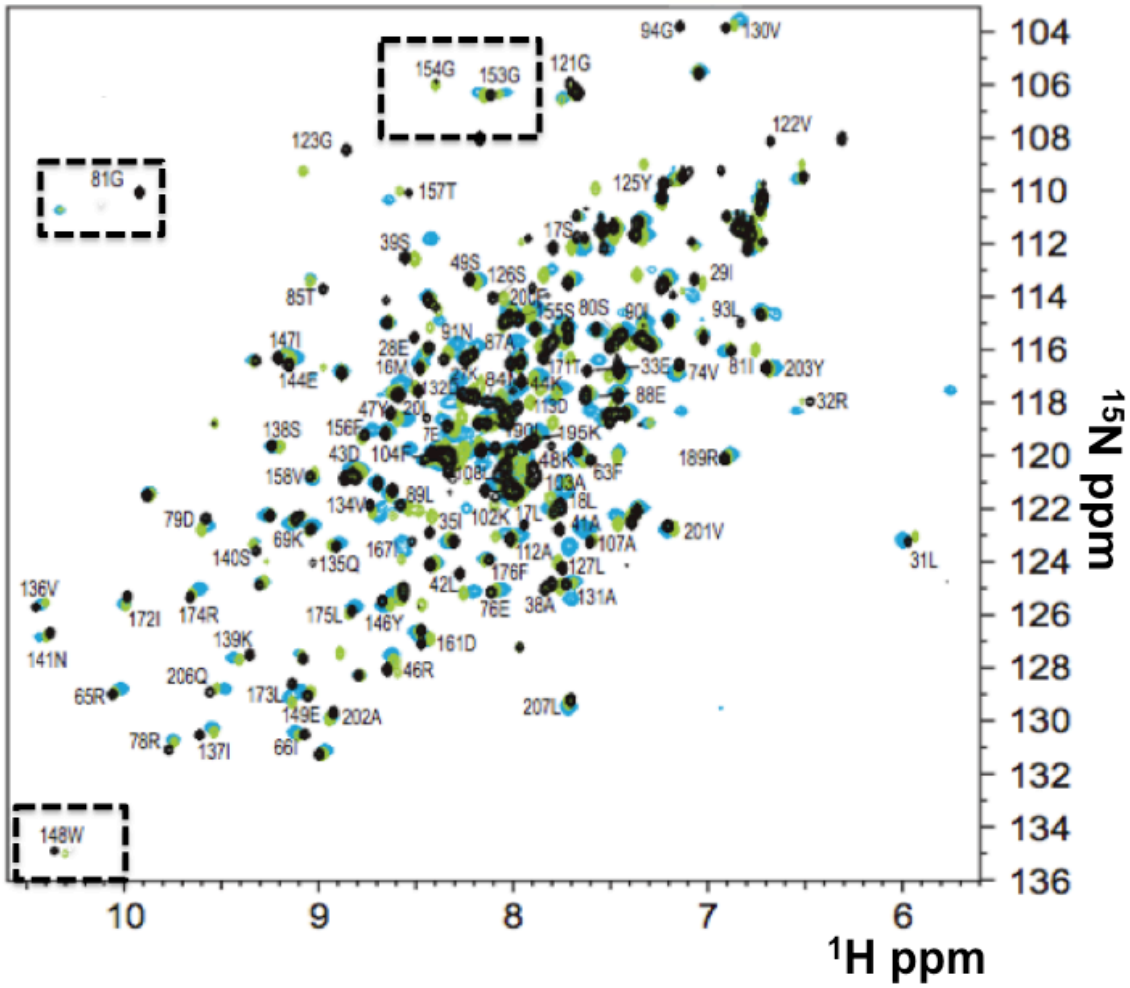

Figure 4.8 Overlay of the HSQC spectra of the apo and AMP-PNP bound N-Hsp90. Highlighting the unique chemical shifts in the interaction of N-Hsp90 on going from apo (black) with AMP-PNP in the presence of Mg^{2+} (cyan).

The chemical shift changes illustrated in the spectra are dramatic when one considers the nature of such large-scale effects as a result of the substitution of the Mg^{2+} ion with a Ca^{2+} ion. Figure 4.9 shows where these residues are located in terms of the N-Hsp90-AMP-PNP structure[16].

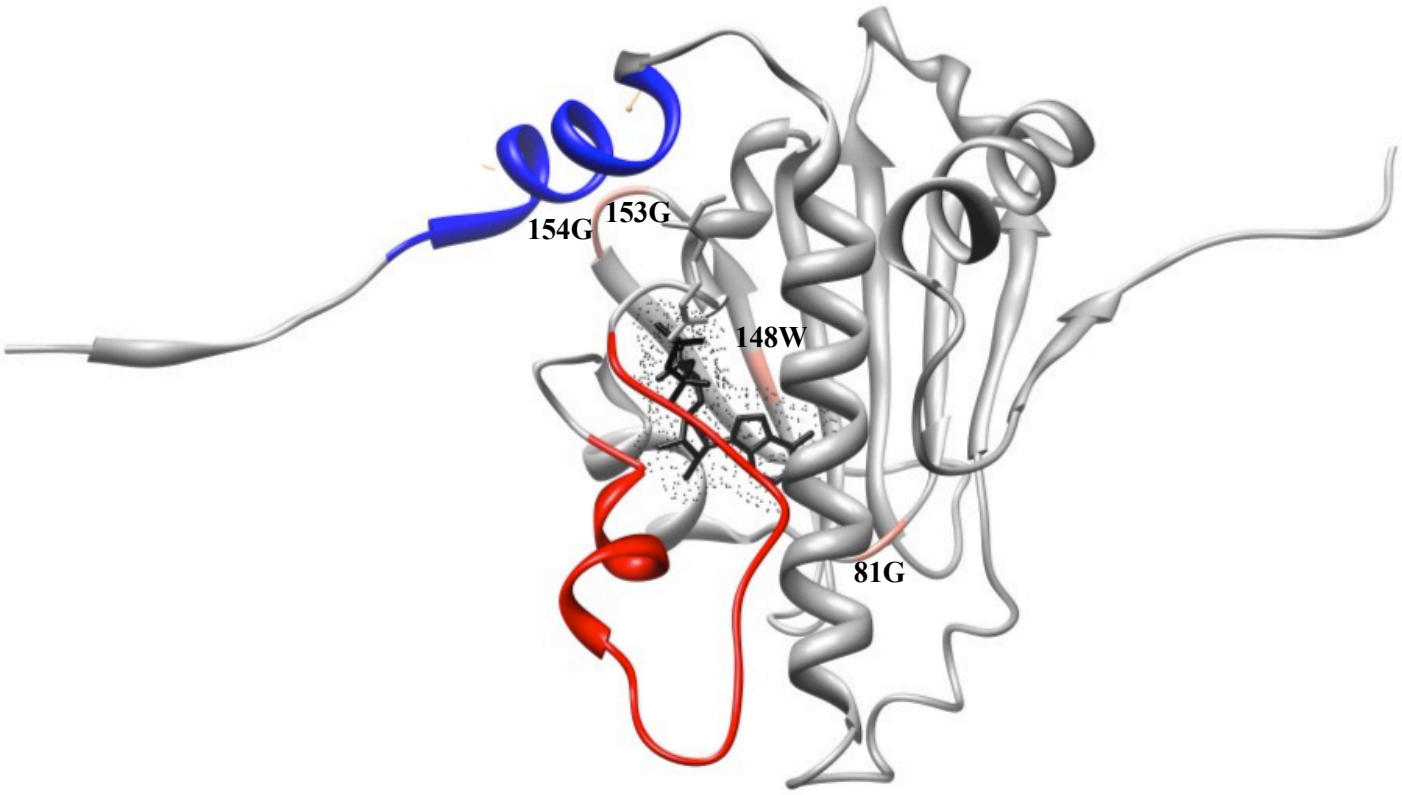

Figure 4.9 N-Hsp90-AMP-PNP complex[16] highlighting residues (pink) unique to the interactions with N-Hsp90 with AMP-PNP in the presence of Ca^{2+} and Mg^{2+}, the ATP lid (red), N-terminal strand (blue), and bound AMP-PNP (black).

Interestingly, residues Gly81, Trp148, Gly153, and Gly154 are located approximately 10-15 Å away from the nucleotide molecule and form part of the β-sheet structure that forms the back of the nucleotide binding pocket. As stated previously, the divalent Mg^{2+} ion although not visible in the available structures of Hsp90, is assumed to reside in the junction between the β and γ phosphates, and as stated by Nilapwar *et al.*[19] most of the interactions between the adenosine ligand and the protein are mediated via water molecules. Clearly the water molecules at the binding interface are an important feature of the interaction between N-Hsp90 its nucleotide ligands. The above observations show that the interaction between N-Hsp90 and AMP-PNP show minor differences in chemical shift perturbations of four distinct residues when the divalent ion is changed between Mg^{2+} and Ca^{2+}. Interestingly, these residues lie relatively far from the presumed ion-binding site; hence this leads to the assumption that since the two metal ions tested differ in their hydration states, the differences in chemical shift changes seen in Figure 4.9 could potentially arise as a result of this characteristic.

4.3 The effect of mutating Gly81, Trp148, Gly153, and Gly154 on the thermodynamic properties of the N-Hsp90/nucleotide interaction

Protein-ligand interactions have been demonstrated to result in a large negative change in $\Delta Cp°_{obs}$ as a result of site-specific binding by means of burying non-polar surface upon complex formation[66]. Contrary to this would be the observation of a positive $\Delta Cp°_{obs}$ resulting from a reduction or removal of polar surface. It has been demonstrated that the association of nucleotide ligands with N-Hsp90 involves a large number of water molecules (detailed in Chapter 3), which are ordered at the binding interface, particularly between the phosphate side chains of the nucleotide molecule, and the burial of these water molecules would result in a negative $\Delta Cp°_{obs}$[19] as is evident for the binding of ADP to N-Hsp90. On the contrary, the binding of AMP-PNP to N-Hsp90 results in a positive $\Delta Cp°_{obs}$, a characteristic more dominant when the interaction takes place in the presence of Ca^{2+} in comparison to the native Mg^{2+}, an effect which was speculated to be the result of the varying hydration shells of both ions.

The results from our NMR studies of the interaction between N-Hsp90 and AMP-PNP in the presence of $CaCl_2$ show slight variations in chemical shift changes corresponding to residues Gly81, Gly153, Gly154, and Trp148 when compared to the interaction in the presence of $MgCl_2$. The effect on residues Gly81 and Trp148 are more distinct as these cross peaks are shown to disappear in either the AMP-PNP-Ca^{2+}/Mg^{2+} spectra, whereas the cross peaks for Gly153 and Gly154 show smaller variations between the two ion interactions. Although these effects are reflective of minor chemical shift changes, these differences are apparent, and therefore it is questionable whether these chemical shift changes arise as a result of ion-specific effects in terms of the hydration shells.

In order to determine whether the differences in the NMR spectra for the interaction between N-Hsp90 and AMP-PNP in the presence of Mg^{2+} and Ca^{2+} is reflective of the metal ion hydration shells, N-Hsp90 mutants where the effected residues were mutated to slightly alter their polarity were experimented on using ITC. Altering the polarity of the effected residues could possibly disrupt the native cooperative hydrogen bonding network that has been extensively demonstrated in the Hsp90-nucletotide system[19], thus the thermodynamics obtained from these mutants may provide further insight into the source of the derived positive $\Delta Cp°_{obs}$ accompanying the N-Hsp90:AMP-PNP interaction.

4.3.1 The effects of Gly81Ala mutation

As illustrated by Figures 4.7 and 4.8, the cross peak corresponding to Gly81 is shifts in the N-Hsp90:AMP-PNP interaction in the presence of Mg^{2+}, but completely disappears in the interaction in the presence of Ca^{2+}. Interestingly, Gly81 lies buried at the base of the β-sheet that forms the back of the nucleotide binding site and faces the adenine ring structure of the nucleotide moiety, but still remains away from the region in which the nucleotide binds.

Considering the location of this residue, it is not surprising to see a shift in the resonance of Gly81 on going from ligand-free to ligand-bound, which is the case with the interaction between N-Hsp90 and AMP-PNP in the presence of both Mg^{2+}. However, the disappearance of the cross peak for this residue in the presence of Ca^{2+} means the environment around this residue is affected differently in the presence of the Ca^{2+} ion, providing implications for the possible role of the hydration shell of this ion being the cause of the disappearance of Gly81.

In order to asses the contribution of Gly81, an alanine mutation was created to see the effect on nucleotide binding of introducing a mildly hydrophobic property at this position. This mutation results in a bulkier amino acid at this position resulting in the loop on which this residue sits on becoming less flexible than it would be. Interestingly, upon attempting to purify this Gly81Ala mutant, the protein showed signs of insolubility despite using various expression conditions such as altering the temperature, IPTG concentrations and length of expression. The insoluble fraction was re-suspended in 8M urea, which then successfully bound to the nickel affinity column due to the N-terminal His-tag, however an attempt at refolding this protein failed and resulted in aggregation. This led me to question of the importance of this residue in Hsp90 and whether this residue was conserved in other Hsp90 homologues somehow causing its mutation to even a small mildly hydrophobic residue such as an alanine to become insoluble.

Figure 4.10 shows 4 homologues of yeast Hsp90 from the species *Homo sapiens, Trypansoma brucei, Leishmania major,* and *Plasmodium falciparum*, all of which exhibit approximately 70% homology to the *Saccharomyces cerevisiae* Hsp90 protein.

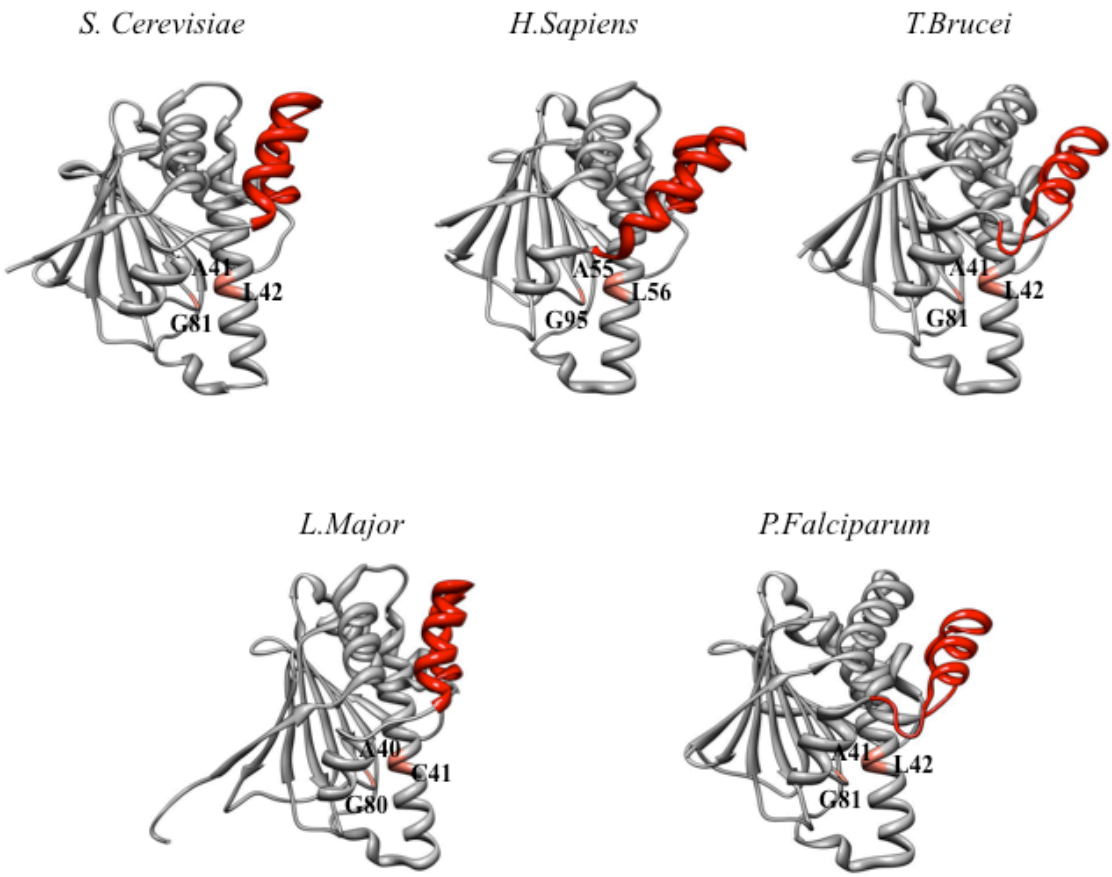

Figure 4.10 Structures of Hsp90 homologues showing 70% homology to *S.Cerevisiae* highlighting the ATP lid (red) and a few selected conserved residues (pink).

The above figure clearly illustrates the presence of a buried glycine residue in all Hsp90 homologues at the same position in which Gly81 resides in the *S.Cerevisiae* structure. In all homologues, this glycine residue lies opposite an Ala/Leu or an Ala/Cys region on α-helix 2 (as illustrated in Figure 4.3) directly opposite the glycine residue. By analysis of the structure, it seems as though the region in which this glycine residue sits leaves no space to accommodate even a small methyl group that would come from an alanine substitution. Furthermore, there is a high chance of the mutated alanine clashing with the conserved alanine on the opposing α-helix, hence it may not be surprising that the Gly81Ala mutant may lead to in an impairment of protein folding of N-Hsp90, resulting in an insoluble product.

4.3.2 The thermodynamic effects of the Gly153Ala and Gly154Ala mutations

Figures 4.7 and 4.8 demonstrate the slight variations in chemical shift changes for residues Gly153 and Gly154. Although the shifts in the cross peaks for these residues are small, they represent two of the four residues shown to be affected

differently with both metal ions and therefore pose as candidates for exploring potential ion-induced effects of the N-Hsp90:AMP-PNP interaction. In order to assess the potential ion-induced effects of these residues, alanine mutations of Gly153 and Gly154 were created and these mutants were experimented on using ITC.

Figure 4.11 and 4.12 show the thermodynamic parameters obtained from the interaction between the Gly153Ala and Gly154Ala N-Hsp90 mutants and AMP-PNP/ADP in the presence of Mg^{2+}, Ca^{2+}, and Mn^{2+}.

Generally, the thermodynamic profiles follow the same trends as with the WT-N-Hsp90:nucleotide interactions in that all interactions are exothermic and enthalpically driven. The interaction of these mutants with ADP in the presence of all metal ions results in a more favourable $\Delta H°_{obs}$ and a less favourable $T\Delta S°_{obs}$, a characteristic thermodynamic effect also seen with the WT-N-Hsp90:ADP interaction.

The data from the interaction of these mutants with AMP-PNP in the presence of Mg^{2+} and Mn^{2+} show similarities with the corresponding WT-N-Hsp90 interactions, whereby the interaction in the presence of Mg^{2+} results in a less favourable $\Delta H°_{obs}$ and a more favourable $T\Delta S°_{obs}$ in comparison to the Mn^{2+} interaction.

.

a

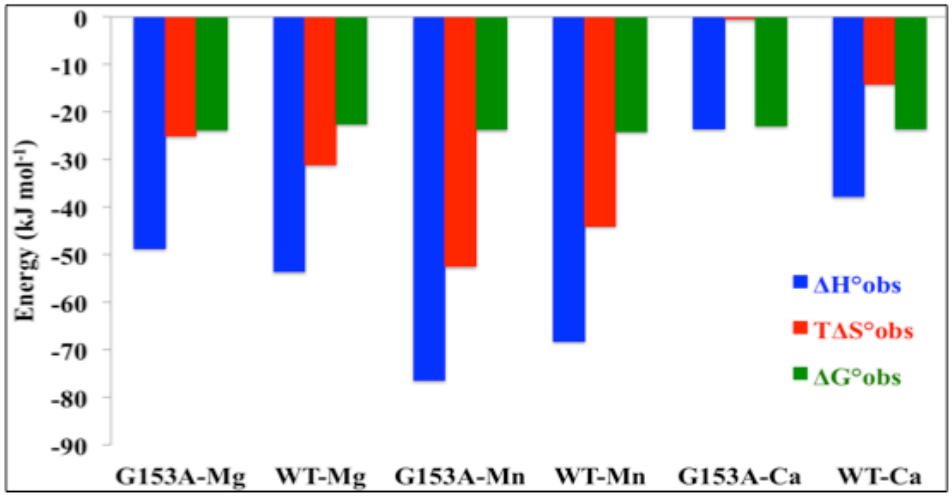

b

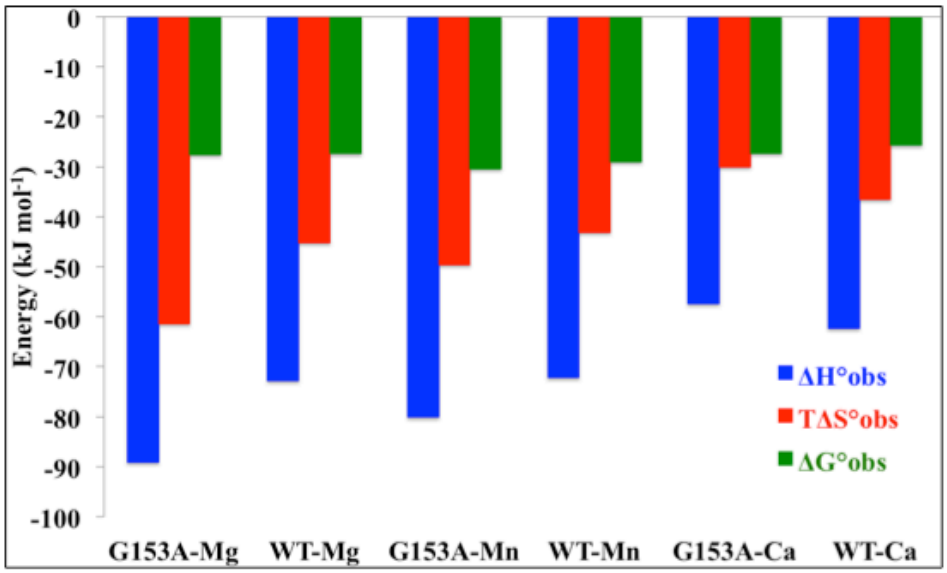

c

N-Hsp90	K_d (μM)	
	AMP-PNP	ADP
G153A-Mg	57.8	12.2
WT-Mg	97	12.8
G153A-Mn	58.8	3.8
WT-Mn	48.7	3.7
G153A-Ca	83.3	13.8
WT-Ca	64.9	25.9

Figure 4.11 Comparison of the thermodynamic profiles of the interaction of N-Hsp90-G153A compared with WT-N-Hsp90 with **a,** AMP-PNP, **b,** ADP, and **c,** binding affinities of corresponding titrations, in the presence of Mg^{2+}, Mn^{2+}, and Ca^{2+}. Data shown for titrations performed at 15°C.

a

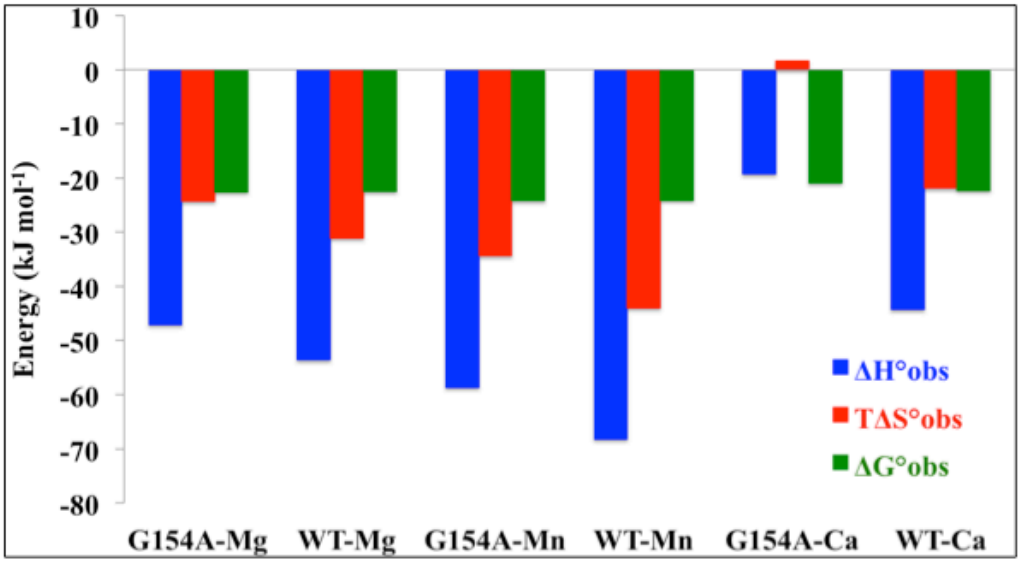

b

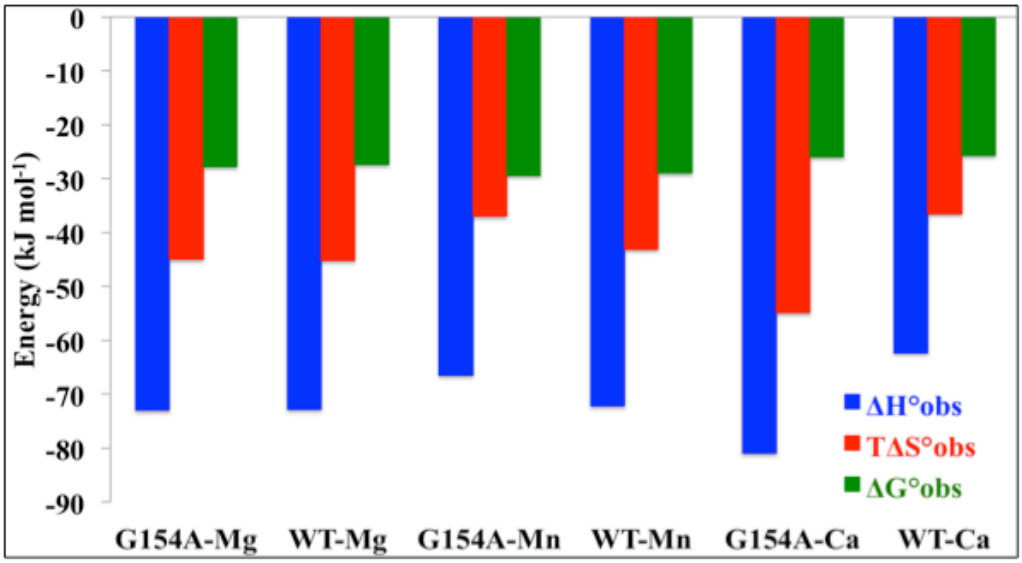

c

N-Hsp90	K_d (μM)	
G154-Mg	93.4	9.1
WT-Mg	97	7.0
G154A-Mn	48.3	5.6
WT-Mn	48.7	3.7
G154A-Ca	159.2	23.3
WT-Ca	88.4	25.9

Figure 4.12 Comparison of the thermodynamic profiles of the interaction of N-Hsp90-G154A compared with WT-N-Hsp90 with **a,** AMP-PNP, **b,** ADP, and **c,** binding affinities of corresponding titrations, in the presence of Mg^{2+}, Mn^{2+}, and Ca^{2+}. Data shown for titrations performed at 15°C.

The data from the interaction of these mutants with AMP-PNP in the presence of Ca^{2+} results in the most significant differences to that of the corresponding WT-N-Hsp90 interaction, in that the data from the mutants show a much more favourable $T\Delta S°_{obs}$ and a much less favourable enthalpy $\Delta H°_{obs.}$ in comparison to WT-N-Hsp90. The WT-N-Hsp90:AMP-PNP interaction in the presence of Ca^{2+} consistently results in a more favourable entropy, and as mentioned earlier this effect possibly reflects its variable hydration shell. The fewer number of water molecules coordinating the Ca^{2+} ion enable it to possibly trap less water present at the interfacial binding site and results in the release of these otherwise well-coordinated water molecules. The introduction of a slight hydrophobic property with the Gly:Ala mutation would result in an even more favourable entropy indicating the trapping of even less water, as would be expected from apolar surface. The calculated $\Delta Cp°_{obs}$ shown in Figure 4.13 of the interaction between N-Hsp90-G153A and AMP-PNP in the presence of Ca^{2+} further strengthens the observation of the effects of introducing a slight hydrophobic property as illustrated by a 3-fold increase in the temperature dependence of the interaction of approximately +2553 J mol^{-1}°/C. The thermodynamic effects seen with the Ca^{2+} interaction are also seen with the Mg^{2+} ion interaction, but to a lesser extent. The thermodynamic effects of the interaction in the presence of Mn^{2+} however results in a negative $\Delta Cp°_{obs}$ of approximately -771 J mol^{-1}°/C, a value comparable to the interaction of this mutant and WT-N-Hsp90 with ADP. This negative $\Delta Cp°_{obs}$ could reflect the presence of more water coordinating the Mn^{2+} ion, which becomes trapped upon nucleotide association, an effect also reflected in the less favourable $T\Delta S°_{obs}$ associated with this interaction in comparison to the WT N-Hsp90 interaction.

On the contrary, the calculated $\Delta Cp°_{obs}$ illustrated in Figure 4.14 for the interaction of N-Hsp90-G154A with AMP-PNP in the presence of Mg/Mn^{2+} show an approximate 6-9-fold increase in comparison to the interactions for WT N-Hsp90, and a 2-fold increase for that of the Ca^{2+} interaction. All interactions of this mutant are associated with a more favourable $T\Delta S°_{obs}$, as would be expected from the introduction of apolar surface area through the Gly:Ala mutation. Going back to the chemical shift changes observed for Gly154 (Figures 4.7 and 4.8), there was no significant change on going from nucleotide-free to nucleotide-bound in the presence of Ca^{2+}, however a shift was

in $\Delta Cp°_{obs}$ for the Gly154A:AMP-PNP:Ca^{2+} interaction of approximately +1661 J mol^{-1}°/C interaction as opposed to the much larger increase observed for the Gly154A:AMP-PNP:Mg/Mn^{2+} interactions of approximately +801 and +1087 J mol^{-1}°/C respectively. However, for the latter interactions, the significantly larger $\Delta Cp°_{obs}$ values suggest an increase in the net degrees of freedom of the waters at the protein:ligand interface and the more favourable entropy indicates trapping of less water by release of the well-coordinated interfacial molecules into bulk solvent. .

a

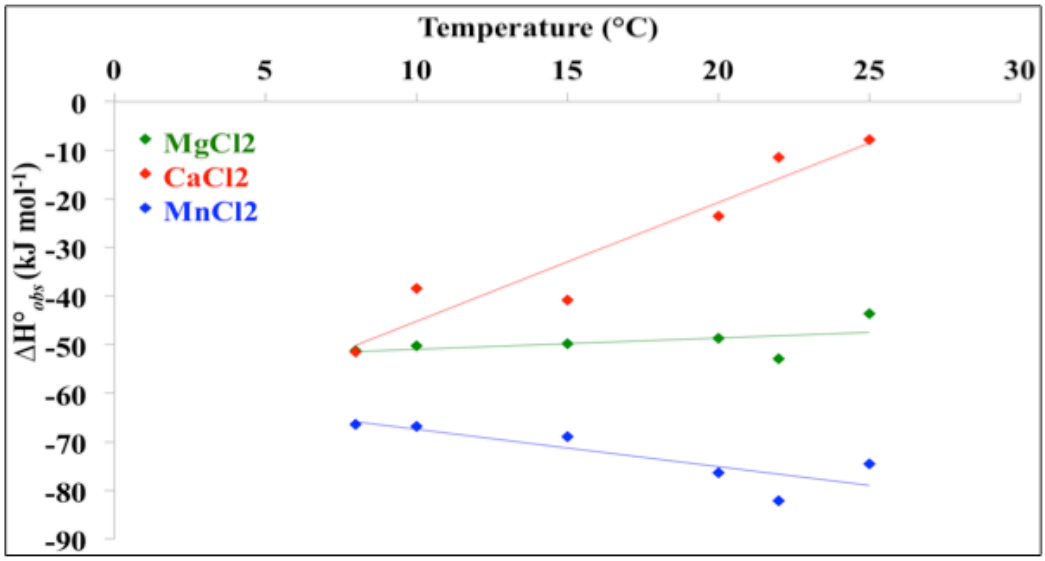

b

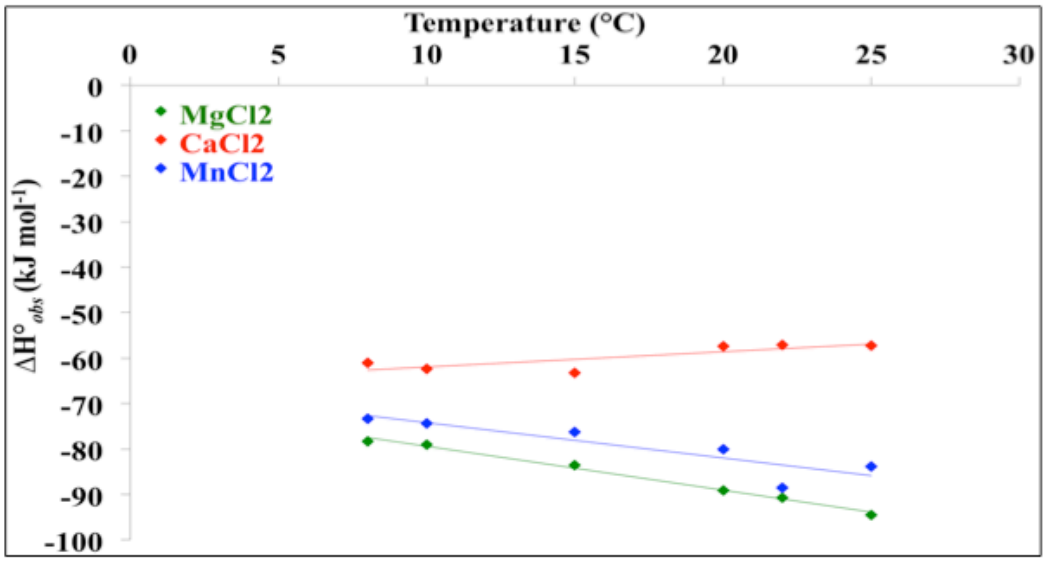

c

N-Hsp90	ΔCp°$_{obs}$ (J mol^{-1}/°C)	
	AMP-PNP	ADP
G153A-Mg	+231	-967
WT-Mg	+180	-850
G153A-Mn	-771	-778
WT-Mn	+109	-911
G153A-Ca	+2446	-335
WT-Ca	+853	-307

Figure 4.13 ΔH°$_{obs}$ against temperature plots for the interaction of N-Hsp90-G153A with **a,** AMP-PNP, **b,** ADP, and **c,** calculated ΔCp°$_{obs}$ compared with WT-N-Hsp90 in the presence of Mg^{2+}, Mn^{2+}, and Ca^{2+}

a

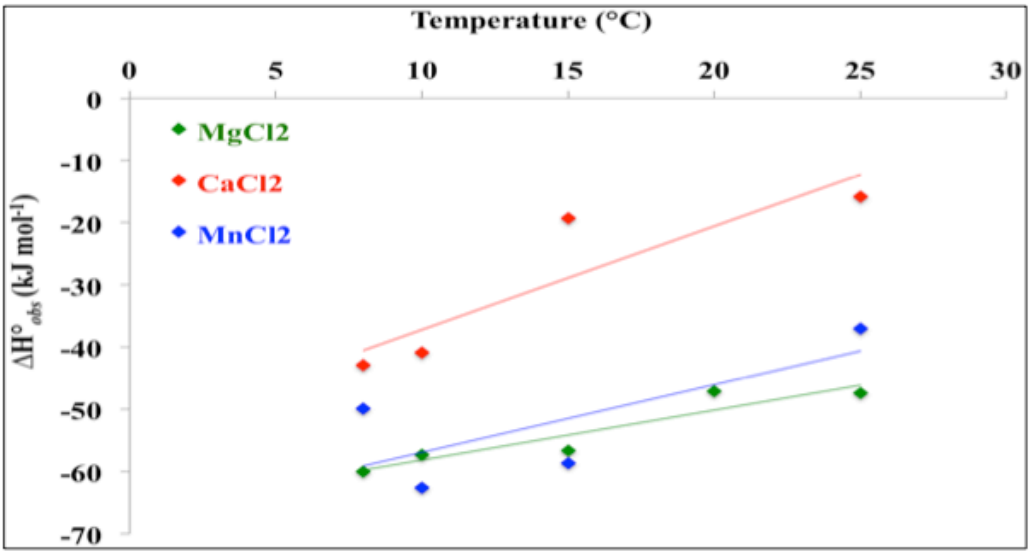

b

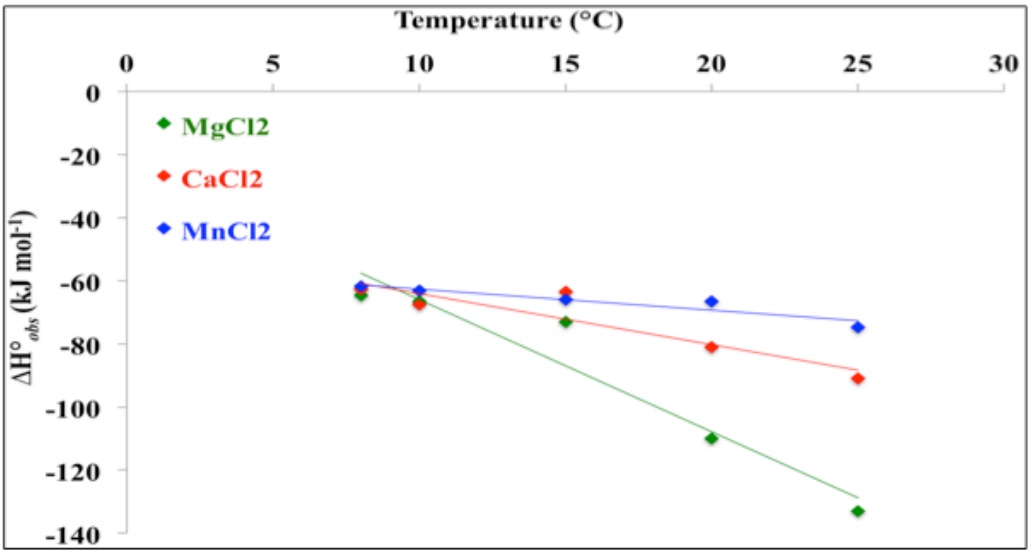

c

N-Hsp90	ΔCp°$_{obs}$ (J mol^{-1}/°C)	
	AMP-PNP	ADP
Mg-G154A	+801	-4187
Mg-WT	+180	-850
Mn-G154A	+1087	-667
Mn-WT	+109	-911
Ca-G154A	+1661	-1618
Ca-WT	+853	-307

Figure 4.14 ΔH°$_{obs}$ against temperature plots for the interaction of N-Hsp90-G154A with **a,** AMP-PNP, **b,** ADP, and **c,** calculated ΔCp°$_{obs}$ compared with WT-N-Hsp90 in the presence of Mg^{2+}, Mn^{2+}, and Ca^{2+}.

In both mutant interactions, binding with ADP is associated with a negative $\Delta Cp°_{obs}$ (in comparison to the binding with AMP-PNP), a trend also seen in the WT-N-Hsp90:ADP interaction. For N-Hsp90-G153A, the data with WT-N-Hsp90 is comparable, whereby the interaction between the mutant and ADP in the presence of Ca^{2+} shows the least negative value of approximately -335 J $mol^{-1}°$/C, indicating a lower number of water molecules coordinating this ion resulting in the entrapment of less water, an observation also reflected by the more favourable $T\Delta S°_{obs}$ in this interaction.

On the contrary, the interaction between N-Hsp90-G154A:ADP in the presence of Mg^{2+} and Ca^{2+} results in a significantly more negative $\Delta Cp°_{obs}$ of approximately -4187 and -1618 J $mol^{-1}°$/C respectively. These values further imply roles of the hydration shells of these ions play in the thermodynamics observed, whereby the higher number of water molecules coordinating the Mg^{2+} ion in addition to the introduction of the hydrophobic alanine residue, would indeed lead to the burial of a large apolar surface in comparison to the fewer number of water molecules coordinating the Ca^{2+}ion.

4.4 Effects of the metal ion hydration shell upon the gross thermodynamics of a system that contains deuterium in comparison to hydrogen as the proton donor

Since water clearly plays a crucial role in the interaction between N-Hsp90 and AMP-PNP, another way of assessing the importance of the waters coordinating the metal ion would be to exchange the hydrogen for deuterium, as this would potentially disrupt or alter the large hydrogen-bonding network present in the N-Hsp90:nucleotide interactions.

Figure 4.15 illustrates the thermodynamic profiles obtained from the interaction between N-Hsp90 and AMP-PNP in the presence of Mg^{2+}, Ca^{2+}, and Mn^{2+} using D_2O as the solvent compared with H_2O. The interactions in D_2O show the same trends as with H_2O in that all interactions are enthalpically driven. All ion interactions show a more favourable $T\Delta S°_{obs}$ when compared to the data in H_2O, which possibly reflect the burial of less apolar surface when the interactions take place in D_2O as opposed to H_2O. These observations appear to be more prominent when the interaction takes place in the presence of Mn^{2+}/Ca^{2+}, further reflecting the possible role of hydration shell of these ions in the thermodynamics observed. The higher number of water molecules speculated to coordinate the Mn^{2+} ion (as mentioned earlier) could reflect the trapping

of more water as implied from the less favourable $T\Delta S°_{obs}$ seen with this ion in comparison to the interaction in the presence of Mg^{2+}.

a

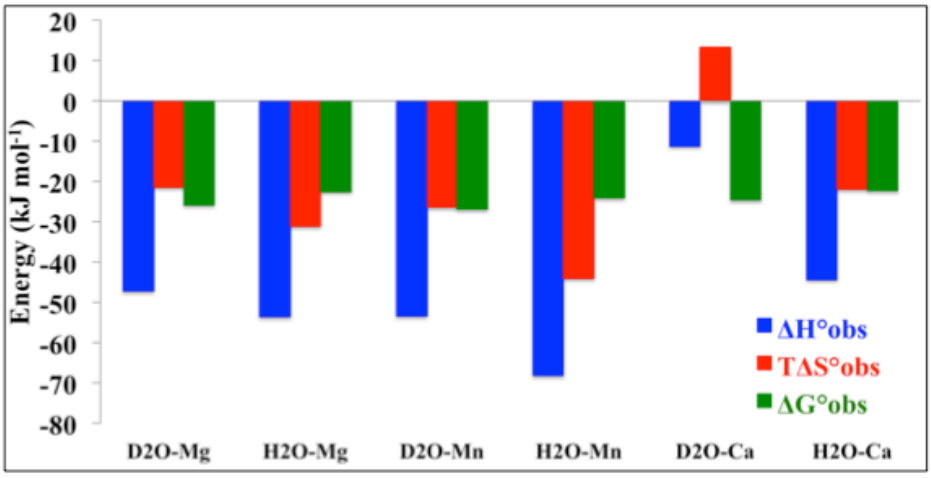

b

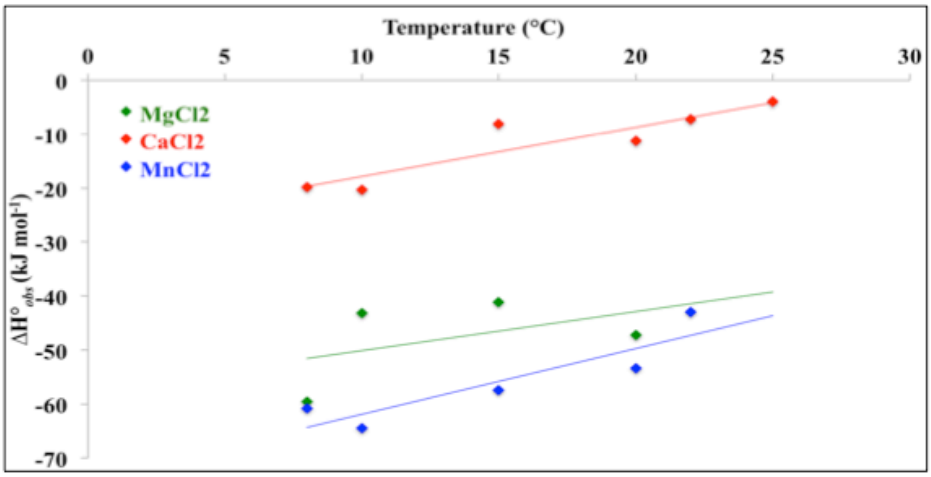

c

	K_d (μM)	$\Delta Cp°_{obs}$ (J mol^{-1}/°C)
D_2O-Mg	26.1	+723
H_2OMg	97	+180
D_2O-Mn	15.7	+1216
H_2O-Mn	48.7	+109
D_2O-Ca	40.6	+915
H_2O-Ca	88.4	+853

Figure 4.15 Comparison of the interaction of N-Hsp90 with AMP-PNP in deuterated buffer compared with WT-N-Hsp90 in the presence of Mg^{2+}, $MnCl_2$, and Ca^{2+}: **a,** thermodynamic profiles, **b,** $\Delta H°_{obs}$ against temperature plots, and **c,** binding affinities and calculated $\Delta Cp°_{obs}$. Data shown for titrations performed at 15°C.

The interaction in the presence of Ca^{2+} (as mentioned above) clearly shows a highly favourable $T\Delta S°_{obs}$ when compared with that of both the same interaction in H2O, but also compared to the other ion interactions with D_2O. These data show implications for the role of the hydration shell of Ca^{2+}, in that the fewer water molecules coordinating this ion would potentially entrap much less water in all of the interactions presented in Figure 4.15, and this effect seems to be more prominent when D_2O is the solvent. Contrary to the latter observation is the observation of a comparable $\Delta Cp°_{obs}$ of the interaction in the presence of the Ca^{2+} ion with both D_2O with H_2O (of +915 and +853 J $mol^{-1}°$/C respectively), indicating that the possible disruption of the hydrogen-bonding network at the protein/ligand interface as a result of substituting the hydrogen atoms with deuterium atoms, does not occur. Although this data remains inconclusive, the variations in the thermodynamics observed with the different metal ions provide a lead for the possibility of the waters coordinating these ions to play an integral role in the interaction between N-Hsp90 and its nucleotide ligands.

4.5 Summary

This chapter further supports the view from the data in Chapter 3 in that there is strong evidence to suggest the hydration shell of the metal ion plays a role in the anomalous $\Delta Cp°_{obs}$ seen in the N-Hsp90:AMP-PNP interaction. Although the data remain ambiguous, the WT-N-Hsp90 data alone suggests that the different metal ions used are giving rise to different effects on the overall $\Delta C_p°_{obs}$, in which data from the interactions in the presence of Mg^{2+} and Mn^{2+} generally share common thermodynamic features, possibly reflecting the similarities these metal ions have share in their hydration shells. Furthermore the interaction of N-Hsp90 in all cases with ADP produces a negative $\Delta C_p°_{obs}$, and only upon introduction of a γ phosphate (with AMP-PNP) do we see large discrepancies in the observed thermodynamics of the interaction in the presence of the different metal ions. Since the region between the β and γ phosphate is where the Mg^{2+} ion is speculated to reside, it is clear that the interactions made via this phosphate between the nucleotide and N-Hsp90 play a key role in the derived positive $\Delta C_p°_{obs}$ observed. The variations observed in this chapter for the different metal ions used in addition with the effects of altering the polarity of selected

importance in the overall $\Delta C_p^{\circ}{}_{obs}$ observed for the N-Hsp90:nucleotide interaction, and this feature has been thoroughly exploited in this thesis, the results of which provide evidence for the contribution of this property in the esoteric $\Delta C_p^{\circ}{}_{obs}$ observed between N-Hsp90 and AMP-PNP.

Chapter 5

Probing conformational changes within the Hsp90 chaperone using SDSL-EPR and DEER

5.1 Introduction

This chapter sets out to establish the dynamic states of the Hsp90 chaperone on going from the nucleotide-free to the nucleotide-bound in solution. Previous studies have extracted extensive information on the complex conformations which Hsp90 adopts during ATP binding and hydrolysis. These studies include investigating the ATP cycle and isolated states of Hsp90 through crystallography[16], cryo-EM[18], FRET[11], and smFRET[24]. The main picture emerging from these studies shows an N- and C-terminally dimerised Hsp90 structure, in which the M domains of the dimer are in close contact with one another. Although these structures provide valuable insight into the potential states of the dimer in the ATP-bound state, it is far from clear how this highly dynamic chaperone behaves in solution with and without nucleotides and without the influence of co-chaperones.

The response of Hsp90 to the non-hydrolysable analogue of ATP, AMP-PNP, was observed using site directed spin labelling (SDSL) and electron paramagnetic resonance (EPR) spectroscopy. Employing four-pulse double electron electron resonance (DEER)[69] we measured distances between two nitroxide spin labels on identical sites within both protomers of the Hsp90 dimer at selected positions. Distances of the labelled Hsp90 were measured in the AMP-PNP-free and AMP-PNP-bound states. These distance measurements allowed us to understand the possible conformations Hsp90 undergoes during its ATP cycle.

5.2 Sample preparation

Protein samples of the full-length Hsp90 dimer were prepared as described in Chapter 2 using the nitroxide spin label MTSSL. This resulted in doubly labelled Hsp90 mutants ($Hsp90^{[MTSSL]}$) suitable for DEER data acquisition.

Details of the full-length *S.Cerevisiae* Hsp90 construct used in this study is given in Chapter 2.

According to Farrelly *et al*.[87], the C domain of the full length Hsp90 protein runs from

which is recognised by TPR motif-containing proteins. The protein construct used in this study has been truncated within this region of the C domain.

5.2.1 Selection of sites for Cysteine residue substitution

A total of nine surface exposed sites on the Hsp90 dimer were selected for site directed mutagenesis of the residues to a cysteine so that the nitroxide spin label could be attached. When deciding which residues on Hsp90 dimer we would mutate, an important factor to consider was whether these mutations would result in structural and/or functional impairment in terms of ATP binding. Fortunately, WT-Hsp90 harbours no cysteine residues and therefore we did not need to mutate any out, which may have led to functional impairment. As a result, we chose to mutate several surface exposed residues, as they are more accessible to the nitroxide label, and probably do not interfere with the structure or function of Hsp90 due to them being on the exterior of the protein. Residues were selected for labelling on all domains of the Hsp90 dimer; residues Ser17, Asp61, and Ala103 were selected for the N domain, residues S297, S363, H430, and T511 were selected for the M domain, and residue M589 was selected for the C domain.

Hsp90$^{[MTSSL]}$ mutants of the N domain

This study focuses on the conformational changes associated with Hsp90 upon AMP-PNP binding and provides a new view of Hsp90s catalytic cycle, which has been demonstrated by other studies, including a crucial study by Hessling *et al*.[11] , who determined three distinct intermediate conformational states of the Hsp90 dimer upon nucleotide binding.

The residues selected for labelling within the N domain were: Ser17, which lies within the N-terminal strand (NTS). The NTS is 11 amino acids in length and is composed of an α-helix. Upon ATP binding, it has been suggested that this strand is involved in a 'strand swap' event with its partner N domain (opposite protomer of the Hsp90 dimer) resulting in dimerisation of the two N domains of Hsp90 (Figure 5.1)[13,15,16,19]; D61, which represents the identical residue chosen in the FRET analysis of Hsp90s catalytic cycle[11], and this study showed that the mutation of Asp61 to a cysteine resulted in no impairment of the Hsp90 in binding ATP. Therefore, the selection of D61 for DEER analysis would act as a positive control for comparison with the distances obtained from the FRET study; and Ala103, which lies within the 'ATP lid' region of the N domain. It

is thought that during the process of ATP binding, the ATP lid closes over the ATP binding site and this conformational change represents one of the major rearrangements in contributing to successful ATP hydrolysis by the Hsp90 chaperone[13,16,19], a conformation also shown in the crystal structure of the Hsp90 dimer in complex with AMP-PNP and the co-chaperone Sba1/p23 (Figure 5.9).

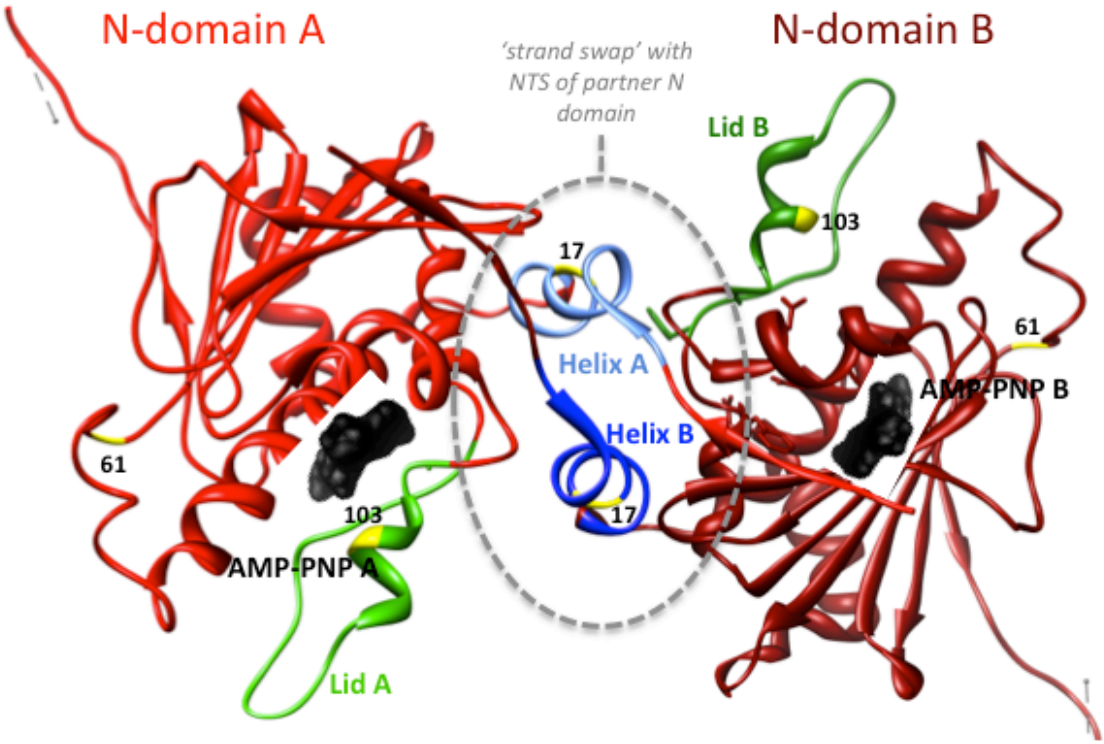

Figure 5.1 Ribbon representation of the N-terminal domains of the Hsp90 dimer (PDB 2CG9[16]; refer to Appendix 1), highlighting the nucleotide (black), lid (L; green) in the closed form, N terminal strand (NTS;blue) showing a 'strand swap' with partner N domains, and residues 17 ($Hsp90^{S17C[MTSSL]}$), 61 ($Hsp90^{D61C[MTSSL]}$), and103 ($Hsp90^{A103C[MTSSL]}$) that were targeted for labelling with the nitroxide spin label MTSSL (yellow). N domain B uses the same colour scheme but in a darker shade.

M domain $Hsp90^{[MTSSL]}$ mutants

The selection for the residues within the M domain domain were based upon studies which have shown that the two M domains of the Hsp90 dimer come into close contact with one another prior to ATP hydrolysis[11,16,18].

The main aim was to select residues which span the length of the M domain so that the suggested contact seen with the M domains would be visible. Residues for mutation

in complex with AMP-PNP and Sba1/p23, which predicted distances between the selected residues within the measurable range of DEER spectroscopy (refer to page 162). Selected residues were Ser297, Ser363, Val391, His430, and Thr511. Figure 5.2 highlights the selected residues.

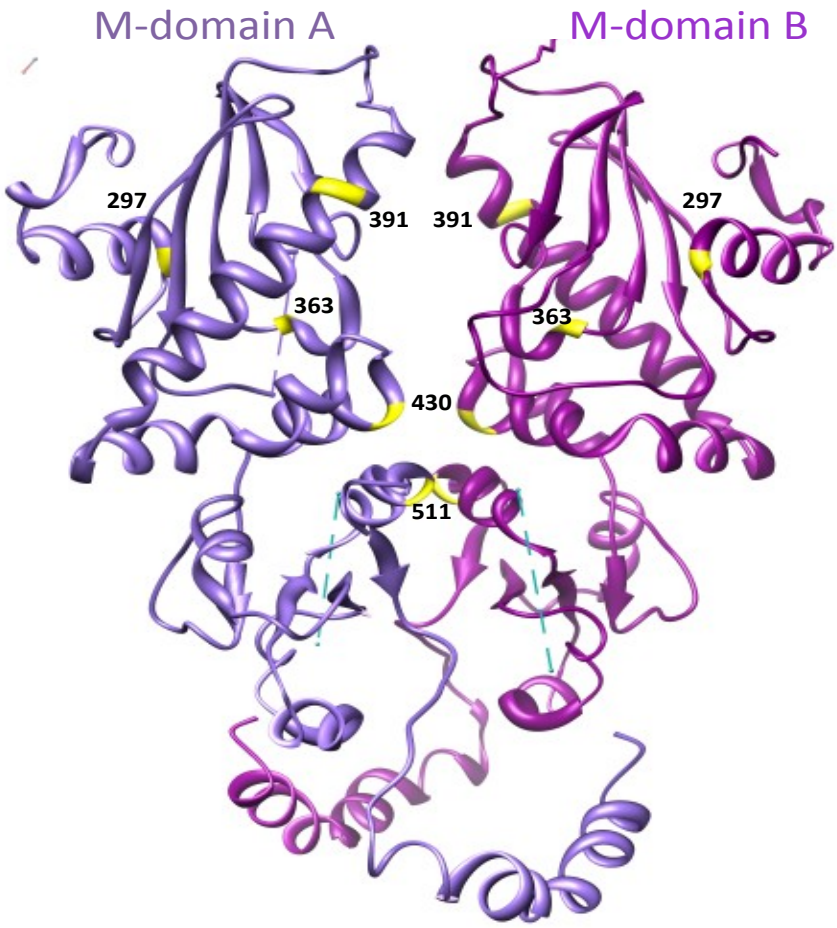

Figure 5.2 Ribbon representation of M domains (purple) of the Hsp90 dimer (PDB 2CG9[16]; refer to Appendix 1), highlighting residues selected for nitroxide labelling (yellow): Ser297 (Hsp90$^{S297C[MTSSL]}$), Ser363 (Hsp90$^{S363C[MTSSL]}$), Val391 (Hsp90$^{V391C[MTSSL]}$), His430 (Hsp90$^{H430C[MTSSL]}$), and Thr511 (Hsp90$^{T511C[MTSSL]}$). M domain B uses same colour scheme but in a darker shade.

C domain Hsp90$^{[MTSSL]}$ mutants

Hsp90 has been extensively studied using various methods, and in all cases it has been assumed that Hsp90 is a homodimer at its C domain. Therefore, selecting a residue for spin labelling within this domain was important for assessing the assumed homodimeric nature of Hsp90. Figure 5.3 highlights the residues which were selected for labelling within the C domain of the Hsp90 dimer.

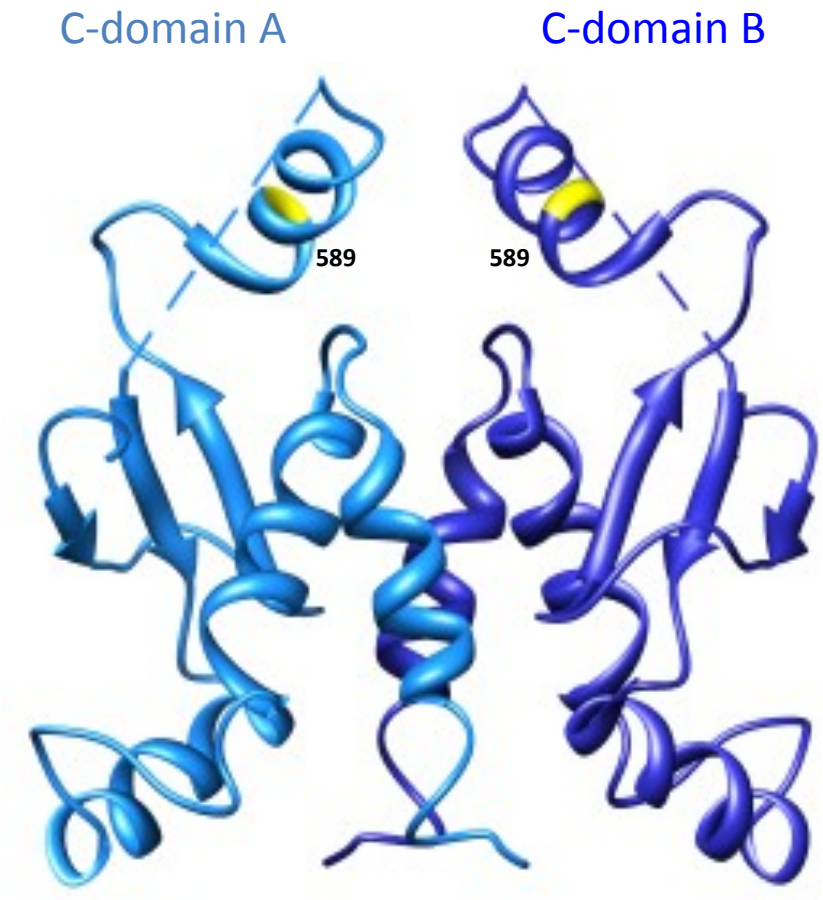

Figure 5.3 Ribbon representation of C domain (blue) of the Hsp90 dimer (PDB 2CG9[16]; refer to Appendix 1), highlighting residue Met589 ($Hsp90^{M589C[MTSSL]}$) selected for nitroxide labelling (yellow). C domain B uses same colour scheme but in a darker shade.

Figure 2.7 (Chapter 2, page 78) shows the polyacrylamide gel electrophoresis (PAGE) analysis of all $Hsp90^{[MTSSL]}$ mutants, which shows the presence of a monomeric (SDS-PAGE) and dimeric (native-PAGE) Hsp90.

5.3 Rotamer library approach (RLA) of the selected $Hsp90^{[MTSSL]}$ mutants

The consideration of the predicted distances between the selected residues was of importance, since this would give an indication of whether these predicted distances would be measureable within the given distance range of DEER spectroscopy. Obtaining these predicted distances is based on the idea of attaching and artificial nitroxide label to the selected residue within a given PDB file; this PDB file would be one which represents the protein under investigation. Since the crystal structure of full-

length Hsp90 in complex with AMP-PNP and Sba1/p23 was solved by Ali *et al.*[16], we were able to use the PDB code of this structure to obtain our predicted distances using the Rotamer library approach (RLA; refer to Chapter 2, page 86). Analysis of the possible orientations of each rotamer position of the attached nitroxide on the selected residue was performed, from which an average distance was given. However, it is important to note that the predicted distances extracted from the rotamer analysis of the the PDB file stated above could not be used as a 'true' representation of the distances that may or may not be observed in our DEER measurements, since this crystal structure is of Hsp90 in complex with AMP-PNP and the co-chaperone Sba1/p23. Furthermore, the protein used to obtain this crystal structure harboured a mutation (A107N) within the N domain of the Hsp90 dimer, which induced ATP lid closure. The DEER measurements carried out in this thesis included measurements both using Sba1/p23, but also in the absence of Sba1/p23, and the latter measurements may produce distances that do not match the predictions from the rotamer analysis. Furthermore, the protein used for our DEER measurements lacked the A107N mutation, and this would also potentially be reflected in the distances measured using DEER, which may differ from that of the predictions.

Table 5.1 shows the results from the rotamer analysis of the PDB file 2CG9, which gave an average distance distribution of nitroxide labels attached to the selected residues. Since Hsp90 is a dimer, the number of possible rotamers for each protomer of the dimer (A and B) and the corresponding average distance distribution is illustrated.

Residue number	Protomer A	Protomer B	Distance (nm)
17	37	38	2.7
61	95	96	8.0
103	35	29	4.5
297	12	14	3.2
363	73	6	2.2
391	5	16	4.4
430	27	27	2.2
511	36	40	3.3
589	17	12	3.3

Table 5.1. RLA analysis of all Hsp90$^{[MTSSL]}$ mutants illustrating the predicted distances of all possible rotamers of the selected residues within each protomer (A and B) of the Hsp90 dimer.

Hsp90 is structurally a homodimer and therefore each protomer should resemble some degree of symmetry, particularly since the crystal structure used in the rotamer analysis shows a Hsp90 dimer bound to two AMP-PNP molecules (one per monomer) and two Sba1/p23 proteins (one per monomer). However, the rotamer analysis revealed variations in the possible rotamer positions for the selected residues within a single site, an observation particularly pronounced for residues Ser363, Val391, and Met589. These variations in rotamer positions indicate the presence of asymmetry in the Hps90 dimer when in complex with AMP-PNP and Sba1/p23. These results further demonstrate how the crystal structure and the structural refinement thereof may give rise to errors, and as a result calculating the motional freedom of the spin labels from the rotamer analysis of this structure is almost impossible.

The residues that showed a low number of possible rotamers in general (Ser297, Val391, Met589, and protomer B of Ser36), indicates that the spatial freedom of the nitroxide label attached to these positions is more restricted due to the surrounding protein atoms, and therefore indicates a lower degree of motional freedom of the nitroxide label. Residues which showed a higher number of possible rotamer positions

(Ser17, Asp61, Ala103, His430, Thr511, and protomer A of Ser363) indicate a nitroxide label that has a high degree of motional freedom, most likely the result of the label being in a region that is solvent exposed. The motions of the attached nitroxide label can be visualised using *cw*-EPR (Chapter 2, page 86), where a label that is able to move freely would be reflected by a sharp nitroxide spectrum, and a label that is restricted or is within a buried region would be reflected by a broad nitroxide spectrum. Apart from one protomer B of residue Ser363 and protomer A of Val391, all other selected residues demonstrate sufficient spatial freedom of the attached nitroxide label, and therefore the *cw*-EPR spectra should reveal relatively mobile features of the label at these positions. However, the mobility of the label may change upon the addition of the nucleotide and the co-chaperone Sba1/p23, an effect that would be evident in the *cw*-EPR spectrum of these samples.

DEER spectroscopy can allow distance measurements in the range of 2–8 nm. Since the predicted distances for all selected residues apart from Asp61 are in the range of 2–5 nm, we can use DEER spectroscopy to measure the distances between the selected residues upon nucleotide and co-chaperone association. The predicted distances presented in Table 5.1 are based on the crystal structure of Hsp90 in complex with AMP-PNP and Sba1/p23, and as a result, any distance(s) that may or may not arise as a result of the nucleotide-free or the nucleotide-bound (minus Sba1/p23) DEER measurements would not be based on these predictions. As mentioned earlier, as of yet there are no structures available of the nucleotide-free or the nucleotide-bound Hsp90 dimer, allowing for the possibility of these states to be assessed by the DEER spectroscopy.

5.4 Mobility measurements and Spin labelling efficiencies of the Hsp90$^{[MTSSL]}$ mutants

Room temperature *cw*-EPR measurements (as described in Chapter 2, page 86) were carried out on a BrukerEMXplus spectrometer operating at 9.4 Ghz equipped with a 4122SHQE resonator. All measurements were carried out 0.2 mW microwave power, 100 KHz modulation frequency, 0.1 mT modulation amplitude and 10 ms conversion time and time constant.

All samples of the Hsp90$^{[MTSSL]}$ mutants contained between 10- 15 % glycerol (w/v) as a cryoprotectant due to the low temperature (50 K) nature of DEER spectroscopy.

Approximately 50μL of sample volume with a protein concentration of 100–150 μM was transferred into an EPR quartz capillary with a 0.9 mm inner diameter. The *cw*-EPR measurements were carried out prior to the DEER measurements in order to calculate the efficiency of the labelling procedure, and also allowing us to observe potential free label within our sample (refer to Chapter 2, page 86), which if present would affect the signal:noise ratio of the DEER measurement. As mentioned above, *cw*-EPR also allowed us to extract information on the environment around the attached nitroxide spin label. The spin labelling efficiencies, based on a standard sample (Tempol at 100 μM) incorporating the spin label MTSSL with a labelling efficiency of 100%, were all calculated between 70-100 % (refer to Chapter 2, page 86).

5.5 Determination of the electron-spin-echo envelope modulation (ESEEM)

The ESEEM experiment is one of many forms of EPR spectroscopy allowing one to extract given parameters from a spin system. This phenomenon appears as a modulation of the intensity of a given 'echo' that is detected after a sequence of two pulses separated by a time on the order of the reciprocal of a hyperfine coupling in frequency units, typically micro-nanoseconds.

This experiment determines a parameter relevant to DEER spectroscopy which results from an approximate exponential decay; this parameter is called the phase memory time, (T_m or T_2)[88] also known as the transverse relaxation time.

To determine the maximum dipolar evolution time τ_2 for each $Hsp90^{[MTSSL]}$ mutant we performed a two-pulse ESEEM sequence prior to each DEER measurement. Due to the four-pulse DEER sequence, the value of τ_2 is half the time value T_{tip}, which is the time in a two-pulse ESEEM where a sufficient echo intensity can still be observed.

The two-pulse ESEEM experiments were performed using the pulse sequence $\pi/2$-τ-π, where τ is increased during the experiment. We used pulse lengths of 16 ns ($\pi/2$) and 32 ns (π). In all measurements, the static magnetic field was set to the maximum of the spin label EPR signal, i.e. the central line of the frozen solution EPR spectrum (refer to Chapter 2, page 86).

Table 5.2 illustrates the results from the two-pulse ESEEM experiments carried out on all measurements for each $Hsp90^{[MTSSL]}$ mutant.

Hsp90$^{[MTSSL]}$ samples	**τ_2 (µs)**	**d_{max} (nm)**	**RLA distances (nm) based on PDB 2CG9**
17 (AMP-PNP free)	2.8	5.3	2.7
17 (AMP-PNP bound)	2.8	5.3	
61 (AMP-PNP bound)	3.2	5.5	8.0
103 (AMP-PNP bound)	3.2	5.5	4.5
103 (AMP-PNPbound/p23)	3.2	5.5	
297 (AMP-PNP bound)	3.2	5.5	3.2
297 (AMP-PNP/p23)	3.2	5.5	
363 (AMP-PNP free)	3.2	5.5	2.2
363 (AMP-PNP bound)	3.2	5.5	
363 (ATP bound)	3.2	5.5	
363 (AMP-PNP/p23)	3.2	5.5	
391 (AMP-PNP bound)	3.2	5.5	4.4
430 (AMP-PNP free)	2.8	5.3	2.2
430 (AMP-PNP bound)	2.8	5.3	
511 (AMP-PNP free)	2.8	5.3	3.3
511 (AMP-PNP bound)	2.8	5.3	
589 (AMP-PNP free)	2.8	5.3	3.3
589 (AMP-PNP bound)	2.8	5.3	

Table 5.2. two-pulse ESEEM analysis of all DEER measurements for each Hsp90$^{[MTSSL]}$ mutant.

The τ_2 determined in the two-pulse ESEEM experiment corresponds to a maximum distance measureable (d_{max}) using DEER spectroscopy. Table 5.3 shows the measurable distances within a given τ_2.

τ_2 (µs)	d_{max} (nm)
0.8	3.5
0.9	3.6
1.0	3.7
1.2	4.0
1.4	4.2
1.6	4.4
1.8	4.5
2.0	4.7
2.4	5.0
2.8	5.3
3.2	5.5
3.6	5.7
4.0	5.9
5.0	6.4
6.0	6.8

Table 5.3. Maximum distances (d_{max}) observeable by DEER spectroscopy for a given τ_2 value.

The observed τ_2 times from the two-pulse ESEEM experiments presented in Table 5.2 are all in the range of 2.4–3.2 µs. This corresponds to a d_{max} in the range of 5.0–5.5 nm for all samples measured using DEER spectroscopy. When considering the average predicted distance distribution resulting from the rotamer analysis of the selected residues for nitroxide labelling (Table 5.1), these distances lie in the range of 2.2 – 4.5 nm for all residues apart from residue D61, for which the which the average predicted distance distribution is 8.0 nm. As mentioned earlier, DEER spectroscopy allows the measurement of distances between 2.0-8.0- nm, therefore it is likely that we may not observe a distance for residue D61. However, as mentioned earlier, the predicted distances are based on a model in which Hsp90 is in complex with AMP-PNP and Sba1/p23, and as such our DEER measurements could potentially yield distances that do not reflect that of the crystal structure. Nevertheless, all other selected residues should yield a distance that is observable within the limitations of DEER spectroscopy.

5.6 Data Acquisition and Processing

DEER measurements were performed at 50 K on a Bruker ELEXSYS E580 spectrometer operating at 9 GHz equipped with an ER-4118-X-MS-3W resonator. The four-pulse DEER sequence was chosen with $\pi/2(\nu_{obs})$-τ_1-$\pi(\nu_{obs})$-τ'- $\pi(\nu_{pump})$-(τ_1+τ_2-t')-$\pi(\nu_{obs})$-τ_2-*echo,* where the observe pulse length was 16 ns for π/2 and 32 ns for π pulses. The pump pulse length was 12 ns, the long interpulse delay τ_2 was determined for each

sample as described earlier. All other parameters were used according to Pannier *et al.*[69].

5.7 The N domains of Hsp90 show dimerisation when bound to AMP-PNP

To assess the juxtaposition and conformation of the N domain, individual *S.Cerevisiae* Hsp90 cysteine mutants at positions 17 (Hsp90 $^{S17C[MTSSL]}$), 61 (Hsp90 $^{D61C[MTSSL]}$), and 103 (Hsp90 $^{A103C[MTSSL]}$) of the N domain mutants were purified and labelled with MTSSL as described in Chapter 2, page 70.

Distances for the N domain Hps90$^{[MTSSL]}$ mutants Hsp90 $^{S17C[MTSSL]}$, Hsp90 $^{D61C[MTSSL]}$, and Hsp90 $^{A103C[MTSSL]}$, were measured in the presence and absence of AMP-PNP. Only if a distance was observed in the AMP-PNP bound conformation (closed dimer), would a distance measurement be performed on the AMP-PNP free conformation (open), due to the fact that if a distance in the closed conformation is not observable (short distance based on N domains being dimerised) then a distance in the open conformation (long distance) would most likely not be seen since the N domains would be farther apart.

For Hsp90$^{S17C[MTSSL]}$, the spin labels are located on the NTS, which has been shown to be involved in a 'strand swap' event on dimer formation (Figure 5.1)[11,16,19,89]. A distance measurement of approximately 2.5 nm between the two labels was observed in the AMP-PNP-bound sample as seen in Figure 5.4c.

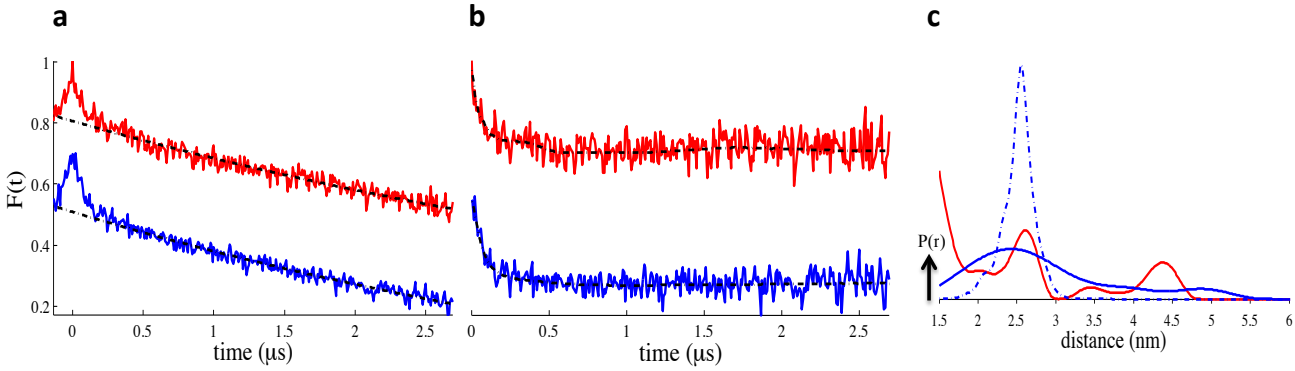

Figure 5.4 DEER measurements of Hsp90$^{S17C[MTSSL]}$ in the AMP-PNP-free and AMP-PNP-bound states. The predicted distance distribution is based on PDB 2CG9[16]. **a,** the raw DEER traces of the AMP-PNP-free and AMP-PNP-bound Hsp90$^{S17C[MTSSL]}$ (red and blue respectively), **b,** the form factor and the fit (black) to the data using DeerAnalysis2011[69]. **c,** the distance distribution of the experimental data (solid lines)

and the predicted distance distribution from the rotamer analysis (dotted line). Colour coding as in Figure 5.4a.

A distance distribution of approximately 2–4.5 nm was observed in the AMP-PNP-free conformation, demonstrating the possible opening and closing of the N domains in the absence of nucleotide. The broad distance populating around 2.5 nm upon AMP-PNP association possibly demonstrates stabilisation of the closed conformation and support the finding that the N domain of Hsp90 forms a dimer upon ATP binding[11,16,19,24,89]. This broad distance around 2.5 nm in the AMP-PNP-bound state agrees well the predicted distance based on rotamer analysis of the crystal structure of Hsp90-AMP-PNP-p23[16].

The DEER measurement between the two nitroxide spin labels on Hsp90$^{D61C[MTSSL]}$ in the AMP-PNP-bound conformation suggest there is no observable distance present in this instance according to the form factor in Figure 5.5b, which shows a flat line. The raw data in Fig. 5.5a, as mentioned in Chapter 2 page 86, is not illustrative of a 3D isotropic decay and suggests that the two spin labels in this instance are outside the limits of the chosen τ_2, therefore preventing the observation of a distance by DEER spectroscopy.

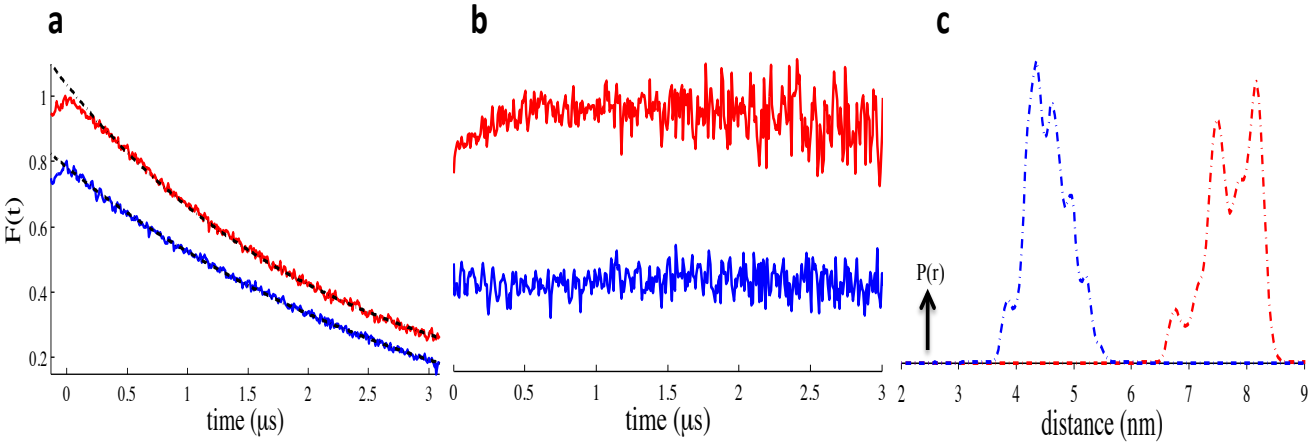

Figure 5.5 DEER measurements of Hsp90$^{D61C[MTSSL]}$ and Hsp90$^{A103C[MTSSL]}$) AMP-PNP-bound states. The predicted distance distributions are based on PDB 2CG9[16]. **a,** the raw DEER traces of Hsp90$^{D61C[MTSSL]}$ and Hsp90$^{A103C[MTSSL]}$ (red and blue respectively), **b,** the form factor. **c,** the predicted distance distribution from the rotamer analysis. Colour coding as in Figure 5.5a.

A τ_2 of 3.2 μs was chosen for both of the measurements presented in Figure 5.5, which allows for a maximum distance measurement by DEER spectroscopy of 5.5 nm. The observation of no distance for the label attached on residue Asp61 is in good agreement with the predicted distance of 8. 0 nm, since a τ_2 of 3.2 μs can only allow distances of up to 5.5 nm to be observed by DEER spectroscopy (Table 5.2).

A distance is also not observable for the labels attached on residue A103. For which a τ_2 of 3.2 μs was chosen. Based on the predicted distance from the rotamer analysis of the selected residue, a distance of 4.5 nm should have been observable by DEER spectroscopy with the chosen τ_2. The discrepancy between the predicted distance and the experimentally found observation of no distance could be related to the A107N mutation present in the crystal structure, which forces the ATP lid closed shown in Figure 5.6. If this were true, then the observation of no distance with the AMP-PNP bound measurement of $Hsp90^{A103[MTSSL]}$ could reflect an ATP lid that may not actually close upon binding of AMP-PNP only, as previously suggested. The observations made in Chapter 3 of an ATP lid that could be in an intermediate state between an open/closed conformation could in fact be true, as a lid that may be partially closed could potentially be outside the distance maximum for the chosen τ_2 of 5.5 nm. Furthermore, additional rearrangements potentially induced by Sba1/p23 could contribute to the predicted distance of 4.5 nm, which would not be reflected in our DEER measurements of the above sample due to the lack of the co-chaperone.

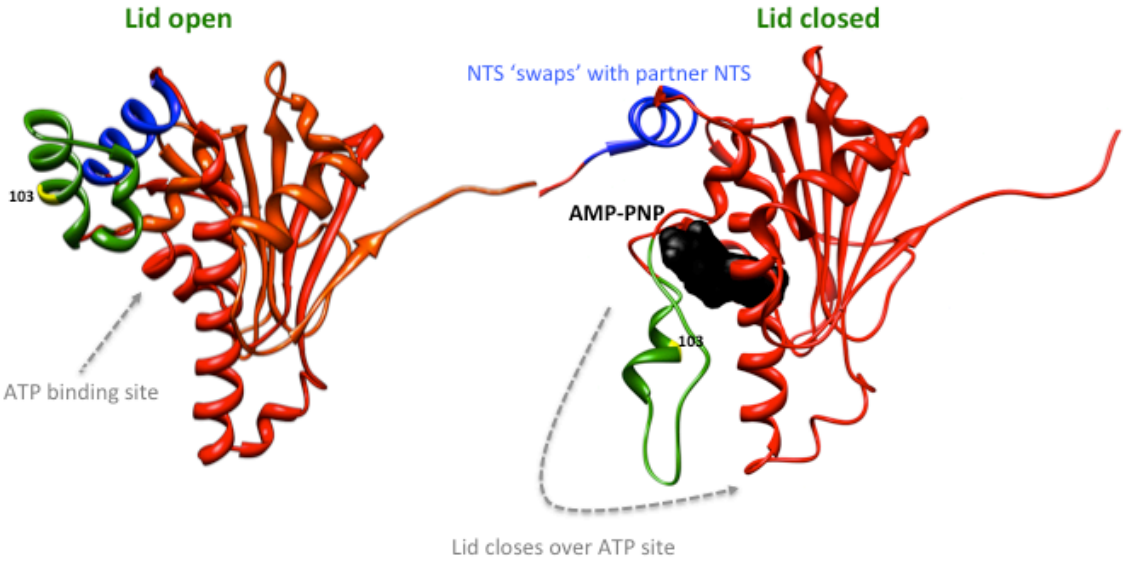

Figure 5.6 Ribbon representations of the N domain of Hsp90. **a,** ATP lid (green) shown in the open conformation with a vacant ATP site and (PDB 1AMW; refer to Appendix 1) **b,** ATP lid shown in the closed conformation over bound AMP-PNP (PDB 2CG9; refer to Appendix 1). Highlighting residue 103 (yellow) and the NTS (blue).

5.8 The M domains of the chaperone do not appear to form a 'twisted' conformation in the nucleotide-bound state

Individual Hsp90 cysteine mutants positions S297 ($Hsp90^{S297C[MTSSL]}$), 363 ($Hsp90^{S363C[MTSSL]}$), and 391 ($Hsp90^{V391C[MTSSL]}$) were purified and labelled with MTSSL as described in Chapter 2, page 86.

Contrary to the predicted distances obtained from the rotamer analysis of the crystal structure, no distances were observed by DEER spectroscopy between the labels attached on residues S297, S363, and V391 in the AMP-PNP-bound measurements as illustrated by the raw data shown in Figure 5.7a. The decay shown in the raw data is not representative of a 3D isotropic decay and therefore the actual distance between the two spin labels is outside the limits of the chosen τ_2 of 3.2 µs, only allowing us to measure a distance of up to 5.5 nm (Table 5.2).

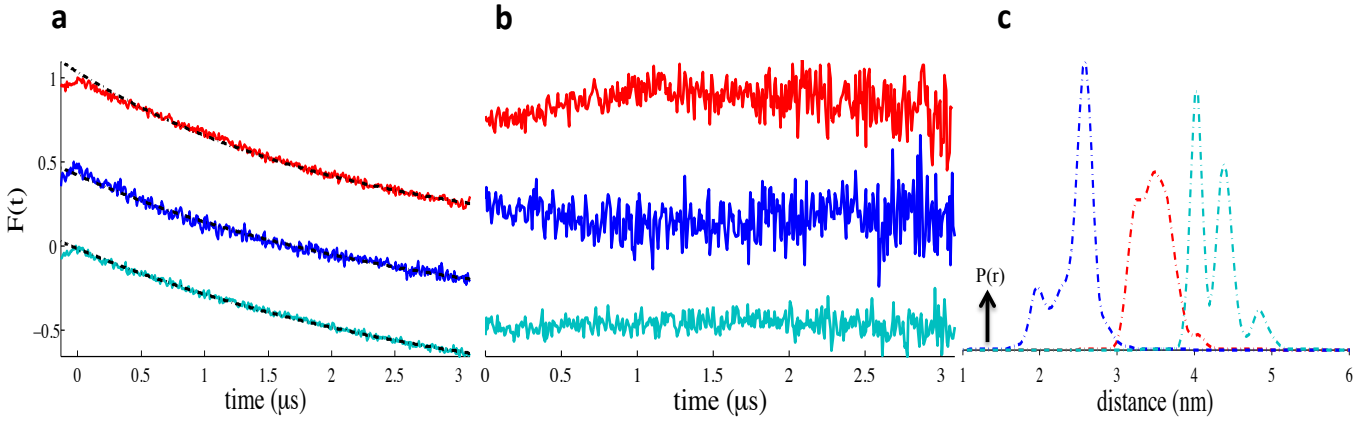

Figure 5.7 DEER measurements of Hsp90$^{S297C[MTSSL]}$, Hsp90$^{S363C[MTSSL]}$, and Hsp90$^{V391C[MTSSL]}$ in the nucleotide-bound states. The predicted distance distributions are based on PDB 2CG9[16]. **a,** the raw DEER traces of Hsp90$^{S297C[MTSSL]}$, Hsp90$^{S363C[MTSSL]}$ and Hsp90$^{V391C[MTSSL]}$ (red, blue, and cyan respectively), **b,** the form factor, **c,** the distance distributions of the predicted distances from the rotamer analysis. Colour coding as in Figure 5.7a.

Our findings show the possibility of a Hsp90-AMP-PNP complex in which the two M domains are not within a distance range of 2.2–4.4 nm as shown in the crystal structure, demonstrating the possibility of the M domains within the labelled regions not forming the 'twisted' complex upon AMP-PNP. Furthermore, since the predicted distances are based on a structure in which the Hsp90 is in complex with AMP-PNP and the co-chaperone Sba1/p23, our DEER results suggest the possibility of the 'twisted' Hsp90 structure being induced by Sba1/p23 association.

Interestingly, our findings are at odds with previous FRET and X-ray crystallographic findings where it was concluded that the final fully closed conformation of Hsp90 in the ATPase cycle, preparing the ATP to commit to hydrolysis, shows the two M domains of the dimer coming into close contact with each other[1,2].

As a control experiment in order to find out if the 'twisted' structure of the M domains of Hsp90 (suggested by previous studies) was due to conformational changes induced upon the hydrolysis of the bound ATP, a distance measurement was carried out between the labels attached at residue Ser363 on the M domains of the Hsp90 dimer with ATP. The reason behind the choice of this particular position was based on the rotamer analysis of the labels attached at this residue, which revealed the shortest predicted

distance (Table 5.2) amongst the three residues (Ser297, Ser363, and Val391 tested above with AMP-PNP, which revealed no observable distance.

A study by Hessling *et al*[11] showed that the Hsp90-ATP closed complex dissociated within 120 s upon binding to ATP. For our experiments, the Hsp90-ATP mixture was allowed to incubate for approximately 60 s prior to freezing in liquid nitrogen, since it has also been reported that Hsp90 turns over one ATP per minute. Hence a 60 s incubation period should potentially allow for sufficient time for the binding of ATP to Hsp90 without any dissociation of the complex. Figure 5.8 shows the results from these DEER measurements in comparison with the data obtained from the AMP-PNP-free and AMP-PNP-bound measurements between the labels attached at residue S363.

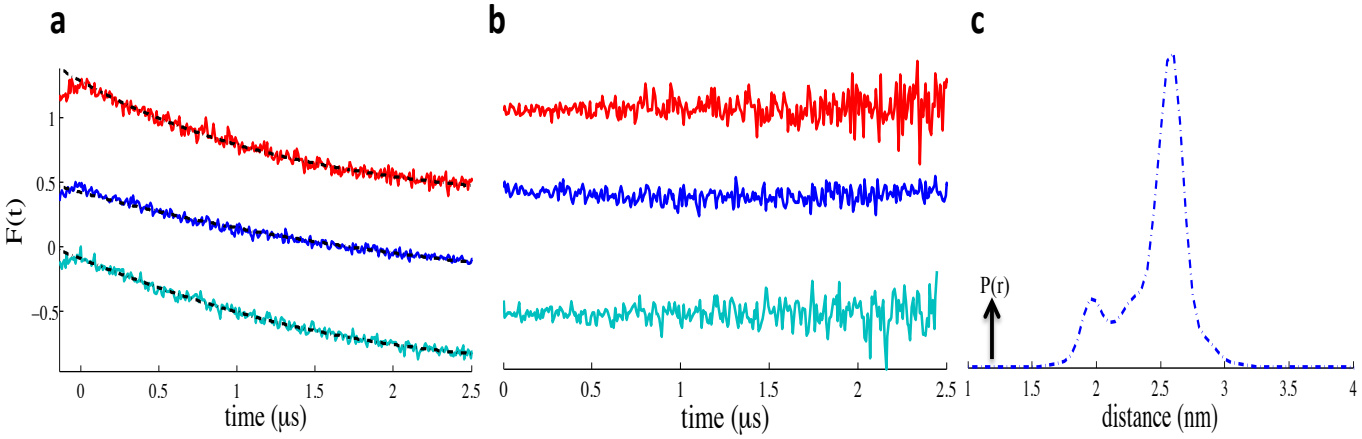

Figure 5.8 DEER measurements of Hsp90$^{S363C[MTSSL]}$ 363 in the nucleotide-free, AMP-PNP-bound and ATP-bound states. The predicted distance distribution is based on PDB 2CG9[16]. **a,** the raw DEER traces of the nucleotide-free, AMP-PNP-bound and ATP-bound Hsp90$^{S363C[MTSSL]}$ (red, blue, and cyan respectively), **b,** the form factor, **c,** the predicted distance distribution from the rotamer analysis. Colour coding as in Figure 5.8a.

The DEER measurements of Hsp90$^{S363C[MTSSL]}$ in the ATP-bound state yielded no observable distance as with the nucleotide-free and AMP-PNP-bound states measured earlier. The raw DEER and form factor profiles shown in Figure 5.8 all share similarities demonstrating that the use of different nucleotides does not appear to result in a difference in the DEER signal of the nitroxide labels attached at residue Ser363.

The data from these measurements further agree with the model in which the M domains of Hsp90 do not appear to form a 'twisted' complex in the AMP-PNP-bound

5.9 The lower M domains of Hsp90 sample opening and closing independent of AMP-PNP binding

The DEER data for the Hsp90$^{[MTSSL]}$ mutant labelled at residue H430 shows a range of distances from our DEER measurements in both the AMP-PNP-free and AMP-PNP-bound states between 1.0-5.0 nm (Fig. 5.9c). The distance distribution for the AMP-PNP-free conformation shows a more pronounced peak at approximately 5.0 nm demonstrating an 'open' lower M domain, and the AMP-PNP-bound conformation of this mutant shows a more pronounced peak at approximately 1.0 nm, demonstrating a 'closed' lower M domain upon AMP-PNP binding.

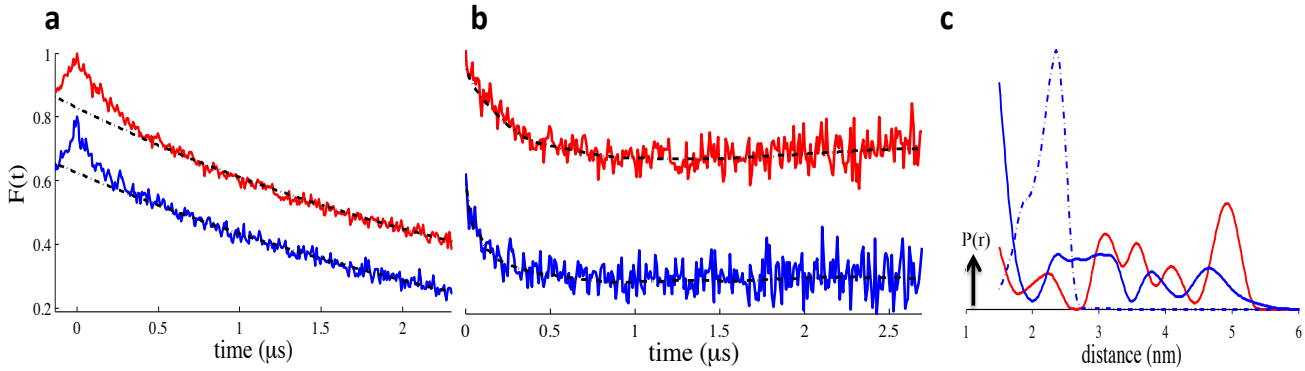

Figure 5.9 DEER measurements of Hsp90$^{H430C[MTSSL]}$ in the nucleotide-free and nucleotide-bound states. The predicted distance distribution is based on PDB 2CG9[16]. **a,** the raw DEER traces of the AMP-PNP-free and AMP-PNP-bound Hsp90$^{[MTSSL]}$ mutant (red and blue respectively), **b,** the form factor and the fit (black) to the data using DeerAnalysis2011[69]. **c,** the distance distributions of the experimental data (solid line) and the predicted distance distribution from the rotamer analysis (dotted line). Colour coding as in Figure 5.9a.

Contrary to the predicted distance distribution of the rotamer analysis of labels attached to residue His430 of approximately 2.0 nm, the experimentally observed shorter distance of approximately 1.0 nm could be due to the modifications made to the crystal structure which are not present in the Hsp90 used in our DEER measurements[16]. The data presented here together with the DEER data from the Hsp90$^{S17C[MTSSL]}$ mutant (Figure 5.4) could provide a potential mechanism in which the N the lower M domains of Hsp90 undergo coupled transient dimerisation, in which both domains are undergoing opening and closing in the nucleotide-free conformation, and AMP-PNP binding leads to the to the closing of both N and lower M domains

5.10 C domains undergo opening and closing independent of N/M domain dimerisation

In order to confirm the homodimerised nature of the Hsp90 chaperone within its C domain, which has been observed as a putative form in many studies[11,16,87], a Hsp90 cysteine mutant at residue 589 ($Hsp90^{M589C[MTSSL]}$) was created and labelled with MTSSL as described in Chapter 2, page 86. Based on the predicted distance distributions of the rotamer analysis of the labels attached at residue M589, our DEER measurements in the AMP-PNP-bound state should have yielded a distance of approximately 3.0 nm (Table 5.2). Figure 5.10 shows the results from the DEER measurements of $Hsp90^{M589C[MTSSL]}$ in the AMP-PNP-free and AMP-PNP-bound conformations.

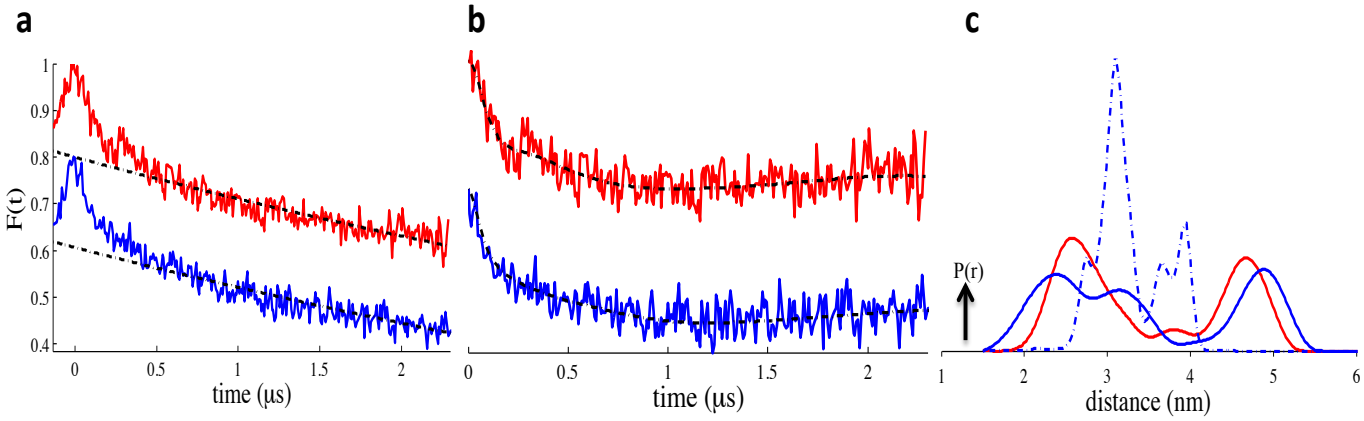

Figure 5.10 DEER measurements of $Hsp90^{M589C[MTSSL]}$ in the AMP-PNP-free and AMP-PNP-bound states. The predicted distance distribution is based on PDB 2CG9[16]. **a,** the raw DEER traces of the AMP-PNP free and AMP-PNP bound $Hsp90^{M589C[MTSSL]}$ (red and blue respectively), **b,** the form factor and the fit (black) to the data using DeerAnalysis2011[69]. **c,** the distance distribution of the experimental data (solid lines) and predicted distance distributions from the rotamer analysis (dotted lines). Colour coding as in Figure 5.10a.

To our surprise, we did not observe a single distance that would indicate the presence of a homodimer at the C domain. Our DEER measurements revealed a range of distances between the labels attached at residue Met589 of 2.0–5.0 nm, in both the AMP-PNP-free and AMP-PNP-bound conformations (Figure 5.10c). However, Met589 is located on an α helix (refer to Figure 5.3) at the top of the C domain and may be subject to

flexibility in both the nucleotide-free and nucleotide-bound states. Therefore in order to validate the findings of our DEER measurements from $Hsp90^{M589[MTSSL]}$, a nitroxide label would need to be attached to a residue directly at the homodimeristion interface, lower down from Met589. Nevertheless, the distances measured on $Hsp90^{M589[MTSSL]}$ could demonstrate the potential opening and closing of the C domains of Hsp90 in both the nucleotide-free and nucleotide-bound states, a finding also demonstrated by Ratzke *et* al[24] who used single-molecule FRET (smFRET) to show the opening and closing of the C domains. This study showed estimated distances of 5.6 nm and 3.5 nm for the open and closed states of the C domains respectively in both the nucleotide-free and nucleotide-bound states. This study demonstrated a model that suggested that C domain dimerisation of Hsp90 had a destabilising effect on nucleotide association. The distances obtained from this study are in good agreement with the distances obtained from our DEER measurements of $Hsp90^{M589C[MTSSL]}$. However, our experiments show no effect of C domain dimerisation becoming destabilized in either nucleotide free or nucleotide bound states.

From the experimental data so far of the DEER measurements made on the $Hsp90^{[MTSSL]}$ mutants, it appears that the N, lower M, and C domains are all sampling opening and closing in both nucleotide-free and nucleotide-bound states. Therefore, the question arises of what is the underlying mechanism of the Hsp90 homodimer if all domains undergo opening and closing? In order to address this question, an Hsp90 cysteine mutant at residue 511 ($Hsp90^{T511C[MTSSL]}$) on the M domain (Figure 5.2) was labelled with MTSSL as described in Chapter 2, page 86.

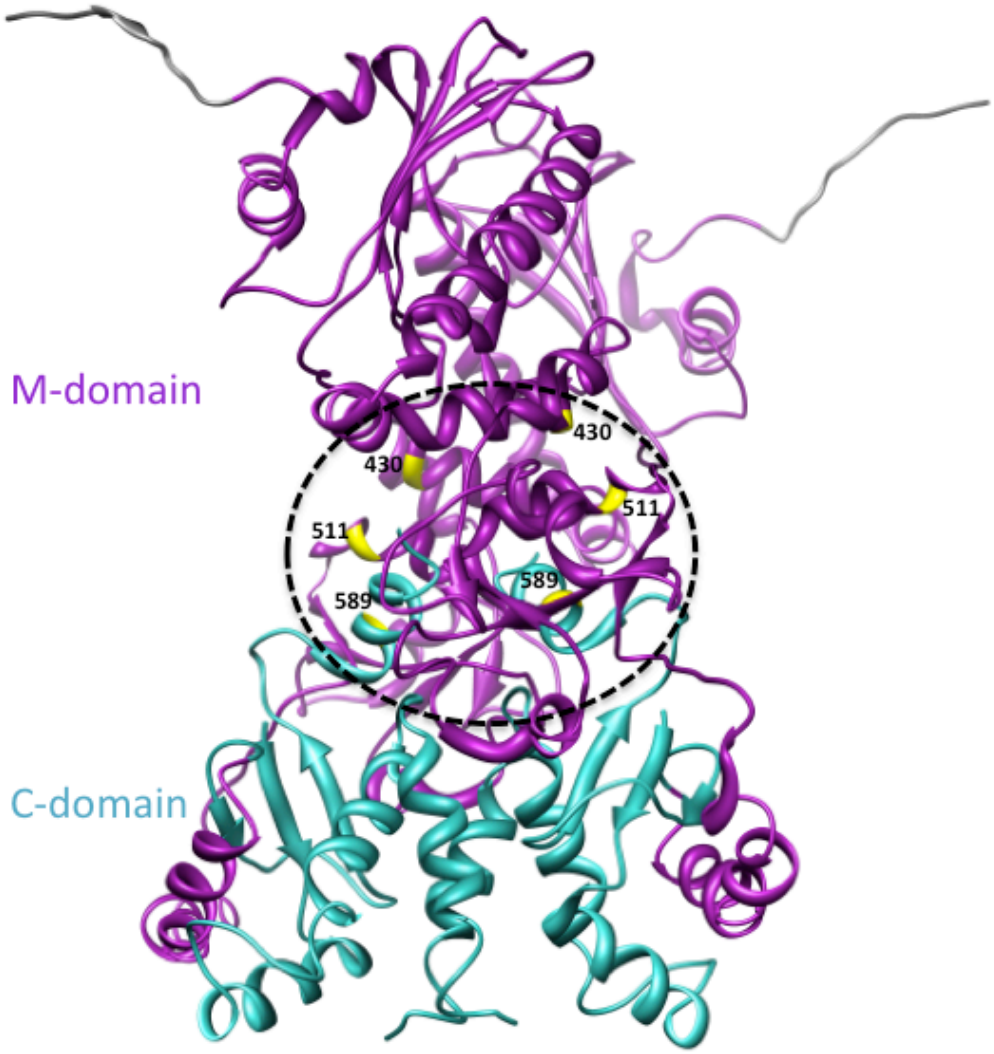

Figure 5.11 Ribbon representation of the M and C domains of the Hsp90 dimer (PDB 2CG9; refer to Appendix 1); M domain (purple) and C domain (blue), highlighting residues 430, 511, and 589 labelled with the nitroxide spin label MTSSL (yellow).

Residue 511 was chosen because it lies between two surfaces, as illustrated by Figure 5.11, of the Hsp90 dimer which sample opening and closing as demonstrated by the DEER measurements carried out on $Hsp90^{H430C[MTSSL]}$ and $Hsp90^{M589C[MTSSL]}$ (Figures 5.9 and 5.10). Figure 5.12 shows the results of the DEER measurements between the labels attached at residue 511 in the AMP-PNP-free and AMP-PNP-bound states.

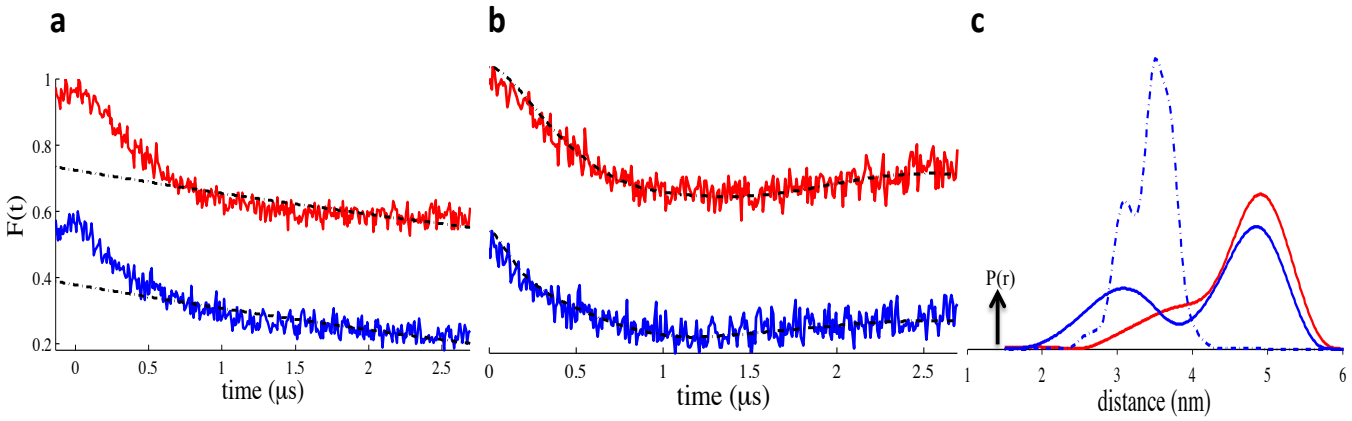

Figure 5.12 DEER measurements of Hsp90$^{T511C[MTSSL]}$ in the AMP-PNP-free and AMP-PNP-bound states. The predicted distance distribution is based on PDB 2CG9[16]. **a,** the raw DEER traces of the AMP-PNP-free and AMP-PNP-bound Hsp90$^{T511C[MTSSL]}$ (red and blue respectively), **b,** the form factor and the fit (black) to the data using DeerAnalysis2011[69]. **c,** the distance distributions of the experimental data (solid lines) and predicted distance distribution from the rotamer analysis (dotted line). Colour coding as in Figure 5.12a.

For both the AMP-PNP-free and AMP-PNP-bound measurements of Hsp90$^{T511C[MTSSL]}$, it appears that there are two distances observed by DEER spectroscopy of approximately 3.0 and 5.0 nm (Figure 5.12c). The shorter experimental distance is in good agreement with the predicted distance distribution of the rotamer positions of the labels attached at residue 511 of approximately 3.3 nm (Table 5.2). However, this shorter distance is less populated than the longer experimental distance of approximately 5.0 nm, which seems to dominate the DEER spectra in both the AMP-PNP-free and AMP-PNP–bound states. Since the shorter distance fits well with crystal structure, the observation of the longer distance in this case may be the result of the Hsp90:AMP-PNP complex not being completely pushed to the fully AMP-PNP-saturated state, particularly since the shorter experimental distance seems to be more pronounced in the AMP-PNP-bound state when compared to the AMP-PNP-free state.

Since the DEER data obtained for Hsp90$^{T511C[MTSSL]}$ also potentially shows an open and closed state, the question still remains as to how the Hsp90 dimer remains intact. Our DEER data for the C domain mutant suggests that C domains of Hsp90 undergo opening and closing in the AMP-PNP-free and AMP-PNP–bound states, whereas the data for the N and lower M domain mutants suggest opening and closing of the dimer in

the absence of nucleotide whereby AMP-PNP association shifts the dimer at these positions to the closed conformation. In light of these results, the data from our DEER measurements strongly suggest that the Hsp90 dimer is kept intact via coupled and synchronised dimerisation between the N, lower M, and C domains. In the absence of nucleotide, all 3 domains sample opening and closing, whereby as N and lower M domains open, C domains close, and as C domains close, N and lower M domains open. Upon AMP-PNP association, the N and lower M domains move to the closed conformation, whereby C domains continue to open and close.

5.11 Co-chaperone induced rearrangement of the M domains of the Hsp90 dimer'

The data in this chapter so far have suggested that the 'twisted' conformation of the M domains of the Hsp90 dimer as seen in the crystal structure[16] could be a result of co-chaperone (Sba1/p23) association to Hsp90. As shown in Figures 5.7 and 5.8, no distances were observable from the DEER measurements made on $Hsp90^{S297C[MTSSL]}$, $Hsp90^{S363C[MTSSL]}$, and $Hsp90^{V391C[MTSSL]}$ in both nucleotide-free and nucleotide-bound states. Contrary to these findings were the predicted distance distributions of the rotamers of the labels attached on residues Ser297, Ser363, and Val391, which present distances between 2.0 – 5.0 nm, all of which should have been observed by DEER spectroscopy with the chosen $\tau 2$ of 3.2 μs.

In order to address the potential mechanism of co-chaperone induced rearrangement of the M domains of Hsp90, DEER measurements were carried out between the labels attached on residues 297 and 363 in the presence of AMP-PNP and the co-chaperone Sba1/p23. Figure 5.13 shows the results of these DEER measurements.

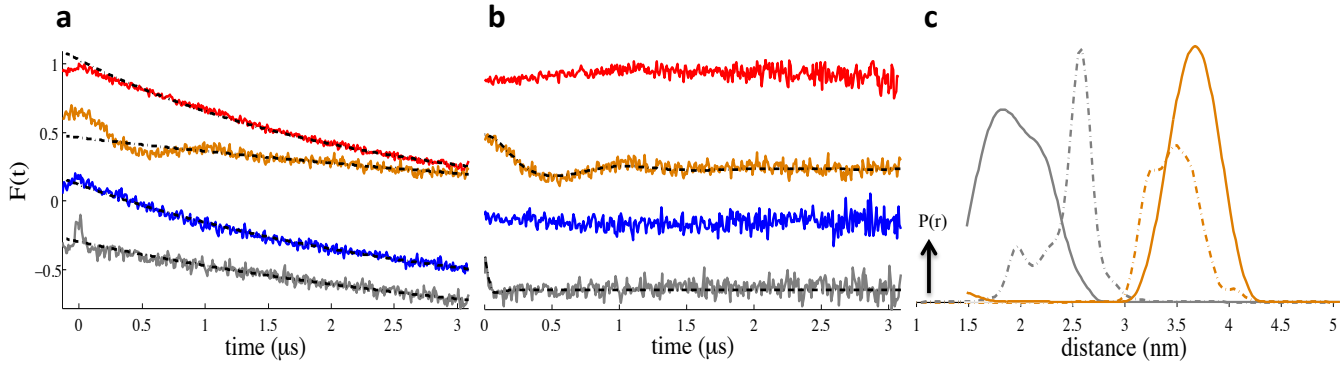

Figure 5.13 DEER measurements of Hsp90^{S297C} and Hsp90$^{S363C[MTSSL]}$ in the AMP-PNP-bound and AMP-PNP-Sba1/p23-bound states. The predicted distance distributions are based on PDB 2CG9[16]. **a,** the raw DEER traces of the AMP-PNP-bound Hsp90$^{S297C[MTSSL]}$ and Hsp90$^{S363C[MTSSL]}$ (red and blue respectively), and the AMP-PNP-p23 bound Hsp90$^{S297C[MTSSL]}$ and Hsp90$^{S363C[MTSSL]}$ (orange and grey respectively), **b,** the form factor and the fit (black) to the data using DeerAnalysis2011[69]. **c,** the distance distributions of the experimental data (solid lines) and predicted distance distributions from the rotamer analysis (dotted lines). Colour coding as in Figure 5.13a.

The data presented in Figure 5.13 is in good agreement with the proposed model of co-chaperone induced rearrangement of the M domains of Hsp90. The distance obtained for Hsp90$^{S297C[MTSSL]}$ in the AMP-PNP-Sba1/p23-bound state of approximately 3.5 nm is in good agreement with the predicted distance from the rotamer analysis of 3.5 nm. The distance obtained for Hsp90$^{S363C[MTSSL]}$ in the AMP-PNP-Sba1/p23-bound state of approximately 2.0 nm however, is shorter than the predicted distance from the rotamer analysis of 2.5 nm. The reason for the shorter distance could be a reflection of the modifications made on the crystal structure, which are not present in the Hsp90 used in our DEER measurements.

Furthermore, it was speculated whether the rearrangement of the M domains of Hsp90 by Sba1/p23 required the presence of AMP-PNP. Figure 5.14 shows the results from the DEER measurements of Hsp90$^{S297C[MTSSL]}$ and Hsp90$^{S363C[MTSSL]}$ with Sba1/p23 in the absence of AMP-PNP. These distance measurements resulted in no observable distance as illustrated by the flat lines of the form factors (Figure 5.14b), suggesting that M domain rearrangement by Sba1/p23 requires the presence of AMP-PNP.

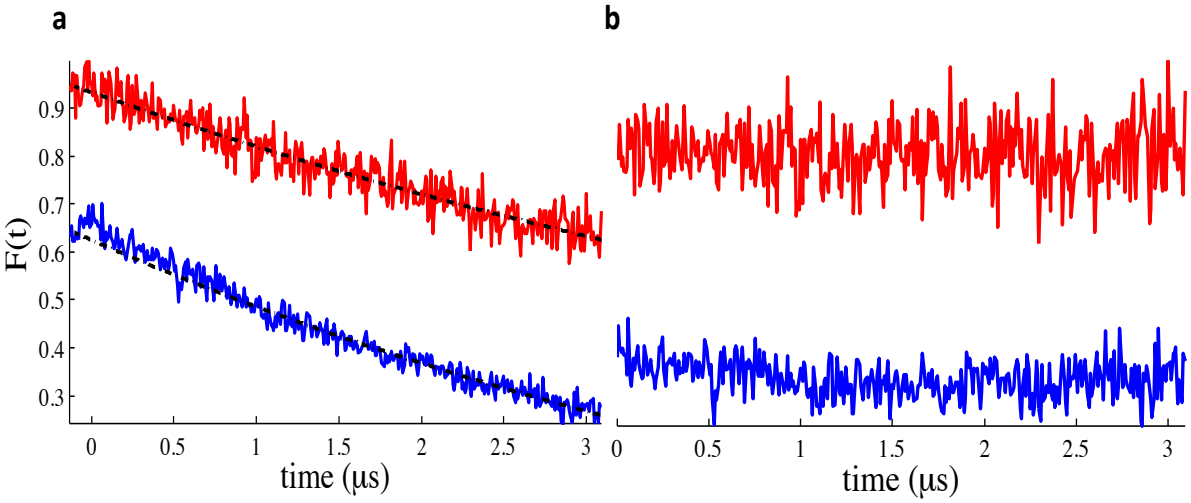

Figure 5.14 DEER measurements of Hsp90$^{S297C[MTSSL]}$ and Hsp90$^{S363C[MTSSL]}$ in the Sba1/p23-bound. a, the raw DEER traces of the Sba1/p23-bound Hsp90$^{S297C[MTSSL]}$ and Hsp90$^{S363C[MTSSL]}$ (red and blue respectively), and **b,** the form factor. Colour coding as in Figure 5.14a.

The results from the distance measurements presented in Figures 5.13 and 5.14 agree with the proposed model of co-chaperone-induced M domain rearrangement, revealing a conformation of Hsp90 that could be a target for the development of potential therapeutics against disease states induced by the Hsp90-Sba1/p23–client machinery.

5.12 Co-chaperone induced ATP lid closure

Sba1/p23 binds to the N and M domains of the Hsp90 dimer, and since the DEER measurements Hsp90$^{A103C[MTSSL]}$ revealed no observable distance, which does not agree with the predicted distance of the rotamer analysis of 4.5 nm, the possibility of co-chaperone-induced ATP lid closure needed to be addressed. A DEER measurement of Hsp90$^{A103C[MTSSL]}$ in AMP-PNP:Sba1/p23-bound state was carried out in order to investigate the possibility of Sba1/p23 inducing lid closure. Figure 5.15 shows the results from this DEER measurement compared with the previous results obtained for Hsp90$^{A103C[MTSSL]}$ in the AMP-PNP-bound state (Figure 5.5).

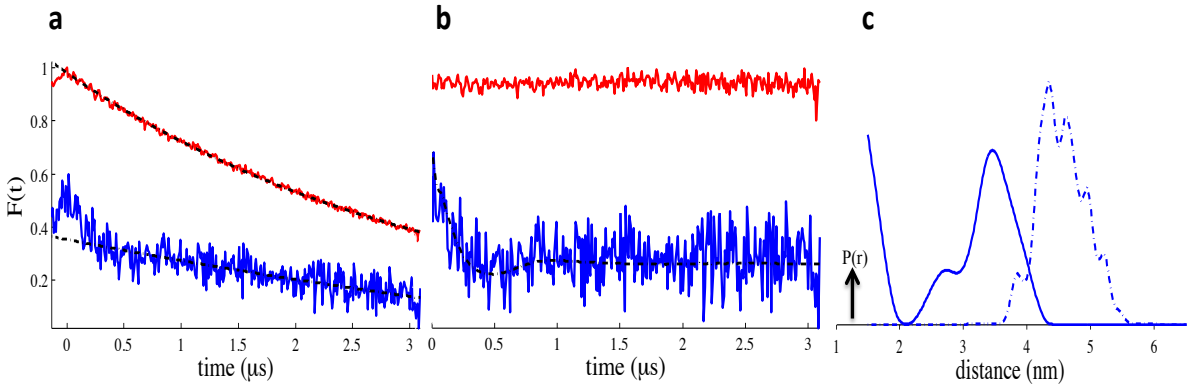

Figure 5.15 DEER measurements of Hsp90$^{A103C[MTSSL]}$ in the AMP-PNP-bound and AMP-PNP:Sba1/p23-bound states. The predicted distance distribution is based on PDB 2CG9[16]. **a,** the raw DEER traces of the AMP-PNP-bound and AMP-PNP:Sba1/p23-bound Hsp90$^{A103C[MTSSL]}$ (red and blue respectively), **b,** the form factor and the fit (black) to the data using DeerAnalysis2011[69]. **c,** the distance distribution of the experimental data (solid line) and predicted distance distribution from the rotamer analysis (dotted line). Colour coding as in Figure 5.15a.

The results presented in Figure 5.15 support the idea of the ATP lid of Hsp90 potentially being in a conformation between open and closed in the AMP-PNP-bound state as suggested by the ITC data presented in Chapter 3. The AMP-PNP–bound Hsp90$^{A103C[MTSSL]}$ yields no observable distance as illustrated by the flat line of the form factor shown in Figure 5.15b, and this does not agree with the predicted distance of 4.5 nm. However, the addition of the co-chaperone Sba1/p23 reveals a distance of approximately 3.5 nm, a distance shorter than the predicted distance. The shorter distance in our experiment could reflect the A107N mutation present in the crystal structure[16], which artificially induces full lid closure. Therefore our results could potentially demonstrate the possibility of Sba1/p23 inducing a less compact lid-closed structure (and therefore shorter distance between labels attached to both lids) for a lid that has no modifications made to it. Nevertheless, these data suggest that Sba1/p23 induces closure of the ATP lid. This conformational change could provide a mechanism by which Sba1/p23 functions, in that Sba1/p23 ‘halts’ the ATP cycle and ‘prepares’ the Hsp90 chaperone for hydrolysis by pushing it towards the ATP ‘active’ state but in a way which prevents hydrolysis, a reaction probably caused by full ATP lid closure.

5.13 A revised ATP cycle for the Hsp90 chaperone

In order to understand the various conformations in the cycle of Hsp90 as it undergoes ATP binding and hydrolysis, we used Hsp90$^{[MTSSL]}$ mutants and DEER spectroscopy to determine distances between nitroxide labels attached to various residues along the length of the Hsp90 dimer. We measured distances of the labelled mutants in the nucleotide-free, nucleotide-bound, and nucleotide:Sba1/p23-bound states. Using the data obtained from the distance measurements of the labelled mutants, we can provide the following revised ATP cycle of Hsp90 as illustrated in Figure 5.16.

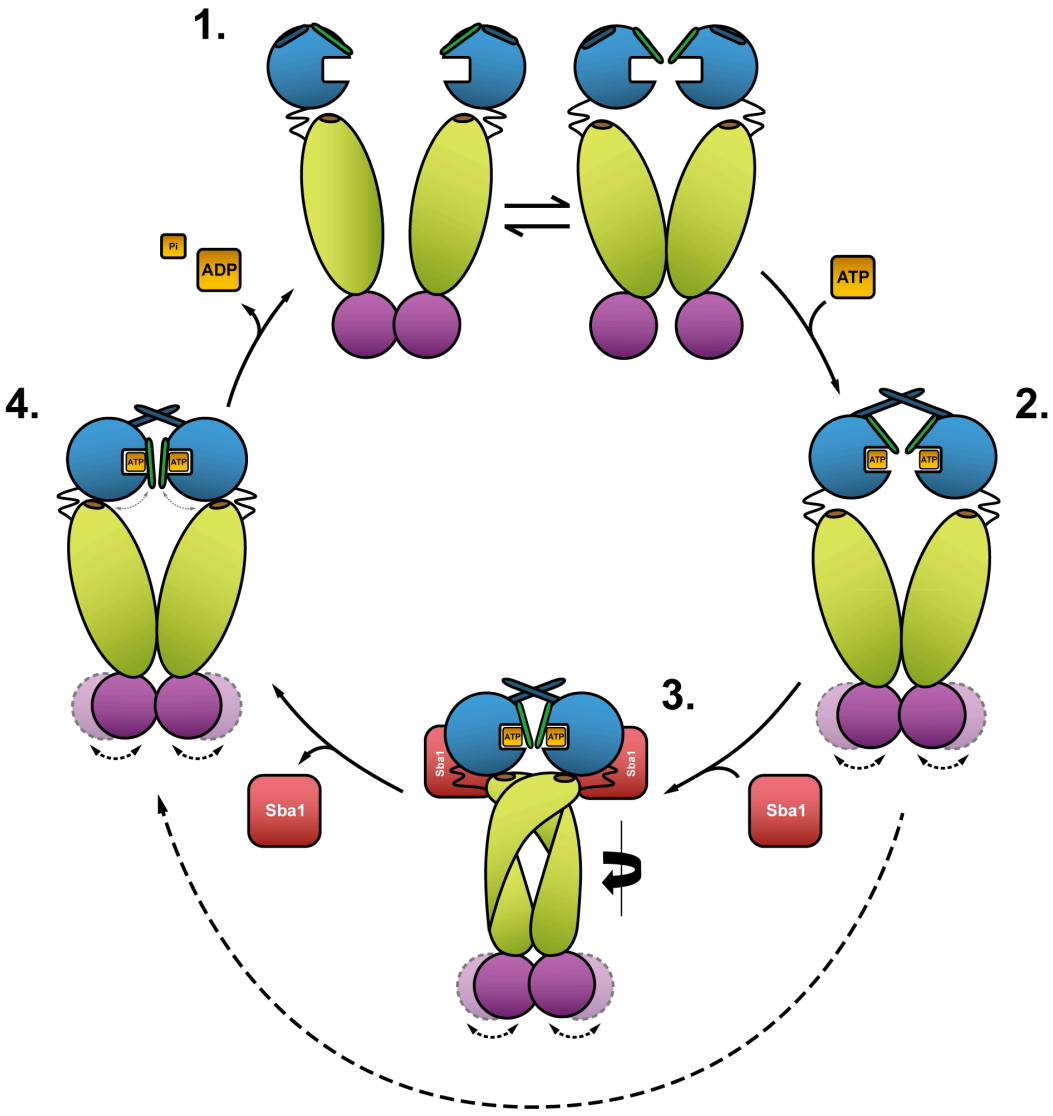

Fig. 5.16 Revised ATPase cycle of the Hsp90 chaperone. Schematic diagram of the Hsp90 ATPase cycle. **1,** Nucleotide-free conformation of Hsp90 in which N (blue) and M (green) domains couple opening and closing in a synchronized manner with C domains (purple), whereby closure of the N and lower M domains lead to opening of

the C domains and the closure of the C domains lead to opening of the N and lower M domains. **2,** After ATP association N domain dimerisation occurs through a 'strand swap' event and partial lid (dark green) closure within the N domains (dark blue); and lower M domains stabilize to the closed conformation, whilst C domains are still undergoing opening and closing (illustrated by the lighter dotted-lined C domains). **3*,** Association of the co-chaperone Sba1/p23 to the N/M domains results in a rearrangement of the M domains in a 'twisted' conformation and further closure of the ATP lid enforcing the ATP 'active' state but in a way which 'halts' ATP hydrolysis. Sba1/p23 can now recruit and process its client(s). **4,** Once Sba1/p23 completes its function as a co-chaperone, it leaves Hsp90 together with its 'folded' client, resulting in the 'unwinding' of the 'twisted' M domains, now allowing the interaction of the N and M domains within individual protomers of the dimer through the catalytic arginine residue (brown) within the M domains via full closure of the ATP lid, ultimately resulting in ATP hydrolysis and the release of ADP + P_i. This reverts the Hsp90 dimer back to the nucleotide-free conformation ready for the recruitment of another ATP molecule (cycle starts from step 1 again).

* At this step, if Hsp90 does not come into contact with any co-chaperone, the cycle goes straight from step 2 to step 4, bypassing step 3.

5.14 Summary

The DEER spectroscopy measurements of the $Hsp90^{[MTSSL]}$ mutants provide a structural overview of the conformational mechanisms involved in the ATP cycle of this therapeutically crucial chaperone. These findings contradict the previously suggested observations of the movements within Hsp90 upon nucleotide association[11,12,16,18,24], which are also not apparent in the crystal structure of the Hsp90-AMP-PNP-p23 complex or the EM structure of the Hsp90-Cdc37-Cdk4 complex[18].

To confirm this model further, previous views of how Hsp90 couples ATP hydrolysis with conformational changes in which the M domains of the dimer come into close contact with one another resulting in a 'twisted' complex committing ATP for hydrolysis were addressed. Nitroxide labels were attached along the length of the M domain and DEER spectroscopy was carried out in the nucleotide-free and nucleotide-bound state, the latte of which forms the dimerised N and lower M domains as shown from the distance measurements on the $Hsp90^{S17C[MTSSL]}$ (Figure 5.4) and $Hsp90^{H430C[MTSSL]}$ (Figure 5.9). These results however, illustrated no contact between

the M domains in the region where residues 297, 363, ad 391 lie, which did not agree with the predicted distances of the rotamer analysis of labels attached to these residues.
It was found that this 'twisted' M domain state of Hsp90 represents a conformation which is achieved after binding of the co-chaperone Sba1/p23 (Figure 5.13). Furthermore, Sba1/p23 induces ATP lid closure as revealed by the DEER measurements of $Hsp90^{A103C[MTSSL]}$ (Figure 5.15), which demonstrates a clear mechanism by which Sba1/p23 could function by 'holding' Hsp90 in an ATP 'active' state but not permitting ATP hydrolysis, and thus allowing Sba1/p23 to process its clientele. The view of Sba1/p23 inducing ATP lid closure fits well with the observations made in Chapter 3 of an ATP lid that could be in an intermediate between open and closed when in the AMP-PNP-bound state, where partial lid closure could also promote N domain dimerisation due to the exposure of partial hydrophobic surface.

Along with the opening and closing of the N and lower M domains of Hsp90 demonstrated by the distances obtained from the DEER measurements on $Hsp90^{S17C[MTSSL]}$ and $Hsp90^{H430C[MTSSL]}$, it was also revealed that the C domains of Hsp90 appear to undergo opening and closing (Figure 5.10), which continue to take place after the dimerisation of the N and lower M domains.
When considering how the opening and closing of all three domains can be structurally feasible, bearing in mind that Hsp90 is natively a homodimer, one potential picture emerges, in which N, M domain and C domain dynamics are coupled and coordinated in a synchronized manner. The binding of ATP then stabilises an N and lower M domain dimerised state, where C domains continue to open and close. N and M domain intra-protomer contacts can now take place via the catalytic Arg^{380} residue[11,15] (Figure 5.16, Step 4). This conformation seems to represent the final fully closed ATP-bound conformation of Hsp90. Any potential continuation of opening and closing motions of the C domains post ATP hydrolysis would not have been seen due to the non-hydrolysable nature of the AMP-PNP. However, as with M domain rearrangements post Sba1/p23 association, C domain dynamics could stabilise to a single state upon binding to a co-chaperone.
The conformational flexibility of this chaperone has been extensively demonstrated both in *vivo* and in *vitro*; this chapter provides us with yet a new understanding in the mechanism with which the dynamics of Hsp90 are choreographed to ultimately hydrolyse ATP.

Chapter 6

Discussion

This thesis has focused on the detailed study of nucleotide binding to the Hsp90 molecular chaperone and the local and global effects thereof, both thermodynamically and structurally. The thermodynamic investigation of nucleotide binding to Hsp90 focused solely on the isolated N-terminal domain (that is N-Hsp90), and the dynamics of the Hsp90 chaperone through its ATP cycle was followed through changes within the full-length dimeric protein. The results from these studies provide sight into the hugely dynamic nature of this molecular chaperone, which is not only confined to the ATP binding domain but extended throughout all domains of the Hsp90.

The ATP interaction of the Hsp90 molecular chaperone and the conformational changes associated have been studied in great detail. However many of these studies yielded static images of either the isolated N-Hsp90 domain in complex with ADP[7] or the full-length Hsp90 in complex with AMP-PNP and the co-chaperone Sba1/p23[16]. The two structures above revealed very distinct conformational changes upon nucleotide binding, particularly concentrated to the NTS and ATP lid regions, whereby the ADP-bound N-Hsp90 illustrated an ATP lid in the 'open' conformation packing against the main body of the N domain structure. In contrast, the AMP-PNP bound full length Hsp90 structure showed an ATP lid that closed over the nucleotide-binding pocket. Furthermore, the NTS in the latter structure was shown to interact with the same region within the partner protomer of the Hsp90 dimer. However, whether the two distinct structures were as a direct result of nucleotide binding remains ambiguous.

6.1 Thermodynamics of nucleotide binding to N-Hsp90

The thermodynamics of nucleotide binding was investigated using ITC, yielding information on the enthalpy, entropy, and affinity of a given interaction. These results were then used to extract information on the changes in the observed free energy and heat capacity of the system under investigation.

Binding of adenine-containing nucleotides to N-Hsp90 revealed exothermic interactions, which were enthalpically driven. ADP binding to N-Hsp90 showed a more favourable $\Delta H°_{obs}$ and a less favourable $T\Delta S°_{obs}$ in comparison to AMP-PNP; this could be reflective of the large amount of water found to be present in the nucleotide binding site in the ADP bound state[7] becoming trapped upon ADP binding, on the contrary, AMP-PNP binding traps less water reflective from the more favourable $T\Delta S°_{obs}$ of this interaction possibly by a means of displacement of some of these waters via formation of indirect hydrogen bonds between the protein and γ phosphate. Furthermore, the addition of the third phosphate in the AMP-PNP interaction resulted in destabilisation of the binding affinity between the nucleotide and N-Hsp90 resulting in ADP bearing an approximate 5 fold stronger affinity than AMP-PNP for N-Hsp90. The weaker affinity of AMP-PNP for N-Hsp90 could indicate changes in the orientation of the nucleotide as a result of conformational change of the ATP lid region.

Previous structures of N-Hsp90 and full-length Hsp90 in complex with ADP[7] and AMP-PNP[7,16] have demonstrated that the majority of the contacts between the nucleotide and the protein are mediated via water molecules whereby only three direct contacts via hydrogen bonds and van der Waals contacts with Asp79, Asn92, and Met84 between the adenine moiety of the nucleotide and protein exist. The phosphate chain of the nucleotide is involved in contacts via hydrogen bonds between the α and β phosphates with Asn37, Phe124, and Lys98, where the latter residue is contacted via the Mg^{2+} ion. Indirect contacts via hydrogen bonds between the γ phosphate and Gln119, Gly121, Val122, and Gly123 were also demonstrated in the full-length Hsp90 structure[16]. When considering the plethora of water molecules in the interaction between Hsp90 and its nucleotide ligands, it becomes increasingly apparent that the clarity of these direct and indirect contacts is crucial if we want to understand the nature of the interaction, and how the binding of two adenine-containing nucleotides to the same binding site on N-Hsp90 revealed completely opposite $\Delta Cp°_{obs}$; an observation initially made by Nilapwar *et al.*[19] and also confirmed in this thesis. The cause of this positive $\Delta Cp°_{obs}$ was explained by the apparent 'closure' of the ATP lid, which reveals a hydrophobic surface to the bulk solvent[19], a conformational change also seen in the full-length Hsp90 in complex with AMP-PNP and the co-chaperone p23[16]. The conformational change associated with the ATP lid could also explain the consistently unfavorable $T\Delta S°_{obs}$ observed with nucleotide binding, as a result of the entrapment of

water molecules at the protein/ligand interface, however the data presented previously does not indicate the extent of lid movement with the different nucleotide ligands and whether these differences are sufficient to explain the different $\Delta Cp°_{obs}$ values observed. Although differing by a single phosphate, these adenine-containing nucleotides must bind to Hsp90 using distinct modes.

6.2 Influence of divalent ion involvement on the thermodynamics of nucleotide association

In the structural detail of the N-Hsp90/nucleotide interaction, metal ions play an integral part of complex formation and previous ITC studies[19] and the data from this thesis revealed no interaction between N-Hsp90 and the nucleotide ligands in the absence of the divalent magnesium ion. Nilapwar *et al.*[19] predicted the location of the magnesium ion to reside in the junction along the phosphate chain in an octahedral manner via the oxygens from the β and γ phosphates, the Asn37, and three water molecules. And indeed this prediction seems to be correct, as the divalent magnesium ion has been found to possess a preferential stable octahedral arrangement in terms of its hydration shell[74]. Furthermore, mutational studies[19] on residues which are involved in indirect hydrogen bonds with the water molecules that coordinate the magnesium ion, through ITC, revealed an inability of AMP-PNP to interact with N-Hsp90 demonstrating the potential importance of these waters in complex formation (refer to Chapter 1).

In this study, ITC revealed that the magnesium ion binds to AMP-PNP in a 1:1 stoichiometry suggesting that the nucleotide-ion complex is formed prior to interacting with N-Hsp90. The ion-nucleotide interaction is enthalpically driven, as is the interaction of AMP-PNP-Mg^{2+} with N-Hsp90, however this interaction is associated with an unfavourable $\Delta H°_{obs}$ and a favourable $T\Delta S°_{obs}$ indicating the displacement or release of water molecules from the magnesium binding site possibly to obtain the preferred octahedral coordination of water around this ion. This complex when bound to N-Hsp90 results in more favourable enthalpic contribution than the ion binding to the nucleotide alone, and a less favourable entropic contribution and results in the destabilisation of the binding affinity possibly due to the entrapment of water molecules within the nucleotide binding site as mentioned in Section 6.1.

Interestingly, the substitution of the divalent Mg^{2+} ion with the Mn^{2+} ion results in a comparable thermodynamic profile including a comparable $\Delta Cp°_{obs}$, however substitution with a Ca^{2+} ion leads to a less favourable $\Delta H°_{obs}$ and a more favourable $T\Delta S°_{obs}$; the $\Delta Cp°_{obs}$ for the latter interaction is approximately 6-fold greater than for the Mg^{2+}/Mn^{2+} ion interactions. These thermodynamic observations implicate the involvement of the hydration shells of the metal ions playing a crucial role, whereby the rather stable hydration shell of Mg^{2+}/Mn^{2+} leads to the entrapment of the water at the protein/ligand interface in a way that limits the inherent vibrational modes of these otherwise well-coordinated waters resulting in a less positive $\Delta Cp°_{obs}$. On the contrary, the less stable hydration shell of the Ca^{2+} ion results in less water being trapped and therefore increases the degrees of freedom of the well-coordinated waters at the protein/ligand interface, possibly by releasing these waters into bulk solvent as reflected by the favourable change in entropy observed with this metal ion. As a result, a larger positive $\Delta Cp°_{obs}$ is observed for this ion interaction.

ADP binding in general is associated with a more favourable enthalpic contribution and less favourable entropic contribution than with AMP-PNP binding for all metal ion interactions, supporting the view of more water being present in the ADP-bound N-Hsp90 interface leading to this excess water becoming trapped upon the binding of ADP. The interactions involving the Ca^{2+} ion produce a much less negative $\Delta Cp°_{obs}$ than the Mg^{2+}/Mn^{2+} ion interactions, further validating the possibility of less water being trapped with the 'water-light' Ca^{2+} ion when compared with the 'water-heavy' Mg^{2+}/Mn^{2+} ions.

The results from the ion substitution interactions provide strong evidence for the hydration states of the ions providing a contribution to the positive $\Delta Cp°_{obs}$ seen with the AMP-PNP interaction, as no difference in $\Delta Cp°_{obs}$ would be observed from substituting the ion if conformational change associated with the interaction was the sole contributor to the anomalous heat capacity demonstrated. Of particular interest is the thermodynamic profiles of the ADP interaction for all metal ions, which produces a consistent negative $\Delta Cp°_{obs}$, an observation more pronounced with water-heavy Mg^{2+}/Mn^{2+} ions. Furthermore, as an additional phosphate is introduced into the binding site, these thermodynamics change dramatically. Since it has been speculated that the region between the β and γ phosphates is where the divalent ion sits, the data from the

metal ion interactions provide strong evidence for the contacts mediated via this region, to be of grave importance in the derived anomalous positive $\Delta Cp°_{obs}$ observed for the N-Hsp90-AMP-PNP interaction.

6.2.1 The effect of the ATP lid on the thermodynamics of the system

In order to distinguish whether the unique thermodynamics of the N-Hsp90/nucleotide interaction is derived from conformational change of the ATP lid and/or metal ion hydration effects, the thermodynamics of N-Hsp90 mutants that stabilised the lid in an open and closed conformation were studied with all metal ions.
The trapping of water at the protein/ligand interface could be due to surface area burial upon nucleotide binding, or due to local conformational changes induced upon AMP-PNP binding, which also results in burial of surface area, or a combination of both effects. ADP-Mg^{2+} binding to N-Hsp90 results in a significantly larger favourable enthalpy and a much less favourable entropy, which as mentioned previously indicates the entrapment of water molecules, particularly when considering the excess water that has been found to reside in the N-Hsp90-ADP structure[7]. The lid dynamics of the ADP structure have been found to result in a 'lid open' N-Hsp90, which explains the consistent negative $\Delta Cp°_{obs}$ seen with the ADP interaction due to burial of non-polar surface area. However the AMP-PNP interaction shows a completely opposite $\Delta Cp°_{obs}$ and a more favourable $T\Delta S°_{obs}$, implying less water is trapped with AMP-PNP than with ADP by increasing the net degrees of freedom of these trapped waters, possibly by release into bulk solvent. The positive $\Delta Cp°_{obs}$ can be partly explained by the conformational change found to be associated with AMP-PNP binding, which although results in burial of non-polar surface area (closure of the ATP lid over the nucleotide binding pocket) leading to trapping of some water, the binding of this nucleotide is also associated with the exposure of hydrophobic surface area (back of the ATP lid) to the bulk solvent, leading to the expulsion of waters and the displacement of water molecules at the protein/ligand interface.

Interestingly, an N-Hsp90 mutant in which the ATP lid could either be in the open or closed (T22I) conformation provides no evidence of a positive change in heat capacity, but rather reflects a negative $\Delta C_p°_{obs}$, as is also seen with the interaction between ADP with N-Hsp90. Since the thermodynamics of T22I are similar to that of the ADP interaction, an interaction which stabilises a lid open N-Hsp90, one may argue

that the T22I mutation may thus stabilise a lid-open N-Hsp90. If this were the case, then the results from the T221 ITC experiments would explain the similarities this mutant shares in terms of thermodynamics with the WT N-Hsp90 and ADP interaction. Similarly, an N-Hsp90 mutant in which the ATP lid is stabilised to the open (T101I) conformation also results in a negative $\Delta C_p°_{obs}$ as would be expected, since the interaction between WT N-Hsp90 with ADP results in an observed negative change in heat capacity caused by ATP lid opening (as mentioned earlier). Therefore, the results from the mutants where the ATP lid is stabilised to open/closed conformation result in a negative $\Delta C_p°_{obs}$, and this suggests that the anomalous positive $\Delta C_p°_{obs}$ seen with the interaction between WT N-Hsp90 and AMP-PNP although may seem to partially relate to the gross dynamics of the ATP lid, must also accrue from some other source.

Furthermore these data suggest that T22I binds with an affinity that is similar to T101I, both of which are stronger than WT N-Hsp90. The similarities in the affinities between T22I and T101I with the adenine-containing nucleotides further implies a lid that could be open for T22I, as a lid closed N-Hsp90 would demonstrate a weak binding affinity in comparison to a lid open N-Hsp90. Additionally, the stronger affinity of the T22I and T101I mutants in comparison to the WT-N-Hsp90 for the adenine-containing nucleotides, indicates that the ATP lid in the WT N-Hsp90 could be in a conformation between open and closed, and that partial closure of the ATP lid upon ATP binding would lead to a destabilisation of the bound ATP as indicated by the weaker binding affinity seen with WT N-Hsp90.

Contrary to the negative heat capacities observed with both N-Hsp90 lid mutants with AMP-PNP binding in the presence of $MgCl_2$, positive heat capacities are observed with $MnCl_2$ and $CaCl_2$, whereby the thermodynamic trends for $MnCl_2$ although enthalpically more favourable and entropically less favourable to $MgCl_2$, are comparable. The thermodynamics of all interactions in the presence of $CaCl_2$ are consistently enthalpically less favourable and entropically more favourable than that with both $MgCl_2$ and $MnCl_2$, demonstrating the possible role of the varied and/or unstable hydration shell of $CaCl_2$ permitting this ion to trap less solvent molecules in a way that increases the net vibrational modes of the water molecules present at the protein/ligand interface by means of releasing them into bulk solvent, as indicated by its largely positive $\Delta C_p°_{obs}$. Such an effect is not achievable by the more stable hydration shells of

both Mg^{2+} and Mn^{2+} ions, which would in fact reduce the net vibrational modes of these waters by displacing them at the protein/ligand interface.

Although a positive change in heat capacity is the general observation of the N-Hsp90/AMP-PNP interaction for all metal ions, the rather varied values of $\Delta C_p°_{obs}$ obtained from these divalent ions suggest alternative mechanisms of action, an effect more pronounced when the gross dynamics of the ATP lid is manipulated.

6.3 Differences in the resonances of residues affected by the presence of two distinct divalent ions

Chapter 4 describes the variations in chemical shift perturbation patterns for residues that are affected differently in the N-Hsp90/AMP-PNP interaction in the presence of the Mg^{2+} and Ca^{2+} ions, differences that can be explained in part by the hydration shells of these divalent ions. Although the thermodynamic data obtained by altering the polarities of the effected residues remains unclear in regards to the waters coordinating the metal ion playing a role in the observed anomalous positive $\Delta C_p°_{obs}$ observed in the WT N-Hsp90/AMP-PNP interaction, clear differences are observable whereby the introduction of a slight hydrophobic property leads to a significant increase in the relative degrees of freedoms of the interfacial water molecules resulting in a much larger temperature dependence of the system under investigation. The observed thermodynamic effects were on a larger scale for interactions of the nucleotides in the presence of the Ca^{2+} ion, a trend that is seen throughout all interactions investigated with this ion. The use of deuterium as the hydrogen donor compared with hydrogen produces a more positive $\Delta C_p°_{obs}$ for the Mg^{2+}/Mn^{2+} interactions with AMP-PNP, possibly reflective of the ability of deuterium to trap of less water by means of disrupting the cooperative hydrogen bonding network between the interacting molecules and the surrounding solvent, resulting in a net increase in the degrees of freedom of the waters at the protein/ligand interface. The water-light Ca^{2+} ion in D_2O interactions however, shows a $\Delta C_p°_{obs}$ comparable to that in H_2O, showing implications for the role of its hydration shell in the derived thermodynamics.

6.4 Global conformational changes upon nucleotide association

Using the distance measurements made in this study we depict a new view of the chaperone cycle, where there is coupled transient dimerisation between the N and

lower M domains of the dimer, which become stabilised to the closed conformation upon AMP-PNP association. The C domains of the Hsp90 dimer open and close in synchronization with N and M domain opening and closing. Once AMP-PNP binds and N and M domain dimerisation takes place our data demonstrate C domain dynamics continuing, possibly even during the step of ATP hydrolysis. However, the latter observation was not seen with our DEER measurements as we used the non-hydrolysable analogue of ATP, AMP-PNP.

To confirm this model further, we addressed previous views of how Hsp90 couples ATP hydrolysis with conformational changes in which the M domains of the dimer come into close contact with one another resulting in a 'twisted' complex committing ATP for hydrolysis; we attached spin labels along the M domain (Hsp90 $^{S297C,S63C,V391C[MTSSL]}$) of residues which showed predicted distances between 2.2-4.4 nm and carried out DEER spectroscopy in the nucleotide-bound state, which forms the N and lower M domain dimerised state as shown from our distance measurements on the N and M domain mutants Hsp90$^{S17C,H430C[MTSSL].}$ The results from these distance measurements illustrated no contact between M domains as suggested by the predicted distances based on the crystal structure of Hsp90 in complex with AMP-PNP and Sba1/p23.

The M domain mutant Hsp90$^{T511C[MTSSL]}$ possibly shows two distances, a shorter and a longer distance, where the longer distance is dominant in both ligand free and ligand bound states. However, since the shorter distance becomes more populated in the ligand-bound state, the data may indicate that the Hsp90 probably did not completely saturate with ligand which is why we see the dominant longer distance, particularly since the shorter distance is in good agreement with the predicted distance of 3.3 nm.

Our study also revealed opening and closing of the C domains of the Hsp90 dimer as illustrated by a broad distance range between 2.5-5.0 nm, which is independent of N domain dimerisation. When considering how these conformations can be structurally feasible bearing in mind Hsp90 is natively a homodimer, one potential picture emerges, in which the N, M and C domain dynamics are coupled until the binding of ATP, after which Hsp90 is fixed and dimerised at both ends of the N and lower M domains, and where N - M domain contacts via the catalytic arginine residue (Arg^{380}) could then take place as previously suggested[11,15]. The structure presented here, in which the N and

lower M domains are dimerised and where the C domains are shown to open and close continuously seems to represent the final fully closed state of the dimer preparing it for association with co-chaperones such as p23 and its clients.

The DEER spectroscopy measurements of the Hsp90$^{[MTSSL]}$ mutants provides a structural overview of the conformational mechanisms involved in the ATP cycle. These findings contradict the previously suggested domain movements within Hsp90 upon nucleotide association[11,12,16,18,24], which are also not apparent in the crystal structure of the Hsp90-AMP-PNP-p23 complex[16] or the EM structure of the Hsp90-Cdc37-Cdk4 complex[18].

6.4.1 Influence of co-chaperones on conformational changes within the Hsp90 chaperone

Our data demonstrate that the previous views on the fully closed conformation of Hsp90 in which the M domains associate in a 'twisted' state represents a conformation which is achieved after binding of the co-chaperone Sba1/p23. Furthermore, the DEER measurements of the ATP lid mutant, A103C, revealed no observation of a distance unless the Sba1/p23 was bound with AMP-PNP to Hsp90. These data demonstrate a clear mechanism in which Sba1/p23 'halts' the Hsp90 chaperone cycle in an ATP 'active' state by closure of the ATP lid but to an extent that does not allow the hydrolysis of the bound ATP by the catalytic arginine residue within the M domain. In this way, Sba1/p23 is able to process its various clientele, after which Sba1/p23 is released from Hsp90 together with its 'folded' client allowing complete lid closure to take place and hence ATP hydrolysis.

Any potential continuation of opening and closing of the C domains of Hsp90 during and after ATP hydrolysis would not have been seen in our experiments due to the non-hydrolysable nature of the AMP-PNP. However as with potential M domain rearrangements after co-chaperone association as shown in our study, C domain dynamics could continue to take place until binding of a co-chaperone proteins in this region or elsewhere on Hsp90 takes place, whereby C domains would potentially become stabilised in the closed conformation.

Our measurements provide the view of co-chaperone induced conformational changes of regions within Hsp90 other than the direct co-chaperone binding site, providing us

with an intermediate to which the development of potential therapeutics could be directed to.

6.5 Future work

The vast conformational flexibility of the Hsp90 chaperone has been extensively demonstrated both in *vivo* and in *vitro*, and there continues to be an ever-growing body of knowledge which provides valuable insight into the highly dynamic nature of this ATPase.

The temperature dependence of the N-Hsp90/nucleotide interactions with the native magnesium ion and the substituted metal ions further confirm the ability of ADP and AMP-PNP to induce different conformational changes upon binding to N-Hsp90. These changes are particularly associated with the rearrangement of the ATP lid. Even in the case of an N-Hsp90 whose lid is stabilised to the open or closed conformation, the ADP interaction reveals extremely comparable thermodynamic profiles. On the other hand, the AMP-PNP interaction reveals a dramatically different thermodynamic profile, whereby the Mg^{2+} and Mn^{2+} interactions show comparable data unlike the Ca^{2+} interactions, which show significantly different trends in thermodynamics. The data from these experiments have implications on two important features that may give rise to the variation in the changes in heat capacity for the N-Hsp90/AMP-PNP interaction; the first being the rearrangement of the ATP lid, which could be in an intermediate between open and closed as opposed to the fully closed conformation that has previously been suggested, and the second is the importance of the hydration shell of the divalent ion, which sits in the junction between the two terminal phosphates of the nucleotide, providing at least part of the source for the derived $\Delta C_p°_{obs}$. The DEER measurements in this study provide us with a new understanding in the mechanism with which the dynamics of Hsp90 are choreographed to ultimately hydrolyse ATP producing a functionally active chaperone.

Overall, the data presented in this thesis demonstrates the importance of determining the solution state structures of the Hsp90/nucleotide complexes as a means of understanding how nucleotide association induces such large scale local and global conformational changes, allowing it to become a fully functional molecular chaperone; one which is able to undergo further conformational change upon co-chaperone

association. Particularly of interest is the closure of the ATP lid and the 'twisted' M domain fully closed state upon Sba1/p23 association, conformational rearrangements previously thought to be induced solely by ATP association. The cascade of conformational change induced during the Hsp90 chaperone cycle may be unique to the various co-chaperones and clientele that it has been found to be associated with, and if one can determine all possible conformational rearrangements this chaperone can adopt by studying the co-chaperone-chaperone interactions ultimately leading to the chaperones activation and hence the processing of client proteins, then this information can be manipulated to design additional and possibly more effective therapeutics against this highly dynamic molecular machinery.

References

1 Picard, D. *et al.* Reduced levels of hsp90 compromise steroid receptor action in vivo. *Nature* 348, 166-168 (1990).

2 Richter, K. & Buchner, J. Hsp90: Chaperoning signal transduction. *Journal of Cellular Physiology* 188, 281-290 (2001).

3 Martinez-Yamout, M. A. *et al.* Localization of Sites of Interaction between p23 and Hsp90 in Solution. *J. Biol. Chem* 281, 14457-14464 (2006).

4 Miyata, Y. & Nishida, E. CK2 Controls Multiple Protein Kinases by Phosphorylating a Kinase-Targeting Molecular Chaperone, Cdc37. *Molecular and Cellular Biology* 24, 4065-4074 (2004).

5 Meyer, P. *et al.* Structural and Functional Analysis of the Middle Segment of Hsp90: Implications for ATP Hydrolysis and Client Protein and Cochaperone Interactions. *Mol. Cell* 11, 647-658 (2003).

6 Mickler, M., Hessling, M., Ratzke, C., Buchner, J. & Hugel, T. The large conformational changes of Hsp90 are only weakly coupled to ATP hydrolysis. *Nat Struct Mol Biol* 16, 281-286 (2009).

7 Prodromou, C. *et al.* Identification and Structural Characterization of the ATP/ADP-Binding Site in the Hsp90 Molecular Chaperone. *Cell* 90, 65-75 (1997).

8 Richter, K. *et al.* Intrinsic Inhibition of the Hsp90 ATPase Activity. *J. Biol. Chem* 281, 11301-11311 (2006).

9 Scheibel, T. *et al.* Contribution of N- and C-terminal domains to the function of Hsp90 in Saccharomyces cerevisiae. *Molecular Microbiology* 34, 701-713 (1999).

10 Weikl, T. *et al.* C-terminal regions of Hsp90 are important for trapping the nucleotide during the ATPase cycle. *J. Mol. Biol* 303, 583-592 (2000).

11 Hessling, M., Richter, K. & Buchner, J. Dissection of the ATP-induced conformational cycle of the molecular chaperone Hsp90. *Nat Struct Mol Biol* 16, 287-293 (2009).

12 Neckers, L., Tsutsumi, S. & Mollapour, M. Visualizing the twists and turns of a molecular chaperone. *Nat Struct Mol Biol* 16, 235-236 (2009).

13 Prodromou, C. *et al.* The ATPase cycle of Hsp90 drives a molecular 'clamp' via transient dimerization of the N-terminal domains. *EMBO J* 19, 4383-4392 (2000).

14 Richter, K. & Buchner, J. hsp90: Twist and Fold. *Cell* 127, 251-253 (2006).

15 Richter, K., Muschler, P., Hainzl, O. & Buchner, J. Coordinated ATP Hydrolysis by the Hsp90 Dimer. *J. Biol. Chem* 276, 33689-33696 (2001).

16 Ali, M. M. U. *et al.* Crystal structure of an Hsp90-nucleotide-p23/Sba1 closed chaperone complex. *Nature* 440, 1013-1017 (2006).

17 Southworth, D. R. & Agard, D. A. Client-Loading Conformation of the Hsp90 Molecular Chaperone Revealed in the Cryo-EM Structure of the Human Hsp90:Hop Complex. *Mol. Cell* 42, 771-781 (2011).

18 Vaughan, C. K. *et al.* Structure of an Hsp90-Cdc37-Cdk4 Complex. *Mol. Cell* 23, 697-707 (2006).

19 Nilapwar, S. *et al.* Structural-Thermodynamic Relationships of Interactions in the N-Terminal ATP-Binding Domain of Hsp90. *J. Mol. Biol* 392, 923-936 (2009).

20 **Siligardi, G. *et al.* Co-chaperone Regulation of Conformational Switching in the Hsp90 ATPase Cycle. *J. Biol. Chem* 279, 51989-51998 (2004).**

21 **Roe, S. M. *et al.* Structural Basis for Inhibition of the Hsp90 Molecular Chaperone by the Antitumor Antibiotics Radicicol and Geldanamycin. *Journal of Medicinal Chemistry* 42, 260-266 (1999).**

22 **Harris, S. F., Shiau, A. K. & Agard, D. A. The Crystal Structure of the Carboxy-Terminal Dimerization Domain of htpG, the Escherichia coli Hsp90, Reveals a Potential Substrate Binding Site. *Structure (London, England : 1993)* 12, 1087-1097 (2004).**

23 **Dehner, A. *et al.* NMR Chemical Shift Perturbation Study of the N-Terminal Domain of Hsp90 upon Binding of ADP, AMP-PNP, Geldanamycin, and Radicicol. *ChemBioChem* 4, 870-877 (2003).**

24 **Ratzke, C., Mickler, M., Hellenkamp, B., Buchner, J. & Hugel, T. Dynamics of heat shock protein 90 C-terminal dimerization is an important part of its conformational cycle. *Proc. Natl. Acad. Sci* USA, 107, 16101-16106 (2010).**

25 **Nathan, D. F. & Lindquist, S. Mutational analysis of Hsp90 function: interactions with a steroid receptor and a protein kinase. *Mol. Cell. Biol* 15, 3917-3925 (1995).**

26 **Rutherford, S. L. & Lindquist, S. Hsp90 as a capacitor for morphological evolution. *Nature* 396, 336-342 (1998).**

27 **Vaughan, C. K. *et al.* Hsp90-Dependent Activation of Protein Kinases Is Regulated by Chaperone-Targeted Dephosphorylation of Cdc37. *Mol. Cell* 31, 886-895 (2008).**

28 **Roe, S. M. *et al.* The Mechanism of Hsp90 Regulation by the Protein Kinase-Specific Cochaperone p50cdc37. *Cell* 116, 87-98 (2004).**

29 **Neckers, L. Hsp90 inhibitors as novel cancer chemotherapeutic agents. *Trends in Molecular Medicine* 8, S55-S61 (2002).**

30 **Sreedhar, A. S. & Csermely, P. Heat shock proteins in the regulation of apoptosis: new strategies in tumor therapy: A comprehensive review. *Pharmacology & Therapeutics* 101, 227-257 (2004).**

31 **Stebbins, C. E. *et al.* Crystal Structure of an Hsp90 Geldanamycin Complex: Targeting of a Protein Chaperone by an Antitumor Agent. *Cell* 89, 239-250 (1997).**

32 **Dunbrack, J. R. L. *et al.* Meeting review: the Second Meeting on the Critical Assessment of Techniques for Protein Structure Prediction (CASP2), Asilomar, California, December 13-16, 1996. *Folding and Design* 2, R27-R42 (1997).**

33 **Bergerat, A. *et al.* An atypical topoisomerase II from archaea with implications for meiotic recombination. *Nature* 386, 414-417 (1997).**

34 **Wigley, D. B., Davies, G. J., Dodson, E. J., Maxwell, A. & Dodson, G. Crystal structure of an N-terminal fragment of the DNA gyrase B protein. *Nature* 351, 624-629 (1991).**

35 **Salek, R. M., Williams, M. A., Prodromou, C., Pearl, L. H. & Ladbury, J. E. Letter to the Editor: Backbone resonance assignments of the 25kD N-terminal ATPase domain from the Hsp90 chaperone. *Journal of Biomolecular NMR* 23, 327-328 (2002).**

36 **Cooper, A., Johnson, C. M., Lakey, J. H. & Nˆllmann, M. Heat does not come in different colours: entropy-enthalpy compensation, free energy windows, quantum confinement, pressure perturbation calorimetry, solvation and the multiple causes of heat capacity effects in biomolecular interactions. *Biophysical Chemistry* 93, 215-230 (2001).**

37 **Prodromou, C., Roe, S. M., Piper, P. W. & Pearl, L. H. A molecular clamp in the crystal structure of the N-terminal domain of the yeast Hsp90 chaperone. *Nat. Struct. Biol* 4, 477-482 (1997).**

38 **Louvion, J.-F. o., Warth, R. & Picard, D. Two eukaryote-specific regions of Hsp82 are dispensable for its viability and signal transduction functions,ÄâiIn,ÄâyeaSt. *Proc. Natl. Acad. Sci* USA, 93, 13937-13942 (1996).**

39 **Hainzl, O., Lapina, M. C., Buchner, J. & Richter, K. The Charged Linker Region Is an Important Regulator of Hsp90 Function. *Journal of Biological Chemistry* 284, 22559-22567 (2009).**

40 **Sato, S., Fujita, N. & Tsuruo, T. Modulation of Akt kinase activity by binding to Hsp90. *Proc. Natl. Acad. Sci* USA, 97, 10832-10837 (2000).**

41 **Phillips, J. J. *et al.* Conformational Dynamics of the Molecular Chaperone Hsp90 in Complexes with a Co-chaperone and Anticancer Drugs. *J. Mol. Biol* 372, 1189-1203 (2007).**

42 **Retzlaff, M. *et al.* Hsp90 is regulated by a switch point in the C-terminal domain. *EMBO Rep* 10, 1147-1153 (2009).**

43 **Shiau, A. K., Harris, S. F., Southworth, D. R. & Agard, D. A. Structural Analysis of E. coli hsp90 Reveals Dramatic Nucleotide-Dependent Conformational Rearrangements. *Cell* 127, 329-340 (2006).**

44 **Pearl, L. H. & Prodromou, C. Structure and Mechanism of the Hsp90 Molecular Chaperone Machinery. *Annual Review of Biochemistry* 75, 271-294 (2006).**

45 **Johnson, J. L. & Toft, D. O. A novel chaperone complex for steroid receptors involving heat shock proteins, immunophilins, and p23. *J. Biol. Chem* 269, 24989-24993 (1994).**

46 **Johnson, J. L. & Toft, D. O. Binding of p23 and hsp90 during assembly with the progesterone receptor. *Molecular Endocrinology* 9, 670-678 (1995).**

47 **Obermann, W. M. J., Sondermann, H., Russo, A. A., Pavletich, N. P. & Hartl, F. U. In Vivo Function of Hsp90 Is Dependent on ATP Binding and ATP Hydrolysis. *J. Cell Biol* 143, 901-910 (1998).**

48 **Chadli, A. *et al.* Dimerization and N-terminal domain proximity underlie the function of the molecular chaperone heat shock protein 90. *Proc. Natl. Acad. Sci* USA, 97, 12524-12529 (2000).**

49 **Panaretou, B. *et al.* Activation of the ATPase Activity of Hsp90 by the Stress-Regulated Cochaperone Aha1. *Mol. Cell* 10, 1307-1318 (2002).**

50 **Richter, K., Walter, S. & Buchner, J. The Co-chaperone Sba1 Connects the ATPase Reaction of Hsp90 to the Progression of the Chaperone Cycle. *J. Mol. Biol* 342, 1403-1413 (2004).**

51 **McLaughlin, S. H. *et al.* The Co-chaperone p23 Arrests the Hsp90 ATPase Cycle to Trap Client Proteins. *J. Mol. Biol* 356, 746-758 (2006).**

52 **Meyer, P. Structural basis for recruitment of the ATPase activator Aha1 to the Hsp90 chaperone machinery. *EMBO J* 23, 1402-1410 (2004).**

53 **Siligardi, G. *et al.* Regulation of Hsp90 ATPase Activity by the Co-chaperone Cdc37p/p50 cdc37. *J. Biol. Chem* 277, 20151-20159 (2002).**

54 **Chang, H. C. & Lindquist, S. Conservation of Hsp90 macromolecular complexes in Saccharomyces cerevisiae. *J. Biol Chem* 269, 24983-24988 (1994).**

55 **Prodromou, C. *et al.* Regulation of Hsp90 ATPase activity by tetratricopeptide repeat (TPR)-domain co-chaperones. *EMBO J* 18, 754-762 (1999).**

56 Chang, H., Nathan, D. & Lindquist, S. In vivo analysis of the Hsp90 cochaperone Sti1 (p60). *Mol. Cell. Biol.* 17, 318-325 (1997).
57 Sambrook, J. *Molecular cloning : a laboratory manual / Joseph Sambrook, David W. Russell.* (Cold Spring Harbor Laboratory, 2001).
58 Bradford, M. M. A rapid and sensitive method for the quantitation of microgram quantities of protein utilizing the principle of protein-dye binding. *Analytical Biochemistry* 72, 248-254 (1976).
59 Pierce, M. M., Raman, C. S. & Nall, B. T. Isothermal Titration Calorimetry of Protein-Protein Interactions. *Methods* 19, 213-221 (1999).
60 Turnbull, W. B. & Daranas, A. H. On the Value of c:,Äâ Can Low Affinity Systems Be Studied by Isothermal Titration Calorimetry? *Journal of the American Chemical Society* 125, 14859-14866 (2003).
61 Ladbury, J. E. & Doyle, M. L. *Biocalorimetry 2: applications of calorimetry in the biological sciences*. (Wiley, 2004).
62 Sturtevant, J. M. Heat capacity and entropy changes in processes involving proteins. *Proc. Natl. Acad. Sci* USA, 74, 2236-2240 (1977).
63 Ladbury, J. E. & Williams, M. A. The extended interface: measuring non-local effects in biomolecular interactions. *Current Opinion in Structural Biology* 14, 562-569 (2004).
64 Gómez, J., Hilser, V. J., Xie, D. & Freire, E. The heat capacity of proteins. *Proteins: Structure, Function, and Bioinformatics* 22, 404-412 (1995).
65 Privalov, P. L. & Makhatadze, G. I. Contribution of hydration and non-covalent interactions to the heat capacity effect on protein unfolding. *J. Mol. Biol* 224, 715-723 (1992).
66 Cooper, A. Heat capacity effects in protein folding and ligand binding: a re-evaluation of the role of water in biomolecular thermodynamics. *Biophysical Chemistry* 115, 89-97 (2005).
67 Delaglio, F. *et al.* NMRPIPE - a multidimensional spectral processing system based on unix pipes. *Journal of Biomolecular NMR* 6, 277-293 (1995).
68 Vranken, W. F. *et al.* The CCPN data model for NMR spectroscopy: Development of a software pipeline. *Proteins: Structure, Function, and Bioinformatics* 59, 687-696 (2005).
69 Pannier, M., Veit, S., Godt, A., Jeschke, G. & Spiess, H. W. Dead-Time Free Measurement of Dipole-Dipole Interactions between Electron Spins. *Journal of Magnetic Resonance* 142, 331-340 (2000).
70 Jeschke, G. *et al.* DeerAnalysis2006—a comprehensive software package for analyzing pulsed ELDOR data. *Applied Magnetic Resonance* 30, 473-498 (2006).
71 Jeschke, G. & Polyhach, Y. Distance measurements on spin-labelled biomacromolecules by pulsed electron paramagnetic resonance. *Physical Chemistry Chemical Physics* 9, 1895-1910, doi:citeulike-article-id:2837612 (2007).
72 Spolar, R. & Record, M. Coupling of local folding to site-specific binding of proteins to DNA. *Science* 263, 777-784 (1994).
73 Murphy, K. P. & Freire, E. in *Advances in Protein Chemistry* Vol. Volume 43 (eds Frederic M. Richards John T. Edsall C.B. Anfinsen & S. Eisenberg David) 313-361 (Academic Press, 1992).
74 Ikeda, T., Boero, M. & Terakura, K. Hydration properties of magnesium and calcium ions from constrained first principles molecular dynamics. *The Journal of Chemical Physics* 127, 074503 (2007).

75 **Carmeli, C., Huang, J. Y., Mills, D. M., Jagendorf, A. T. & Lewis, A. Extended X-ray absorption fine structure of Mn^{2+} and Mn^{2+} X ATP complex bound to coupling factor 1 of the H+-ATPase from chloroplasts. *J. Biol. Chem* 261, 16969-16975 (1986).**

76 **Cowan, J. A. Metal Activation of Enzymes in Nucleic Acid Biochemistry. *Chemical Reviews* 98, 1067-1088 (1998).**

77 **Maguire, M. E. & Cowan, J. A. Magnesium chemistry and biochemistry. *BioMetals* 15, 203-210 (2002).**

78 **Sousa, M. C. & McKay, D. B. The Hydroxyl of Threonine 13 of the Bovine 70-kDa Heat Shock Cognate Protein Is Essential for Transducing the ATP-Induced Conformational Change, *Biochemistry* 37, 15392-15399 (1998).**

79 **Torres, R. A., Himo, F., Bruice, T. C., Noodleman, L. & Lovell, T. Theoretical Examination of Mg2+-Mediated Hydrolysis of a Phosphodiester Linkage as Proposed for the Hammerhead Ribozyme. *Journal of the American Chemical Society* 125, 9861-9867 (2003).**

80 **Weis, W. I., Drickamer, K. & Hendrickson, W. A. Structure of a C-type mannose-binding protein complexed with an oligosaccharide. *Nature* 360, 127-134 (1992).**

81 **Bock, C. W., Katz, A. K., Markham, G. D. & Glusker, J. P. Manganese as a Replacement for Magnesium and Zinc:,Äâ Functional Comparison of the Divalent Ions. *Journal of the American Chemical Society* 121, 7360-7372 (1999).**

82 **Morton, C. J. & Ladbury, J. E. Water mediated protein-DNA interactions: The relationship of thermodynamics to structural detail. *Protein Science* 5, 2115-2118 (1996).**

83 **Ladbury, J. E., Wright, J. G., Sturtevant, J. M. & Sigler, P. B. A Thermodynamic Study of the trp Repressor operator Interaction. *J. of Mol. Biol* 238, 669-6811994).**

84 **Bergqvist, S., Williams, M. A., O'Brien, R. & Ladbury, J. E. Heat Capacity Effects of Water Molecules and Ions at a Protein,ÄìDNA Interface. *J. Mol. Biol* 336, 829-842 (2004).**

85 **Bergqvist, S., Williams, M. A., O'Brien, R. & Ladbury, J. E. Heat Capacity Effects of Water Molecules and Ions at a Protein-DNA Interface. *J. Mol. Biol* 336, 829-842 (2004).**

86 **HOOGSTRATEN, C. G. & BRITT, R. D. Water counting: Quantitating the hydration level of paramagnetic metal ions bound to nucleotides and nucleic acids. *RNA* 8, 252-260 (2002).**

87 **Farrelly, F. W. & Finkelstein, D. B. Complete sequence of the heat shock-inducible HSP90 gene of Saccharomyces cerevisiae. *J. Biol. Chem* 259, 5745-5751 (1984).**

88 **Rieger, P. H. (Royal Society of Chemistry).**

89 **Karag√∂z, G. E. *et al.* N-terminal domain of human Hsp90 triggers binding to the cochaperone p23. *Proc. Natl. Acad. Sci* USA, (2010).**

Appendix 1 - Table illustrating details of all Hsp90 crystal structures presented in this thesis:

Structure	Species	PDB code	Resolution	Reference
N domain	*S.Cerevisiae*	1AMW	1.85	[7]
N domain	*H.Sapiens*	1YES	2.20	[31]
N domain-Geldanamycin	*S.Cerevisiae*	1A4H	2.50	[7]
N domain-Radicicol	*S.Cerevisiae*	1BGQ	2.50	[21]
N domain-p50^{Cdc37}	*S.Cerevisiae*	1US7	2.30	[28]
M domain	*S.Cerevisiae*	1HK7	2.50	[5]
M domain-Aha1	*S.Cerevisiae*	1USU	2.15	[52]
C domain	*E.coli*	1SF8	2.60	[22]
Hsp90-AMPPNP-Sba1/p23	*S.Cerevisiae*	2CG9	3.10	[16]
HtpG-nucleotide free	*E.coli*	2IOQ	3.50	[43]
HtpG-ADP bound	*E.coli*	2IOP	3.55	[43]